Cover art: Kimmo Rantalainen - 2014 - www.sciencewithfiction.com
Layout and design: Anna Gram and Oliver Wicht
Print: Kruse Digitaldruck, Stralsund - www.mv-druck.de

Copyright: Oliver Wicht, 2014. All rights reserved.
No part of this publiation may be reproduced, stored in a retreival system, or transmitted in any form without prior permission of the author. For the copyrights of articles that have been accepted for publication, please refer to the policy of the respective journal.

Proteolytic Activation of the Coronavirus Fusion Protein

Activatie van het coronavirus fusie-eiwit

(met een samenvatting in het Nederlands)

Proefschrift

ter verkrijging van de graad van doctor aan de Universiteit Utrecht op gezag van de rector magnificus, prof.dr. G.J. van der Zwaan, ingevolge het besluit van het college voor promoties in het openbaar te verdedigen op

maandag 30 juni 2014 des ochtends te 10.30 uur

door

Oliver Wicht
geboren op 28 juli 1983 te Stralsund (Duitsland)

Promotor: Prof.dr. P.J.M Rottier
Copromotor: Dr. B.J. Bosch

The research described in this thesis was financially supported by the EU Framework 7 program PITN-GA-2009-235649-Virus Entry.

Table of Contents

General Introduction

Viruses depend on the host's transcription and translation machinery for propagation. For transfer of viral genomes between host cells, virions are the principle transport vehicles. Virions must enter a host cell to deliver genetic information – an essential step in the viral life cycle. Cells are separated from their environment by lipid membranes, thereby imposing a biophysical barrier that is challenging to cross. The virus particle of enveloped viruses is also encapsulated by a lipid membrane. Enveloped viruses carry highly specialized glycoproteins that control and catalyze fusion of the viral and the host cell membrane. For some viruses, all necessary functions, such as receptor binding, regulation of fusion, and the fusion machinery itself, are combined in a single fusion protein, whereas others require the help of auxiliary viral proteins.

Common virus-membrane fusion process

About three decades of research on viral fusion proteins led to detailed biochemical and structural knowledge and enabled the development of a general virus-membrane fusion model (1). Fusion proteins of enveloped viruses are type I integral membrane proteins that share functional and structural features. Before interaction with the host cell, they exist in a metastable pre-fusion conformation (Figure 1a). Membrane fusion is driven by transition of the fusion protein into a thermodynamically favorable post-fusion conformation (Figure 1e). Thereby, they perturb the target cell membrane structure and provide the free energy to overcome the biophysical barrier. The pre- and post-fusion conformations are studied in great detail for a number of viral fusion proteins (for comparison see (2)). The following intermediate steps complete the model of the fusion process.

The fusion process begins with the interaction of the virus with a cell. After attachment to the host cell, the viral fusion machinery typically requires a trigger like low pH or receptor binding to come into action. The triggered fusion protein adopts an extended intermediate conformation that reaches out (Figure 1b). An amphipathic fusion peptide or fusion loop at the top of the fusion protein inserts into a target membrane, thereby crosslinking two membranes. Subsequently, the two membranes are forced into juxtaposition by a structural

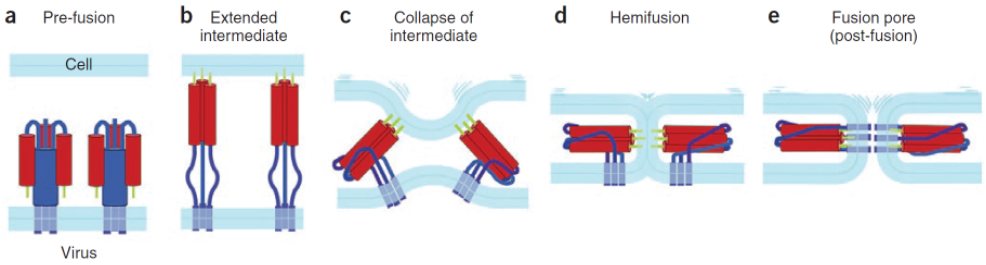

Fig.1. Membrane fusion process by viral fusion proteins (figure reproduced from (1). (a) Fusion-ready, metastable fusion proteins protrude from the viral envelope. The fusion peptide (green) is not exposed. A fusion trigger is required to reorganize the fusion protein yielding (b) an extended intermediate conformation. The fusion peptide is presented at the membrane-distal end of the fusion subunit and can be inserted into the cell membrane. (c) Collapse of fusion protein by zipping up against a central domain. As a result, the membrane associated domains are forced into juxtaposition, bending the membranes. (d) Upon contact of the bilayers the apposed outer leaflets fuse, forming a hemifusion stalk. (e) A fusion pore is formed while the fusion proteins adopt the final post-fusion conformation. Expansion of this pore enables the content of the virions to be released into the cytoplasm of the cell. Reprinted by permission from Macmillan Publishers Ltd: Nat Struct Mol Biol. 2008 Jul; 15(7):690-8, copyright 2008.

collapse of the fusion protein (Figure 1c). By this hairpin formation, the membranes come into close contact and the opposed, outer lipid layers merge and create a hemifusion stalk first (Figure 1d). This is followed by the fusion of the inner leaflets that results in the formation of a fusion pore. Expansion of the fusion pore releases the content of the virus into the cell. Despite high sequence variation, all viral fusion proteins fold into a trimer-of-hairpins post-fusion conformation.

Three classes of viral fusion glycoproteins

Viral fusion proteins are classified into class I, II, or III according to their structural features and distinct organization (3). The best studied *class I* fusion protein is the influenza virus hemagglutinin (HA). Crystal structures of different conformational states are available that lead to the development of a detailed fusion model (4). Like all class I fusion proteins, hemagglutinin occurs as a homotrimer that is oriented perpendicular to the viral envelope. The precursor HA0 is cleaved by host cell proteases to separate the N-terminal HA1 and C-terminal HA2 subunit which remain covalently linked by a disulfide bond near the transmembrane domain (Figure 2A). Proteolysis of precursor class I fusion proteins primes their membrane fusion potential, i.e., they become fusion-ready. The HA1 subunit constitutes a head domain and contains the sialic acid receptor binding domain, whereas three HA2 subunits comprise the fusion machinery and carry the fusion peptide (5), a sequence of apolar amino acids at the newly formed N-terminus (Figure 2B). Acidification of the environment triggers the fusion reaction. The cleaved hemagglutinin trimers undergo large structural rearrangements. HA2 refolds into an extended intermediate conformation. It exposes the fusion peptide at the membrane-distal tip of the molecule, enabling its insertion into the target membrane (Figure 2C). Two coiled-coil domains composed of heptad repeats that are typical for class I fusion proteins, zip up and fold against each other (Figure 2D, yellow and blue). Thereby, the protein is bend around to create a hairpin and force the two membrane-interacting parts into juxtaposition. The final post-fusion conformation is characterized by a stable six-helix bundle composed of a trimer-of-hairpins.

The afore mentioned common features and structures of class I fusion proteins are: i) orientation of prefusion trimers perpendicular to the membrane, ii) proteolytic priming to gain fusion capacity, iii) a fusion peptide at the N-terminus of the membrane-anchored subunit, iv) heptad repeat domains enabling formation of a six-helix bundle made of a trimer-of-hairpins.

The best studied *class II* fusion proteins are the E proteins of flaviviruses (1). Their structures contain predominantly beta-sheets rather than alphahelices. The viral envelope is covered by an array of pre-fusion dimers that are arranged in a symmetric, often icosahedral grid. Class II fusion proteins are locked by an auxiliary protein to prevent premature fusion activity and proteolytic priming of the auxiliary protein makes them fusion-ready. Low-pH-induced protonation is generally required to trigger the fusion process. Upon transition to the elongated intermediate conformation, the fusion proteins reorganize into trimers. Instead of a fusion peptide, an internal hydrophobic fusion loop is presented at the tip of the molecule and connects with the target membrane. Parallel interactions of the beta-sheets zip up the proteins, pulling the membranes together and resulting in a thermodynamically favorable post-fusion timer-of-hairpins.

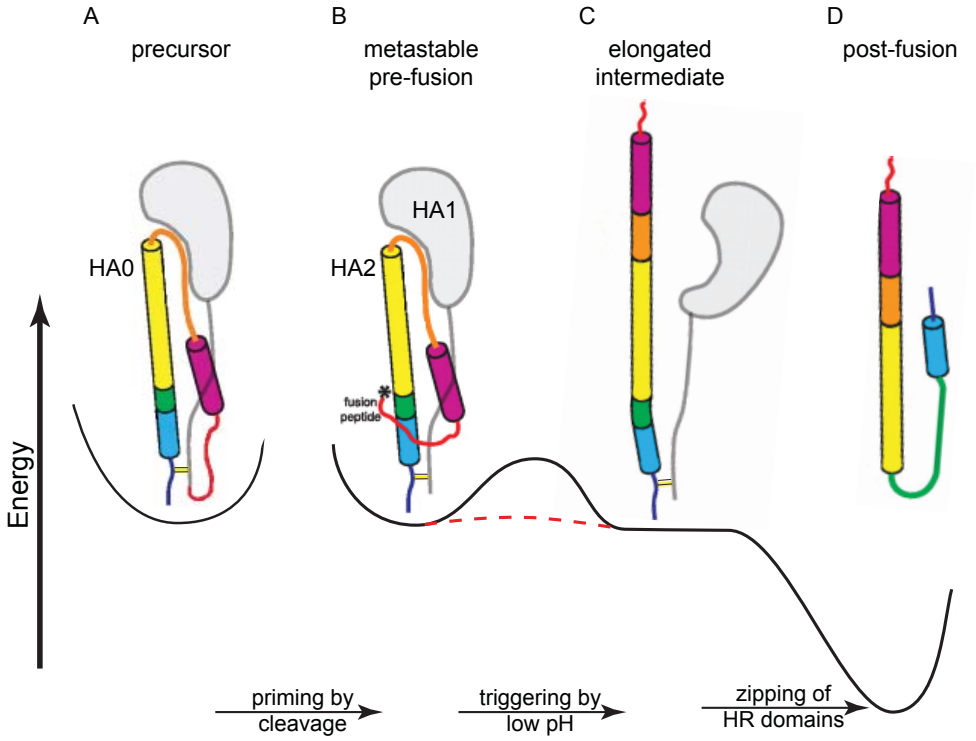

Fig.2: Structures and function of influenza virus hemagglutinin, a prototype class I fusion protein. A schematic representation is shown alongside the level of thermodynamic energy. For simplicity, only a monomer is shown. (A) Priming of the HA0 precursor by proteolytic cleavage renders the protein fusion-ready. (B) The HA1 subunit (grey) remains covalently connected by an intramolecular disulfide bond (yellow bond) and contains the receptor binding domain. The membrane-anchored HA2 subunit comprises the fusion machinery (color) and contains the thermodynamic energy required for membrane merger. The fusion peptide (red) is located at the newly formed N-terminus and remains buried in the protein. (C) Acidic pH lowers the energy barrier (red dotted line) and facilitates dramatic rearrangements in HA. The fusion process is initiated by HA1 moving aside and HA2 adopting an elongated intermediate conformation. The FP is projected at the tip and can insert into the target membrane. This links the viral and the host membrane. (D) The HA2 subunit collapses into an energetically favorable post-fusion conformation, providing the energy for membrane fusion. A hairpin structure forms that juxtaposes the membrane-associated parts (dark blue and red pointing upwards). Figure was adapted from (6).

Class III fusion proteins enable virus-cell fusion of e.g., rhabdoviruses and herpesviruses (1). Part of their structure is made of coiled-coils resembling pivotal features of class I fusion proteins. In addition, the N-terminal part of the fusion machinery is rich in beta-sheets and has two internal fusion loops, resembling the overall structure of class II fusion proteins. Proteolytic priming is not required for activation of the fusion capacity. So far, no common fusion trigger has been identified; some class III fusion proteins require low pH and others can fuse after receptor binding (7). By analogy to other fusion proteins, an elongated intermediate conformation connects the opposing membrane surfaces. Zipping up against the central domain brings the membranes together. The post-fusion structure of class III fusion proteins complies with the unifying trimer-of-hairpins model (Figure 1).

Proteolytic priming and the fusion trigger of viral fusion proteins

A selective interplay between host cells and virions controls the progression of the fusion process at two major checkpoints: priming and triggering (2). Fusion proteins are synthesized at the rough endoplasmic reticulum. When trafficking along the slightly acidic secretory pathway, the ectodomains are exposed to cellular membranes and potential fusion activators like low pH and receptor molecules (8). Hence, protection of the metastable fusion protein against a pre-mature fusion reaction is required. In fact, the majority of fusion proteins of enveloped viruses is unable to fuse at this stage. They require an essential maturation step called priming to become fusion-ready. Priming is typically characterized by a proteolytic cleavage of the fusion protein or an auxiliary protein. This releases structural constrains and enables the fusion proteins to acquire the fusion-competent metastable prefusion conformation. Only after priming, a fusion trigger, typically in the form of an environmental stimulus, is able to initiate the fusion reaction. Whereas priming often occurs in the process of virion biogenesis, the triggers for fusion are encountered at or in a target cell.

Fusion protein activation is controlled by environmental stimuli

A particular signature of preconditions and stimuli govern the timing and site of virus entry. Priming of class I fusion proteins is affected by the type of cleavage site in the fusion protein, the nature of a priming protease, and the accessibility of both. Proteolytic cleavage of class I fusion proteins can occur at three different locations, as illustrated by some examples. Human immunodeficiency virus (HIV) Env protein and the respiratory syncytial virus F protein are proteolytically primed by furin or furinlike proteases in the virus producing cell before virions are released (9). Some viral fusion proteins are cleaved upon virion transit through the extracellular milieu, where they can encounter proteases and become primed as well. An example is the activation of influenza virus hemagglutinin by tryptase clara or mini-plasmin, two proteases that occur in the airways (10, 11). Other fusion proteins only get cleaved after binding to the target cell by cellular transmembrane proteases, either directly or upon receptor-induced conformational changes. For example, the type II transmembrane serine proteases (TTSP) proteolytically prime human pathogenic severe acute respiratory syndrome coronavirus (SARS-CoV) spike and influenza virus HA proteins (12, 13).

Receptor interaction can promote binding to a coreceptor or trigger the fusion reaction of primed fusion proteins at the plasma membrane. Yet, most viruses do not fuse at the plasma membrane, but are internalized and subsequently experience a dramatic change in environmental conditions along the endolysosomal degradation pathway (14). The endosomal pH typically drops from neutral to acidic (pH 7.4 to 4.5) and this cue triggers the fusion reaction of influenza virus HA, hepatitis C virus E1/E2 glycoproteins, vesicular stomatitis virus G protein, and many more (2). Furthermore, low-pH-activated proteases can proteolytically prime viral fusion proteins, rendering them fusion-ready only in the endolysosomal compartment. Cathepsin proteases, for example, have been found to promote cell entry of SARS-CoV and Ebola virus (15, 16). Proteolytic activation is necessary for most class I fusion proteins. In contrast, class III fusion proteins like vesicular stomatitis virus G protein do not require proteolytic priming for function.

Priming of viral fusion proteins has been observed in the virus producing cell, in the extracellular milieu, and at or in a target cell. Receptor binding and low pH or a combination of both represent fusion triggers for most viral fusion proteins, although for others the

trigger still remains to be identified (2). Depending on the virus, priming and triggering occur as clearly separated events or in close succession. Both processes sometimes require similar environmental stimuli.

Coronaviruses use class I fusion proteins for entry. The aim of the studies described in the present dissertation was to elucidate the mechanism of action and the regulation of coronavirus fusion proteins. To that end, we investigated the entry of the prototype coronavirus mouse hepatitis virus (MHV) and of the emerging porcine epidemic diarrhea virus (PEDV).

Coronaviruses

Coronaviruses have received much attention due to the identification of the human pathogenic SARS-CoV in 2003 and the Middle East respiratory syndrome coronavirus (MERS-CoV) in 2012 (17, 18). The emergence of both coronaviruses demonstrates the zoonotic potential and the consequential threat of coronaviruses to human health (19). Coronaviruses have been isolated from various mammals and birds including beluga whales and thrushes. They can cause severe diseases among farm and companion animals such as avian infectious bronchitis or feline infectious peritonitis (20). PEDV infections frequently recur in East-Asia, where they cause severe economic damage due to high mortality rates amongst suckling piglets (21). PEDV has been introduced on the North American subcontinent in 2013 (22) and since then, the number of reported cases continues to rise (weekly case report http://www.aasv.org). The virus infects the epithelia of the small intestine, and causes villous atrophy resulting in diarrhea and dehydration.

The spherical, pleiomorphic coronavirion is about 80-120 nm in diameter and contains at least four structural proteins ((23) and (20) for detailed information on coronavirus biology). The triple spanning membrane protein (M) and the small hydrophobic envelope protein (E) facilitate virus assembly. The spike protein (S) is a homotrimeric surface glycoprotein that protrudes perpendicular from the viral envelope and is responsible for the characteristic crown-like appearance of the coronavirion in the electron microscope. S proteins mediate attachment to and fusion with the host cells and represent the main target for neutralizing antibodies. Inside the virion, the 5‘-capped, poly-adenylated, positive-sense RNA genome is packaged by the nucleocapsid (N) protein. Virions of some coronaviruses carry a fifth structural protein, the hemagglutinin esterase glycoprotein. It can bind to the cellular glycocalyx and its enzymatic activity destroys acetylated sialic acids. The hemagglutinin esterase seems to be essential for viral fitness in vivo but is dispensable in vitro (24).

With up to 31.700 nucleotides, coronaviruses have the longest non-segmented RNA genome known. Replication and transcription are controlled by structural elements in the untranslated regions at the 5’ and 3’ end of the genome and by promoter-like elements. These so called transcription regulatory sequences (TRS) precede each open reading frame (ORF). The 5’ end of the genome contains the large ORF1ab, which encodes the nonstructural proteins. ORF1ab accounts for two thirds of the genetic information and is translated into two large precursor polyproteins. Processing by viral proteases is required to generate functional replicase proteins. For example, mouse hepatitis virus (MHV) encodes two papain-like cysteine proteinases, and a 3C-like proteinase for polyprotein processing. The previously mentioned structural genes are expressed from a nested set of subgenomic mRNAs derived from the 3’ third of the genome. The subgenomic transcripts are generated with a 5’ leader

sequence followed by a TRS that serves as a transcription signal on the negative strand RNA during genome replication. Replication of coronaviruses occurs on membranous structures in the cytoplasm and involves characteristic double membrane vesicles, whose precise function remains unclear. New virions are assembled in the endoplasmic reticulum / Golgi intermediate compartment and are released through the secretory pathway. Coronavirus entry is the first step in the next round of the viral life cycle and its prevention can foster our efforts to prevent and treat disease.

The coronavirus spike protein

The coronavirus S protein is the sole determinant for coronavirus entry and cell-cell fusion, thereby determining critical features like host range and pathogenesis (25). It is heavily Nglycosylated (MHV and feline infectious peritonitis virus (FIPV) S proteins have 21 and 35 predicted N-glycosylation sites, respectively) and occurs in trimers on the virus envelope ((26-28) for reviews of the S protein). Composed of up to 1450 amino acids, S proteins are the largest class I fusion proteins known to date and feature typical structural elements (Figure 3). As a type I integral membrane protein, it contains an N-terminal signal peptide which is removed after translocation into the endoplasmic reticulum, and a transmembrane domain close to the C-terminus that anchors the protein in the membrane. A short cysteine-rich cytoplasmic or intra-virion tail can be palmitoylated and has been reported to play a role in intracellular trafficking and membrane fusion (29). C-terminal targeting signals direct newly synthesized S proteins to the site where virions bud. The large ectodomain comprises two functionally distinct domains. The N-terminal part (S1) contains the receptor binding domain and forms a globular head domain that is placed on the C-terminal stem-like domain (S2) containing the fusion machinery. The S2 subunit includes a well-conserved sequence of apolar amino acids representing the putative fusion peptide (30) and the two heptad repeat (HR) regions HR1 and HR2 that adopt alpha-helical structures and can form coiled-coils characteristic for class I fusion proteins. During fusion, the HR1 and HR2 domains of the three S proteins interact with each other in an antiparallel manner, eventually assembling into a stable six-helix bundle whose structure has been solved for SARS-CoV and MHV (31, 32). Small peptides corresponding to the HR domains inhibit the membrane fusion process by interfering with HR interactions (33).

Proteolytic priming of spike proteins

Fundamental aspects of the fusion mechanism of class I fusion proteins apply to the coronavirus S protein. However, the regulation of its proteolytic priming seems to differ considerably and is incompletely understood. Studies have correlated protease activity with virus fusion competence by diverse approaches: application of pharmacological protease inhibitors to block infection, manipulation of potential cleavage sites using reverse-genetic systems, investigation of the cell-cell fusion capacity of the fusion protein, experimental expression of proteases, and mimicking the milieu of the fusion site to simulate the priming and triggering events using recombinant proteases and soluble receptors in vitro. Despite the importance of proteolytic priming, direct biochemical evidence for cleavage of coronavirus S proteins at or in the target cell is lacking for all coronaviruses; i.e., cleaved S proteins have not been isolated and analyzed after virus entry. I will review the current understanding of proteolytic priming of coronavirus S proteins by presenting some examples.

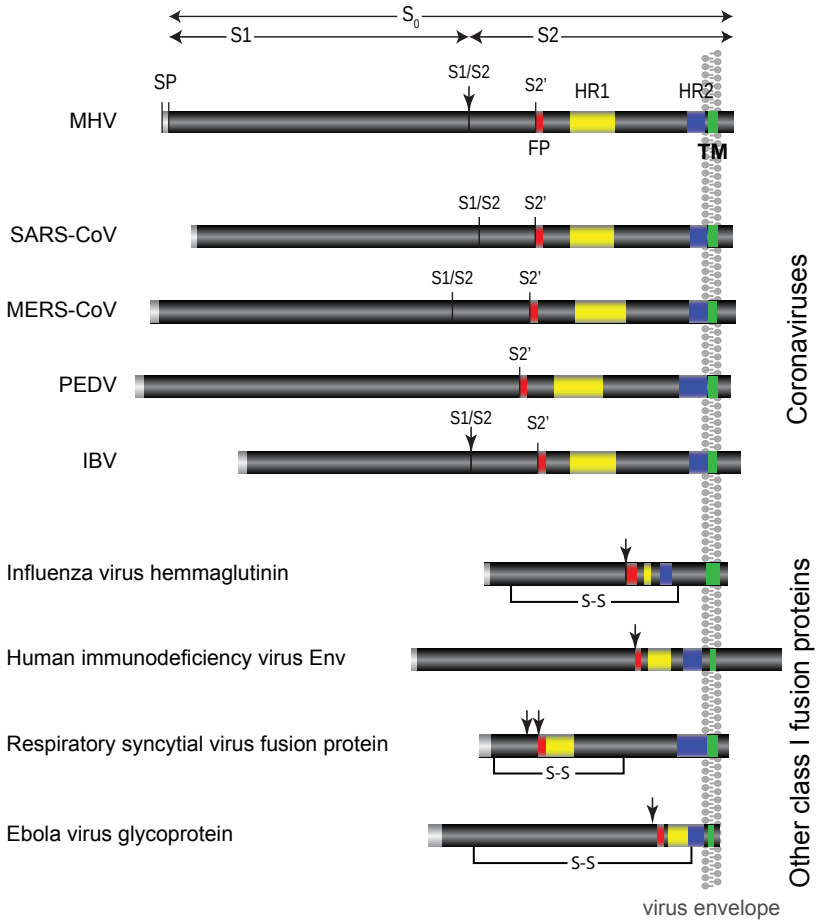

Fig.3. Schematic presentation of various class I fusion proteins drawn to scale. The spike proteins of three betacoronaviruses mouse hepatitis virus (MHV), severe acute respiratory syndrome coronavirus (SARS-CoV), and Middle East respiratory syndrome coronavirus (MERS-CoV), the alphacoronavirus porcine epidemic diarrhea virus (PEDV), and the gammacoronavirus infectious bronchitis virus (IBV) are shown next to the fusion proteins influenza virus hemagglutinin (orthomyxovirus), human immunodeficiency virus Env (retrovirus), respiratory syncytial virus fusion protein (paramyxovirus) and Ebola virus glycoprotein (filovirus). Common structural features are depicted: the N-terminal signal peptide (light gray), the fusion peptide (FP, shown in red), the heptad repeat regions (yellow and blue), and the transmembrane domain that anchors the fusion proteins in the viral envelope (green). Arrows point to the furin cleavage sites that separate the N-terminal from the C-terminal domain. In coronaviruses, the furin cleavage site in MHV and IBV S proteins allows to deduce the putative S1/S2 junction in S of SARS-CoV and MERS-CoV from sequence alignments. Another putative cleavage site in coronavirus S proteins (S2') is located just upstream of the fusion peptide. Disulfide bridges link the N- and C-terminal subunits after proteolytic priming of some fusion proteins (S-S).

The S proteins of most beta- and gammacoronaviruses like MHV-A59 and IBV, as well as few alphacoronaviruses, in particular feline coronavirus (FCoV) serotype 1 strains, are proteolytically cleaved at the S1/S2 junction. Cleavage results in a noncovalently associated conjugate of S1 and S2 domains (review (26)). The S1/S2 junction typically consists of a furin cleavage site (FCS) with the R-X-(R/K)-R (R = arginine, K = lysine, X = any aa) consensus motif,

which is used by furin or furin-like serine proteases during virus biogenesis in the secretory pathway ((34); overview of cleavage sites in Chapter 6 Table 2). Cleavage of S proteins in the host cell correlates with the ability to induce cell-cell fusion resulting in giant multinucleated syncytia. For example, MHVA59 S protein contains a suboptimal FCS. Hence, ~30% of S proteins become cleaved in the secretory pathway and can induce large syncytia in cell culture (35). Inhibition of furin-like proteases during virus production by specific compounds, as well as mutation or deletion of the FCS, yields uncleaved S proteins. This strongly reduces cell-cell fusion activity, but has no impact on viral infectivity or pathogenicity (34, 36, 37). The extent of MHV S protein cleavage varies with the cell type used to propagate the virus (38). The FCS in coronavirus S proteins is atypically positioned, i.e. more than 100 amino acids upstream of the putative FP (30). Based on the N-terminal location of the FP in other class I fusion proteins, the furin cleavage at the S1/S2 junction may not generate a fusion-ready S2 domain (Figure 3). Furthermore, most coronavirions carry uncleaved S proteins. Strong evidence has been obtained that proteolytic processing at or in the target cell is required for fusion. For SARSCoV and MHV, the fusion process has been characterized in more detail, illustrating different principles of controlling this important step of the viral life cycle.

S proteins of MHV strain 2 (MHV-2) were shown to become activated by proteolytic priming at the S1/S2 junction (39). Blocking endosomal proteases, in particular the low-pH-activated cysteine proteases cathepsin B and L, by protease inhibitors or by preventing endosomal acidification, inhibited the infection of MHV2 in vitro (40). Priming in the endolysosomal compartment can be bypassed by either genetically introducing an alternative protease cleavage site or by the addition of exogenous proteases to the inoculum (41). Furthermore, biochemical analysis of MHV-2 S proteins showed that cleavage alone does not enable transition into the proteinase K resistant post-fusion trimer-of-hairpins (42). Addition of soluble receptor was required for cleavage of S proteins at an alternative cleavage site. This truncated S2 subunit was found to organize into stable multimers indicating the formation of the post-fusion six-helix bundle. Furthermore, coincubation with soluble receptor also enabled association of the virions with lipid membranes as measured by liposome cofloatation, suggesting the induction of a receptor-mediated conformational rearrangement in the S protein. The membrane fusion of MHV-2 is controlled by at least two checkpoints: receptor binding, which enables subsequent cleavage, and the cleavage itself, which requires an active protease.

Virus entry of SARS-CoV can be blocked by specific cathepsin L inhibitors, lysosomotropic agents and inhibitors of endocytosis in vitro (43). The proteolytic priming of its naturally uncleaved S protein by cathepsin L became more evident by the identification of the cathepsin cleavage site (16). Like MHV-2, SARS-CoV S protein mediated entry can be rescued by supplementing trypsin during inoculation (44). Alternatively, the expression of thermolysin, HAT, or TMPRSS by the target cells enables SARS-CoV entry (12, 45). By mutagenesis of the S protein, candidate cleavage sites were identified Nterminally of the putative fusion peptide, a typical class I fusion protein feature (46). Genetic modification of the putative S protein cleavage site and treatment with exogenous trypsin or elastase augmented S protein activation, supporting the hypothesis that S proteins can be sequentially cleaved [(47), reviewed in (28)]. An early cleavage at the S1/S2 junction apparently facilitates a second cleavage within the S2 subunit to release an N-terminal fusion peptide. SARS-CoV S protein

proteolytic priming is controlled mainly by the availability of protease activity, whereas it seems independent of receptor binding or a low-pH environment *per se*. Studies indicate that natural infections of SARS-CoV are preferentially targeting tissues that express high levels TMPRSS2 (48). Nevertheless, receptor binding is necessary to establish contact with the target cell, hence bringing the virus in proximity to priming proteases and the target membrane (25).

Besides SARS-CoV and MHV-2 S protein, the proteolytic priming of other S proteins is not well understood. For example, infection of some coronaviruses with uncleaved S proteins like human CoV (HCoV) NL63 is insensitive to protease inhibitors and lysosomotropic agents, making the priming step enigmatic (49). In contrast, coronaviruses like IBV carry almost fully cleaved S proteins. Sequence analysis indicated that they are primed by furin-like proteases at the S1/S2 junction before virus release (50), much like HIV Env. However, the cell-culture-adapted IBV Beaudette strain contains an additional FCS immediately upstream of the fusion peptide. It supports furin mediated entry, suggesting an alternative cleavage at the FP (51). The entry stage of many other important coronaviruses like PEDV, canine coronavirus (CCoV), and transmissible gastroenteritis coronavirus (TGEV) is barely investigated.

Proteolytic priming may also have profound effects on the disease outcome of a virus infection. FCoV virions mostly carry uncleaved S proteins. The pathogenicity of different isolates was described to correlate with differential fusion-activating cleavage of the S protein (52). Furthermore, the switch from a mildly pathogenic biotype to a highly pathogenic, lethal biotype is accompanied by amino acid substitutions in the S1/S2 cleavage site (53).

The endolysosomal compartment offers a diverse spectrum of proteases with the potential to prime virus fusion proteins. However, premature and unspecific proteolysis can cause irreversible damage. A fine balance between beneficial and detrimental proteolytic activity has to be maintained. Notably, natural infections by FECV, CCoV and PEDV, the latter also carrying uncleaved S proteins, occur in the intestine, an environment rich in gastric and pancreatic proteases. To stay infectious, the viruses require a distinct mechanism that tightly controls proteolytic priming to avoid premature activation or destruction of their fusion proteins.

Triggering of spike proteins

Before membrane fusion can occur, primed, fusion-ready class I fusion proteins have to pass the last checkpoint that controls the fusion machinery: the fusion trigger. In contrast to prototype class I fusion proteins, coronavirus S protein-mediated membrane fusion is generally believed to be independent of low pH. MHV-A59 infection and, under conditions of trypsin supplementation, also IBV and PEDV infection induce cell-cell fusion at neutral pH (35, 44, 54, 55). Moreover, the infection of MHV-2 and SARS-CoV can occur under conditions where lysosomal acidification is blocked, although it requires to bypass the requirement for low pH-activated proteases for priming by the addition of proteases to the inoculum (40, 56). Yet, certain coronaviruses like IBV and MHV-A59 were reported to rely on acidification for productive infection (57, 58). Particularly the low pH requirement of MHV-A59 infection is under debate. Qiu et al. found the virus to be insensitive to lysosomotropic agents, although Eifart et al. reported low-pH induced conformational changes and loss of infectivity after low pH treatment (40, 58).

Alternatively, receptor binding has been implicated to act as a trigger for membrane fusion. The formation of protease resistant post-fusion structures and the cofloatation of virus with liposomes after incubation with soluble receptor were interpreted to reflect receptor-induced conformational rearrangements in S proteins (strain A59, JHM and MHV-2, (42, 59-61)). The receptor protein or specific antibodies were able to induce the formation of proteinase K resistant multimers, indicative of a post-fusion structure (62). Notably, the transmembrane domain and the C-terminus of the receptor do not play a role, since MHV can be redirected to nonnatural glycoproteins like Fc receptors or EGF receptors (63, 64). In contrast, the infection mediated by FIPV S protein was independent of specific receptor interaction, as bipartite antibodies that link the virion via the S protein to a nonnatural EGF receptor promoted virus entry and syncytia formation (65). Furthermore, receptor-interaction of the SARS-CoV S protein induced minor conformational reorganization as observed by electron microscopy (66). This interaction can expose a cleavage site for activation of S protein by particular human airway proteases (67). However, other studies observed that trypsin inactivates the SARS-CoV S proteins even in the absence of receptor (43). Thus, the exact effects of receptor interaction for SARS-CoV entry are unknown.

Receptors serve as attachment molecules and primarily determine the tropism of coronaviruses. The consequences of receptor binding for structure and function of many coronavirus S proteins remain elusive. Importantly, rather than serving as fusion trigger, receptor binding can stimulate proteolytic priming. At this point, it is largely unclear whether coronavirus entry requires specific fusion triggers and if so of what nature they are.

Outline of this thesis

Whereas the class I fusion proteins of prototype viruses are well described, the features and mechanism of action of coronavirus S proteins are less clear, leaving fundamental aspects of spatiotemporal regulation of virus entry obscure. Especially the current concepts of proteolytic priming and fusion triggering of class I fusion proteins do not reflect the complex situation and diversity seen for coronaviruses. No crystal structure of the full-length S protein has been solved; hence details of the structural reorganization of S proteins resulting in membrane fusion remain enigmatic. Understanding coronavirus fusion proteins will deepen our knowledge concerning other viral class I fusion proteins as well and facilitate the development of prevention and treatment strategies against virus infections.

Proteolytic priming is required for class I fusion proteins to become fusion-ready. Instead of during biogenesis of the virions, this activation of coronaviruses often occurs in the context of the target cell. However, the fusion-ready subunit of coronavirus S proteins has not yet been observed upon an infection. In chapter 2 we aimed to determine the S protein cleavage product that actually mediates membrane fusion with the host cell. We developed an unbiased assay to determine the cleavage status of MHV-A59 S proteins directly after membrane fusion has occurred. Our entry assay enables the specific identification and biochemical characterization of viral S proteins that were partitioning in successfully fusing virions.

Specific proteases are involved in priming of the S proteins. The study in chapter 3 was designed to identify the protease(s) which mediate proteolytic priming of the MHV-A59 S protein by RNA interference technology and by using pseudotyped virus-like particles.

Besides studying the very details of MHV-A59 entry, we investigated the particular

growth requirements for PEDV. The propagation of PEDV field isolates is strictly dependent on the supplementation of active trypsin to the cell culture medium. To set the stage for the investigation of PEDV, a reverse genetic system was established that allows the modification of the viral genome (Chapter 4). By adopting the targeted recombination system as described for MHV, we were able to generate PEDV derivatives that express reporter genes. This system is based on the cell culture-adapted PEDV strain DR13, which we found to propagate independent of trypsin. Genetic manipulation of the S gene enabled us to study details of PEDV entry. Therefore, we compared the S proteins of the trypsin dependent field isolate CV777 and the cell culture-adapted PEDV DR13 (Chapter 5).

In the final chapter, I will reevaluate the current understanding of the various steps leading to coronavirus membrane fusion and compare it to typical class I fusion proteins to illustrate similarities and differences. Reviewing our results from the MHV and PEDV studies, I will discuss the underlying mechanism and the putative biological role of proteolysis in the coronavirus life cycle. I will also discuss the putative enzymes involved in cleavage and their potential as antiviral drug targets.

References

1. Harrison SC. 2008. Viral membrane fusion. Nature structural & molecular biology 15:690-698.
2. White JM, Delos SE, Brecher M, Schornberg K. 2008. Structures and mechanisms of viral membrane fusion proteins: multiple variations on a common theme. Critical reviews in biochemistry and molecular biology 43:189-219.
3. Igonet S, Rey FA. 2012. SnapShot: Viral and eukaryotic protein fusogens. Cell 151:1634-1634 e1631.
4. Skehel JJ, Wiley DC. 2000. Receptor binding and membrane fusion in virus entry: the influenza hemagglutinin. Annual review of biochemistry 69:531-569.
5. Epand RM. 2003. Fusion peptides and the mechanism of viral fusion. Biochimica et biophysica acta 1614:116-121.
6. Xu R, Wilson IA. 2011. Structural characterization of an early fusion intermediate of influenza virus hemagglutinin. Journal of virology 85:5172-5182.
7. Eisenberg RJ, Atanasiu D, Cairns TM, Gallagher JR, Krummenacher C, Cohen GH. 2012. Herpes virus fusion and entry: a story with many characters. Viruses 4:800-832.
8. Alberts B, Johnson A, Lewis J, Raff M, Roberts K, Alberts B 2007, posting date. Molecular biology of the cell Fifth edition. [Online.]
9. Garten W, Hallenberger S, Ortmann D, Schafer W, Vey M, Angliker H, Shaw E, Klenk HD. 1994. Processing of viral glycoproteins by the subtilisin-like endoprotease furin and its inhibition by specific peptidylchloroalkylketones. Biochimie 76:217-225.
10. Kido H, Yokogoshi Y, Sakai K, Tashiro M, Kishino Y, Fukutomi A, Katunuma N. 1992. Isolation and characterization of a novel trypsin-like protease found in rat bronchiolar epithelial Clara cells. A possible activator of the viral fusion glycoprotein. The Journal of biological chemistry 267:13573-13579.
11. Murakami M, Towatari T, Ohuchi M, Shiota M, Akao M, Okumura Y, Parry MA, Kido H. 2001. Mini-plasmin found in the epithelial cells of bronchioles triggers infection by broad-spectrum influenza A viruses and Sendai virus. European journal of biochemistry / FEBS 268:2847-2855.
12. Matsuyama S, Nagata N, Shirato K, Kawase M, Takeda M, Taguchi F. 2010. Efficient activation of the severe acute respiratory syndrome coronavirus spike protein by the transmembrane protease TMPRSS2. Journal of virology 84:12658-12664.
13. Bottcher E, Matrosovich T, Beyerle M, Klenk HD, Garten W, Matrosovich M. 2006. Proteolytic activation of influenza viruses by serine proteases TMPRSS2 and HAT from human airway epithelium. Journal of virology 80:9896-9898.
14. Mercer J, Schelhaas M, Helenius A. 2010. Virus entry by endocytosis. Annual review of biochemistry 79:803-833.
15. Chandran K, Sullivan NJ, Felbor U, Whelan SP, Cunningham JM. 2005. Endosomal proteolysis of the Ebola virus glycoprotein is necessary for infection. Science (New York, N.Y.) 308:1643-1645.
16. Bosch BJ, Bartelink W, Rottier PJ. 2008. Cathepsin L functionally cleaves the severe acute respiratory syndrome coronavirus class I fusion protein upstream of rather than adjacent to the fusion peptide. Journal of virology 82:8887-8890.
17. Drosten C, Gunther S, Preiser W, van der Werf S, Brodt HR, Becker S, Rabenau H, Panning M, Kolesnikova L, Fouchier RA, Berger A, Burguiere AM, Cinatl J, Eickmann M, Escriou N, Grywna K, Kramme S, Manuguerra JC, Muller S, Rickerts V, Sturmer M, Vieth S, Klenk HD, Osterhaus AD, Schmitz H, Doerr HW. 2003. Identification of a novel coronavirus in patients with severe acute

respiratory syndrome. The New England journal of medicine 348:1967-1976.

18. Zaki AM, van Boheemen S, Bestebroer TM, Osterhaus AD, Fouchier RA. 2012. Isolation of a novel coronavirus from a man with pneumonia in Saudi Arabia. The New England journal of medicine 367:1814-1820.
19. Drexler JF, Corman VM, Drosten C. 2014. Ecology, evolution and classification of bat coronaviruses in the aftermath of SARS. Antiviral research 101:45-56.
20. Fields BN, Knipe DM, Howley PM. 2013. Fields virology, Sixth edition ed. Wolters Kluwer/ Lippincott Williams & Wilkins Health, Philadelphia.
21. Li W, Li H, Liu Y, Pan Y, Deng F, Song Y, Tang X, He Q. 2012. New variants of porcine epidemic diarrhea virus, China, 2011. Emerging infectious diseases 18:1350-1353.
22. Huang YW, Dickerman AW, Pineyro P, Li L, Fang L, Kiehne R, Opriessnig T, Meng XJ. 2013. Origin, evolution, and genotyping of emergent porcine epidemic diarrhea virus strains in the United States. mBio 4:e00737-00713.
23. Perlman S, Holmes KV. 2006. The nidoviruses toward control of SARS and other nidovirus diseases, p. 1 online resource (xxxvii, 617 p.), Advances in experimental medicine and biology v. 581. Springer Science+Business Media, New York, NY.
24. Lissenberg A, Vrolijk MM, van Vliet AL, Langereis MA, de Groot-Mijnes JD, Rottier PJ, de Groot RJ. 2005. Luxury at a cost? Recombinant mouse hepatitis viruses expressing the accessory hemagglutinin esterase protein display reduced fitness in vitro. Journal of virology 79:15054-15063.
25. Perlman S, Gallagher T, Snijder EJ. 2008. Nidoviruses. ASM Press, Washington, DC.
26. Belouzard S, Millet JK, Licitra BN, Whittaker GR. 2012. Mechanisms of coronavirus cell entry mediated by the viral spike protein. Viruses 4:1011-1033.
27. Heald-Sargent T, Gallagher T. 2012. Ready, set, fuse! The coronavirus spike protein and acquisition of fusion competence. Viruses 4:557-580.
28. Simmons G, Zmora P, Gierer S, Heurich A, Pohlmann S. 2013. Proteolytic activation of the SARS-coronavirus spike protein: cutting enzymes at the cutting edge of antiviral research. Antiviral research 100:605-614.
29. Thorp EB, Boscarino JA, Logan HL, Goletz JT, Gallagher TM. 2006. Palmitoylations on murine coronavirus spike proteins are essential for virion assembly and infectivity. Journal of virology 80:1280-1289.
30. Madu IG, Roth SL, Belouzard S, Whittaker GR. 2009. Characterization of a highly conserved domain within the severe acute respiratory syndrome coronavirus spike protein S2 domain with characteristics of a viral fusion peptide. Journal of virology 83:7411-7421.
31. Xu Y, Liu Y, Lou Z, Qin L, Li X, Bai Z, Pang H, Tien P, Gao GF, Rao Z. 2004. Structural basis for coronavirus-mediated membrane fusion. Crystal structure of mouse hepatitis virus spike protein fusion core. The Journal of biological chemistry 279:30514-30522.
32. Supekar VM, Bruckmann C, Ingallinella P, Bianchi E, Pessi A, Carfi A. 2004. Structure of a proteolytically resistant core from the severe acute respiratory syndrome coronavirus S2 fusion protein. Proceedings of the National Academy of Sciences of the United States of America 101:17958-17963.
33. Bosch BJ, van der Zee R, de Haan CA, Rottier PJ. 2003. The coronavirus spike protein is a class I virus fusion protein: structural and functional characterization of the fusion core complex. Journal of virology 77:8801-8811.
34. de Haan CA, Stadler K, Godeke GJ, Bosch BJ, Rottier PJ. 2004. Cleavage inhibition of the murine coronavirus spike protein by a furin-like enzyme affects cell-cell but not virus-cell fusion. Journal of virology 78:6048-6054.
35. Sturman LS, Ricard CS, Holmes KV. 1985. Proteolytic cleavage of the E2 glycoprotein of murine coronavirus: activation of cell-fusing activity of virions by trypsin and separation of two different 90K cleavage fragments. Journal of virology 56:904-911.
36. Gombold JL, Hingley ST, Weiss SR. 1993. Fusion-defective mutants of mouse hepatitis virus A59 contain a mutation in the spike protein cleavage signal. Journal of virology 67:4504-4512.
37. Bos EC, Luytjes W, Spaan WJ. 1997. The function of the spike protein of mouse hepatitis virus strain A59 can be studied on virus-like particles: cleavage is not required for infectivity. Journal of virology 71:9427-9433.
38. Frana MF, Behnke JN, Sturman LS, Holmes KV. 1985. Proteolytic cleavage of the E2 glycoprotein of murine coronavirus: host-dependent differences in proteolytic cleavage and cell fusion. Journal of virology 56:912-920.
39. Yamada YK, Takimoto K, Yabe M, Taguchi F. 1998. Requirement of proteolytic cleavage of the murine coronavirus MHV-2 spike protein for fusion activity. Advances in experimental medicine and biology 440:89-93.
40. Qiu Z, Hingley ST, Simmons G, Yu C, Das Sarma J, Bates P, Weiss SR. 2006. Endosomal proteolysis by cathepsins is necessary for murine coronavirus mouse hepatitis virus type 2 spike-mediated entry. Journal of virology 80:5768-5776.
41. Yamada YK, Takimoto K, Yabe M, Taguchi F. 1997. Acquired fusion activity of a murine coronavirus MHV-2 variant with mutations in the proteolytic cleavage site and the signal sequence of the S protein. Virology 227:215-219.
42. Matsuyama S, Taguchi F. 2009. Two-step conformational changes in a coronavirus envelope glycoprotein mediated by receptor binding and proteolysis. Journal of virology 83:11133-11141.
43. Simmons G, Gosalia DN, Rennekamp AJ, Reeves JD, Diamond SL, Bates P. 2005. Inhibitors of cathepsin L prevent severe acute respiratory syndrome coronavirus entry. Proceedings of the National Academy of Sciences of the United

States of America 102:11876-11881.

44. Simmons G, Reeves JD, Rennekamp AJ, Amberg SM, Piefer AJ, Bates P. 2004. Characterization of severe acute respiratory syndrome-associated coronavirus (SARS-CoV) spike glycoprotein-mediated viral entry. Proceedings of the National Academy of Sciences of the United States of America 101:4240-4245.
45. Bertram S, Glowacka I, Muller MA, Lavender H, Gnirss K, Nehlmeier I, Niemeyer D, He Y, Simmons G, Drosten C, Soilleux EJ, Jahn O, Steffen I, Pohlmann S. 2011. Cleavage and activation of the severe acute respiratory syndrome coronavirus spike protein by human airway trypsin-like protease. Journal of virology 85:13363-13372.
46. Belouzard S, Chu VC, Whittaker GR. 2009. Activation of the SARS coronavirus spike protein via sequential proteolytic cleavage at two distinct sites. Proceedings of the National Academy of Sciences of the United States of America 106:5871-5876.
47. Belouzard S, Madu I, Whittaker GR. 2010. Elastase-mediated activation of the severe acute respiratory syndrome coronavirus spike protein at discrete sites within the S2 domain. The Journal of biological chemistry 285:22758-22763.
48. Bertram S, Heurich A, Lavender H, Gierer S, Danisch S, Perin P, Lucas JM, Nelson PS, Pohlmann S, Soilleux EJ. 2012. Influenza and SARS-coronavirus activating proteases TMPRSS2 and HAT are expressed at multiple sites in human respiratory and gastrointestinal tracts. PloS one 7:e35876.
49. Huang IC, Bosch BJ, Li F, Li W, Lee KH, Ghiran S, Vasilieva N, Dermody TS, Harrison SC, Dormitzer PR, Farzan M, Rottier PJ, Choe H. 2006. SARS coronavirus, but not human coronavirus NL63, utilizes cathepsin L to infect ACE2-expressing cells. The Journal of biological chemistry 281:3198-3203.
50. Cavanagh D, Davis PJ, Pappin DJ, Binns MM, Boursnell ME, Brown TD. 1986. Coronavirus IBV: partial amino terminal sequencing of spike polypeptide S2 identifies the sequence Arg-Arg-Phe-Arg-Arg at the cleavage site of the spike precursor propolypeptide of IBV strains Beaudette and M41. Virus research 4:133-143.
51. Yamada Y, Liu DX. 2009. Proteolytic activation of the spike protein at a novel RRRR/S motif is implicated in furin-dependent entry, syncytium formation, and infectivity of coronavirus infectious bronchitis virus in cultured cells. Journal of virology 83:8744-8758.
52. Regan AD, Shraybman R, Cohen RD, Whittaker GR. 2008. Differential role for low pH and cathepsin-mediated cleavage of the viral spike protein during entry of serotype II feline coronaviruses. Veterinary microbiology 132:235-248.
53. Licitra BN, Millet JK, Regan AD, Hamilton BS, Rinaldi VD, Duhamel GE, Whittaker GR. 2013. Mutation in spike protein cleavage site and pathogenesis of feline coronavirus. Emerging infectious diseases 19:1066-1073.
54. Otsuki K, Tsubokura M. 1981. Plaque formation by avian infectious bronchitis virus in primary chick embryo fibroblast cells in the presence of trypsin. Archives of virology 70:315-320.
55. Hofmann M, Wyler R. 1988. Propagation of the virus of porcine epidemic diarrhea in cell culture. Journal of clinical microbiology 26:2235-2239.
56. Follis KE, York J, Nunberg JH. 2006. Furin cleavage of the SARS coronavirus spike glycoprotein enhances cell-cell fusion but does not affect virion entry. Virology 350:358-369.
57. Chu VC, McElroy LJ, Chu V, Bauman BE, Whittaker GR. 2006. The avian coronavirus infectious bronchitis virus undergoes direct low-pH-dependent fusion activation during entry into host cells. Journal of virology 80:3180-3188.
58. Eifart P, Ludwig K, Bottcher C, de Haan CA, Rottier PJ, Korte T, Herrmann A. 2007. Role of endocytosis and low pH in murine hepatitis virus strain A59 cell entry. Journal of virology 81:10758-10768.
59. Matsuyama S, Taguchi F. 2002. Receptor-induced conformational changes of murine coronavirus spike protein. Journal of virology 76:11819-11826.
60. Sturman LS, Ricard CS, Holmes KV. 1990. Conformational change of the coronavirus peplomer glycoprotein at pH 8.0 and 37 degrees C correlates with virus aggregation and virus-induced cell fusion. Journal of virology 64:3042-3050.
61. Zelus BD, Schickli JH, Blau DM, Weiss SR, Holmes KV. 2003. Conformational changes in the spike glycoprotein of murine coronavirus are induced at 37 degrees C either by soluble murine CEACAM1 receptors or by pH 8. Journal of virology 77:830-840.
62. Miura HS, Nakagaki K, Taguchi F. 2004. N-terminal domain of the murine coronavirus receptor CEACAM1 is responsible for fusogenic activation and conformational changes of the spike protein. Journal of virology 78:216-223.
63. Wurdinger T, Verheije MH, van der Aa LM, Bosch BJ, de Haan CA, van Beusechem VW, Gerritsen WR, Rottier PJ. 2006. Antibody-mediated targeting of viral vectors to the Fc receptor expressed on acute myeloid leukemia cells. Leukemia 20:2182-2184.
64. Wurdinger T, Verheije MH, Broen K, Bosch BJ, Haijema BJ, de Haan CA, van Beusechem VW, Gerritsen WR, Rottier PJ. 2005. Soluble receptor-mediated targeting of mouse hepatitis coronavirus to the human epidermal growth factor receptor. Journal of virology 79:15314-15322.
65. Wurdinger T, Verheije MH, Raaben M, Bosch BJ, de Haan CA, van Beusechem VW, Rottier PJ, Gerritsen WR. 2005. Targeting non-human coronaviruses to human cancer cells using a bispecific single-chain antibody. Gene therapy 12:1394-1404.
66. Beniac DR, deVarennes SL, Andonov A, He R, Booth TF. 2007. Conformational reorganization of the SARS coronavirus spike following receptor binding: implications for membrane fusion. PloS one 2:e1082.
67. Kam YW, Okumura Y, Kido H, Ng LF, Bruzzone R, Altmeyer R. 2009. Cleavage of the SARS coronavirus spike glycoprotein by airway proteases enhances virus entry into human bronchial epithelial cells in vitro. PloS one 4:e7870.

Chapter 2

Identification and Characterization of a Proteolytically Primed Form of the Murine Coronavirus Spike Proteins after Fusion with the Target Cell

Oliver Wicht, Christine Burkard, Cornelis A.M. de Haan, Frank J.M. van Kuppeveld, Peter J.M. Rottier, Berend Jan Bosch

Virology Division, Department of Infectious Diseases and Immunology, Faculty of Veterinary Medicine, Utrecht University, Utrecht, The Netherlands

Journal of Virology, 2014 May;88(9):4943-52

Abstract

Enveloped viruses carry highly specialized glycoproteins that catalyze membrane fusion under strict spatial and temporal control. To prevent premature activation after biosynthesis, viral class I fusion proteins adopt a locked conformation and require proteolytic cleavage to render them fusion-ready. This priming step may occur during virus exit from the infected cell, in the extracellular milieu or during entry at or in the next target cell. Proteolytic processing of coronavirus spike (S) fusion proteins during virus entry has been suggested but not yet formally demonstrated, while the nature and functionality of the resulting subunit is still unclear. We used the prototype coronavirus mouse hepatitis virus (MHV) to develop a conditional biotinylation assay that enables the specific identification and biochemical characterization of viral S proteins on virions that mediated membrane fusion with the target cell. We demonstrate that MHV S proteins are indeed cleaved upon virus endocytosis and we identified a novel processing product S2* with characteristics of a fusion-active subunit. The precise cleavage site and the enzymes involved remain to be elucidated.

Introduction

Enveloped viruses must fuse their envelope with a target cell membrane to get access to host cells and deliver their genetic information. They carry specialized surface glycoproteins that mediate attachment to and fusion with the host membrane. Viral fusion proteins can generally be divided into three distinct classes according to their molecular organization and fusion mechanism (1). Class I fusion proteins like the influenza virus hemagglutinin and the human immunodeficiency virus *env* occur as homotrimeric glycoproteins that are oriented perpendicular to the viral membrane and contain typical structural elements, including a receptor binding domain, heptad repeat regions (HR), an amphipathic fusion peptide (FP), and a C-terminal transmembrane domain (2). These fusion proteins also feature a common fusion mechanism (3). Initial conformational rearrangements triggered by cues like receptor binding or low pH lead to the exposure and insertion of the FP into the target membrane. Subsequent structural reorganization pulls the two membranes together to achieve fusion. The free energy is provided by the S proteins and released by zipping up of the heptad repeat regions into an energetically favorable, stable six-helix bundle (1). To prevent premature activation, class I fusion proteins are produced in a locked conformation that needs proteolytic cleavage to acquire fusion competence. Cleavage typically occurs just upstream of the FP and causes N-terminal liberation thereof (4). Furin or furin-like proteases often prime the fusion proteins in the producer cell before virions are released. Alternatively, the cleavage event can take place after the release of virions from the infected cell, i.e. in the extracellular space or upon entry into new host cells (5-7). Prevention of fusion protein cleavage by mutagenesis of the cleavage site as well as by inhibition of cellular proteases often renders viruses noninfectious (8-10).

Coronavirus (CoV) entry is mediated by the spike (S) protein, an exceptionally large glycoprotein of approximately 1200-1450 amino acid residues in length that comprises the canonical structural features of class I fusion proteins and shares the typical fusion mechanism (11). The trimeric S proteins characteristically decorate the extracellular virus particles and two subunits of similar size can be distinguished. The Nterminal S1 subunit contains the receptor binding domain while the Cterminal S2 subunit comprises the fusion machinery including a putative FP, HR regions and transmembrane domain.

Some CoV S proteins are cleaved at the S1/S2 junction during biogenesis by furin(-like) proteases, but many CoV lack a furin cleavage site at the S1/S2 junction and hence carry uncleaved S protein in their virions (12). Other cellular proteases have been reported to cleave CoV S proteins, but those are only available upon attachment or during uptake of virions by the next target cells (13). The infection of some CoV can be blocked by protease inhibitors, thereby underlining the importance of proteolytic activation that should render class I fusion proteins into their fusion-competent form (6, 14-16). Remarkably, a cleavage at the S1/S2 junction does not liberate a putative FP at the Nterminus of S2 (17). Rather than at the S1/S2 junction, cleavage can occur at alternative positions within the S2 domain of the protein to promote the fusion competence. Such alternative cleavage sites have been described within the S2 subunit for the S proteins of severe acute respiratory syndrome coronavirus (SARS)-CoV, mouse hepatitis virus (MHV), and infectious bronchitis virus (IBV) (16, 18, 19). In general, a variety of putative, alternative cleavage sites and cleavage timings have been reported or suggested for CoV, yet the role of S-protein cleavage remains largely undefined.

Despite extensive research on the proteolytic requirements for entry, the exact cleavage position within the CoV S protein generating the fusogenic subunit has been difficult to predict and the formal demonstration of S-protein cleavage upon entry is currently lacking. In this study, we developed a novel unbiased approach to selectively identify and characterize the S proteins of incoming viruses that accomplish fusion. The assay employs a combination of a protein biotin ligase (BirA) and a biotin acceptor peptide added as an extension to the cytoplasmic tail of the S protein. When incoming viral proteins gain access to the cytoplasm of cells expressing BirA ligase, they are specifically labeled with biotin which then enables isolation, enrichment and detection. With this assay, we investigated the S glycoprotein of the prototype coronavirus MHV (strain A59). The MHV S proteins are partially cleaved into the noncovalently linked subunits at the S1/S2 junction by furin or furin-like proteases (20). Intriguingly, preventing furin cleavage by mutation or the use of furin inhibitors has no effect on virus infectivity of MHV (21-23). With our new approach we demonstrate that the MHV S proteins participating in fusion are proteolytically processed in the target cells at a different position in the S2 subunit. The newly identified S2* subunit has characteristics of the functional fusion machinery.

Materials and Methods

Cells, viruses, antibodies and HR2 peptide

HEK-293T, HeLa, Vero-CCL81 and LR7 (24) cells were maintained in Dulbecco modified Eagle medium supplemented with 10% fetal bovine serum. Generally, murine hepatitis viruses (MHV, strain A59) were propagated and titrated in LR7 cells in culture medium supplemented with 20 mM HEPES. For the immune detection of S protein in virus supernatants, MHV was grown to high titers in Dulbecco modified Eagle medium supplemented with 0.3% tryptose phosphate broth (Sigma, T9157). For immunoprecipitation (IP) and immune detection, MHV S protein was reacted with polyclonal rabbit anti-BAP antibody (Genscript, A00674) or mouse monoclonal anti-S2 (10G) antibody and subsequently with anti-mouse or anti-rabbit immunoglobulin G conjugated horseradish peroxidase (Dako, P0217) (25, 26). A polyclonal rabbit antiMHV serum (K135) was used to detect infected cells by reacting with anti-rabbit immunoglobulin G conjugated horseradish peroxidase. Biotin was detected by streptavidin-HRP conjugate (Themo Scientific, 21126). The MHV fusion inhibitor HR2 peptide (DLSLDFEKLNVTLLDLTYEMNRIQDAIKKLNESYINLKE) was synthesized by GenScript (11).

Construction of recombinant viruses

Recombinant MHVs were generated by targeted recombination as described earlier (27). A transfer vector based on pXHERLM was generated to create the recombinant MHV-BAP virus encoding a tandem repeat of the 15 amino acid long biotin acceptor peptide including linkers DLPGGLNDIFEAQKIEWHEPPGGLNDIFEAQKIEWHE (BAP sequence is underlined) as a Cterminal extension of the S protein (28). The recombinant viruses MHV^{FCS}BAP and MHV^{S2^*}BAP were generated by introducing additional point mutations into the transfer vector using site directed mutagenesis. MHV^{FCS}BAP S protein carries three point mutations R713S, R7174, and R717S that substitute all arginines at the furin cleavage site by serines. MHV^{S2^*}BAP S protein carries two point mutations R867S and R869S that substitute the arginines at the putative S2' cleavage site by serines.

Generation of stable cell lines

The pQCXIN-CCM plasmid encoding the MHV receptor - murine carcinoembryonic antigen-related cell adhesion molecule 1a (CCM) - was generated by cloning the CCM gene into the pQCXIN Moloney murine leukemia virus (MLV) packaging vector (Clontech) (29). Likewise, the human codon optimized gene encoding Biotin Protein Ligase (BirA) with an N-terminal HA- and FLAG-tag (the pUM376-BirA PCR template was kindly provided by V. Ogryzko) was cloned into the pQCXIP vector (Clontech), generating the pQCXIP-BirA packaging vector (30). HEK-293T, HeLa and Vero-CCL81 cell lines expressing the CCM receptor were made after transduction with vesicular stomatitis virus G protein pseudotyped MLV using the pQCXIN-CCM packaging vector. The polyclonal HEKCCM, HeLaCCM, VeroCCM cell lines stably expressing CCM, as well as murine LR7 cells were selected and maintained with G418 (PAA). CCM expression was confirmed by immune detection using mouse monoclonal anti-CCM (mAb CC1 provided by K. Holmes (31)). Polyclonal LR7 cells stably expressing biotin protein ligase (LR7-BirA) were similarly made with the MLV-pseudotyped virus using the pQCXIP-BirA packaging vector. LR7-BirA cells were selected at 15 µg/ml and maintained at 10 µg/ml puromycin (Sigma, P8833). BirA expression was confirmed by immune detection using Cy3 conjugated mouse monoclonal anti-FLAG (Sigma, A9594). No BirA enzyme was detected in the cell culture supernatants of LR7-BirA cells after 72 hours incubation as analyzed by western blot using a mouse monoclonal anti-FLAG antibody conjugated horseradish peroxidase.

Conditional biotinylation assay

LR7 or LR7-BirA cells were cultured to confluence in 6 well clusters. Cells were inoculated with virus-containing cell culture supernatant supplemented with 50 µg/ml DEAE-dextran (Sigma, D9885) and 10 µM biotin (Sigma, B4639) with a multiplicity of infection (MOI) of 10. After 30 min, protein biosynthesis was inhibited by addition of 50 µg/ml cycloheximide (Sigma C7698) to prevent S-protein synthesis from virus infections. At 90 min postinfection (p.i.), the cells were chilled on ice, washed twice with ice-cold phosphate buffered saline (PBS) and lysed in ice-cold radio immunoprecipitation assay buffer (RIPA, 150 mM NaCl, 1% Nonidet P-40, 0.5% Sodium deoxycholate, 0.1% Sodium dodecyl sulfate (SDS), 50 mM Tris-HCl pH 8) supplemented with Complete Protease Inhibitor Cocktail Tablets (Roche 11836153001) to prevent further proteolysis and with or without 6 mM Napyrophosphate (PP, Sigma, 71516) to quench the activity of BirA in cell lysates (32). The cell lysates were cleared by centrifugation at 10,000 x *g* for 10 min at 4°C. The supernatants were combined with 20 µl 50:50 slurry of protein G sepharose (Biovision, 6511) supplemented with 0.5 mg polyclonal anti-BAP antibody (Genscript, A00674) and incubated under rotation for 2 h at 8°C to immunoprecipitate the S proteins. Next, sepharose beads were pelleted at 6,000 x *g* for 5 min at 4°C and washed trice with an excess of ice-cold RIPA buffer. Excess supernatant was carefully removed and, finally, samples were denatured by addition of sample buffer and subjected to western blotting.

If inhibitory compounds were used during the infection, cells were pretreated for 30 min at 37°C followed by infection in the presence of the respective compounds. The following protease inhibitors were used at their highest recommended working range concentration according to Sigma's protease inhibitor technical bulletin INHIB1 (final concentration): Pepstatin A (1.5 µM, Sigma, P5318), Leupeptin (100 µM, Sigma, L2023), E64d (10 µM, Sigma,

E8640), phosphoramidon (10 µM, Sigma, R7385) AEBSF (100 µM, Sigma, A8456). HR2 peptide was used at 25 µM concentration. The following lysosomotropic agents were used (final concentration): ammonium chloride (25 mM NH_4Cl, Merck, Darmstadt), Bafilomycin A1 (125 µM, Enzo Life sciences).

Time course biotinylation assay

LR7 or LR7-BirA cells were cultured to confluence on 10 cm dishes and the inoculum was prepared similar to the conditional biotinylation assay. First, cells were washed twice with ice-cold PBS and ice-cold inoculum was added for 45 min to allow attachment of the virus to the target cells at 8°C. Next, inoculum was removed and cell layer washed once with ice-cold PBS, followed by the addition of 37°C culture medium supplemented with 10 µM biotin. Differential periods of infection were achieved by successively delaying the start of attachment and infection while maintaining an equal duration. All samples were harvested at the same time to even out the time between lysis and immunoprecipitation. 50 µg/ml cycloheximide was added 30 min after warming up the infection to 37°C for all samples with an infection period longer than 30 min or at the end of the infection. The sample for 0 min was prepared for lysis after 1 minute at 37°C. Lysis and immunoprecipitation was performed as described in the conditional biotinylation assay and IP-samples were analyzed by western blotting.

HR2 inhibition of MHV infection

Multiple wells containing LR7 cells were infected with wild-type MHV for 1.5 min to synchronize infection. Inoculum was replaced by culture medium at the start of infection. At increasing time points supernatants of individual wells were replenished with culture medium supplemented with 20 µM HR2 peptide to block MHV entry. 4 h p.i., supernatant was replaced with culture medium containing 1 µM HR2 peptide to inhibit syncytia formation. 7 h p.i., cells were fixed with 3.7% formalin and immunoperoxidase staining was performed using K135 serum and visualized with AEC substrate kit (Vector Laboratories). The extent of infection relative to noninhibited virus infection was calculated from the number of plaques observed.

Deglycosylation

LR7 or LR7-BirA cells were cultured to confluence in 10 cm dishes and the virus infection was performed similar to the conditional biotinylation assay. After immunoprecipitation, samples on the sepharose beads were denatured and deglycosylated with PNGase F (New England BioLabs, P0704) according to the manufacturer's protocol. Finally, samples were denatured by addition of sample buffer and subsequently analyzed by western blotting.

Western blot analysis

For the detection of S protein in virus containing cell culture supernatants, aliquots were directly lysed and denatured in sample buffer containing 50 mM Tris-HCl pH 6.8, 5 % glycerol, 5% 2-mercaptoethanol, 1% SDS and bromophenol blue and boiled at 95°C for 10 min. Samples after immunoprecipitation were eluted from beads by boiling at 95°C for 10 min in sample buffer. Supernatant was subjected to SDSpolyacrylamide gel electrophoresis (SDS-PAGE) in a discontinuous gel with 8% acryl amide in the separating gel (33). Next,

samples were transferred to a polyvinylidene fluoride membrane (BioRad, 1620176). Membranes were blocked with bovine serum and reacted with antibodies or streptavidin-HRP in PBS with bovine serum and 0.5% Tween20. For detection we used Amersham ECL Western Blotting Analysis System (GE healthcare, RPN2109) with X-Omat LS films (Kodak, Sigma F1149).

Computational analysis

The transmembrane domain of MHV S protein was predicted by TMHMM 2.0 and the signal peptide by SignalP 4.1. HR1 and HR2 regions were defined according to Bosch et al. (11). Glycosylation sites were predicted with NetNGlyc 1.0 (Technical University of Denmark). Western blot signals were quantified using ImageJ. Amino acid sequence alignment was performed by ClustalW2 using S sequences of infectious bronchitis virus (IBV strain Beaudette, NP_040831.1), Middle East respiratory syndrome coronavirus (MERS-CoV strain HCoV-EMC, AFS88936.1), mouse hepatitis virus (MHV strain 2, AAF19386.1 and strain MHV-A59, NP_045300.1), severe acute respiratory syndrome coronavirus (SARS-CoV strain Tor2, NP_828851.1) and transmissible gastroenteritis virus (TGEV strain TO14, AF302263_1).

Results

A biotinylation assay to label S protein after virus-cell fusion

During inoculation, not all virions successfully fuse with the target cell and deliver their genome into the cytoplasm. According to the current model of class I protein fusion, the Cterminal tail of the CoV S protein is hidden internally in the intact virion. It will be introduced into the cytoplasm after virus and cell membrane have fused. In order to be able to discriminate S proteins coming from virions that successfully achieved fusion from those that failed, we designed a biotinylation assay that uses selective intracellular biotin labeling of the protein's Cterminus. To that end, we generated a recombinant MHV-A59 derivative carrying an S protein with a Cterminally appended 37 amino acid biotin acceptor peptide (MHVBAP; Fig. 1A) and a recombinant murine cell line that constitutively expresses BirA in its cytoplasm (LR7BirA). BirA recognizes the biotin acceptor peptide (BAP) as substrate for biotin ligation in the presence of ATP and free biotin. In intact virions, the BAP faces the luminal side and is protected from modification by BirA, but upon virus-cell fusion it becomes exposed to the enzyme (Fig. 1B). Consequently, BirA can biotinylate the BAP-tag of S proteins of virions that underwent fusion, enabling the selection and characterization of postfusion S proteins via the biotin label. MHVBAP displayed similar growth kinetics but yielded 10-fold reduced titers compared to wild-type MHV (data not shown).

To characterize the S protein of MHV-BAP and to demonstrate biotinylation of the BAP-tag, we propagated wildtype MHV and the recombinant MHVBAP in LR7 cells and LR7-BirA cells. The cell culture supernatants were analyzed by western blotting with antibodies recognizing the S2 subunit or the BAP-tag, or with the biotin-binding streptavidin (Fig. 1C). The monoclonal antibody recognizing the S2 subunit detected the full-length S protein (S_0) and the S2 subunit of all virus preparations. A polyclonal antibody directed against the BAP specifically detected (S_0) and the S2 subunit of MHVBAP, but not those of wild-type MHV. Importantly, biotinylation of BAP-tagged S protein was only detected for MHV-BAP viruses produced in LR7-BirA cells, demonstrating the BirA dependent biotinylation of the BAP.

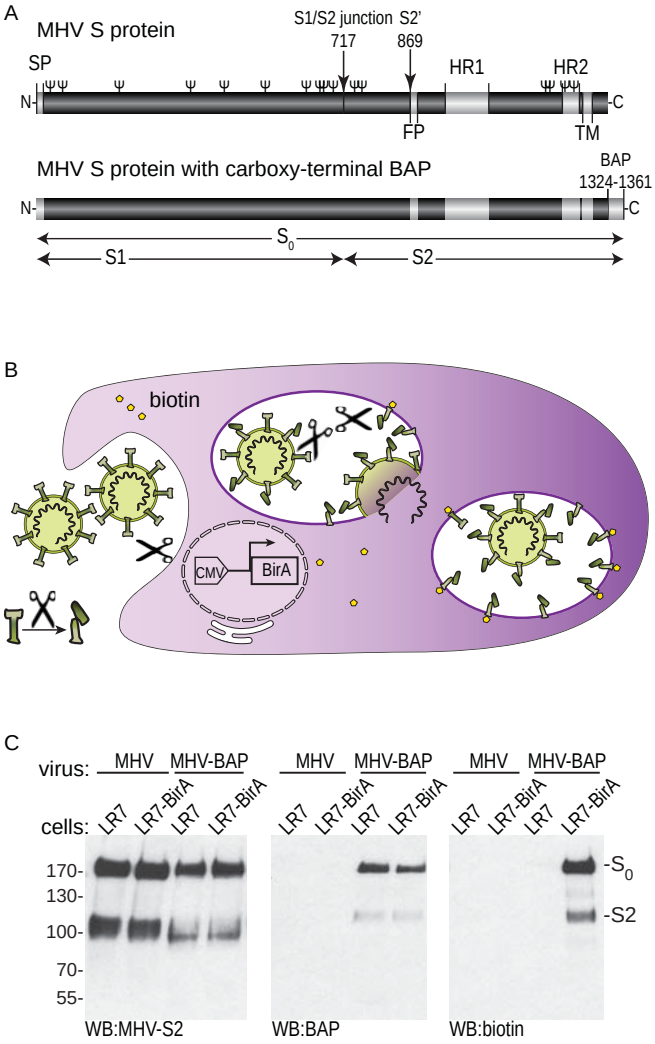

Fig.1 Recombinant MHV-BAP for the detection of biotinylated S proteins. (A) Schematic organization of wild-type (1324 aa) and BAP-tagged MHV (strain A59) S protein (1361 aa) drawn to scale. The S protein has an N-terminal S1 domain, responsible for receptor binding, and a C terminal S2 domain that holds the fusion machinery. Positions of the signal peptide (SP), predicted N-glycosylation sites (Ψ), the putative fusion peptide (FP), two heptad repeat (HR) regions, the transmembrane domain (TM) and the biotinylation acceptor peptide (BAP) are indicated. MHV S protein contains two predicted protease cleavage sites: a furin cleavage site at the S1/S2 junction and a putative second cleavage site (S2') just upstream of the fusion peptide. (B) A biotinylation assay was designed to selectively identify and characterize S protein of MHV virions that underwent membrane fusion with the cellular target membrane. The biotin acceptor peptide was fused to the C-terminus of the S protein. Target cells stably express cytoplasmic protein biotin ligase (BirA) from a CMV promoter. Upon membrane fusion, the C-terminal BAP of S protein will be introduced into the cytoplasm and can be accessed and biotinylated by BirA. (C) Characterization of recombinant MHV-BAP. Virus stocks of MHV-A59 with wild-type S protein (MHV) or with BAP-tagged S protein (MHV-BAP) were produced in LR7 cells or LR7 cells expressing BirA (LR7-BirA) and subjected to western blotting (WB) using a MHV-S2 monoclonal antibody, an anti-BAP polyclonal antibody and streptavidin-HRP for detection of proteins. Full length S protein (S0) and S2 subunit resulting from cleavage at the S1/S2 junction were detected with antibodies directed against the S2 domain or BAP, and with streptavidin for detection of biotinylation. Size and position of marker proteins (in kilodalton) are indicated at the left.

Recognition of the BAP-tag by the anti-BAP polyclonal antibody was not influenced by its biotinylation status; tagged and nontagged S proteins were detected equally efficient.

Biotinylated S proteins after virus-cell fusion: detection of S2*

Next, we assessed the biotinylation of S proteins after membrane fusion of virions with BirA expressing target cells. The LR7-BirA cells were inoculated with MHV-BAP (MOI = 10) for 90 min to enable binding and fusion. To detect the biotinylated S proteins, anti-BAP antibody was used to immunoprecipitate the BAP-tagged S proteins from whole cell lysates. This purification and concentration step was essential for detection. The BirA enzyme maintains its activity in the lysis buffer, even at low temperatures. Consequently, all S protein present in the cell lysate became biotinylated post lysis and could be detected using streptavidin-HRP conjugate (Fig. 2A lane 1). In addition to the S_0 and S2 forms, which could already be observed in the virus stock (Fig. 1C), an additional product of ~80 kDa was detected which we named S2*. To prevent post lysis biotinylation and analyze the S proteins as they occur in the intact cell, BirA activity was quenched by product feedback inhibition by addition of PP to the lysis buffer and during the IP procedure (Fig. 2A lane 2) (32). Now, the S2* was the most abundant S-protein product detected and only limited amounts of S_0 and S2 were observed.

To test whether the appearance of the S2* protein indeed correlates with successful infection, we exploited the HR2 peptide, a synthetic peptide fusion inhibitor, which

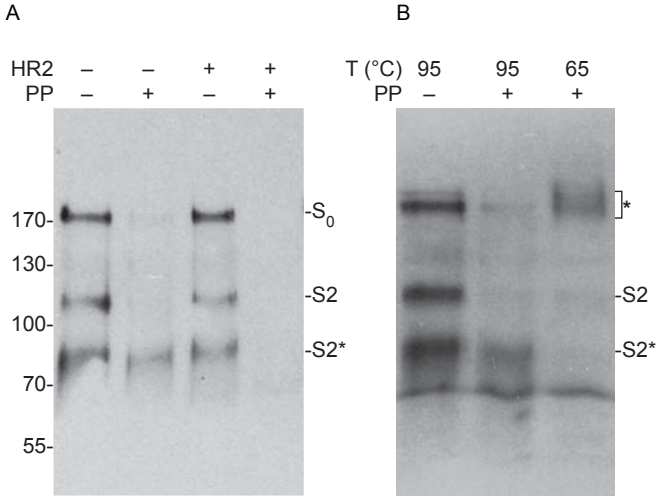

Fig.2 Detection of S protein after membrane fusion with target cells. (A) LR7-BirA cells were inoculated with MHV-BAP for 90 min in the absence or presence of peptidic fusion inhibitor (HR2) and lysed in the absence or presence of the BirA inhibitor PP. Immunoprecipitated S proteins were analyzed by western blotting. Only biotinylated S protein was detected by streptavidin-HRP conjugate. Upon cell lysis in the absence of PP, all S protein was allowed to be biotinylated by BirA; thus full-length (S0), S protein cleaved at the S1/S2 junction (S2), and a novel product of lower molecular mass designated S2* was detected. The presence of PP during lysis allowed the exclusive detection of S protein that was biotinylated during infection and mainly shows the S2* fragment. (B) IP samples were denatured at 95°C or 65°C before western blot. In the presence of PP, the S2* fragment constitutes the majority of biotinylated S proteins migrating at ~80 kDa position. After heating IP samples at 65°C - instead of 95°C - a larger product was present around the ~200 kDa position (indicated by the asterisk).

effectively blocks the membrane fusion activity of the S protein (11). Addition of the HR2 peptide efficiently abrogated biotinylation of the S protein in the presence of PP (Fig. 2A lane 4). The experiment confirmed that biotinylation of S proteins only occurs after virus-cell fusion, and further demonstrated that the proteolytic processing of S protein is not affected by addition of HR2 peptide (Fig. 2A lane 3). We hypothesized that the S2* subunit represents the proteolytically primed subunit of MHV S protein.

The S2* subunit occurs in stable multimers

We examined the novel S2* subunit for characteristic features of the fusion machinery. To drive membrane fusion, the membrane-anchored domains of class I fusion proteins fold into a highly SDS-stable and temperature-resistant postfusion trimer, facilitated by the zipping up of the two HR domains into six-helix bundles (11, 34). To test whether S2* forms such stable trimers, we analyzed the SDSPAGE migration of the biotinylated S-protein variants after heat treatment of the samples at 65°C, rather than 95°C. The S2* subunit that was biotinylated upon infection of target cells migrated at ~ 80 kDa if denatured at 95°C. This species was, however, absent after denaturation at 65°C; instead, a larger band was observed at ~ 200 kDa, in line with the S2* subunit actually occurring as a stable, multimeric postfusion complex (Fig. 2B).

Kinetics of S2* appearance, virus cell fusion and MHV infection coincide

If the novel S2* subunit represents the proteolytically primed form, the kinetics of S-protein cleavage should be equal to or faster than productive MHV infection. We monitored the kinetics of S-protein cleavage and fusion by performing a time course of infection with MHV-BAP on LR7-BirA cells. To synchronize infections, virus was allowed to bind to cells at 8°C for 1 h, followed by removal of the inoculum after which infection was continued at 37°C. Omitting PP during IP procedure revealed the overall biochemical fate of all (i.e. fused and nonfused) S proteins over a 90 minute time period (Fig. 3A). Western blot analysis of IP samples indicated that the relative amount of the S2* cleavage product increased over time, while the S_0 and S2 signal slowly vanished. To prevent the maturation of endosomes and the acidification of endo-lysosomal compartments, 25 mM NH_4Cl was added to the cells throughout infection (35). This treatment resulted in a net increase of S protein, suggesting that the time dependent overall decrease of S protein in the absence of NH_4Cl was due to lysosomal degradation. In contrast, the proteolytic process leading to S2* formation was not blocked by NH_4Cl. Quantification of the density of the S-protein bands over 90 min of infection showed that the fraction of the S2* subunit increased from 3% to 50% (Fig. 3A, bar chart). Yet, not all S proteins had undergone proteolytic processing after 90 min. By performing the analysis in the presence of PP during the sample preparation, only S protein from virus-cell fusion events was monitored (Fig. 3B). The appearance of the S2* subunit started early and continued increasingly for at least 90 min.

To confirm the kinetics of virus-cell fusion by an independent approach, we examined the inhibition of MHV infection by HR2 peptide fusion inhibitor. LR7 cells were pulse-inoculated for 1.5 min with wild-type MHV to synchronize binding. Inocula were replaced by culture medium after which HR2 peptide was added to individual samples at successive time points. The relative amount of infection was determined at 7 h p.i. by immune staining of the cells against MHV. The presence of HR2 peptide from the start completely abolished

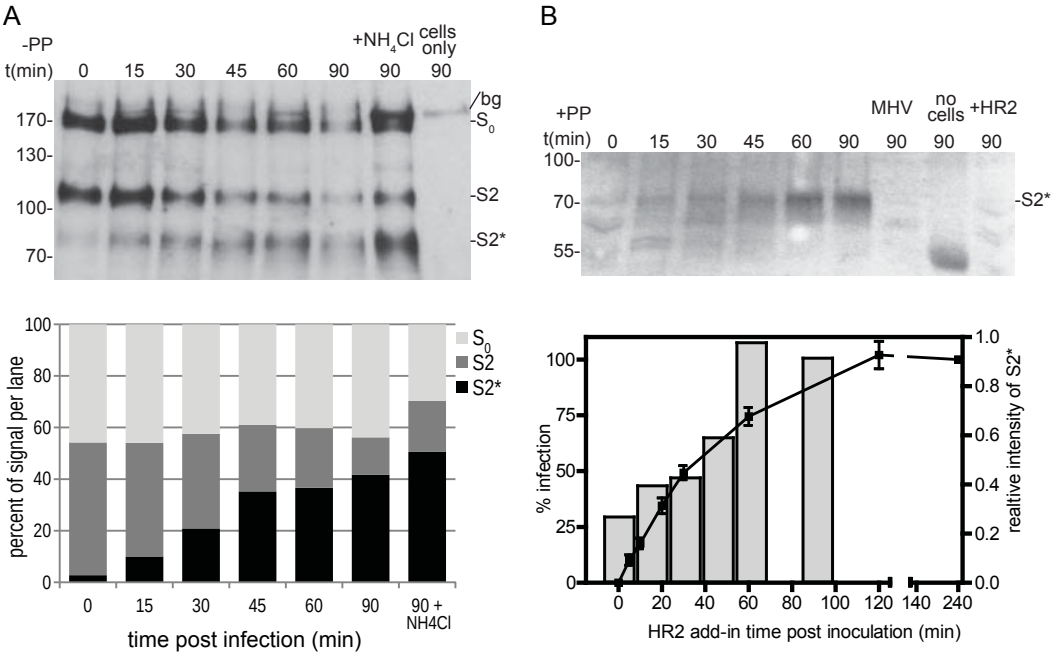

Fig.3 S2* fragment is generated during virus entry. (A) MHV-BAP was bound to LR7-BirA cells and excess virus was removed to synchronize the infection. The infection was stopped at the indicated times post infection by cell lysis in the absence of the BirA inhibitor PP. Immunoprecipitated S proteins were analyzed by western blot and biotinylated protein detected by a streptavidin-HRP conjugate. To assess lysosomal degradation, ammonium chloride (NH4Cl) was added during infection. A background band (bg) is indicated. The relative amounts of S0, S2 and S2* protein per lane were quantified to illustrate the proteolytic processing over time (lower panel). (B) Same as 3A, except that by addition of PP during lysis, only S protein that has been biotinylated during infection was detected. As controls, MHV-BAP in the absence of cells, infection with wild-type MHV and MHV-BAP infection performed in the presence of the HR2 fusion inhibitor was taken along. The intensity of the S2* fragment was quantified and displayed as a bar diagram below. In addition, to determine the kinetics of virus entry independently, MHV infections were supplemented in time with the HR2 fusion inhibitor after a synchronized infection (line diagram). At 7 h post infection, infected cells were detected by immunostaining and relative amount of infection was determined.

infection, but showed no effect when added 120 min after inoculation (Fig. 3B, line chart). The MHV infection deduced from the HR2 peptide time-of-addition experiment showed similar kinetics to proteolysis of S protein yielding the S2* product but was slower. MHV infection coincided with the accumulation of the S2* subunit as monitored by intracellular biotinylation. In comparison, the intensities of the biotinylated S2* protein bands observed in the virus-cell fusion experiment were quantified and included in the same graph as a bar chart (Fig. 3B, bar chart).

Conserved arginine is not the cleavage site that yields the S2* subunit

The identification of the proteolytic cleavage site that yields the fusion active S2* subunit, could provide further information about the requirements for gaining fusion competence. Judged from the molecular weight of the S2* protein, the cleavage site is located within the N-terminal half of the S2 subunit. This region comprises a conserved arginine, previously

described as a potential protease target site and termed S2' in the S proteins of SARSCoV and IBV (18, 36) (Fig. 4A). Cleavage at this arginine would truncate the S2 domain by approximately 15 kDa and remove two glycosylation sites which is in agreement with the observed difference between the S2 and S2* band. We used a reverse genetic approach to determine whether the MHV S2* subunit indeed results from proteolysis at the putative S2' cleavage site. To that end, mutant MHV-BAP was generated containing two serine substitutions of arginines occurring at or close to the S2' cleavage ($MHV^{S2'-}$BAP, Fig. 4A, table). Another MHV variant with a mutated furin cleavage site at the S1/S2 junction was generated by replacing the arginines by serines (MHV^{FCS-}BAP). Mutant viruses were viable and used to infect LR7BirA cells for 90 min at equal MOI after which IP samples were prepared in the absence or presence of PP. Western blot analysis of IP samples showed that the knock-out of the furin cleavage site at the S1/S2 junction in MHV^{FCS-}BAP prevented the appearance of the S2 form (22) (Fig. 4A lower panel). In contrast, serine substitution of the two arginines at the presumed S2´ cleavage site in $MHV^{S2'-}$BAP did not prevent the formation of the S2* subunit. When IP was performed in the presence of PP, only allowing the detection of the S proteins involved in fusion, the S2* subunit was clearly detected for all three viruses. The S2* product of the mutant viruses migrated with similar mobility and represented the major form of S protein that underwent fusion. Arginine substitutions at the S1/S2 or S2' site had no detectable effect on virus titers, which remained comparable to MHV-BAP (Figure 4A). As reported earlier, the deletion of the S1/S2 arginine motif resulted in reduced syncytia formation capacity of the virus (22).

Prediction of the S2' cleavage site from the molecular weight of the S2* subunit after deglycosylation

As we could not predict other protease cleavage sites from the S-protein amino acid sequence, we tried to identify the S2' cleavage site by alternative approaches. The biotinylation assay did not yield sufficient amount and purity of the S2* subunit to allow Nterminal amino acid sequencing. Instead, we deglycosylated the S protein to more precisely determine the molecular weight of S2*, from which the approximate location of the cleavage site might then be deduced. To that end, LR7-BirA cells were inoculated with MHV-BAP for 90 min and samples prepared in the absence or presence of PP. After the IP, S protein bound to protein G sepharose beads was denatured and samples were deglycosylated by PNGase F to remove all N-linked glycans. Successful deglycosylation was revealed by the S proteins migrating with higher electrophoretic mobility (Fig. 4B, top and middle panel). Deglycosylation of all S proteins (- PP) and of S proteins from virions that had fused (+ PP) showed a similar effect. The theoretical molecular weight was predicted to be 70 kDa for the S2 domain and 54 kDa for S2* if the cleavage occurs close to the putative FP. The deglycosylated S2 subunit shifted from the 105 kDa position to 80 kDa, slightly higher than predicted, and migrated as a welldefined band. In contrast, the S2* protein also shifted to a lower molecular mass, yet it remained heterogeneous after deglycosylation ranging in size from 60 to 65 kDa. Similar to S2, the S2* subunit appears larger than its predicted molecular mass of 54 kDa, hence cleavage may occur at the putative S2' cleavage site or further upstream. The blot was restained with antiserum against the BAP in order to visualize the S proteins from infections of LR7 cell without BirA (Fig. 4B, lower panel) and independent of biotinylation. Of note, the prior streptavidin-biotin interaction reduces

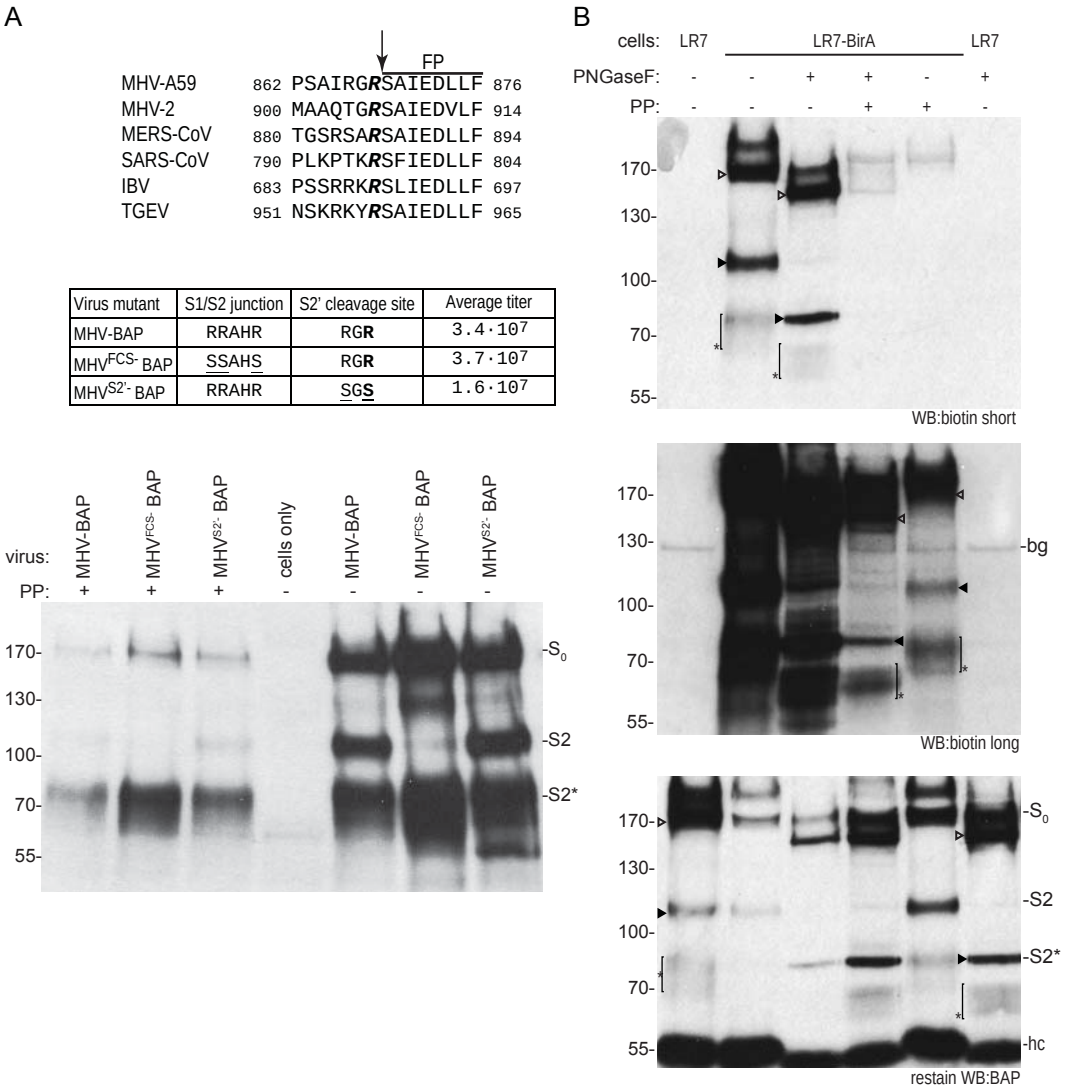

Virus mutant	S1/S2 junction	S2' cleavage site	Average titer
MHV-BAP	RRAHR	RG**R**	3.4·10^7
MHV^{FCS-} BAP	SSAHS	RG**R**	3.7·10^7
MHV$^{S2'-}$ BAP	RRAHR	SG**S**	1.6·10^7

Fig.4 Characterization of the S2* fragment. (A) Sequence alignment of an S-protein segment of representative coronaviruses containing the putative S2' cleavage site (arrow) and part of the fusion peptide (FP). The conserved arginine residue adjacent to the putative fusion peptide (FP, (37)) is shown in bold. Table indicates the mutations of generated recombinant MHV viruses, carrying serine substitutions of arginines (underlined) at the furin cleavage site at the S1/S2 junction (MHVFCS-BAP) and the putative S2' site (MHVS2'-BAP). The average titer of three independent virus preparations was determined by end point dilution and reported as TCID50/ml. BirA-cells, infected with the recombinant viruses for 90 minutes, were lysed in the absence and presence of pyrophosphate (PP). Biotinylation of immunoprecipitated S proteins was detected by western blotting, as described in the text. (B) Deglycosylation of biotinylated S proteins. The biotinylation assay was performed with MHV-BAP as described under A. Prior to western blot analysis, all samples were denatured and selected samples subsequently deglycosylated using PNGaseF. Biotinylated S protein was detected with streptavidin (two exposure times shown) and the same blot was restained with anti-BAP antibody to detect (nonbiotinylated) S proteins (of note: streptavidin binding to biotinylated BAP limits detection with the anti-BAP antibody). Full length S protein is indicated by open triangles, S protein cleaved at the S1/S2 junction by solid triangles and S2* fragment by asterisks. All S proteins show faster migration after deglycosylation; S0 and S2 are reduced to a defined band upon deglycosylation, whereas the S2* fragment band remains diffuse. A cellular background band is indicated (bg).

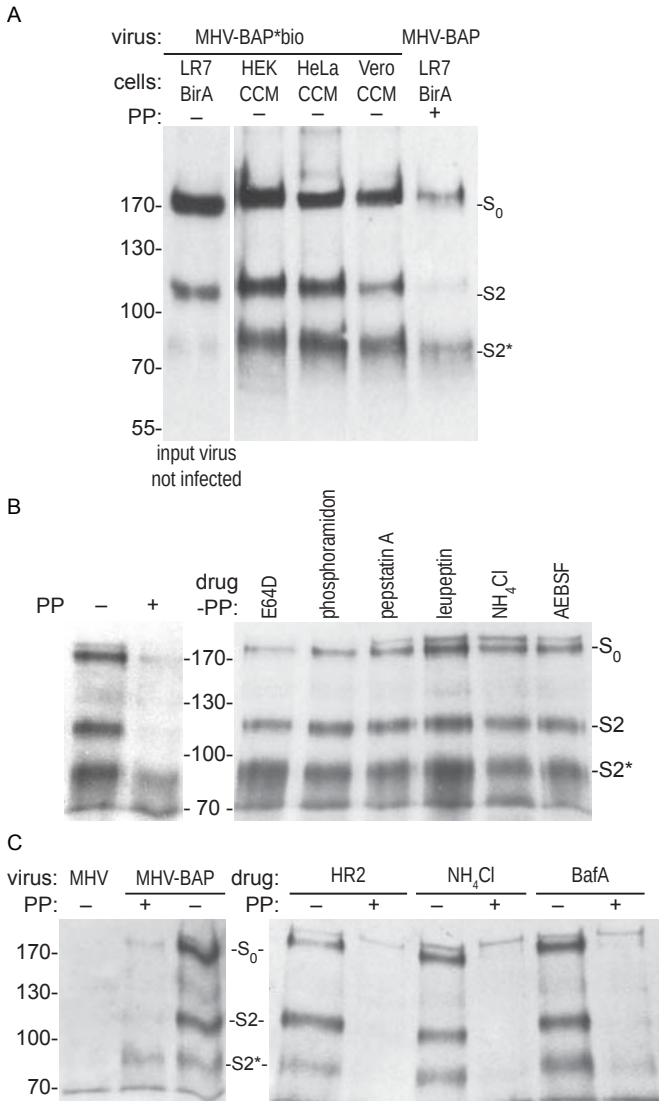

Fig. 5 Protease inhibitors or lysosomotropic agents do not prevent S2* formation. (A) Biotinylated MHV-BAP (MHV-BAP*bio) progeny viruses were produced in LR7-BirA cells. Cells overexpressing the MHV receptor Ceacam1a (CCM) were infected with MHV BAP*bio for 90 min. Immunoprecipitated S proteins were analyzed by western blot and biotinylation detected by the streptavidin-HRP conjugate. Cleavage status of MHV-BAP*bio prior to infection was visualized by inoculating LR7-BirA with virus-containing cell culture supernatant for 2 h 15 min at 4°C and direct lysis without warming (first lane). (B) LR7-BirA target cells were pretreated with various broad spectrum protease inhibitors for 30 min. Infection with MHV-BAP was allowed in the presence of protease inhibitors for 90 min and subsequently sample preparation was performed in the absence of PP as described in A. (C) Same as B, infection with MHV or MHV-BAP, infections were performed in the presence of HR2 fusion inhibitor, ammonium chloride (NH4Cl), or bafilomycin A1 (BafA). Lysates were prepared in the absence or presence of PP.

the anti-BAP antibody reactivity, particularly in fully biotinylated samples prepared in the absence of PP (Fig. 4B, lane 2 & 3).

Inhibition of cellular proteases that generate the S2* subunit

To obtain information on the S-protein cleavage site and the functional aspect of proteolysis during virus infection we attempted to identify the responsible host cell proteases. SARS-CoV S protein can be cleaved by multiple proteases and availability of those proteases has been linked to the tissue tropism of the virus (7). Yet, expression of the MHV receptor can render cell lines of different species susceptible to MHV infection (31) and if the S2* subunit represents the fusion active form, the priming protease(s) should occur in various cell lines. To test this, we monitored S-protein cleavage in nonmurine cell lines stably expressing the MHV receptor. Virus preparations containing prebiotinylated S protein were produced after a single passage on LR7-BirA (MHV-BAP*bio) and typically contained about 70% of S_0, 30% of S2 and a marginal fraction of S2* (Fig. 5A, lane1). After 90 min of inoculation of two human and one simian cell line (i.e. HEK 293T, HeLa and Vero cells, respectively), the pattern of S_0, S2 and S2* was similar compared to that in the murine LR7-BirA cell line (Fig. 5A). Broad spectrum protease inhibitors can affect various classes of proteases. In order to characterize the proteases involved in S-protein cleavage, a virus entry assay was performed in the presence of various protease inhibitors, suppressing the activity of the main classes of proteases. MHV-BAP infection was performed on LR7-BirA cells for 90 min in the presence of the cysteine protease inhibitor E64d, the metalloprotease inhibitor phosphoramidon, the aspartyl protease inhibitor pepstatin A, the serine and thiol protease inhibitor leupeptin, the serine protease inhibitor AEBSF (Fig. 5B) as well as the serine protease inhibitor camostat or 1x concentrated Roche mini cocktail inhibitor (data not shown). In addition, the involvement of low-pH dependent proteases was probed using the lysosomotropic agents NH_4Cl and bafilomycin A1 (Fig. 5C). None of the applied agents could prevent the S-protein cleavage that results in the formation of the S2* subunit. The lysosomotropic agents NH_4Cl and bafilomycin A1 abolished fusion similar to HR2 peptide peptide fusion inhibitor as indicated by the lack of biotinylated S when IP was performed in the presence of PP (Fig. 5C).

Discussion

We studied cleavage of the MHV S glycoprotein during virus entry by an unbiased approach that allowed us to isolate fusion proteins of virions that accomplished virus-cell fusion and we newly identified an S2* subunit. It displayed features of the fusion machinery, suggesting that the S2* subunit represents the fusion-active part of the S protein. In support of this, the majority of the postfusion S proteins were cleaved into the S2* protein and formed heat- and SDS-stable multimers that resemble the postfusion six-helix bundle. Furthermore, the kinetics of appearance of the biotinylated S2* protein coincided with the kinetics of virus entry as determined by monitoring sensitivity of infection to the HR2 peptide fusion inhibitor. The size of the S2* protein indicates cleavage to occur in the S2' region just upstream of the putative FP. We could not determine the exact cleavage site by reverse genetics, and the low mass amounts of the S2* protein did not allow its identification by mass spectrometry. Deglycosylation of the S2* protein resulted in a heterogeneous product suggesting that

cleavage can occur at alternative sites in proximity to the S2' site. Protease inhibitors used to identify the protease responsible for S-protein cleavage could not prevent the formation of the S2* subunit. Although the precise details of the cleavage process remain enigmatic, the appearance and characteristics of the S2* subunit support the idea that it represents the fusion-ready subunit.

Previous investigations of CoV fusion protein cleavage have monitored the infectivity of viruses or virus like particles in the presence of protease inhibitors or after genetically modifying the fusion protein. (14, 16, 21, 23, 36, 37). Many studies demonstrate cleavage of S proteins displayed on the cell surface by recombinant proteases, but only few verify proteolysis in virus preparations upon exposure to recombinant proteases and soluble receptor (38, 39). These studies convincingly correlated cleavage of S protein with its membrane fusion capacity, but failed to demonstrate cleavage during virus entry or identifying the fusion competent subunit. In fact, the biochemical fate of viral glycoproteins on virions that are entering host cells at physiological MOIs is difficult to study. Given the limited amount of virus even at high MOI, the significant fraction of noninfectious particles in each virus preparation, and the relatively low number of S proteins per virion, the specific detection of S proteins on successfully fusing virions is a great challenge. In this study we established a novel biochemical assay based on the conditional biotinylation of proteins to concentrate and purify MHV S proteins involved in functional virus-cell fusion events. This enables the identification and characterization of fused S proteins in combination with more classical experiments using site-directed mutagenesis and protease inhibitors. Our approach excludes contributions of nonfused virions hence focuses on functional fusion events. As the infecting virions take a physiological entry route, we do not rely on mimicking the fusion process by addition of soluble receptor, exogenous protease treatment or pH shock. The assay can be adapted to monitor the biochemical fate of structural virion components of any enveloped or nonenveloped virus upon entry.

The entry of various CoV is supported by distinct proteases that can act at the plasma membrane of the target cell or in the endosomal compartments (10, 13). For MHV-A59, proteolytic processing at the S1/S2 junction enables efficient cell-cell fusion resulting in syncytia formation (40) and mutagenesis of the cleavage site limits the syncytia size (23, 41). However, as we showed earlier (22) and confirmed here by substituting all arginines at the S1/S2 junction, the S1/S2 cleavage is dispensable for fusion activity and virus infectivity. This is supported by observations with a natural isolate, MHV-2 (42), or with a cell passaged isolate MHV/BHK (43), which both lack a genuine furin cleavage site and hence carry uncleaved S proteins on their virions. In our study, only small amounts of the S2 subunit were present on virions that had fused, suggesting that S2 is not the fusion-active form. Nevertheless, cleavage of MHV S protein at the S1/S2 junction may provide additional structural flexibility to increase the accessibility of a cleavage site for priming, as suggested earlier for SARSCoV (36). It is possible that S proteins are processed into S2*, perhaps via a short-lived intermediate S2 form that is not detected. With less priming proteases on the cell surface than in the endolysosomal compartments, this may explain the cell-cell fusion inability of the MHV spikes lacking a functional furin cleavage site.

We observed that S-protein cleavage upon MHV infection occurred downstream of the S1/S2 junction and released an S2* fragment of ~80 kDa, which is ~25 kDa smaller than the S2 subunit. Assuming this membrane-bound subunit to carry the membrane fusion function

we probed the S2* subunit for criteria of the fusion machinery. First of all, the S2* subunit was the most abundant S-protein species observed after virus-cell fusion and hence likely to be involved in membrane fusion. We assume that S_0 and S2 protein decorate virions which failed to reach the cellular compartment where the appropriate stimuli and proteolytic activity occur for S-protein activation. However, a limited number of virions reaches the fusion compartment, where a majority of S proteins are proteolytically processed and triggered for fusion. Second, S2* occurred in heat- and detergent-resistant multimers indicative of the characteristic class I postfusion sixhelix bundle. Similarly, treatment of MHV-2 virions with soluble receptor followed by protease treatment revealed an equivalent pattern of S_0, S2 and S2*(38). Cathepsin L and trypsin cleaved the S protein yielding a 71 kDa fragment which appeared as a stable, postfusion form, similar to S2* (38). Proteolytic priming of the MHV-2 S proteins upon virus entry was earlier implicated by studies with inhibitors of endolysosomal proteases and lysosomotropic agents, and by trypsin bypass experiments, but the actual processing in cells was not confirmed (6). In our study, proteolytic processing of the S protein and virus-cell fusion, as measured by intracellular biotinylation of the S protein and by an independent virus infection assay, occurred with similar kinetics. The HR2 peptide fusion inhibitor prevents virus from fusion by inhibiting six-helix bundle formation (11). Consistently, it also prevented S proteins of incoming virions from becoming biotinylated, hence allowing us to discriminate the sequential order of cleavage and fusion. If cleavage is a prerequisite for the S protein to mediate fusion, then HR2 must take effect after the proteolytic event and HR2 peptide indeed did not affect the cleavage of S protein. Taken together, we argue that the S2* fragment fulfills the criteria of the functional fusion protein.

The difference in molecular weight between the S2 and S2* subunits predicts the suspected cleavage site to map approximately 230 amino acids downstream of the S1/S2 junction. Furthermore, priming of the class I fusion proteins often occurs directly N-terminal of the FP which has been described as a conserved sequence of apolar amino acids in the CoV S protein (16, 36, 37). Both predictions point towards two critical arginine residues in the MHV S2 domain and intriguingly, cleavage at the same position (S2') has been implicated to enable SARS-CoV S-protein fusion (8, 10). By analogy, we suspected the S2' cleavage site to be used in MHV-A59 S protein, but after mutagenesis of both arginines the infectivity of MHV remained unaffected and the S-protein cleavage pattern upon fusion unaltered.

In an attempt to deduce the cleavage site from its molecular weight we enzymatically removed the N-linked glycans of the S2* glycoprotein and analyzed its size. Although the deglycosylated S_0 and S2 proteins were reduced to sharply defined products, S2* remained ill-defined, migrating as a heterogeneous band ranging from 60 to 65 kDa. Assuming that the S2 and S2* product underwent similar posttranslational modifications, the variable size of the S2* fragment can be best explained by promiscuous proteolytic cleavages, whereas S2 is formed by cleavage precisely at the S1/S2 junction. Heterogeneity of cleavage products might result from a certain degree of plasticity of S2' cleavage either by the existence of alternative cleavage sites or by involvement of multiple or alternative proteolytic enzymes, analogous to the fusion activation of the SARS-CoV S protein (13). The plasticity of the cleavage site also suggests that cleavage directly adjacent to the FP may not be an absolute requirement for fusion.

In search for the cleavage site, we applied broad spectrum protease inhibitors to identify corresponding (classes of) proteases. Testing protease inhibitors in SARS-CoV entry highlighted involvement of cathepsin L and eventually led to the identification of the cathepsin L cleavage site in the S protein (15, 17). In contrast to SARS-CoV, the protease inhibitors leupeptin, E64d and specific cathepsin L/B inhibitors failed to block MHV-A59 infection (6, 14). We observed no effect on the proteolytic processing of MHV S proteins for broad range protease inhibitors targeting cysteine, aspartyl, serine, thiol and metallo proteases. We conclude that heterogeneity of the S2* subunit, our failure to knock-out the S2' cleavage site by mutation and the insensitivity of MHV towards individual protease inhibitors are all consequences of redundant proteases and/or multiple cleavage sites that mediate MHV S-protein priming. However, a given protease inhibitor may not block all individual proteases of a specific class and our inhibitor panel was lacking threonine protease inhibitors and aminopeptidases inhibitors that potentially prime the S protein (44). Plasticity in cleavage is further supported by the similarity of S-protein processing in various cell lines and may confer flexibility to the virus in infecting different tissues (45). Alternatively, heterogeneous S2* fragment could be explained in analogy to filovirus fusion protein processing which requires gradual trimming by low pH activated endosomal proteases to reach fusion competence (46). However, we do not observe an enrichment of a particular S2* species over time and lysosomotropic agents did not prevent cleavage. Nevertheless, MHV S-protein priming is a distinct event that is timed after virus attachment and before lysosomal degradation. Binding to cells alone (Fig. 3A, time course) or incubation of virus preparations with cell lysates (data not shown) was not sufficient to trigger the cleavage event. On the other hand, the application of lysosomotropic agents, which can prevent endosome maturation at higher concentrations, prevented the S protein signal from declining over time. The quantification of the different S forms after 90 min of inoculation in the absence or presence of NH_4Cl indicated that this lysosomal degradation equally affects all forms of S, but did not block cleavage into the S2* subunit. Hence, the S2* fragment is not the product of an unspecific lysosomal degradation processes, but is cleaved by cellular proteases that are active prior to fusion and before degradation in the lysosomal system.

All class I viral fusion proteins have to minimally meet two requirements to accomplish fusion: proteolytic priming and triggering of membrane fusion. Priming by cleavage is a common maturation step to bring fusion proteins into the fusion-ready, metastable form (1, 2). Our data suggest that the S2* subunit represents primed MHV-A59 S protein and indicate, in combination with other observations, that many if not all CoV fusion proteins need cleavage to achieve the fusion-ready form (6, 8, 20, 39). In contrast to many typical class I fusion proteins, priming of S proteins does not occur in the producer cell; cleavage in the target cell provides an extra level of spatial and temporal control of virus fusion. Thus, MHV receptor-induced conformational changes are initiated at the target cell exposing a proteolytic cleavage site (19, 38, 47). SARS CoV S proteins require a first cleavage to facilitate a consecutive cleavage that then renders the S-protein fusion competent (36). Nevertheless, an additional trigger of unknown nature is probably necessary to initiate the membrane fusion, since we could block virus-cell fusion - using lysosomotropic agents - but not S-protein cleavage. Low pH in the endolysosomal compartment may itself be a trigger but may as well be necessary for priming by low pH-activated proteases (14, 48, 49). Triggers of an alternative nature seem, however, more likely because the infection of some CoV can be

bypassed using recombinant proteases without pH decrease, whereas syncytia formation typically occurs at neutral pH (6, 20, 22, 39, 40). In summary, the priming of S proteins plays a pivotal role in the temporal and spatial regulation of CoV entry. With the conditional biotinylation assay described here, the priming events that occur after receptor binding and depend on cellular proteases can be characterized in detail.

Acknowledgements

We acknowledge Zou Yong for kindly providing Vero CCL-81 cells. This study was supported by EU Framework 7 program PITN-GA-2009-235649-Virus Entry.

References

1. Harrison SC. 2008. Viral membrane fusion. Nature structural & molecular biology 15:690-698.
2. White JM, Delos SE, Brecher M, Schornberg K. 2008. Structures and mechanisms of viral membrane fusion proteins: multiple variations on a common theme. Critical reviews in biochemistry and molecular biology 43:189-219.
3. Melikyan GB, Smith EC, Dutch RE. 2012. 5.15 Mechanisms of Enveloped Virus Entry by Membrane Fusion, p. 290-311. In Editor-in-Chief: Edward HE (ed.), Comprehensive Biophysics. Elsevier, Amsterdam.
4. Epand RM. 2003. Fusion peptides and the mechanism of viral fusion. Biochimica et biophysica acta 1614:116-121.
5. Chandran K, Sullivan NJ, Felbor U, Whelan SP, Cunningham JM. 2005. Endosomal proteolysis of the Ebola virus glycoprotein is necessary for infection. Science (New York, N.Y.) 308:1643-1645.
6. Qiu Z, Hingley ST, Simmons G, Yu C, Das Sarma J, Bates P, Weiss SR. 2006. Endosomal proteolysis by cathepsins is necessary for murine coronavirus mouse hepatitis virus type 2 spike-mediated entry. Journal of virology 80:5768-5776.
7. Bertram S, Heurich A, Lavender H, Gierer S, Danisch S, Perin P, Lucas JM, Nelson PS, Pohlmann S, Soilleux EJ. 2012. Influenza and SARS-coronavirus activating proteases TMPRSS2 and HAT are expressed at multiple sites in human respiratory and gastrointestinal tracts. PloS one 7:e35876.
8. Kawase M, Shirato K, van der Hoek L, Taguchi F, Matsuyama S. 2012. Simultaneous treatment of human bronchial epithelial cells with serine and cysteine protease inhibitors prevents severe acute respiratory syndrome coronavirus entry. Journal of virology 86:6537-6545.
9. Burri DJ, da Palma JR, Kunz S, Pasquato A. 2012. Envelope glycoprotein of arenaviruses. Viruses 4:2162-2181.
10. Heald-Sargent T, Gallagher T. 2012. Ready, set, fuse! The coronavirus spike protein and acquisition of fusion competence. Viruses 4:557-580.
11. Bosch BJ, van der Zee R, de Haan CA, Rottier PJ. 2003. The coronavirus spike protein is a class I virus fusion protein: structural and functional characterization of the fusion core complex. Journal of virology 77:8801-8811.
12. de Haan CA, Haijema BJ, Schellen P, Wichgers Schreur P, te Lintelo E, Vennema H, Rottier PJ. 2008. Cleavage of group 1 coronavirus spike proteins: how furin cleavage is traded off against heparan sulfate binding upon cell culture adaptation. Journal of virology 82:6078-6083.
13. Belouzard S, Millet JK, Licitra BN, Whittaker GR. 2012. Mechanisms of coronavirus cell entry mediated by the viral spike protein. Viruses 4:1011-1033.
14. Eifart P, Ludwig K, Bottcher C, de Haan CA, Rottier PJ, Korte T, Herrmann A. 2007. Role of endocytosis and low pH in murine hepatitis virus strain A59 cell entry. Journal of virology 81:10758-10768.
15. Simmons G, Gosalia DN, Rennekamp AJ, Reeves JD, Diamond SL, Bates P. 2005. Inhibitors of cathepsin L prevent severe acute respiratory syndrome coronavirus entry. Proceedings of the National Academy of Sciences of the United States of America 102:11876-11881.
16. Watanabe R, Matsuyama S, Shirato K, Maejima M, Fukushi S, Morikawa S, Taguchi F. 2008. Entry from the cell surface of severe acute respiratory syndrome coronavirus with cleaved S protein as revealed by pseudotype virus bearing cleaved S protein. Journal of virology 82:11985-11991.
17. Bosch BJ, Bartelink W, Rottier PJ. 2008. Cathepsin L functionally cleaves the severe acute respiratory syndrome coronavirus class I fusion protein upstream of rather than adjacent to the fusion peptide. Journal of virology 82:8887-8890.
18. Yamada Y, Liu DX. 2009. Proteolytic activation of the spike protein at a novel RRRR/S motif is implicated in furin-dependent entry, syncytium formation, and infectivity of coronavirus infectious bronchitis virus in cultured cells. Journal of virology 83:8744-8758.
19. Matsuyama S, Taguchi F. 2002. Receptor-induced conformational changes of murine coronavirus spike protein. Journal of virology 76:11819-11826.
20. Sturman LS, Ricard CS, Holmes KV. 1985. Proteolytic cleavage of the E2 glycoprotein of

murine coronavirus: activation of cell-fusing activity of virions by trypsin and separation of two different 90K cleavage fragments. Journal of virology 56:904-911.

21. Bos EC, Luytjes W, Spaan WJ. 1997. The function of the spike protein of mouse hepatitis virus strain A59 can be studied on virus-like particles: cleavage is not required for infectivity. Journal of virology 71:9427-9433.
22. de Haan CA, Stadler K, Godeke GJ, Bosch BJ, Rottier PJ. 2004. Cleavage inhibition of the murine coronavirus spike protein by a furin-like enzyme affects cell-cell but not virus-cell fusion. Journal of virology 78:6048-6054.
23. Gombold JL, Hingley ST, Weiss SR. 1993. Fusion-defective mutants of mouse hepatitis virus A59 contain a mutation in the spike protein cleavage signal. Journal of virology 67:4504-4512.
24. Kuo L, Godeke GJ, Raamsman MJ, Masters PS, Rottier PJ. 2000. Retargeting of coronavirus by substitution of the spike glycoprotein ectodomain: crossing the host cell species barrier. Journal of virology 74:1393-1406.
25. Janes PW, Griesshaber B, Atapattu L, Nievergall E, Hii LL, Mensinga A, Chheang C, Day BW, Boyd AW, Bastiaens PI, Jorgensen C, Pawson T, Lackmann M. 2011. Eph receptor function is modulated by heterooligomerization of A and B type Eph receptors. The Journal of cell biology 195:1033-1045.
26. Taguchi F, Shimazaki YK. 2000. Functional analysis of an epitope in the S2 subunit of the murine coronavirus spike protein: involvement in fusion activity. The Journal of general virology 81:2867-2871.
27. de Haan CA, Haijema BJ, Masters PS, Rottier PJ. 2008. Manipulation of the coronavirus genome using targeted RNA recombination with interspecies chimeric coronaviruses. Methods in molecular biology (Clifton, N.J.) 454:229-236.
28. Beckett D, Kovaleva E, Schatz PJ. 1999. A minimal peptide substrate in biotin holoenzyme synthetase-catalyzed biotinylation. Protein science : a publication of the Protein Society 8:921-929.
29. Rossen JW, Bekker CP, Strous GJ, Horzinek MC, Dveksler GS, Holmes KV, Rottier PJ. 1996. A murine and a porcine coronavirus are released from opposite surfaces of the same epithelial cells. Virology 224:345-351.
30. Mechold U, Gilbert C, Ogryzko V. 2005. Codon optimization of the BirA enzyme gene leads to higher expression and an improved efficiency of biotinylation of target proteins in mammalian cells. Journal of biotechnology 116:245-249.
31. Dveksler GS, Pensiero MN, Cardellichio CB, Williams RK, Jiang GS, Holmes KV, Dieffenbach CW. 1991. Cloning of the mouse hepatitis virus (MHV) receptor: expression in human and hamster cell lines confers susceptibility to MHV. Journal of virology 65:6881-6891.
32. Ng B, Polyak SW, Bird D, Bailey L, Wallace JC, Booker GW. 2008. Escherichia coli biotin protein ligase: characterization and development of a high-throughput assay. Analytical biochemistry 376:131-136.
33. Laemmli UK. 1970. Cleavage of structural proteins during the assembly of the head of bacteriophage T4. Nature 227:680-685.
34. Miura HS, Nakagaki K, Taguchi F. 2004. N-terminal domain of the murine coronavirus receptor CEACAM1 is responsible for fusogenic activation and conformational changes of the spike protein. Journal of virology 78:216-223.
35. Ohkuma S, Chudzik J, Poole B. 1986. The effects of basic substances and acidic ionophores on the digestion of exogenous and endogenous proteins in mouse peritoneal macrophages. The Journal of cell biology 102:959-966.
36. Belouzard S, Chu VC, Whittaker GR. 2009. Activation of the SARS coronavirus spike protein via sequential proteolytic cleavage at two distinct sites. Proceedings of the National Academy of Sciences of the United States of America 106:5871-5876.
37. Madu IG, Roth SL, Belouzard S, Whittaker GR. 2009. Characterization of a highly conserved domain within the severe acute respiratory syndrome coronavirus spike protein S2 domain with characteristics of a viral fusion peptide. Journal of virology 83:7411-7421.
38. Matsuyama S, Taguchi F. 2009. Two-step conformational changes in a coronavirus envelope glycoprotein mediated by receptor binding and proteolysis. Journal of virology 83:11133-11141.
39. Matsuyama S, Ujike M, Morikawa S, Tashiro M, Taguchi F. 2005. Protease-mediated enhancement of severe acute respiratory syndrome coronavirus infection. Proceedings of the National Academy of Sciences of the United States of America 102:12543-12547.
40. Frana MF, Behnke JN, Sturman LS, Holmes KV. 1985. Proteolytic cleavage of the E2 glycoprotein of murine coronavirus: host-dependent differences in proteolytic cleavage and cell fusion. Journal of virology 56:912-920.
41. Bos EC, Heijnen L, Luytjes W, Spaan WJ. 1995. Mutational analysis of the murine coronavirus spike protein: effect on cell-to-cell fusion. Virology 214:453-463.
42. Yamada YK, Takimoto K, Yabe M, Taguchi F. 1997. Acquired fusion activity of a murine coronavirus MHV-2 variant with mutations in the proteolytic cleavage site and the signal sequence of the S protein. Virology 227:215-219.
43. de Haan CA, Li Z, te Lintelo E, Bosch BJ, Haijema BJ, Rottier PJ. 2005. Murine coronavirus with an extended host range uses heparan sulfate as an entry receptor. Journal of virology 79:14451-14456.
44. Lopez-Otin C, Bond JS. 2008. Proteases: multifunctional enzymes in life and disease. The Journal of biological chemistry 283:30433-30437.
45. Slobodskaya O, Snijder EJ, Spaan WJ. 2012. Organ tropism of murine coronavirus does not correlate with the expression levels of the membrane-anchored or secreted isoforms of the carcinoembryonic antigen-related cell adhesion molecule 1 receptor. The Journal of general virology 93:1918-1923.

46. Hunt CL, Lennemann NJ, Maury W. 2012. Filovirus entry: a novelty in the viral fusion world. Viruses 4:258-275.

47. Holmes KV, Zelus BD, Schickli JH, Weiss SR. 2001. Receptor specificity and receptor-induced conformational changes in mouse hepatitis virus spike glycoprotein. Advances in experimental medicine and biology 494:173-181.

48. Sturman LS, Ricard CS, Holmes KV. 1990. Conformational change of the coronavirus peplomer glycoprotein at pH 8.0 and 37 degrees C correlates with virus aggregation and virus-induced cell fusion. Journal of virology 64:3042-3050.

49. Zelus BD, Schickli JH, Blau DM, Weiss SR, Holmes KV. 2003. Conformational changes in the spike glycoprotein of murine coronavirus are induced at 37 degrees C either by soluble murine CEACAM1 receptors or by pH 8. Journal of virology 77:830-840.

50. Pensaert MB, de Bouck P. 1978. A new coronavirus-like particle associated with diarrhea in swine. Archives of virology 58:243-247.

51. AASV. 2013. Porcine Epidemic Diarrhea Information. American Association of Swine Veterinarians

52. Li W, Li H, Liu Y, Pan Y, Deng F, Song Y, Tang X, He Q. 2012. New variants of porcine epidemic diarrhea virus, China, 2011. Emerging infectious diseases 18:1350-1353.

53. Huang YW, Dickerman AW, Pineyro P, Li L, Fang L, Kiehne R, Opriessnig T, Meng XJ. 2013. Origin, evolution, and genotyping of emergent porcine epidemic diarrhea virus strains in the United States. mBio 4.

54. Hofmann M, Wyler R. 1988. Propagation of the virus of porcine epidemic diarrhea in cell culture. Journal of clinical microbiology 26:2235-2239.

55. Park JE, Cruz DJ, Shin HJ. 2011. Receptor-bound porcine epidemic diarrhea virus spike protein cleaved by trypsin induces membrane fusion. Archives of virology 156:1749-1756.

56. Duarte M, Tobler K, Bridgen A, Rasschaert D, Ackermann M, Laude H. 1994. Sequence analysis of the porcine epidemic diarrhea virus genome between the nucleocapsid and spike protein genes reveals a polymorphic ORF. Virology 198:466-476.

57. Cavanagh D. 1983. Coronavirus IBV: structural characterization of the spike protein. The Journal of general virology 64 (Pt 12):2577-2583.

58. Xiao X, Chakraborti S, Dimitrov AS, Gramatikoff K, Dimitrov DS. 2003. The SARS-CoV S glycoprotein: expression and functional characterization. Biochemical and biophysical research communications 312:1159-1164.

59. Li C, Li Z, Zou Y, Wicht O, van Kuppeveld FJ, Rottier PJ, Bosch BJ. 2013. Manipulation of the porcine epidemic diarrhea virus genome using targeted RNA recombination. PloS one 8:e69997.

60. Song DS, Yang JS, Oh JS, Han JH, Park BK. 2003. Differentiation of a Vero cell adapted porcine epidemic diarrhea virus from Korean field strains by restriction fragment length polymorphism analysis of ORF 3. Vaccine 21:1833-1842.

61. Egberink HF, Ederveen J, Callebaut P, Horzinek MC. 1988. Characterization of the structural proteins of porcine epizootic diarrhea virus, strain CV777. American journal of veterinary research 49:1320-1324.

62. Park SJ, Moon HJ, Yang JS, Lee CS, Song DS, Kang BK, Park BK. 2007. Sequence analysis of the partial spike glycoprotein gene of porcine epidemic diarrhea viruses isolated in Korea. Virus genes 35:321-332.

63. Shirato K, Maejima M, Matsuyama S, Ujike M, Miyazaki A, Takeyama N, Ikeda H, Taguchi F. 2011. Mutation in the cytoplasmic retrieval signal of porcine epidemic diarrhea virus spike (S) protein is responsible for enhanced fusion activity. Virus research 161:188-193.

64. Shirato K, Matsuyama S, Ujike M, Taguchi F. 2011. Role of proteases in the release of porcine epidemic diarrhea virus from infected cells. Journal of virology 85:7872-7880.

65. Kido H, Okumura Y, Takahashi E, Pan HY, Wang S, Chida J, Le TQ, Yano M. 2008. Host envelope glycoprotein processing proteases are indispensable for entry into human cells by seasonal and highly pathogenic avian influenza viruses. Journal of molecular and genetic medicine : an international journal of biomedical research 3:167-175.

66. Kantanen ML, Leinikki P, Kuismanen E. 1995. Endoproteolytic cleavage of HIV-1 gp160 envelope precursor occurs after exit from the trans-Golgi network (TGN). Archives of virology 140:1441-1449.

67. Bugge TH, Antalis TM, Wu Q. 2009. Type II transmembrane serine proteases. The Journal of biological chemistry 284:23177-23181.

68. Bottcher E, Matrosovich T, Beyerle M, Klenk HD, Garten W, Matrosovich M. 2006. Proteolytic activation of influenza viruses by serine proteases TMPRSS2 and HAT from human airway epithelium. Journal of virology 80:9896-9898.

69. Matsuyama S, Nagata N, Shirato K, Kawase M, Takeda M, Taguchi F. 2010. Efficient activation of the severe acute respiratory syndrome coronavirus spike protein by the transmembrane protease TMPRSS2. Journal of virology 84:12658-12664.

70. Krzyzaniak MA, Zumstein MT, Gerez JA, Picotti P, Helenius A. 2013. Host cell entry of respiratory syncytial virus involves macropinocytosis followed by proteolytic activation of the F protein. PLoS pathogens 9:e1003309.

71. Li BX, Ge JW, Li YJ. 2007. Porcine aminopeptidase N is a functional receptor for the PEDV coronavirus. Virology 365:166-172.

72. Bertram S, Dijkman R, Habjan M, Heurich A, Gierer S, Glowacka I, Welsch K, Winkler M, Schneider H, Hofmann-Winkler H, Thiel V, Pohlmann S. 2013. TMPRSS2 activates the human coronavirus 229E for cathepsin-independent host cell entry and is expressed in viral target cells in the respiratory epithelium. Journal of virology 87:6150-6160.

73. Licitra BN, Millet JK, Regan AD, Hamilton BS, Rinaldi VD, Duhamel GE, Whittaker GR. 2013.

Mutation in spike protein cleavage site and pathogenesis of feline coronavirus. Emerging infectious diseases 19:1066-1073.

74. Kido H, Okumura Y, Takahashi E, Pan HY, Wang S, Yao D, Yao M, Chida J, Yano M. 2012. Role of host cellular proteases in the pathogenesis of influenza and influenza-induced multiple organ failure. Biochimica et biophysica acta 1824:186-194.
75. Tay FP, Huang M, Wang L, Yamada Y, Liu DX. 2012. Characterization of cellular furin content as a potential factor determining the susceptibility of cultured human and animal cells to coronavirus infectious bronchitis virus infection. Virology 433:421-430.
76. Baker M, Prasad BV. 2010. Rotavirus cell entry. Current topics in microbiology and immunology 343:121-148.
77. Kweon CH, Kwon BJ, Lee JG, Kwon GO, Kang YB. 1999. Derivation of attenuated porcine epidemic diarrhea virus (PEDV) as vaccine candidate. Vaccine 17:2546-2553.
78. Park SJ, Song DS, Ha GW, Park BK. 2007. Cloning and further sequence analysis of the spike gene of attenuated porcine epidemic diarrhea virus DR13. Virus genes 35:55-64.
79. Huang IC, Bosch BJ, Li F, Li W, Lee KH, Ghiran S, Vasilieva N, Dermody TS, Harrison SC, Dormitzer PR, Farzan M, Rottier PJ, Choe H. 2006. SARS coronavirus, but not human coronavirus NL63, utilizes cathepsin L to infect ACE2-expressing cells. The Journal of biological chemistry 281:3198-3203.
80. Kawase M, Shirato K, Matsuyama S, Taguchi F. 2009. Protease-mediated entry via the endosome of human coronavirus 229E. Journal of virology 83:712-721.
81. Gierer S, Bertram S, Kaup F, Wrensch F, Heurich A, Kramer-Kuhl A, Welsch K, Winkler M, Meyer B, Drosten C, Dittmer U, von Hahn T, Simmons G, Hofmann H, Pohlmann S. 2013. The spike protein of the emerging betacoronavirus EMC uses a novel coronavirus receptor for entry, can be activated by TMPRSS2, and is targeted by neutralizing antibodies. Journal of virology 87:5502-5511.
82. Sato T, Takeyama N, Katsumata A, Tuchiya K, Kodama T, Kusanagi K. 2011. Mutations in the spike gene of porcine epidemic diarrhea virus associated with growth adaptation in vitro and attenuation of virulence in vivo. Virus genes 43:72-78.
83. Park SJ, Moon HJ, Luo Y, Kim HK, Kim EM, Yang JS, Song DS, Kang BK, Lee CS, Park BK. 2008. Cloning and further sequence analysis of the ORF3 gene of wild- and attenuated-type porcine epidemic diarrhea viruses. Virus genes 36:95-104.
84. Kaverin NV, Webster RG. 1995. Impairment of multicycle influenza virus growth in Vero (WHO) cells by loss of trypsin activity. Journal of virology 69:2700-2703.
85. Zamolodchikova TS. 2012. Serine proteases of small intestine mucosa--localization, functional properties, and physiological role. Biochemistry. Biokhimiia 77:820-829.
86. Simmons G, Zmora P, Gierer S, Heurich A, Pohlmann S. 2013. Proteolytic activation of the SARS-coronavirus spike protein: cutting enzymes at the cutting edge of antiviral research. Antiviral research 100:605-614.

Chapter 3

Proteolytic Activation of the Murine Coronavirus Spike Protein for Membrane Fusion

Oliver Wicht, Eelke P. Béguin, Lione Willems,

Cornelis A.M. de Haan, Peter J.M. Rottier and

Berend Jan Bosch

Virology Division, Department of Infectious Diseases and Immunology, Faculty of Veterinary Medicine, Utrecht University, Utrecht, The Netherlands

Manuscript in preparation

Abstract

Cell entry of enveloped viruses requires a membrane fusion event that is catalyzed by highly specialized surface glycoproteins. Class I viral fusion proteins can be primed for fusion by proteolysis that releases the fusion protein into a fusion-competent, metastable conformation. In chapter 2, we demonstrate that the spike (S) fusion protein of the coronavirus mouse hepatitis virus (MHV; strain A59) is indeed proteolytically processed at the stage of virus entry. However, the priming protease remained unknown; hence we aimed to identify proteases that are required for MHV S protein priming using different approaches. Based on candidates obtained by a large primary small interfering RNA (siRNA) screen, we investigate the role of human elastase 2B, a potential priming protease, and SERPINA1, a natural inhibitor of serine proteases, in MHV infection by small interfering RNA mediated knockdown and overexpression of the genes. Moreover, broad spectrum protease inhibitors were tested for their ability to block MHV infection. Serine protease inhibitors reduced MHV infection, but by using retrovirus-based pseudo-particles bearing different fusion proteins, a specific effect of these inhibitors on MHV S protein mediated entry was not observed. At last, we could not identify a protease that proteolytically activates the MHV S protein. Protease requirements for MHV entry remain unclear, may be due to a variable protease cleavage sites or redundancy in activating proteases.

Introduction

Virus-cell membrane fusion is essential for enveloped virus infection and is catalyzed by specialized viral glycoproteins. The fusion proteins can be divided into classes according to structural and functional features. Class I fusion proteins typically pass three checkpoints to accomplish membrane fusion: priming, receptor binding, and triggering. This tight control of the fusion protein activity at multiple levels ensures virus-cell fusion at the appropriate time with the proper membrane of the target cell supporting productive infection. The priming stage is characterized by proteolytic cleavage of the fusion protein that separates an N-terminal subunit with receptor binding function from a C-terminal membrane-anchored subunit carrying the fusion machinery. Cleavage generates a fusion subunit with a hydrophobic sequence close to the Nterminus, which serves as a fusion peptide. Priming of the premature fusion protein is required to create a fusion-ready, metastable conformation. Structural and mechanistic details have been best characterized for the influenza virus hemagglutinin and human immunodeficiency virus Env fusion proteins that are primed for fusion by furin-like enzymes before release of progeny virus from producer cells (1, 2).

Growing evidence demonstrates that proteolysis is also required for the functioning of the class I spike (S) fusion protein of coronaviruses (CoVs) (reviewed in (3)). Instead of priming during virus exit, cleavage of S proteins can also occur in the extracellular milieu or after binding to the target cells. Activity of proteases – sometimes of a specific type – can determine the susceptibility of cultured cells to CoV (Chapter 5, (4-7). Entry of severe acute respiratory syndrome CoV (SARS-CoV) and the natural mouse hepatitis virus isolate strain 2 (MHV-2) can be blocked by protease inhibitors. These inhibitor studies helped to identify proteases and subsequent studies illuminated mechanistic details of proteolytic activation (8, 9). The SARSCoV S protein is sequentially cleaved at multiple positions to acquire fusion competence (10), whereas MHV-2 S protein undergoes receptor-induced conformational rearrangements that are necessary to expose the proteolytic cleavage site (11). However, requirements for proteolysis and priming of other coronaviruses like the human coronavirus NL63 and the laboratory isolated, prototype MHV strain A59 (MHVA59) remain elusive (9, 12, 13). MHV-A59 S protein can be cleaved in the producer cell at a furin cleavage site (FCS) that separates the receptor binding domain (S1) from the subunit comprising the fusion machinery (S2) (14). However, cleavage at the S1/S2 junction is dispensable for virus viability, as disabling of the FCS by mutation and production of viruses in presence of furin inhibitors did not abolish infectivity (15-17). Nevertheless, proteolytic priming of fusion

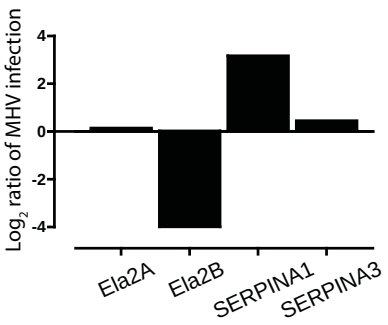

Fig. 1 Candidate genes from the RNAi druggable genome screen. An siRNA-based screen for MHV host factors was performed on HeLa cells. siRNAs targeting the serine protease elastase 2B (Ela2B) and serine protease inhibitor clade A (SERPINA1) genes were amongst the top hits and had opposite effects on MHV infection. Knockdown of the related genes Ela2A and SERPINA3 had no effect. Data provided by: M.H. Verheije, C.A.M. de Haan, L. Pelkmans, Institute for Molecular Systems Biology, ETH, Zürich, Switzerland.

proteins is a requirement for the function of class I fusion proteins. This probably holds true for coronavirus S proteins as well. Until today, the activating proteases for MHV-A59 were not yet identified.

To identify essential host factors in MHV infection, a microscopy-based high-throughput RNA interference (RNAi) screen targeting the druggable genome has been performed in HeLa cells (data kindly provided by Hélène Verheije; experiments done in collaboration with Lucas Pelkmans, ETH Zürich, Switzerland). In search for proteolysis related genes, data analysis yielded two candidates: human chymotrypsin-like serine protease elastase 2B (Ela2B, gene symbol CELA2B) and human serine proteinase inhibitor clade A (SERPINA1). Knockdown of Ela2B reduced MHV infection by 16-fold with two (out of three) small interfering RNAs (siRNA) (Figure 1). In vivo, this enzyme is predominantly expressed by the pancreas and secreted into the gastro-intestinal tract (18). Human Ela2B shares 90% sequence homology with human elastase2A (Ela2A, gene symbol CELA2A), whereas other species like mice contain only a single elastase 2 gene. On the other hand, knockdown of SERPINA1 – an irreversible inhibitor of several serine proteases – did raise MHV infection by 10fold with all three siRNAs tested (Figure 1). Inhibitor alpha-antitrypsin SERPINA1 is found in blood plasma and deregulated SERPINA1 expression has been associated with obesity and cancer (19, 20).

Intriguingly, SERPINA1 is a potential inhibitor of elastases (reviewed in (21)), which corresponds to the opposite phenotype on infection found after siRNA knockdown. This indicates that SERPINA1 and Ela2B expression may be inversely linked to MHV infection. Moreover, the potential of elastase to activate coronavirus S proteins has been demonstrated by the proteolytic activation of the SARS-CoV S protein at multiple positions by bacterial elastase (22). We hypothesized that Ela2B activates MHV-A59 S protein by proteolytic processing, whereas SERPINA1 acts as inhibitor of Ela2B activity in cultured cells.

In this study, we aimed to characterize the cellular protease that activates MHV-A59 S protein and renders it fusion-competent. Following the lead from the siRNA screen, we studied the impact of Ela2B and SERPINA1 on MHV infection. In an attempt to reproduce the Ela2B and SERPINA1 knockdown phenotype on MHV infection a validation siRNA mediated knockdown of the genes was performed. In parallel, we assessed MHV infection of target cells that overexpressed Ela2B and SERPINA1 to directly characterize their role and complement the validation siRNA experiment. In addition, an unbiased approach was taken to characterize the activating protease for MHV S protein. We tested the effects of a variety of protease inhibitors on MHV infection and used pseudotyped retrovirus-based pseudo-particles to control the specificity of the inhibitors.

Material and Methods

Cells and viruses

HEK-293T, HeLa-TDS (high-throughput Technology Development Studio, MPI Dresden, Germany), and murine LR7 cells (23) were maintained in Dulbecco modified Eagle medium (DMEM, Lonza BE12-741F) supplemented with 10% fetal bovine serum (FBS) and penicillin and streptomycin (100 units/ml and 100 µg/ml, respectively, Life Technologies). Recombinant HEK-293T and HeLa cell lines expressing the MHV receptor murine carcinoembryonic antigen-related cell adhesion molecule 1a (CCM) have been described earlier (24). HEKCCM,

HeLaCCM and LR7 and were maintained in culture medium supplemented with G418 (PAA). MHV (strain A59) and recombinant MHV variants were propagated and titrated on LR7 cells in culture medium. The recombinant MHV-A59 derivative MHV-2aFLS carries firefly luciferase gene between ORF 2a and the S gene (25). In MHV-2aFLSrec the S gene is substituted by the S gene of virus MHV/BHK (26) in the isogenic background of MHV-2aFLS. MHV-ERLM carries the Renilla luciferase gene between the E and M genes (27).

Small interfering RNA-mediated knockdown experiments

Small interfering RNA (siRNA) oligonucleotide sequences, target genes and manufacturer are reported in Table 1. HeLa or HeLaCCM cells were seeded in 96-well clusters. 24 h after seeding, cells were transfected with 10 nM siRNA oligos using oligofectamine (Invitrogen) according to manufacturer's protocol. Four hours post transfection, supernatant was supplied with 50 µl DMEM + 30% FBS + penicillin and streptomycin (300 units /ml and 300 µg /ml, respectively). Per experiment, siRNA transfection was performed in triplicates and the control siRNA targeting kinesin family member 11 (Eg5), firefly luciferase (Luc), Scrambled, green fluorescent protein (GFP), ADP-Ribosylation Factor 1 (Arf1), as well as conditions without siRNA (complex) and untreated (mock) were included on every plate. At 64 h after transfection, cells were inoculated with MHV-2aFLSrec at a multiplicity of infection (MOI) corresponding to 10 to 20% infection on mock treated cells as predetermined by immunoperoxidase staining of infected cells using a polyclonal rabbit anti MHV serum (K135) in combination with an horseradish peroxidase conjugated anti-rabbit immunoglobulin G and visualized with AEC substrate kit (Vector Laboratories). After 6 h 30 min incubation, the supernatant was exchanged for Wst1 (Roche) in culture medium to determine cell number and viability according to the manufacturer's protocol. Finally, cells were lysed using 40 µl cell culture lysis reagent (Promega, E1531). Luciferase expression was determined in 10 µl lysate using a luminescence plate reader (Berthold Centro LB 960) with the luciferase assay system (Promega, E152A). Luciferase counts were corrected for the cell number and viability as determined by the Wst1 assay. Individual siRNA were marked with asterisks if the knockdown resulted in a pvalue $p<0.05$ compared to Scr siRNA according to Dunnett's statistical test that compares multiple samples to a single control, whereas the error variance is based on the pool of all measurements.

Expression plasmids

To generate pCAGGS-Ela2BST, pCAGGS-Ela2AST, pCAGGS-SERPINA1ST, and pCAGGS-SERPINA3ST, the open reading frames of Elastase2A (Gene Bank Accession No. BC069331), Elastase2B (BC069412), SERPINA1 (BC015642), and SERPINA3 (BC010530) were PCR-amplified from commercially available cDNA (Openbiosystems) and cloned into pCAGGS expression plasmids with a C-terminal sequence encoding three consecutive Strep tag II (NWSHPQFEK). The human codon optimized gene encoding Biotin Protein Ligase (BirA) with an N-terminal HA- and FLAG-tag (the pUM376-BirA PCR template was kindly provided by V. Ogryzko) was cloned into the pCAGGS vector (pCAGGS-hBirA, (28)). pCAGGS expression plasmid containing the MHV-A59 S gene (pCAGGS-MHV-S) was kindly provided by Stefan Pöhlmann (DPZ, Göttingen, Germany). Site directed mutagenesis was used to create pCAGGS-MHV-S^{-FCS} and MHV-S^{+FCS} expression plasmids encoding MHV-S variants with arginine to serine substitution at position 868 and a histidine to arginine substitution at position 867,

resulting in disruption or augmentation of the furin cleavage site, respectively (see table 2). All plasmids generated in this study were confirmed by sequencing the open reading frame. To express the human transmembrane protease serine 2 (TMPRSS2) gene and the murine transmembrane protease serine 4 (TMPRSS4) gene, pCMV-SPORT6 expression plasmids were purchased from (Openbiosystems). The retroviral packaging construct pQCXIX containing eGFP (pQeGFP) gene and pCAGGS expression plasmid containing vesicular stromatitis virus glycoprotein (VSV-G) gene was kindly provided by H. Choe (from Harvard Medical School, Boston, USA). pCD5 plasmid encoding hemagglutinin of the pandemic H1N1 influenza virus with a C-terminally appended GCN4 trimerization motif and Strep tag I (sHA-ST) have been described before (29).

Virus infection

HeLa-CCM or LR7 cells were inoculated at an MOI of 0.1 with MHV-2aFLS or MHV-ERLM (Figure 3C, Figure 4); alternatively, HeLa cells were inoculated with MHV-2aFLSrec (Figure 3B) at an MOI of 0.1. To express proteases and protease inhibitors (SERPINA), target cells were transiently transfected with expression plasmids using JetPrime according to the manufacturer's protocol. After 20 h, cells were dispensed into 96-well clusters. At 48 h post transfection, the inoculum was then added without removing the cell culture supernatant (Figure 3). At 3 to 5 h post infection, all MHV infections were supplemented with peptidic fusion inhibitor HR2 (5 µM) to prevent cell-cell fusion events. After 6.5 to 8 h, virus infection was quantified by determining luciferase expression. Therefore, cells were lysed using 40 µl cell culture lysis reagent (Promega, E1531). Luciferase expression was determined by a luciferase assay using 10 µl lysate with the luciferase assay system (Promega, E152A) in a luminescence plate reader (Berthold Centro LB 960).

Inhibitors of MHV infection

The effect of various compounds on MHV infection was tested. Cells were pretreated for 30 min at 37°C followed by inoculation in the presence of individual compounds. The following protease inhibitors were used at their highest and lowest recommended working range concentration according to Sigma's protease inhibitor technical bulletin INHIB1 (final concentration): Pepstatin A (1.5 or 0.7 µM, Sigma, P5318), E64d (10 or 1 µM, Sigma, E8640), phosphoramidon (10 or 1 µM, Sigma, R7385), and AEBSF (1 or 0.1 mM, Sigma, A8456). Complete Protease Inhibitor Cocktail was toxic to cells at a concentration recommended by the manufacturer to block proteolytic activity in cell extracts. Therefore, we used Complete Protease Inhibitor Cocktail at lower concentrations (Roche 11836153001, dilutions are indicated in figures). To block infection, peptidic fusion inhibitor HR2 (25 µM) or the lysosomotropic agent ammonium chloride (20 or 30 mM NH_4Cl, Merck, Darmstadt) was added.

Cell viability assay

Eight hours after application of HR2 peptide (25 µM), AEBSF (10 - 100 µM), NH_4Cl (30 mM) or Complete Protease Inhibitor Cocktail (0.5x – 0.08x concentrated) to the cell culture supernatant of HEK293T or LR7 cells, we performed a Wst1 (Roche) cell viability assay according to the manufacturer's protocol. Viable cells convert the Wst1 substrate into a colorimetric product that was measured by an ELISA reader (EL-808, BioTEK) at 450 nm.

Table 1. siRNA target sequences.

Name (alias)	Target gene ; accession number	Mfr	Catalog number	Target sequence (5'-3')
Eg5	Kinesin Family Member 11; NM_004523	Am	AM4639	unknown
Luc	Firefly Luciferase; X65324	Am	AM4629	unknown
Scr -	non-targeting	Am	AM4635	unknown
Arf1	ADP-Ribosylation Factor 1; NM_001658	Dh	M-011580-00	unknown
GFP	green fluorescent protein; U55761	Am	AM4626	unknown
Ela2A1	Elastase 2A; NM_033440	TS	D-008368-18	GUGAAAACCAGUAUGAUCU
Ela2A2	Elastase 2A; NM_033440	TS	D-008368-19	AAUUACAUCGACUGGAUCA
Ela2A3	Elastase 2A; NM_033440	TS	D-008368-20	CAUCGUCAGCUUCGGGUCU
Ela2A4	Elastase 2A; NM_033440	TS	D-008368-21	CCACAAGCCCUCCGUCUUC
Ela2A/B1	Elastase 2A & B; NM_033440 & NM_015849	TS	D-008368-01	CUAAGAUUGUGGUGCACAA
Ela2A/B1	Elastase 2A & B; NM_033440 & NM_015849	TS	D-008368-02	GGGGAAGGCUGCAGACCAA
Ela2A/B1	Elastase 2A & B; NM_033440 & NM_015849	TS	D-008368-03	GCUCCAAUGGCAAGUGGUA
Ela2B1	Elastase 2B; NM_015849	TS	D-005862-02	UCACGCGGGUCUCCAACUA
Ela2B2	Elastase 2B; NM_015849	TS	D-005862-03	GCAGCACCGUGAAGACGAA
Ela2B3	Elastase 2B; NM_015849	TS	D-005862-05	CAACGGGGCUCUCCCUGAU
Ela2B4*	Elastase 2B; NM_015849	Qia	Hs_ELA2B_1	CACCGTGAAGACGAATATGAT
Ela2B5*	Elastase 2B; NM_015849	Qia	Hs_ELA2B_3	CAGCATAACCTCTACGTTGCA
SERPINA11	Serpin Peptidase Inhibitor, Clade A, Member 1; NM_001127707	TS	D-008847-01	AGAAACAGAUCAACGAUUA
SERPINA12	Serpin Peptidase Inhibitor, Clade A, Member 1; NM_001127707	TS	D-008847-02	GAGCAUCGCUACAGCCUUU
SERPINA13	Serpin Peptidase Inhibitor, Clade A, Member 1; NM_001127707	TS	D-008847-03	GCCUGAAGCUAGUGGAUAA
SERPINA14*	Serpin Peptidase Inhibitor, Clade A, Member 1; NM_001127707	Qia	Hs_SERPINA1_6	CACCCACGATATCATCACCAA
SERPINA15	Serpin Peptidase Inhibitor, Clade A, Member 1; NM_001127707	Qia	Hs_SERPINA1_7	CCCGAGGTCAAGTTCAACAAA
SERPINA31	Serpin Peptidase Inhibitor, Clade A, Member 3; NM_001085	TS	D-009576-01	CUAAGAAGCUCAUCAACGA
SERPINA32	Serpin Peptidase Inhibitor, Clade A, Member 3; NM_001085	TS	D-009576-02	CAAGGACCAUUGUGCGUUU
SERPINA33	Serpin Peptidase Inhibitor, Clade A, Member 3; NM_001085	TS	D-009576-03	CCAAGAUACUCAUCAGUCA

Specific siRNAs and control siRNAs were purchased from various manufacturers (Mfr). Am = Ambion, TS = Thermo Scientific, Qia = Qiuagen, Dh = Dharmacon. Asterisks indicate siRNAs which were used in the primary siRNA screen.

Retroviral pseudo-particles carrying virus fusion proteins

Moloney murine leukemia virus (MLV)-based pseudo-particles were pseudotyped with MHV-S, MHV S^{FCS}, $MHVS^{+FCS}$, VSVG, or without a fusion protein (MLV-S, $MLVS^{-FCS}$, $MLVS^{+FCS}$, MLV-G, MLV-null, respectively). Pseudo-particles were produced by cotransfecting HEK-293T cells with the MLV packaging construct encoding the MLV gag-pol polyprotein (kindly provided by H.Choe, Harvard Medical School, Boston, USA), an MLV-based transfer vector encoding firefly luciferase (pQCXIN-FL), and the expression plasmid for MHV-S, $MLVS^{FCS}$, $MLVS^{+FCS}$, VSV-G, or pCAGGS vector. The pQCXIN-FL transfer vector was constructed by cloning the PCR-amplified firefly luciferase gene into the multiple cloning site of the pQCXIN vector (Clontech). Transfection was performed using JetPrime according to manufacturer's manual (Polyplus, 114-15) and 24 h later cell culture supernatant was replenished and incubation was continued at 31°C for 48 h. Pseudo-particle containing supernatants were filtered through 0.45 µm pore-size membranes and diluted 1:2 in culture medium before transduction. HEK293T or HEKCCM cells grown in 96-well clusters were inoculated with pseudo-particles supplemented with HR2 peptide (16.6 µM), AEBSF (100 µM), or Complete Protease Inhibitor Cocktail (0.25x concentrated). At 24 h post transfection, luciferase expression was measured as described above.

Western Blot

To confirm the secretion of Strep-tagged proteins from transfected HeLa cells, cell culture supernatants were sampled 70 h post transfection (50 h after redistribution into 96-well clusters), supplemented with Laemmli buffer, and denatured at 95°C for 10 min (30). To confirm incorporation of virus membrane fusion glycoproteins into the retrovirus-based pseudo-particles, 2.5 ml of pseudo-particles containing cell culture supernatant was purified and concentrated (factor 1:100 v/v) by sedimentation through a cushion of 20% sucrose in TN buffer (10 mM Tris, 100 mM NaCl, pH 7.2) at 115,000 x *g* for 1 h at 4°C. Proteins were separated by sodium dodecyl sulfate polyacrylamide gel electrophoresis (SDS-PAGE) in a discontinuous gel with 10% acryl amide in the separating gel and subsequently transferred to a polyvinylidene fluoride membrane (BioRad, 162 0176). Membranes were blocked with 2% FBS in PBS and 0.5% Tween-20 and then reacted with antibodies and signals detected with Amersham ECL Western Blotting Analysis System (GE healthcare, RPN2109) using X-Omat LS films (Kodak, Sigma F1149). For detection of Strep-tagged proteins after overexpression, a mouse monoclonal anti-Strep tag antibody (IBA, 2-1507-001) and an anti-mouse immunoglobulin G conjugated horseradish peroxidase (Dako, P0161) was used. For detection of MHV S proteins incorporated into pseudo-particles, a polyclonal rabbit anti MHV serum (K135) and an anti-rabbit immunoglobulin G conjugated horseradish peroxidase (Dako, P0217) was used.

Results

Validation of RNAi-mediated elastase 2B and SERPINA1 knockdown phenotypes in MHV infection

To evaluate the role of the secretory proteins Ela2B and SERPINA1 in MHV infection, an siRNA knockdown experiment was carried out similar to the earlier performed primary siRNA screen. We assessed the effects of alternative siRNAs on MHV infection using a luciferase-expressing recombinant MHV. HeLa or HeLa cells stably expressing the MHV receptor CCM were transfected with 10 nM siRNA oligos for 72 h prior to inoculation with recombinant MHV (MOI = 0.1). As controls, cells were also transfected without siRNA (oligofect) or left untreated (mock) before inoculation with MHV-2aFLSrec, a recombinant MHV-A59. This virus contains the MHV/BHK S gene, which conferrs an extended host range by enabling CCM independent infection via heparan sulfate. It also codes a firefly luciferase reporter gene (31). A similar virus with a GFP gene instead of the luciferase gene had been used in the primary siRNA screen together with the siRNA oligos against Ela2B4, Ela2B5, and SERPINA14 (Table 1). After 6.5 h incubation, cell viability was determined by a colorimetric assay using Wst-1. MHV infection was determined by measuring firefly luciferase expression in cell lysates. For individual siRNAs, at least 3 independent wells were analyzed per experiment and the complete validation experiment was performed five times on HeLa cells and three times on HeLa-CCM cells. Knockdown of the mitotic motor protein Eg5 is lethal to cells and visual inspection of the cell layer confirmed a killing effect on >90% cells upon Eg5 siRNA transfection for each experiment (32). Small GTPase Arf1 knockdown, a known host factor of MHV replication, significantly reduced MHV infection to 30 to 40% (33)(Figure 2). Introduction of siRNA targeting the firefly luciferase gene (Luc) diminished infection of HeLa cells to about 20% and reduced infection of HeLa-CCM cells to background levels. Compared to controls with non-targeting siRNA (GFP) or lacking siRNA (oligofect and mock), transfection of unspecific siRNA (Scr) slightly reduced MHV infection. Four siRNAs targeting Ela2A, five siRNAs against Ela2B, three siRNAs with a dual specificity for Ela2A and 2B, as well as five siRNAs against SERPINA1 and three against SERPINA3 were tested. We considered it an acceptable reproducibility if more than 50% of the individual siRNAs against a single gene were significantly affecting MHV infection in a similar fashion.

In HeLa cells, out of five siRNAs against Ela2B, siRNAs #1 and #3 diminished MHV infection while the Ela2B #5 oligo had the opposite effect (Figure 2, left panel). Also knockdown with bispecific Ela2A/B #2 and #3 oligos increased MHV infection, hampering the interpretation of the result for Ela2B. Knockdown of other genes in HeLa cells had no significant effect for the majority of siRNAs tested and contradicting phenotypes by individual siRNAs against the same target gene were observed.

In HeLa-CCM cells only SERPINA1 knockdown showed reproducible reduction of MHV infection (Figure 2, right panel). However, SERPINA1 knockdown enhanced virus infection in the primary screen. Knockdown of other genes had no significant effect for the majority of siRNAs tested. Contradicting phenotypes by individual siRNAs against the same target gene were observed for SERPINs and when using bispecific Ela2A/B oligos. The siRNA validation screen gave a similar result if HeLaCCM cells were inoculated with recombinant MHV carrying the normal S protein of MHV-A59 (data not shown) or if the period of siRNA knockdown was reduced to 48 h (data not shown). In summary, the results of our validation screen did not reproduce the hits from the primary screen. The tested siRNAs often showed only

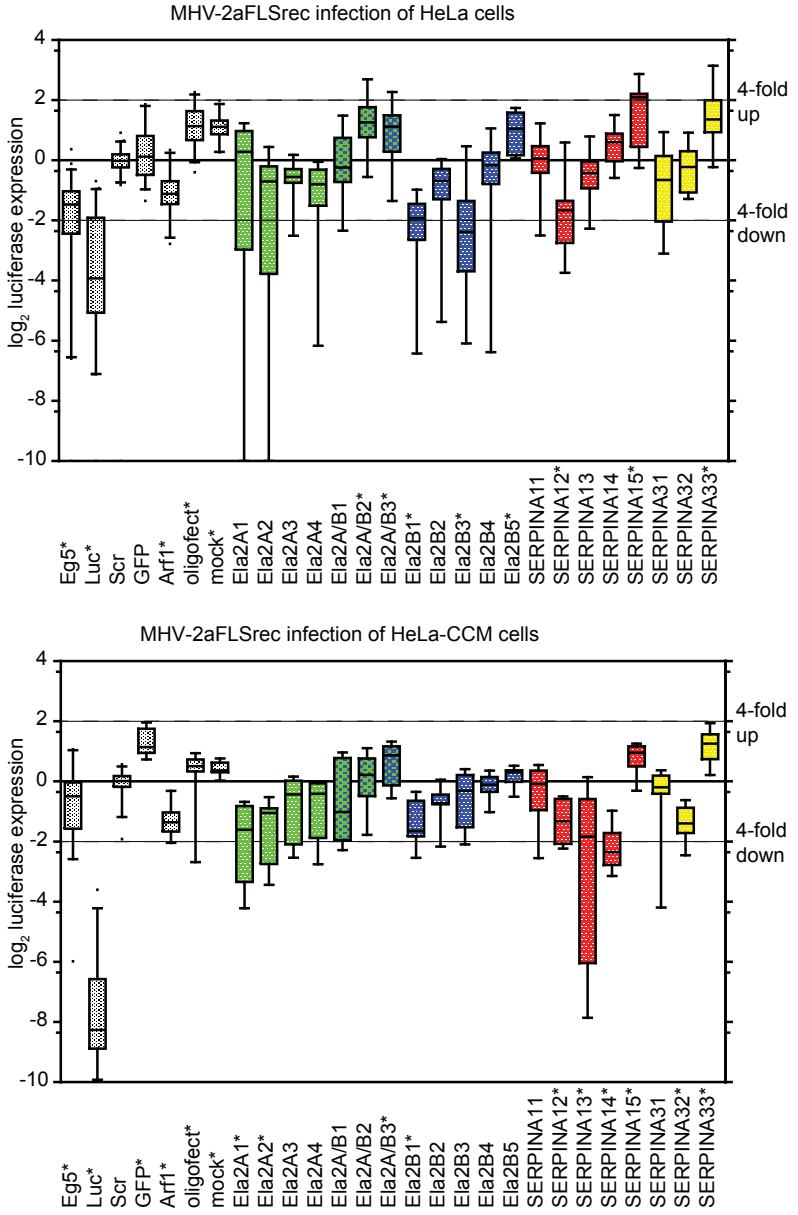

Fig. 2 Effects of siRNAs targeting the serine proteases elastase 2A and 2B (Ela2A, Ela2B) and serine protease inhibitor clade A SERPINA1 and SERPINA3 genes on MHV infection. Transfection with individual siRNA (details in Table 1), mock transfection (oligofect) or no treatment (mock) of HeLa or HeLa-CCM cells was performed for each experiment in triplicate. Candidate genes were targeted by at least three unique siRNA. After 72 h, cells were inoculated with MHV-2aFLSrec and the cell viability was determined at 6.5 h post infection (p.i.) by Wst1 reagent. At 7 h p.i. MHV replication was determined by measuring luciferase activity in cell lysates. Luciferase counts were reduced by cellular background, corrected for cell viability and normalized to non-targeting scrambled control siRNA (Scr). Boxes with whiskers showing the 95% confidence interval are plotted and samples with p-value <0.05 compared to Scr control according to Dunnett's statistical test are marked with asterisks. The bispecific siRNA Ela2A/B(1-3) target the Ela2A and Ela2B gene. Experiment was repeated five times on HeLa and three times on HeLa-CCM cells.

insignificant effects on MHV infection if compared to the untreated control. Furthermore, the effect amongst siRNAs targeting the same gene was inconsistent.

To confirm the specific knockdown of Ela2A/B mRNA after siRNA transfection, we performed semiquantitative real-time PCR (qRT-PCR). First, cellular RNA was purified and mRNA was either reverse-transcribed before qRT-PCR with oligo(dT) primers (two-step protocol) or a one-step qRT-PCR protocol was used that contains a cDNA synthesis step. Real-time PCR kits were based on non-specific fluorochromes for detection (Sybr Green) and successfully detected the housekeeping genes human glyceraldehyde 3-phosphate dehydrogenase (GAPDH, high expression) and human hydroxymethyl-bilane synthase (HMBS, low expression (34)) in human HeLa cells and murine LR7 cells (data not shown). However, we failed to detect endogenous levels of Ela2A and Ela2B mRNA (data not shown). As a positive control for the qRT-PCR assay, the full length Ela2A and 2B genes with a C-terminal Strep-Tag were cloned into eukaryotic expression vectors. After transient expression of Ela2A/B genes in HeLa cells, mRNA was successfully detected by qRT-PCR.

Overexpression of putative entry effectors

Parallel to the siRNA knockdown, we followed a complementary approach to assess the role of Ela2A/B or SERPINA1/A3 in MHV entry. We hypothesized that if the Ela2B protease activates MHV S protein, its transient expression in target cells may have an enhancing effect on MHV infection whereas SERPIN overexpression may diminish MHV infection. In addition, since SARS-CoV has been shown to be activated by transmembrane protease serine 2 (TMPRSS2), we also tested the effect of TMPRSS2 overexpression for enhancement of MHV infection (35). Genes encoding Ela2A, Ela2B, SERPINA1, and SERPINA3, each provided with a C-terminal Strep tag II encoding sequence (Ela2BST, Ela2AST, SERPINA1ST, and SERPINA3ST), as well as genes encoding human TMPRSS2 and murine transmembrane protease serine 4 (TMPRSS4), or the control genes encoding biotin protein ligase (BirA), GFP, or a Strep-tagged, soluble influenza virus hemagglutinin (sHAST) were cloned into eukaryotic expression vectors and transiently transfected into HeLa or HeLaCCM cells. Approximately 30% of cells became transfected as judged by the percentage of GFP-positive cells after transfection with a GFP-encoding plasmid. To confirm the expression of proteins, cell culture supernatants were analyzed by western blot using a mouse monoclonal anti-Strep tag antibody. The expression and secretion of Ela2BST (calculated MW = 34 kDa), Ela2AST (34 kDa), SERPINA1ST (52 kDa), and SERPINA3ST (53 kDa) were confirmed (Figure 3A). Also sHAST was detected in the supernatant, whereas we observed no background bands in culture supernatants of BirA and GFP gene transfected cells. Next, transfected HeLa-CCM and HeLa cells were inoculated with recombinant CCM-dependent MHV-2aFLS or CCM-independent MHV2aFLSrec, respectively, by adding the inoculum without removing the cell culture supernatants containing the secretory proteins. Three hours post infection (p.i.) the inoculum was replaced by fresh culture medium supplemented with 5 µM HR2 peptide – a potent inhibitor of MHV fusion – to prevent further infection and syncytia formation. Incubation was continued until 6.5 h p.i. before MHV infection was determined by measuring intracellular luciferase expression. HeLa and HeLa-CCM cells infected with MHV2aFLSrec and MHV-2aFLS, respectively, showed a clear increase in luciferase expression (Figure 3B and 3C, respectively). However, expression of recombinant proteases or protease inhibitor proteins had no effect on MHV infection in comparison to BirA expressing control cells.

Protease inhibitor sensitivity of MHV infection

Although we could not confirm a role of elastase in MHV infection, a proteolytic cleavage event is generally thought to be required for coronavirus entry. Therefore, we aimed to identify the class of proteases which is responsible for MHV S protein activation by testing MHV entry for susceptibility to broad spectrum protease inhibitors. One hour prior to inoculation with MHV-2aFLS (MOI = 0.1), LR7 cells were pretreated with lysosomotropic ammonium chloride (NH_4Cl), the cysteine protease inhibitor E64d, the metalloprotease inhibitor phosphoramidon, the aspartyl protease inhibitor pepstatin A, or the serine protease inhibitor AEBSF at the maximum and minimum concentration recommended for use in cell culture by the manufacturer (Sigma INHIB1). Inoculation was performed in

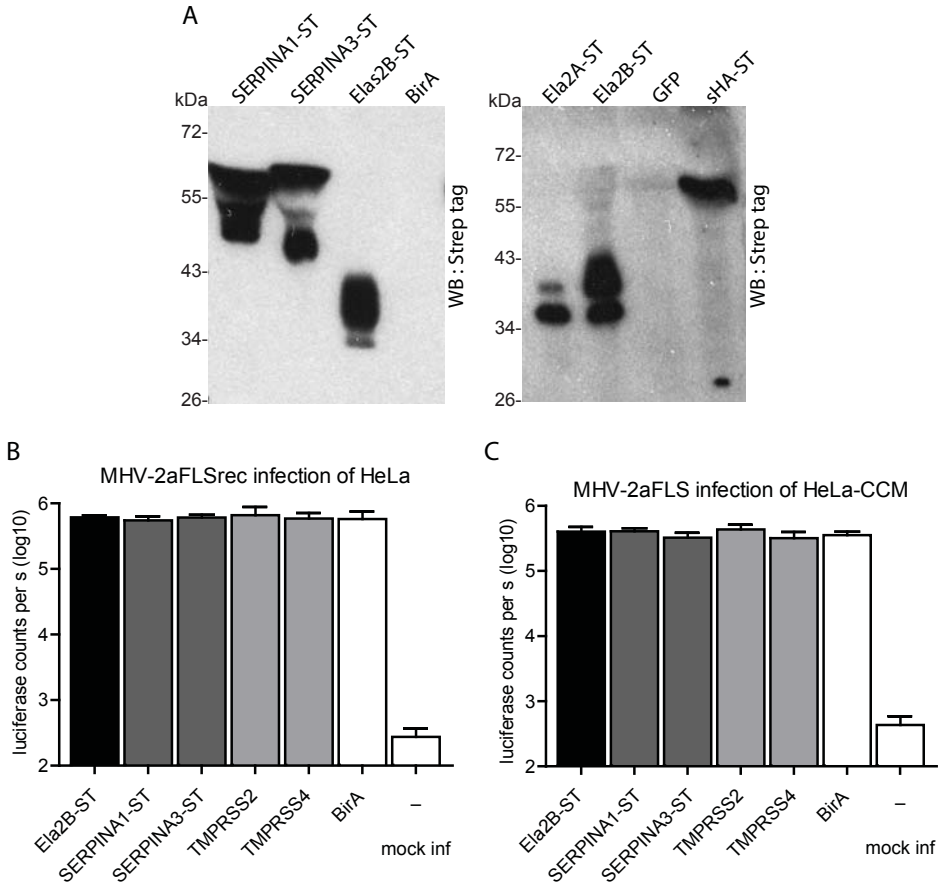

Fig. 3 Effect of overexpression of proteases and SERPIN protease inhibitors on MHV infection.
(A) Strep-tagged (ST) Ela2A-ST, Ela2B-ST, SERPINA1-ST, SERPINA3-ST, and influenza virus hemagglutinin (sHA-ST), as well as non-tagged GFP and protein biotin ligase (BirA) were transiently expressed in HeLa cells. Cell culture supernatants were analyzed by western blot and stained with a monoclonal antibody against ST.
(B) HeLa cells expressing Ela2B-ST, SERPINA1-ST, SERPINA3-ST, as well as non-tagged BirA, type II transmembrane serine proteases TMPRSS2 or TMPRSS4 were transiently expressed in HeLa cells or left untreated ( ). At 48 h after transfection, cells were inoculated with MHV-2aFLSrec for 6.5 h or left uninfected (mock inf) and MHV infection was determined by measuring luciferase activity in cell lysates. (C) Same as B but HeLa-CCM were inoculated with MHV-2aFLS.

the presence of protease inhibitors. At 4 h p.i. HR2 peptide (5 µM) was added to the cell culture supernatant to prevent cell-cell fusion. After 7 h, MHV infection was determined by measuring intracellular luciferase expression. A robust MHV infection was observed in the absence of protease inhibitors. Supplementation of NH_4Cl, a known agent to inhibit MHV infection, reduced luciferase expression by >10-fold (Figure 4A). The protease inhibitors pepstatin A, E64d, and phosphoramidon had no effect, but addition of AEBSF reduced MHV infection by approximately 500-fold at 1 mM and 0.1 mM concentrations.

Quantification of infection relies on expression of the luciferase reporter gene, but live cells as well as MHV replication are dependent on the function of proteases and may suffer

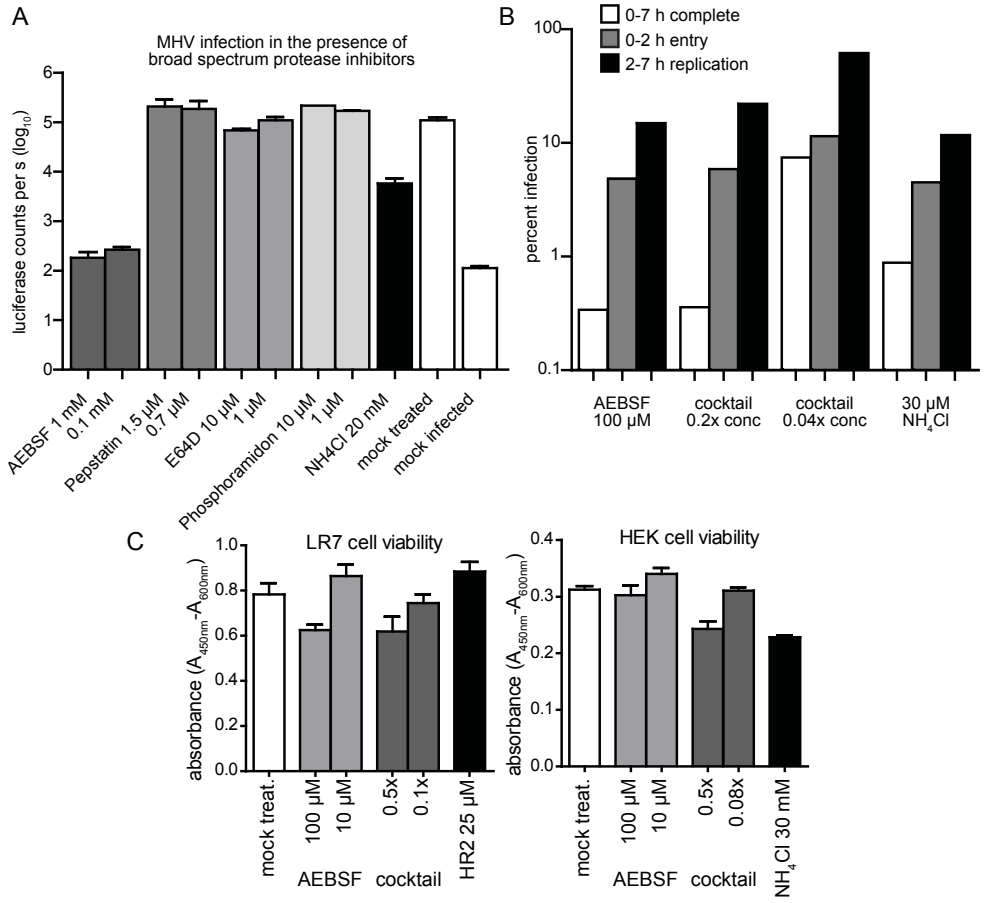

Fig. 4 Inhibition of MHV infection by protease inhibitors. (A) LR7 cells were pretreated with AEBSF, pepstatin A, E64d, phosphoramidon, or NH4Cl for 1 h or left untreated (mock treated). Cells were subsequently inoculated with MHV-2aFLS in the presence of compounds, or left uninfected (mock infected). At 7 h p.i. MHV infection was determined by measuring luciferase activity in cell lysates. (B) Cell culture supernatant was supplemented with AEBSF, NH4Cl, and an inhibitor cocktail or left untreated (100% infection) either from the start of inoculation until cell lysis (0 to 7 h), during inoculation (0 to 2 h), or during replication phase only (2 to 7 h). LR7 cells were inoculated with MHV-ERLM for 2 h before replenishing the medium. At 7 h p.i. MHV infection was determined by measuring luciferase activity in cell lysates and expressed as percent of untreated infection. (C) LR7 and HEK cells were incubated with AEBSF, an inhibitor cocktail, NH4Cl, peptidic MHV fusion inhibitor HR2 or left untreated. After 8 h, cell viability was measured by Wst-1 assay according to the manufacturer's protocol.

from off target effects by the inhibitors. To distinguish between effects on MHV entry versus replication, AEBSF, a commercially available broad spectrum protease inhibitor mixture (Roche complete mini) or NH_4Cl were applied either over the entire infection period (0 to7 h), during the entry (0 to 2 h) or the replication (2 to 7 h) phase of MHV infection. The inhibitor cocktail is meant for protease inhibition in cell lysates. It was toxic at 1x concentration and resulted in rounding up and detachment of cells, hence we used it at lower concentration. HeLa-CCM cells were inoculated with MHV-A59 carrying a Renilla luciferase (RL) reporter gene between the E and M gene (MHV-ERLM), infection was measured by a luciferase assay and presented relative to mock treated samples. The inhibitor cocktail at 0.04x concentration reduced the infection when present during the entry phase or throughout the experiment (Figure 4B). It no effect was observed if added only during replication phase. The supplementation of AEBSF, NH_4Cl and inhibitor cocktail at 0.2x concentration reduced infectivity by more than 100-fold when treatment was done from the 0 to 7 h.

It also inhibited MHV infection up to 10-fold when applied during replication only (2 to 7 h). However, the application of inhibitors from 0 to 2 h p.i. decreased infection by over 10-fold, indicative of an effect of protease inhibitors on MHV entry. We note that one representative experiment is depicted, but a similar outcome was observed for virus infections at an MOI of 0.5 or 0.02 as well as if infection was quantified after 10 h of infection. Moreover, the serine and thiol protease inhibitor leupeptin (100 μM) and the serine protease inhibitor camostat (1 mM) were tested, but they had no effect on MHV infection (data not shown).

Our experiments indicated that AEBSF and the inhibitor cocktail can block MHV entry, but also cause off-target effects or cytotoxicity. Although off-target effects are difficult to identify and measure, cell viability can be determined to assess a compound's impact on the metabolic state of cells. Colorimetric Wst1 reagent was used to quantify proliferation and viability of live LR7 or HEK-293T cells after 8 h of treatment with AEBSF, inhibitor cocktail, ammonium chloride or HR2 fusion inhibitor. LR7 cell viability was reduced in the presence of 100 μM AEBSF and 0.5x concentrated inhibitor cocktail, while lower inhibitor concentrations and HR2 peptide had little or no effect, respectively (Figure 4C). In general HEK-293T cells were less affected by the compounds, but 0.5x concentrated inhibitor cocktail and ammonium chloride reduced the cell viability as well.

Protease inhibitors block fusion of pseudo-particles carrying MHV S or VSV G protein

Virus entry can be addressed independently of coronavirus-specific replication by using Moloney murine leukemia virus (MLV)-based pseudo-particles. Entry of pseudo-particles depends on the fusion protein of choice that is incorporated into the retroviral envelope. After fusion, genomic integration of a retroviral transfer vector drives expression of a firefly luciferase reporter gene. Pseudo-particles were produced in HEK-293T cells and pseudotyped with the MHV S protein (MLV-S) or no fusion protein (MLV-Null). Full length MHV S protein

Recombinant S protein	Furin cleavage site	Furin cleavage
MHV-S	RRAHR	+/-
MHV-S^{-FCS}	RRAHS	-
MHV-S^{+FCS}	RRARR	+
Minimal FCS	RXXR	+/-

Table 2. Site directed mutagenesis of the furin cleavage site (FCS) in MHV S protein. The genuine MHV S protein S1/S2 junction contains a minimal FCS, causing the cleavage of a proportion of S proteins that are incorporated into pseudo-particles. Expression plasmids were generated for S protein with single amino acid substitutions, resulting in a destroyed furin cleavage site (MHV-S^{-FCS}) or a dual furin cleavage site (MHV-S^{+FCS}).

(S_0) and S protein that was cleaved at the authentic furin cleavage site (FCS) located at the S1/S2 junction (S2) were detected in MLV-S preparations. The FCS in the S protein was modified by site directed mutagenesis of the S gene. Substitution of the arginine residue at the P1 position by serine destroys the FCS (Table 2) and results in entirely uncleaved S proteins that can also be incorporated into MLV-S^{FCS}. An S protein carrying a dual FCS (S^{+FCS}), created by substituting the histidine at the P2 position by an arginine, could not be incorporated into

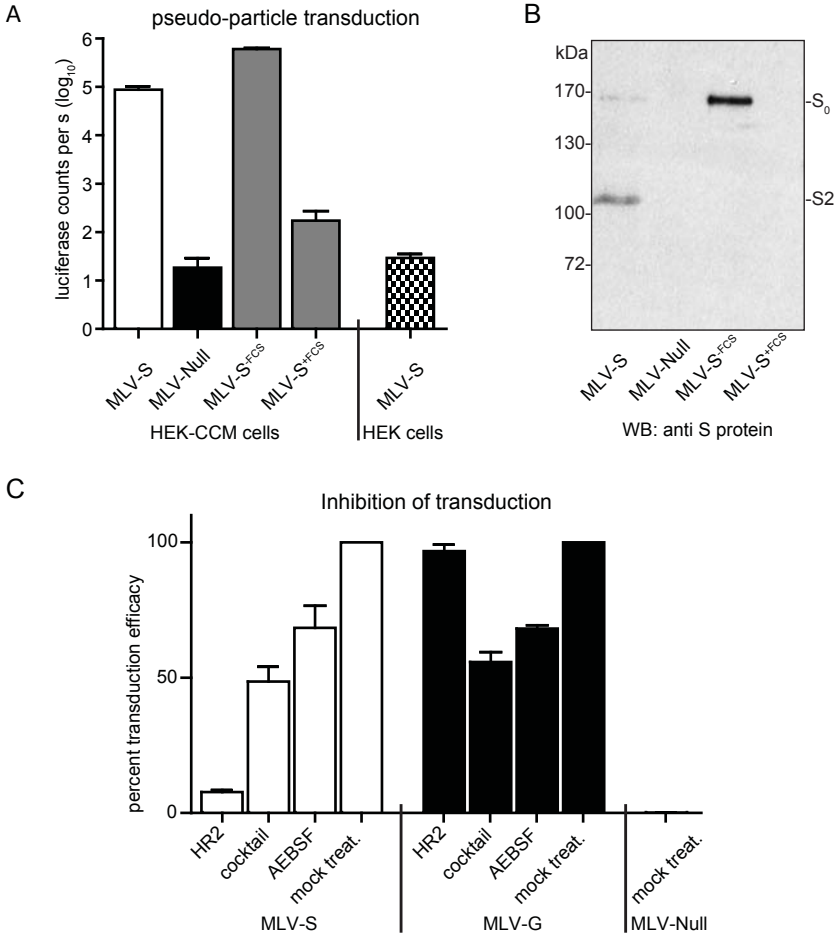

Fig. 5 Studying virus fusion characteristics using pseudo-particles. A) Retrovirus based pseudo-particles (MLV-Null) were pseudotyped with wild-type MHV S protein (MLV-S), MHV S protein containing a knockout of the furin cleavage site (MLV-S-FCS) or MHV S protein harboring a dual furin cleavage site (MLV-S+FCS). Amino acid substitutions at the furin cleavage site are shown in Table 2. MLV pseudo-particles were produced in HEK-293T cells and used for transduction of HEK-CCM or HEK cells. 24 h later, transduction efficacy was determined by measuring luciferase activity in cell lysates. (B) Pseudotyped MLV was pelleted through a 20% sucrose cushion and analyzed by western blot using monoclonal anti-MHV S protein antibody (10G). Position of the full-length S protein (S0) and S protein cleaved at the furin cleavage site (S2) are indicated. (C) HEK-CCM cells were transduced (mock treat.) with MLV-S, MLV-Null, and MLV pseudotyped with vesicular stromatitis virus G fusion protein (MLV G) or transduced in the presence of MHV-specific peptidic fusion inhibitor HR2 (16.6 µM), cocktail protease inhibitor (0.25x concentrated), and AEBSF (100 µM). Transduction efficiency was determined as described for A and expressed relative to the mock treated control (set to 100%).

pseudo-particles. Non-purified pseudo-particle preparations were used to transduce HEK-293T cells or HEK-293T cells stably expressing the MHV receptor molecule (HEK-CCM (24)). Firefly luciferase expression was allowed for 1 day before determining the transduction efficiency by measuring intracellular luciferase expression. MLV pseudotyped with MHV S proteins specifically transduced HEKCCM cells but not HEK-293T cells, whereas MLV-Null and MLVS^{+FCS}, lacking fusion protein incorporation, failed to transduce HEK-CCM cells (Figure 5A). Notably, average transduction mediated by S protein was approximately 100-fold or 10-fold less efficient compared to transduction by MLV pseudotyped with VSV G protein (MLV-G) or SARSCoV S protein, respectively (data not shown). Supernatants containing pseudo-particles were harvested at day 4, concentrated by sedimentation through a 20% sucrose cushion and analyzed by western blotting using a mouse monoclonal anti-S2 (10G) antibody (36)(Figure 5B).

Since integration and expression of firefly luciferase is independent on the fusion protein, we can compare the effect of protease inhibitors on the MHV S protein versus vesicular stomatitis virus (VSV) G protein mediated pseudo-particle-cell fusion, the latter being protease independent (2). Effects of AEBSF and protease inhibitor cocktail on the transduction efficiency of MLV-S and MLV pseudotyped with the VSV G protein (MLV-G) were compared. The application of AEBSF and inhibitor cocktail equally reduced the transduction efficiency of MLVS and MLV-G to approximately 50% (Figure 5C). In contrast, the MHV inhibitor HR2 selectively blocks transduction of MLVS but not MLVG. In summary, no specific effect of AEBSF and the inhibitor cocktail on MLV transduction mediated by the MHV S protein was observed.

Discussion

The details of functional activation of MHV S protein have remained elusive, but are believed to depend on proteases of the target cell by analogy to S proteins of other coronaviruses. We studied whether the chymotrypsin-like serine protease elastase 2B (Ela2B) and serine proteinase inhibitor clade A (SERPINA1), two candidate genes identified in a primary siRNA-based screen for MHV host factors, play a role in MHV-A59 S protein activation. We aimed to reproduce and rescue their siRNA knockdown phenotype on MHV infection. In addition to the siRNAs used in the primary screen, we ordered siRNA's from alternative suppliers. They were chosen to individually target different mRNA regions in the genes to avoid systematic misinterpretation of the results due to siRNA design, siRNA preparations and off-targeting (37). A number of individual siRNA knockdowns showed a significant effect on MHV infection, but the phenotype was either not consistent amongst multiple siRNAs targeting the same gene and/or less than half of the tested siRNAs targeting the same gene resulted in a phenotype. Hence, we could not draw a thorough conclusion from the validation screen and could not reproduce the primary screen results. Notably, the control siRNAs targeting luciferase, Arf1, and Eg5 did show the anticipated phenotypes and verified that setup and execution of the assay were suited to verify siRNA hits. For example, Arf1 knockdown is known to diminish MHV infection and we could reproduce that phenotype in our screen (33). We were unable to detect endogenous mRNA levels of Ela2A/B in HeLa cells. Since the same HeLa cell clone was used in the primary screen, the Ela2B and SERPINA1 knock down phenotypes for MHV infected cells are most likely

false positive hits. Indeed, low levels of Ela2A/B mRNA in HeLa cells were only detected in approximately 1/3 of the microarray data deposited at gene expression omnibus (http://www.ncbi.nlm.nih.gov/geo/) and Ela2A/B are not amongst the expressed sequence tags for humans in the MEROPS database (38). The Human Protein Atlas does not report expression of Ela2A, Ela2B, SERPINA1 or SERPINA3 in HeLa cells based on the lack of mRNA transcript (39). In contrast to neutrophil elastase (gene symbol ELANE, formally ELA2), Ela2A/B are mainly expressed in pancreatic tissue (18, 39).

The discrepancy between the results of the primary screen and the present study may be multifactorial. RNAi is a technically challenging method and small variations in the experimental procedure, type of readout, quality of compounds and variations in biological material can alter results. To compensate, a large number of measurements is required. This paragraph will exemplify some aspects with respect to our study and the development of RNAi technology at large. The primary large-scale MHV screen was examined by automated image acquisition and single cell analysis. Infection was scored by measuring GFP fluorescence intensities using a threshold above which a cell was counted as infected. In contrast, the luciferase assay used for validation was based on a cell population-based readout. Hence, the luciferase assay is independent from the subcellular distribution of luciferase and siRNA knockdown stimulated changes are easier to detect in a cell population (40). Like all 'omics' approaches, large scale siRNA screens also have an inherent rate of false-negative and false-positive results (41). For example, three genome-wide siRNA screens for HIV host factors identified only 3 to 6% overlapping genes (42). The development of RNAi techniques initially focused on the optimization of siRNA libraries to reduce off-target effects and on technical automation in screening facilities (43). Today, the field has advanced and computational data analysis, data integration and high-content screening make the tools even more powerful which has led to many successful discoveries (44). New technology can correct for false results, making recent studies more accurate, but it may cause variation to previous outcomes. The primary MHV screen was also re-analyzed by high-content algorithms, integrating the cell state parameters like cell cycle phase or cell size and the cell's microenvironment considering local cell density (45-47). A second assessment of primary screen data that integrates current knowledge about MHV infection determinants may help to identify false positive or negative samples in the future and increase sensitivity (48).

To investigate the role of the primary siRNA screen hit candidates Ela2B and SERPINA1 as well as to validate the primary results, we tested the involvement of Ela2B and SERPINA1 by overexpression in parallel. siRNA knockdowns can be further validated by rescuing the siRNA target gene knockdown either by co-expression of a RNAi resistant version or by transient overexpression (37). Although the overexpression and secretion of the recombinant proteases and SERPIN could be demonstrated by western blot, they had no influence on virus infection. Since SERPINs and elastase are secretory proteins, we expected them to function on the entire cell population, despite our inability to transfect all cells. In addition, we expressed TMPRSS2 and TMPRSS4, two out of 16 members from the transmembrane serine protease family, but could not observe effects on MHV infection either, although the transfection rate and expression efficiency may have been insufficient to observe significant effects. The expression of cellular proteases can have a stimulating effect on virus entry as is exemplified by TMPRSS2, which was reported to support entry of influenza A virus, SARS-CoV, and others (35, 49). The influenza virus hemagglutinin and SARS-CoV S protein

become fusion-ready by TMPRSS2 cleavage and the availability of TMPRSS2 has been correlated with the tropism of the viruses (50, 51). In contrast, MHV-A59 infection in cell culture does not rely on Ela2A, Ela2B, TMPRSS2 or TMPRSS4. MHV receptor expression is sufficient to render HeLa and Vero cells susceptible, two cell types that are often used for propagation of viruses and lack endogenous expression of TMRSS2 and TMPRSS4 (39, 52, 53). Nevertheless, proteolytic processing of S proteins occurs and is probably carried out by alternative proteases ((24)). We did not test the enzymatic activity of the proteases or the inhibitory capacity of the SERPINs on ELA activity after overexpression. Elastases are chymotrypsin-like proteases that naturally occur in blood serum and are produced by various cell types (54). Despite the presence of potential elastase inhibitors like the alpha-1-antitrypsin SERPINA1 in blood serum, elastase activity is maintained and was associated with artherosclerosis (55, 56). Since we cultured our cells in medium containing FBS, we cannot exclude that overexpressed proteases were readily inactivated by inhibitors present in the serum. Nervertheless, MHV is not relying on Ela2A or Ela2B for productive infection, hence another protease must be activating the MHV S protein for fusion.

Many cellular proteases that are necessary for virus entry have been identified by studying the effects of protease inhibitors on virus infections. We performed virus infection in the presence of broad spectrum protease inhibitors. AEBSF - a compound with inhibition constants similar to PMSF and with higher bioavailability - reduced MHV infection. AEBSF blocks serine proteases including elastase (57), trypsin, thrombin and plasmin (58). By differentiating the timing of protease inhibitor addition during MHV infection, we could detect an inhibitory effect of AEBSF on MHV entry; however, the compound also affected viral replication. To circumvent interference of the inhibitor with MHV replication and consequently reporter gene expression, we made use of retroviral pseudo-particles. MLV based particles were pseudotyped with SARS-CoV S protein in previous studies and here we demonstrate that pseudotyping can be achieved with MHV S protein as well (59). The G protein of vesicular stomatitis virus - a class III fusion protein - mediates membrane fusion independent of a proteolytic cleavage event. By comparison of MHV S protein to VSV G protein mediated entry, no selective effect of AEBSF or an inhibitor cocktail on MHV S protein mediated entry was observed. In summary, we could not find a protease inhibitor that specifically blocked MHV entry, although inhibitors against the major classes of proteases were tested: cysteine, serine, aspartic and metallo-proteases, but not threonine proteases which are mainly found in the archaea and bacteria and account for only 21 of the approximately 500 expressed protease genes of human cells (60, 61). Confirming earlier studies, we found MHV infection to be independent of the protease inhibitors E64d, leupeptin (62), as well as cathepsin L and B inhibitors (9, 63), and extended the list by AEBSF, phosphoramindon, pepstatin A, and camostat.

We previously performed a conditional biotinylation assay, which enabled isolation and characterization of the S proteins of virions after accomplishing membrane fusion with the target cell. We demonstrated that MHV S proteins that are part of fusing virions are indeed cleaved during virus entry (24). The cleavage product showed a remarkable variation in the molecular weight of the deglycosylated membrane-anchored subunit. This led us to hypothesize that proteolytic processing of MHV-A59 S protein may not occur at a precise position but that cleavage has to occur in a certain region of the protein: further C-terminal than the S1/S2 junction but upstream of the fusion peptide. A panel of protease inhibitors

failed to block the cleavage of MHV-A59 S proteins after endocytosis in these studies. In combination with the protease inhibitors tested here, we support the hypothesis that MHV S protein may not have a strict requirement for a specific protease or cleavage site. Rather, proteolytic processing may well be a redundant process that can be achieved by a range of proteases with multiple cleavage specificities at various functional cleavage sites. As long as cleavage is performed within a certain critical range MHV becomes fusion-ready, allowing the virus to fuse under varying conditions as it infects different cell types in natural infections. This is in contrast to other CoV such as SARS-CoV, MHV-2, and PEDV that rely on the activity of specific proteases for virus entry in vitro such as cathepsin L or exogenous trypsin.

References

1. Harrison SC. 2008. Viral membrane fusion. Nature structural & molecular biology 15:690-698.
2. White JM, Delos SE, Brecher M, Schornberg K. 2008. Structures and mechanisms of viral membrane fusion proteins: multiple variations on a common theme. Critical reviews in biochemistry and molecular biology 43:189-219.
3. Belouzard S, Millet JK, Licitra BN, Whittaker GR. 2012. Mechanisms of coronavirus cell entry mediated by the viral spike protein. Viruses 4:1011-1033.
4. Matsuyama S, Ujike M, Morikawa S, Tashiro M, Taguchi F. 2005. Protease-mediated enhancement of severe acute respiratory syndrome coronavirus infection. Proceedings of the National Academy of Sciences of the United States of America 102:12543-12547.
5. Yamada Y, Liu DX. 2009. Proteolytic activation of the spike protein at a novel RRRR/S motif is implicated in furin-dependent entry, syncytium formation, and infectivity of coronavirus infectious bronchitis virus in cultured cells. Journal of virology 83:8744-8758.
6. Regan AD, Shraybman R, Cohen RD, Whittaker GR. 2008. Differential role for low pH and cathepsin-mediated cleavage of the viral spike protein during entry of serotype II feline coronaviruses. Veterinary microbiology 132:235-248.
7. Kawase M, Shirato K, Matsuyama S, Taguchi F. 2009. Protease-mediated entry via the endosome of human coronavirus 229E. Journal of virology 83:712-721.
8. Simmons G, Gosalia DN, Rennekamp AJ, Reeves JD, Diamond SL, Bates P. 2005. Inhibitors of cathepsin L prevent severe acute respiratory syndrome coronavirus entry. Proceedings of the National Academy of Sciences of the United States of America 102:11876-11881.
9. Qiu Z, Hingley ST, Simmons G, Yu C, Das Sarma J, Bates P, Weiss SR. 2006. Endosomal proteolysis by cathepsins is necessary for murine coronavirus mouse hepatitis virus type 2 spike-mediated entry. Journal of virology 80:5768-5776.
10. Belouzard S, Chu VC, Whittaker GR. 2009. Activation of the SARS coronavirus spike protein via sequential proteolytic cleavage at two distinct sites. Proceedings of the National Academy of Sciences of the United States of America 106:5871-5876.
11. Matsuyama S, Taguchi F. 2009. Two-step conformational changes in a coronavirus envelope glycoprotein mediated by receptor binding and proteolysis. Journal of virology 83:11133-11141.
12. Kawase M, Shirato K, van der Hoek L, Taguchi F, Matsuyama S. 2012. Simultaneous treatment of human bronchial epithelial cells with serine and cysteine protease inhibitors prevents severe acute respiratory syndrome coronavirus entry. Journal of virology 86:6537-6545.
13. Huang IC, Bosch BJ, Li F, Li W, Lee KH, Ghiran S, Vasilieva N, Dermody TS, Harrison SC, Dormitzer PR, Farzan M, Rottier PJ, Choe H. 2006. SARS coronavirus, but not human coronavirus NL63, utilizes cathepsin L to infect ACE2-expressing cells. The Journal of biological chemistry 281:3198-3203.
14. Sturman LS, Ricard CS, Holmes KV. 1985. Proteolytic cleavage of the E2 glycoprotein of murine coronavirus: activation of cell-fusing activity of virions by trypsin and separation of two different 90K cleavage fragments. Journal of virology 56:904-911.
15. Bos EC, Luytjes W, Spaan WJ. 1997. The function of the spike protein of mouse hepatitis virus strain A59 can be studied on virus-like particles: cleavage is not required for infectivity. Journal of virology 71:9427-9433.
16. de Haan CA, Stadler K, Godeke GJ, Bosch BJ, Rottier PJ. 2004. Cleavage inhibition of the murine coronavirus spike protein by a furin-like enzyme affects cell-cell but not virus-cell fusion. Journal of virology 78:6048-6054.
17. Gombold JL, Hingley ST, Weiss SR. 1993. Fusion-defective mutants of mouse hepatitis virus A59 contain a mutation in the spike protein cleavage signal. Journal of virology 67:4504-4512.
18. Kawashima I, Tani T, Shimoda K, Takiguchi Y. 1987. Characterization of pancreatic elastase II cDNAs: two elastase II mRNAs are expressed in human pancreas. DNA (Mary Ann Liebert, Inc.) 6:163-172.
19. Mansuy-Aubert V, Zhou QL, Xie X, Gong Z, Huang

JY, Khan AR, Aubert G, Candelaria K, Thomas S, Shin DJ, Booth S, Baig SM, Bilal A, Hwang D, Zhang H, Lovell-Badge R, Smith SR, Awan FR, Jiang ZY. 2013. Imbalance between neutrophil elastase and its inhibitor alpha1-antitrypsin in obesity alters insulin sensitivity, inflammation, and energy expenditure. Cell metabolism 17:534-548.

20. El-Akawi ZJ, Al-Hindawi FK, Bashir NA. 2008. Alpha-1 antitrypsin (alpha1-AT) plasma levels in lung, prostate and breast cancer patients. Neuro endocrinology letters 29:482-484.
21. Abboud RT, Nelson TN, Jung B, Mattman A. 2011. Alpha1-antitrypsin deficiency: a clinical-genetic overview. The application of clinical genetics 4:55-65.
22. Belouzard S, Madu I, Whittaker GR. 2010. Elastase-mediated activation of the severe acute respiratory syndrome coronavirus spike protein at discrete sites within the S2 domain. The Journal of biological chemistry 285:22758-22763.
23. Kuo L, Godeke GJ, Raamsman MJ, Masters PS, Rottier PJ. 2000. Retargeting of coronavirus by substitution of the spike glycoprotein ectodomain: crossing the host cell species barrier. Journal of virology 74:1393-1406.
24. Wicht O, Burkard C, de Haan CA, van Kuppeveld FJ, Rottier PJ, Bosch BJ. 2014. Identification and Characterization of a Proteolytically Primed Form of the Murine Coronavirus Spike Proteins after Fusion with the Target Cell. Journal of virology.
25. de Haan CA, Haijema BJ, Boss D, Heuts FW, Rottier PJ. 2005. Coronaviruses as vectors: stability of foreign gene expression. Journal of virology 79:12742-12751.
26. Schickli JH, Zelus BD, Wentworth DE, Sawicki SG, Holmes KV. 1997. The murine coronavirus mouse hepatitis virus strain A59 from persistently infected murine cells exhibits an extended host range. Journal of virology 71:9499-9507.
27. de Haan CA, van Genne L, Stoop JN, Volders H, Rottier PJ. 2003. Coronaviruses as vectors: position dependence of foreign gene expression. Journal of virology 77:11312-11323.
28. Mechold U, Gilbert C, Ogryzko V. 2005. Codon optimization of the BirA enzyme gene leads to higher expression and an improved efficiency of biotinylation of target proteins in mammalian cells. Journal of biotechnology 116:245-249.
29. Bosch BJ, Bodewes R, de Vries RP, Kreijtz JH, Bartelink W, van Amerongen G, Rimmelzwaan GF, de Haan CA, Osterhaus AD, Rottier PJ. 2010. Recombinant soluble, multimeric HA and NA exhibit distinctive types of protection against pandemic swine-origin 2009 A(H1N1) influenza virus infection in ferrets. Journal of virology 84:10366-10374.
30. Laemmli UK. 1970. Cleavage of structural proteins during the assembly of the head of bacteriophage T4. Nature 227:680-685.
31. de Haan CA, Li Z, te Lintelo E, Bosch BJ, Haijema BJ, Rottier PJ. 2005. Murine coronavirus with an extended host range uses heparan sulfate as an entry receptor. Journal of virology 79:14451-14456.
32. Blangy A, Lane HA, d'Herin P, Harper M, Kress M, Nigg EA. 1995. Phosphorylation by p34cdc2 regulates spindle association of human Eg5, a kinesin-related motor essential for bipolar spindle formation in vivo. Cell 83:1159-1169.
33. Verheije MH, Raaben M, Mari M, Te Lintelo EG, Reggiori F, van Kuppeveld FJ, Rottier PJ, de Haan CA. 2008. Mouse hepatitis coronavirus RNA replication depends on GBF1-mediated ARF1 activation. PLoS pathogens 4:e1000088.
34. Vazquez-Blomquist D, Fernandez JR, Miranda J, Bello C, Silva JA, Estrada RC, Novoa LI, Palenzuela D, Bello I. 2012. Selection of reference genes for use in quantitative reverse transcription PCR assays when using interferons in U87MG. Molecular biology reports 39:11167-11175.
35. Matsuyama S, Nagata N, Shirato K, Kawase M, Takeda M, Taguchi F. 2010. Efficient activation of the severe acute respiratory syndrome coronavirus spike protein by the transmembrane protease TMPRSS2. Journal of virology 84:12658-12664.
36. Taguchi F, Shimazaki YK. 2000. Functional analysis of an epitope in the S2 subunit of the murine coronavirus spike protein: involvement in fusion activity. The Journal of general virology 81:2867-2871.
37. Echeverri CJ, Beachy PA, Baum B, Boutros M, Buchholz F, Chanda SK, Downward J, Ellenberg J, Fraser AG, Hacohen N, Hahn WC, Jackson AL, Kiger A, Linsley PS, Lum L, Ma Y, Mathey-Prevot B, Root DE, Sabatini DM, Taipale J, Perrimon N, Bernards R. 2006. Minimizing the risk of reporting false positives in large-scale RNAi screens. Nat Meth 3:777-779.
38. Rawlings ND, Barrett AJ, Bateman A. 2012. MEROPS: the database of proteolytic enzymes, their substrates and inhibitors. Nucleic acids research 40:D343-350.
39. Uhlen M, Oksvold P, Fagerberg L, Lundberg E, Jonasson K, Forsberg M, Zwahlen M, Kampf C, Wester K, Hober S, Wernerus H, Bjorling L, Ponten F. 2010. Towards a knowledge-based Human Protein Atlas. Nature biotechnology 28:1248-1250.
40. Moffat J, Sabatini DM. 2006. Building mammalian signalling pathways with RNAi screens. Nature reviews. Molecular cell biology 7:177-187.
41. Boutros M, Ahringer J. 2008. The art and design of genetic screens: RNA interference. Nature reviews. Genetics 9:554-566.
42. Bushman FD, Malani N, Fernandes J, D'Orso I, Cagney G, Diamond TL, Zhou H, Hazuda DJ, Espeseth AS, Konig R, Bandyopadhyay S, Ideker T, Goff SP, Krogan NJ, Frankel AD, Young JA, Chanda SK. 2009. Host cell factors in HIV replication: meta-analysis of genome-wide studies. PLoS pathogens 5:e1000437.
43. Pei Y, Tuschl T. 2006. On the art of identifying effective and specific siRNAs. Nature methods 3:670-676.
44. Brodin P, Christophe T. 2011. High-content screening in infectious diseases. Current opinion in chemical biology 15:534-539.
45. Snijder B, Sacher R, Ramo P, Damm EM, Liberali P, Pelkmans L. 2009. Population context determines

cell-to-cell variability in endocytosis and virus infection. Nature 461:520-523.

46. Raj A, van Oudenaarden A. 2008. Nature, nurture, or chance: stochastic gene expression and its consequences. Cell 135:216-226.
47. Snijder B, Sacher R, Ramo P, Liberali P, Mench K, Wolfrum N, Burleigh L, Scott CC, Verheije MH, Mercer J, Moese S, Heger T, Theusner K, Jurgeit A, Lamparter D, Balistreri G, Schelhaas M, De Haan CA, Marjomaki V, Hyypia T, Rottier PJ, Sodeik B, Marsh M, Gruenberg J, Amara A, Greber U, Helenius A, Pelkmans L. 2012. Single-cell analysis of population context advances RNAi screening at multiple levels. Molecular systems biology 8:579.
48. Knapp B, Rebhan I, Kumar A, Matula P, Kiani NA, Binder M, Erfle H, Rohr K, Eils R, Bartenschlager R, Kaderali L. 2011. Normalizing for individual cell population context in the analysis of high-content cellular screens. BMC bioinformatics 12:485.
49. Bottcher E, Matrosovich T, Beyerle M, Klenk HD, Garten W, Matrosovich M. 2006. Proteolytic activation of influenza viruses by serine proteases TMPRSS2 and HAT from human airway epithelium. Journal of virology 80:9896-9898.
50. Bertram S, Heurich A, Lavender H, Gierer S, Danisch S, Perin P, Lucas JM, Nelson PS, Pohlmann S, Soilleux EJ. 2012. Influenza and SARS-coronavirus activating proteases TMPRSS2 and HAT are expressed at multiple sites in human respiratory and gastrointestinal tracts. PloS one 7:e35876.
51. Hatesuer B, Bertram S, Mehnert N, Bahgat MM, Nelson PS, Pohlman S, Schughart K. 2013. Tmprss2 Is Essential for Influenza H1N1 Virus Pathogenesis in Mice. PLoS pathogens 9:e1003774.
52. Shirato K, Kawase M, Matsuyama S. 2013. Middle East respiratory syndrome coronavirus infection mediated by the transmembrane serine protease TMPRSS2. Journal of virology 87:12552-12561.
53. Bertram S, Glowacka I, Blazejewska P, Soilleux E, Allen P, Danisch S, Steffen I, Choi SY, Park Y, Schneider H, Schughart K, Pohlmann S. 2010. TMPRSS2 and TMPRSS4 facilitate trypsin-independent spread of influenza virus in Caco-2 cells. Journal of virology 84:10016-10025.
54. Zureik M, Robert L, Courbon D, Touboul PJ, Bizbiz L, Ducimetiere P. 2002. Serum elastase activity, serum elastase inhibitors, and occurrence of carotid atherosclerotic plaques: the Etude sur le Vieillissement Arteriel (EVA) study. Circulation 105:2638-2645.
55. Bauman SJ, Whinna HC, Church FC. 2002. Serpins (serine protease inhibitors). Current protocols in protein science / editorial board, John E. Coligan ... [et al.] Chapter 21:Unit 21 27.
56. Garcia-Touchard A, Henry TD, Sangiorgi G, Spagnoli LG, Mauriello A, Conover C, Schwartz RS. 2005. Extracellular proteases in atherosclerosis and restenosis. Arteriosclerosis, thrombosis, and vascular biology 25:1119-1127.
57. Wen W, Moses MA, Wiederschain D, Arbiser JL, Folkman J. 1999. The generation of endostatin is mediated by elastase. Cancer research 59:6052-6056.
58. Hedstrom L. 2002. An overview of serine proteases. Current protocols in protein science / editorial board, John E. Coligan ... [et al.] Chapter 21:Unit 21 10.
59. Giroglou T, Cinatl J, Jr., Rabenau H, Drosten C, Schwalbe H, Doerr HW, von Laer D. 2004. Retroviral vectors pseudotyped with severe acute respiratory syndrome coronavirus S protein. Journal of virology 78:9007-9015.
60. Powers JC, Asgian JL, Ekici OD, James KE. 2002. Irreversible inhibitors of serine, cysteine, and threonine proteases. Chemical reviews 102:4639-4750.
61. Lopez-Otin C, Bond JS. 2008. Proteases: multifunctional enzymes in life and disease. The Journal of biological chemistry 283:30433-30437.
62. Eifart P, Ludwig K, Bottcher C, de Haan CA, Rottier PJ, Korte T, Herrmann A. 2007. Role of endocytosis and low pH in murine hepatitis virus strain A59 cell entry. Journal of virology 81:10758-10768.
63. Zhou H, Perlman S. 2006. Preferential infection of mature dendritic cells by mouse hepatitis virus strain JHM. Journal of virology 80:2506-2514.

Chapter 4

Manipulation of the porcine epidemic diarrhea virus genome using targeted RNA recombination

Chunhua Li[1], Zhen Li[1], Yong Zou[1], Oliver Wicht[2], Frank J.M. van Kuppeveld[2], Peter J.M. Rottier[2] and Berend Jan Bosch[2]

[1] Institute of Animal Science and Veterinary Medicine, Shanghai Academy of Agricultural Sciences, Shanghai, P.R. China

[2] Department of Infectious Diseases and Immunology, Virology Division, Faculty of Veterinary Medicine, Utrecht University, Utrecht, The Netherlands

PLoS One. 2013 Aug 2;8(8):e69997

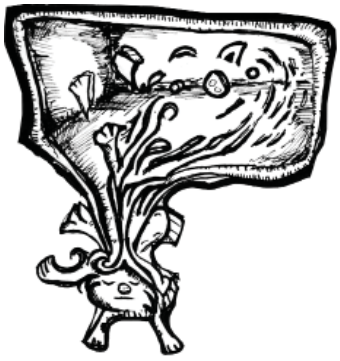

Abstract

Porcine epidemic diarrhea virus (PEDV) causes severe economic losses in the swine industry in China and other Asian countries. Infection usually leads to an acute, often lethal diarrhea in piglets. Despite the impact of the disease, no system is yet available to manipulate the viral genome which has severely hampered research on this virus until today. We have established a reverse genetics system for PEDV based on targeted RNA recombination that allows the modification of the 3´-end of the viral genome, which encodes the structural proteins and the ORF3 protein. Using this system, we deleted the ORF3 gene entirely from the viral genome and showed that the ORF3 protein is not essential for replication of the virus *in vitro*. In addition, we inserted heterologous genes (*i.e.* the GFP and *Renilla* luciferase genes) at two positions in the viral genome, either as an extra expression cassette or as a replacement for the ORF3 gene. We demonstrated the expression of both GFP and *Renilla* luciferase as well as the application of these viruses by establishing a convenient and rapid virus neutralization assay. The new PEDV reverse genetics system will enable functional studies of the structural proteins and the accessory ORF3 protein and will allow the rational design and development of next generation PEDV vaccines.

Introduction

Porcine epidemic diarrhea virus (PEDV) causes diarrhea and dehydration in newborn piglets. The virus infects the epithelial cells of the small intestine resulting in severe mucosal atrophy and consequent malabsorption. PEDV is common and the cause of serious problems, particularly in pigs in Asia. The disease usually appears in winter during which it can cause high fatalities in suckling piglets (see for a recent review (1)). From 2010, an outbreak of PEDV has swept China with over 1 million fatalities among newborn piglets causing substantial economic losses in the swine industry (2). The characteristics of the infection and its epidemiology were quite dramatic with morbidity and fatality approaching 100% in one-week old piglets, despite the use of commercial, inactivated vaccines. Virus transmission occurs via the fecal-oral route and possibly also by vertical transmission through lactation (2). Currently there is no efficient way of treatment of the disease. Prevention of the infection usually relies on vaccination with cell culture adapted live-attenuated or inactivated viruses although the efficacy of current vaccines has been questioned (2, 3).

PEDV belongs to the alphacoronavirus genus within the *Coronavirinae* subfamily of the *Coronaviridae* family. Coronaviruses are important pathogens of concern for human and animal health. They occur in almost any species, usually causing respiratory or intestinal infections. Interest in these viruses has increased significantly as a result of the SARS epidemic in 2002 and 2003. Coronaviruses are enveloped viruses and possess a positive-sense RNA genome ranging from 26 to 32 kilobases, which is the largest viral RNA genome known (Fig.1A). The 5' two-third of the viral genome contains two large open reading frames (ORFs), 1a and 1b, which encode two non-structural polyproteins, pp1a and pp1ab, that direct genome replication and transcription. The remaining part of the genome contains ORFs specifying structural and non-structural proteins. They are expressed via a 3'-terminal nested set of subgenomic messenger RNAs, the transcription of which is regulated by conserved six-nucleotides transcription-regulating sequences (TRSs; in PEDV XUA(A/G)AC (4)). These subgenomic mRNAs encode at least four structural proteins, three membrane anchored proteins called the spike (S), membrane (M) and envelope (E) protein, and the nucleocapsid (N) protein that encapsidates the genomic RNA. The non-structural proteins expressed from the subgenomic mRNAs encode one or more accessory proteins, which are specific for each coronavirus genus. The genome structures of alphacoronaviruses including PEDV and related members such as the human coronavirus (hCoV) strains 229E and NL63 show the typical set of essential core genes but they share only one accessory gene, ORF3, located between the S and the E gene (Fig.1A). The PEDV ORF3 gene encodes a 224 amino acids (aa) long protein with three to four predicted transmembrane domains (5).

Entry of coronaviruses into their host cells is mediated by the approximately 200 kDa large S glycoprotein. Trimers of S form the characteristic spikes on the viral surface which interact with the host receptor and mediate membrane fusion. PEDV was reported to utilize the porcine aminopeptidase N as a receptor (6). Yet, PEDV is usually propagated in VERO cells, which are derived from the African green monkey kidney, indicating that PEDV can utilize non-porcine receptors for cell entry. Propagation of PEDV in cell culture requires addition of trypsin which is believed to prime or activate the S protein for membrane fusion during virus cell entry and syncytia formation (7). Recently it was demonstrated that trypsin cleavage may also play a role in detachment of the virus from infected cells (8). Interestingly, a cell

culture adapted strain was reported to replicate in the absence of trypsin (9), which suggests that the virus acquired mutations in the S protein conferring its trypsin-independence. The S protein also stimulates the induction of neutralizing antibodies and hence is an important target in developing effective vaccines.

Research on the molecular biology and pathogenicity of PEDV has been severely hampered by the lack of a reverse-genetic system. Here we report the first reverse genetic system for PEDV based on targeted RNA recombination. Establishment of the reverse genetic system included two stages (Fig.1B). One was the generation of the chimeric virus mPEDV, a PEDV derivative carrying spikes derived from the murine coronavirus mouse hepatitis virus (MHV), hence growing only in murine cells. In the second stage the mPEDV virus was used as a recipient virus to reintroduce the PEDV spike along with other genome alterations, *in casu* the deletion of the ORF3 gene or the insertion of foreign, reporter genes. The generated PEDV derivatives now carrying again PEDV spikes could be easily selected by their regained tropism for non-murine cells.

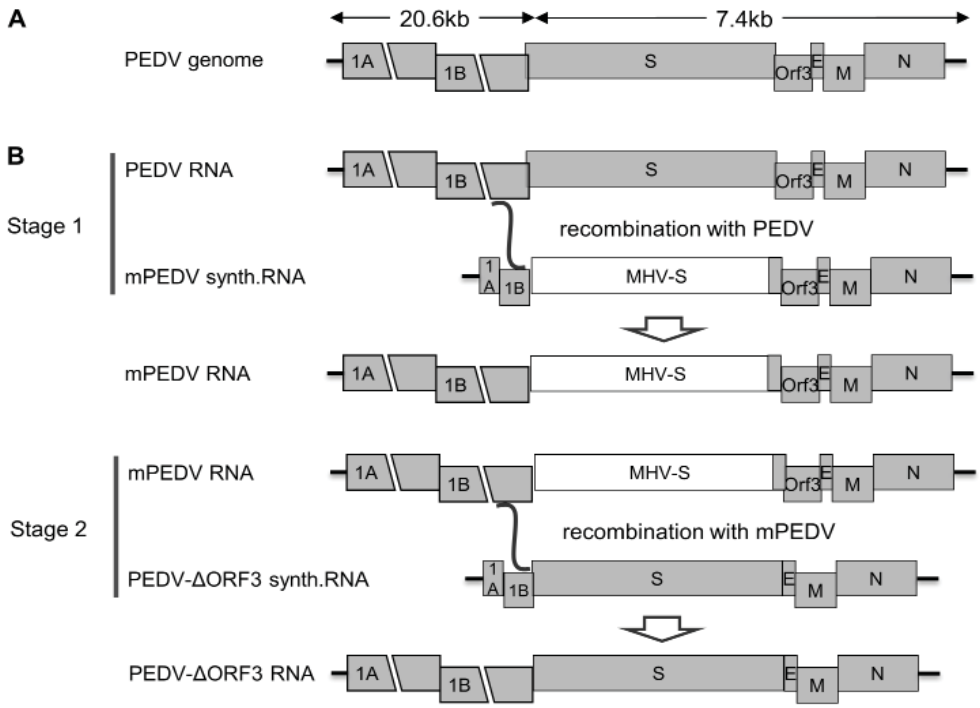

Fig.1 Coronavirus genome organization and targeted RNA recombination scheme. (A) Genomic organization of PEDV. (B) Targeted RNA recombination scheme to make the interspecies chimeric virus mPEDV (Stage 1) or recombinant PEDV derivatives e.g. lacking the ORF3 gene as shown here (Stage 2). The ectodomain-encoding region of the MHV S gene is shown as a light-grey box in the mPEDV genome. Synthetic RNAs transcribed from the transfer vectors (Fig.2A) were electroporated into PEDV (Stage 1) or mPEDV (Stage 2) infected cells, respectively. A single recombination event (indicated by a curved line) anywhere within the 3' region of ORF1b present in the donor RNA and viral genome generates a recombinant genome. Selection of recombinant progeny viruses against parental viruses was done on the basis of the acquired ability to form plaques in murine cell monolayers (Stage 1) or on the basis of the ability to infect VERO cells and the concomitantly lost ability to infect murine cells (Stage 2).

Materials and Methods

Cells, viruses and antibodies

L (12) and VERO CCL81 cells (purchased from ATCC) were maintained as monolayer cultures in Dulbecco's modified Eagle medium containing 10% fetal calf serum, 100 IU of penicillin/ml, and 100 µg of streptomycin/ml (all from Life Technologies, Ltd., Paisley, United Kingdom). PEDV (isolated from a commercial vaccine of GreenCross, South Korea) was propagated in Vero cells in the absence of trypsin. Virus was harvested by three cycles of freeze-thawing the infected cells and supernatant followed by removal of cell debris by centrifugation at 3,000 x *g* for 20 minutes. Virus infectivity in the supernatant was measured by an end-point dilution assay on VERO cells and 50% tissue culture infectious doses ($TCID_{50}$) were calculated. MHV (strain A59) was propagated in mouse L cells as described previously (12). The rabbit anti-MHV serum K135 raised against purified MHV has been described elsewhere (30). The monoclonal antibody (MAb) 3F12 recognizing the PEDV nucleocapsid protein was obtained from BioNote, Korea. Polyclonal PEDV serum from a pig experimentally infected with PEDV (strain CV777) was kindly provided by Dr. Kristin van Reeth (Gent University). PEDV antibody-negative control serum was obtained from a newborn piglet deprived of colostrum.

Construction of pPEDV transfer vector and derivatives

pPEDV vector. A cDNA clone encompassing the 3'-terminal 7,832 nt part of the PEDV genome starting within ORF1b was obtained by reverse transcription-PCR (RT-PCR) with viral genomic RNA isolated from virions as a template and primers 4922 and 4815 as plus- and minus-strand primers (for primer sequences see Table I), respectively. The overhang of primer 4922 and primer 4815 contained a *Bgl*II and a *Pac*I restriction site, respectively. The *Bgl*II-*Pac*I digested fragment was cloned into the *Bam*HI-*Pac*I digested pMH54 vector (12), creating the plasmid pPEDV-1b-3T. The 5´-terminal 605 nt of ORF1a was amplified using primers 4884 and 4885. Primer 4884 contains a T7 polymerase recognition site, as well as a *Bgl*II restriction site and primer 4885 contained a *Bam*HI restriction site. The *Bgl*II-*Bam*HI digested fragment was ligated into the *Bam*HI site of the pPEDV-1b-3T plasmid, resulting in the pPEDV vector.

p-rPEDV vector. A transfer vector was constructed in which the partly overlapping ORF1b and S gene were separated by introduction of a unique *Bam*HI site to facilitate further cloning. The stop codon of ORF1b was mutated to TAA to knock out the overlapping ATG start codon of the spike gene. First, the forward primer 5127 containing the *Bam*HI site and a TRS (TAAAC), and the reverse primer 4815 containing a unique *Pac*I site were used to amplify the 3´ proximal 7,332 nt of the PEDV genome starting with the spike gene. This fragment was cloned into the *Bam*HI-*Pac*I site of pMH54 vector, creating the pPEDV-S-3T vector. Second, primers 4884 and 4885 containing a *Bgl*II and *Bam*HI site, respectively, were used to RT-PCR amplify the ORF1a fragment which was introduced into the *Bam*HI digested pPEDV-S-3T vector creating the pPEDV-1a-S-3T plasmid. Third, primers 4922 and 4923 that contain a *Bgl*II and *Bam*HI in the overhang, respectively, were used to amplify the ORF1b fragment by RT-PCR. This fragment was cloned into the *Bam*HI site of the pPEDV-1a-S-3T vector, creating the p-rPEDV vector.

p-mPEDV vector. First, the plasmid pTUMS (31) encoding the MHV spike was used as an intermediate vector to construct a chimeric spike composed of the ectodomain of MHV and the transmembrane and cytoplasmic domain of PEDV. For the construction of the hybrid gene, a *Sty*I restriction site was used that is located in both S genes at the transition between the protein's ectodomain and transmembrane domain. The forward primer 4814 (*Sty*I site in overhang) and reverse primer 4924 (*Eag*I site in overhang) were used to amplify the 3' end of the PEDV S gene and downstream sequences and cloned into the *Sty*I-*Eag*I digested pTUMS plasmid, creating the pTUMS(MP) vector. Second, to create the p-mPEDV vector, the PEDV S gene in the p-rPEDV vector was replaced by the chimeric MHV-PEDV spike gene by cloning the *Bam*HI-*Pml*I digested fragment of pTUMS(MP) into the *Bam*HI-*Pml*I digested p-rPEDV vector.

pPEDV-ΔORF3 vector. Primers 5300 and 5301 were used to amplify the E gene and downstream sequences using the pPEDV vector as a template. The forward primer 5300 contained a *Pml*I and an *Eco*RV restriction site and the reverse primer 5301 contained an restriction *Eco*NI site to facilitate further cloning. The *Pml*I-*Eco*NI digested PCR fragment was cloned into the *Pml*I-*Eco*NI digested pPEDV vector to create the pPEDV-ΔORF3 vector.

pPEDV-RLuc and pPEDV-ΔORF3/RLuc vector. The *Renilla* luciferase gene was excised from the pRLnull vector (Promega) using enzymes *Nhe*I and *Xba*I, blunted with DNA-polymerase I large (Klenow) fragment and ligated into the *Bam*HI digested and blunted p-rPEDV vector or the *Eco*RV digested pPEDV-ΔORF3 vector, resulting in the pPEDV-RLuc and pPEDV-ΔORF3/RLuc transfer vector, respectively.

pPEDV-ΔORF3/GFP vector. The GFP gene was excised from the pEGFP-N1 plasmid (Clontech) with enzymes *Nco*I and *Not*I, blunted with DNA-polymerase I large (Klenow) fragment and ligated into the *Eco*RV digested pPEDV-ΔORF3 vector yielding the pPEDV-ΔORF3/GFP transfer vector.

The identity of all generated transfer vectors was verified by sequencing.

Targeted RNA recombination

A targeted recombination system was established for PEDV in a two-stage process as outlined in Fig.1B.

Stage 1 Generation of mPEDV: Introduction of the hybrid MHV-PEDV S gene into the PEDV genome by targeted RNA recombination was carried out essentially as described previously for MHV and FIPV (12, 13). Briefly, capped runoff donor RNA transcripts were synthesized from the *Pac*I-linearized p-mPEDV vector using a T7 RNA polymerase kit (Ambion) as specified by the manufacturer. Donor RNA was electroporated (Gene Pulser electroporation apparatus [Bio-Rad]; two consecutive pulses of 0.3 kV/975 µF) into PEDV-infected (multiplicity of infection [MOI] of 0.4) VERO cells (2×10^7 cells) at 8 hours post infection (p.i.). The electroporated cells were co-cultured in a 25-cm^2 flask with 5×10^6 murine L cells. After 48-60 h of incubation at 37°C, when syncytia could be detected in the murine L cells, progeny virus in the culture supernatant was harvested and mPEDV recombinant virus was purified by two consecutive cycles of plaque purification on L cells at 37°C.

Stage 2 Generation of recombinant PEDVs: The construction of PEDV recombinant viruses that had regained the PEDV S gene was carried out in a reverse process by using pPEDV-derived donor RNAs and mPEDV as the recipient virus. Capped runoff transcripts were synthesized from *Pac*I-linearized pPEDV, pPEDV-Rluc, pPEDV-ΔORF3, pPEDV-ΔORF3/Rluc, or

Table 1. Primers

Primer	Location[a] (nucleotides)	Sense	Sequence (5'-3')[b]
4535	S / 22164-22187	-	GCCGCAGAGACAGTAATATTAACA
4538	S / 23484-23507	+	GTATAGTGCGTCTCTCATCGGTGG
4814	S / 24603-24624	+	GTGG**CCTTGG**TGGGTTTGGTTG
4815	3'UTR / 28012-28033	-	GC**TTAATTAA**TTTTTTTTTGTGTATCCATATCAACACCGTC
4884	5'UTR / 1-25	+	GC**AGATCT**TAATACGACTCACTATAGGGACTTAAAAAGAT TTTCTATCTACGG
4885	1A / 584-605	-	**GGATCC**GAGCTCTAACTCTTCGAGGAAG
4886	1B / 20156-20176	+	**GGATCC**GAGAACGTGTCTAAAGAAGGC
4921	T7 / N.A.	+	GC**AGATCT**TAATACGACTCACTATAGGG
4922	1B / 20156-20173	+	GC**AGATCT**GAGAACGTGTCTAAAGAAGG
4923	1B / 20618-20649	-	GC**GGATCC**TTATTTGTTTACGTTGACCAAATG
4924	E / 25655-25674	-	GC**CGGCCG**AGATCTTTATATGTCAATAACAGTAC
4977	M / 25942-25962	-	ATTATCCACAGCATAAGAGTG
5109	1B / 20396-20416	+	GACGGCAACACCATGCATGCC
5127	S / 20629-20655	+	**GGATCC**GTAAACAAATGACGCCTTTAATTTAC
5300	E / 25403-25446	+	GGTC**CACGTG**CAGT**GATATC**ACTCAATTCAACTAGACGA GTATG
5301	N / 26458-26477	-	GCGAGTA**CCTTAGAAAGG**GG

a The location of primers is relative to the full genome sequence of the PEDV CV777 strain (GenBank accession No. AF353511).
b Endonuclease restriction sites used for cloning are indicated in bold.

pPEDV-ΔORF3/GFP, respectively, with a T7 RNA polymerase kit (Ambion) as specified by the manufacturer. The donor transcripts were electroporated (as specified above) into murine L cells (2×10^7 cells) that had been infected 4 h earlier with mPEDV (MOI = 1). These cells were then plated onto a monolayer of VERO cells. After 4-5 days of incubation at 37°C progeny virus in the culture supernatant was harvested by freeze-thawing and candidate recombinant viruses were purified by two rounds of end-point dilutions on VERO cells. Recombinant genotypes were confirmed by RT-PCR on purified genomic RNA and subsequent sequencing.

(Immuno)fluorescence microscopy

L cells and VERO cells were inoculated with MHV, mPEDV or PEDV (MOI = 0.05). After 2 hours of incubation the cells were washed with PBS and incubated in culture medium. At 6.5 hours p.i., the cells were rinsed with PBS and fixed with 3.7% formaldehyde for 20 min at room temperature. The cells were washed three times with PBS and incubated with the K135 rabbit-α-MHV serum and the 3F12 mouse MAb α-PEDV-N. After 30 min at room temperature, the cells were rinsed three times with PBS and stained with goat α-rabbit FITC-conjugated and donkey-α-mouse Cy3 conjugated secondary antibodies (Cappel). Nuclei were

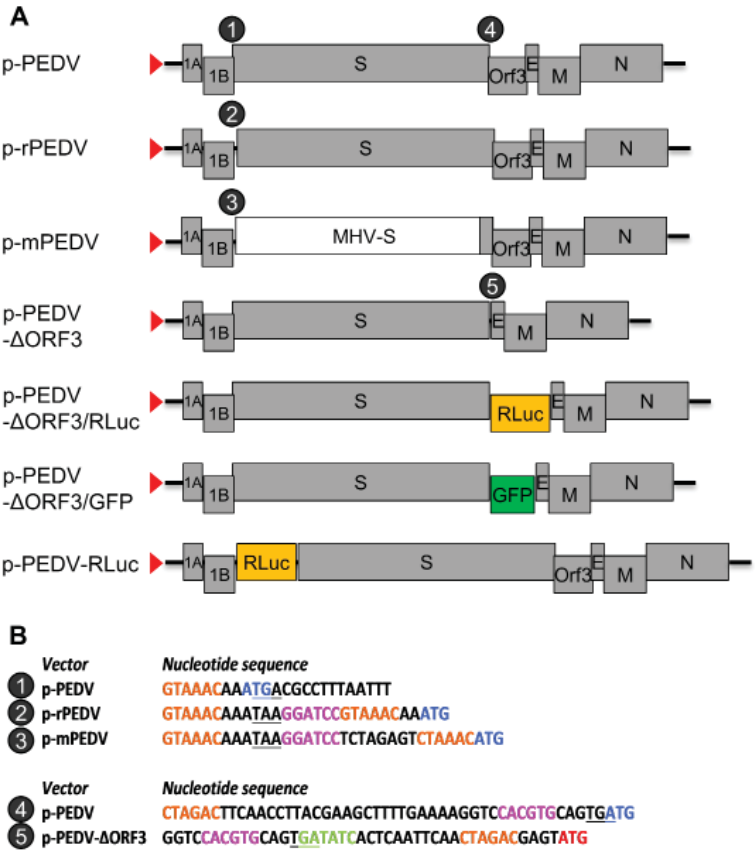

Fig.2 PEDV transfer vectors. (A) The pPEDV transfer vector contains the 5´-proximal 605 nt fused to the 3´ approximately 8 kilobases of the PEDV genome. All other vectors are derivatives thereof. The red triangle indicates the T7 promoter in the transfer vectors from which synthetic RNAs were made in vitro using T7 RNA polymerase. (B) Nucleotide sequences of junctions in the PEDV transfer vectors. Encircled numbers correspond to the numbered positions in the vector maps as indicated in Fig2A. (upper panel) The stop codon of ORF1b is underlined, the start codon of S is in blue, the transcription regulatory sequences (XUA(A/G)AC; (4)) are in orange and the BamHI site is indicated in purple. (lower panel) The stop codon of the S gene is underlined, the start codon of the ORF3 gene is in blue, the start codon of E gene is in red, the transcription regulatory sequences are in orange and the unique PmlI and EcoRV sites are indicated in purple and green, respectively.

stained with DAPI (Molecular Probes) for 10 min at room temperature. Finally, the cells were washed three times with PBS and fluorescence was viewed with an EVOS-fl fluorescence microscope (Advanced Microscopy Group) at 10x magnification. The EVOS-fl was also used to view GFP fluorescence from PEDV-ΔORF3/GFP infected cells after paraformaldehyde fixation.

Renilla luciferase assay

VERO cell monolayers were infected as described above with the PEDV-Rluc and PEDV-ΔORF3/Rluc viruses at indicated MOI's. At indicated times post infection, cell lysate samples were assayed for luciferase activity using the *Renilla* Luciferase Assay system (Promega)

according to the manufacturer's instructions, and the relative light units (RLU) were determined with a Berthold Centro LB 960 plate luminometer.

Virus neutralization assay

PEDV-ΔORF3/Rluc or PEDV-ΔORF3/GFP were mixed with serial dilutions of positive or negative piglet serum or with cell culture medium. The inoculum was incubated for 30 minutes at room temperature to allow virus neutralization before inoculating VERO cell monolayers as described above. Cells were either lysed at 8 hours post infection and assayed for *Renilla* luciferase activity as described above or subjected to fluorescence microscopy as described above at 9 hours post infection.

Results

To set up a targeted RNA recombination system for PEDV we first created a recombinant PEDV virus carrying MHV spikes (mPEDV). To this end a transfer vector p-mPEDV was construced (Fig.2A) that was composed of a 5'-terminal genomic cDNA fragment ligated to a cDNA representing the entire 3'-terminal part of the genome starting within ORF1b, except for the S gene. This gene was replaced by a hybrid gene encoding a chimeric S protein composed of the 1,263 aa long ectodomain from MHV S and the transmembrane domain plus cytoplasmic tail (61 aa) from PEDV S. RNA was transcribed from the T7 promotor of this vector and electroporated into PEDV-infected VERO cells after which the cells were overlaid onto a murine cell (L cells) monolayer. The recombinant mPEDV virus generated during subsequent incubation was cloned by two rounds of plaque selection on L cells.

The identity of purified mPEDV viruses was checked at a genetic level by RT-PCR sequencing of the ORF1b-S gene junction (data not shown) and at the protein level by an immunofluoresence assay (Fig.3A). All mPEDV infected cells stained positive both with the polyclonal MHV serum and with the monoclonal antibody directed against the PEDV nucleocapsid protein confirming the purity and the identity of the chimeric virus. In contrast to the parental virus, mPEDV displayed the ability to induce syncytia in the absence of trypsin (Fig.3A). As predicted, cell-cell fusion mediated by mPEDV could be inhibited by a MHV S specific, peptidic fusion inhibitor (Fig.3B).

The generated mPEDV virus was used as a recipient virus to reintroduce by similar procedures the PEDV spike along with other genome modifications by targeted RNA recombination. Candidate recombinant viruses carrying the PEDV spikes can be selected by their regained ability to replicate in VERO cells. Apart from the wild-type recombinant virus (r-wtPEDV) we aimed at constructing a virus lacking the ORF3 gene (PEDV-ΔORF3). A number of cell culture adapted viruses including the strain used in this study have each acquired during passaging an identical 51 nucleotide in-frame deletion in the ORF3 gene, giving rise to a 17 amino acid deletion (aa 82-98) in their ORF3 protein (10). We constructed a transfer vector (pPEDV-ΔORF3, Fig.2A) from which the entire ORF3 gene was deleted. Donor RNAs transcribed from the pPEDV and pPEDV-ΔORF3 transfer vectors were electroporated into mPEDV-infected L cells after which we were able to recover and purify the r-wtPEDV and PEDV-ΔORF3 viruses in VERO cells. RT-PCR analysis confirmed the intended loss of the ORF3 gene from the viral genome (Fig.4A) and the genetic identity of the ORF3 lacking virus was further verified by sequencing of the RT-PCR product (data not shown). The PEDV-ΔORF3

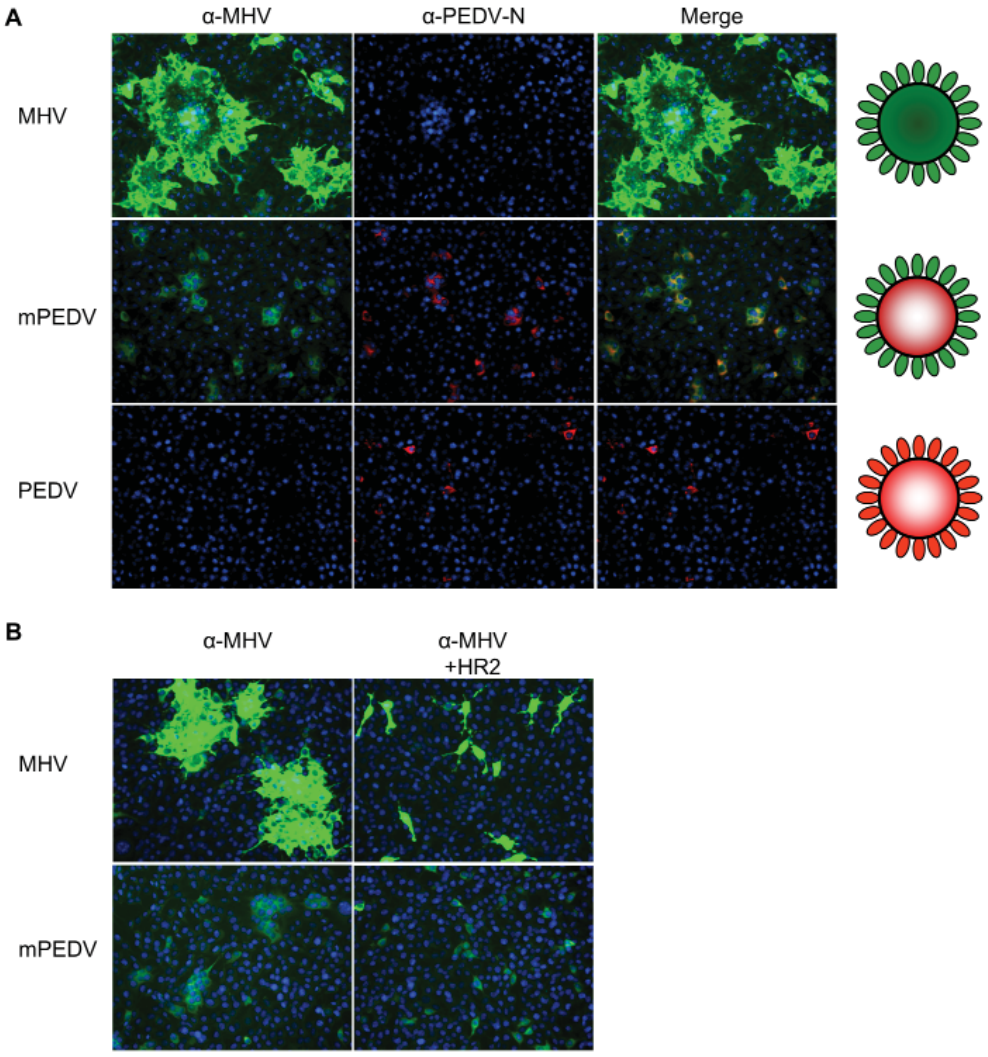

Fig.3 Characterization of a chimeric PEDV carrying MHV spikes. (A) Immunofluorescence analysis of mPEDV, MHV and PEDV infected cells. L cells infected with mPEDV were fixed and double immunolabeled with a polyclonal antibody against MHV (green) and a monoclonal antibody against the PEDV nucleocapsid (red). MHV and PEDV infected L cells were taken along for comparison. Nuclei are visualized with DAPI (blue). Overlay pictures (Merge) and graphical presentation of the MHV, mPEDV and PEDV virions are indicated at the right. Of note, the α-MHV fluorescence signal for MHV is significantly stronger than that for mPEDV due to the contribution of antibodies directed against other MHV proteins in the polyclonal MHV serum. (B) Inhibition of syncytia formation by the MHV-S HR2-peptide fusion inhibitor. HR2 peptide (4 μM; (32)) was added to MHV and mPEDV infected cells at 2 hours p.i. and kept present until 6.5 hours p.i. when cells were fixed and immunolabeled with the polyclonal MHV serum (green). Nuclei are visualized with DAPI (blue).

grew unimpaired in cell culture (Fig.4B), demonstrating that the ORF3 gene product is not required for virus propagation *in vitro*. In addition, the successful deletion of the ORF3 gene from the viral genome demonstrated the feasibility of the mPEDV-based targeted RNA recombination system to manipulate the 3´ end of the viral genome.

We next explored the possibilities of expressing heterologous proteins from the PEDV genome by inserting reporter genes at different genomic positions. Transfer vectors were made with the *Renilla* luciferase gene (936 nt) and the GFP gene (720 nt) at the position of ORF3, creating the pPEDV-ΔORF3/Rluc and pPEDV-ΔORF3/GFP vectors (Fig.2A). These marker genes are under the transcriptional control of the TRS of ORF3 (CTAGAC) which is located in the 3´end of the S gene, 46 nucleotides upstream of the ORF3 gene. The *Renilla* luciferase gene was also inserted as an extra expression cassette between the ORF1b and S gene, creating the pPEDV-Rluc vector. To this end the otherwise overlapping ORFs 1b and S were first separated and a unique *Bam*HI restriction site was introduced (p-rPEDV vector, Fig.2A and B), which did not hamper the generation of a viable virus (data not shown). The *Renilla* luciferase gene was subsequently cloned into the *Bam*HI site of the p-rPEDV vector under control of the TRS in ORF1B (GTAAAC) originally driving S gene expression, whereas the S gene was provided with a new TRS (GTAAAC; Fig.2B). The PEDV-ΔORF3/GFP, PEDV-ΔORF3/Rluc and PEDV-Rluc recombinant viruses were successfully recovered by the targeted RNA recombination procedure. RT-PCR analyses confirmed the insertion of both reporter genes at the intended positions (Fig.5A), which was further confirmed by sequencing.

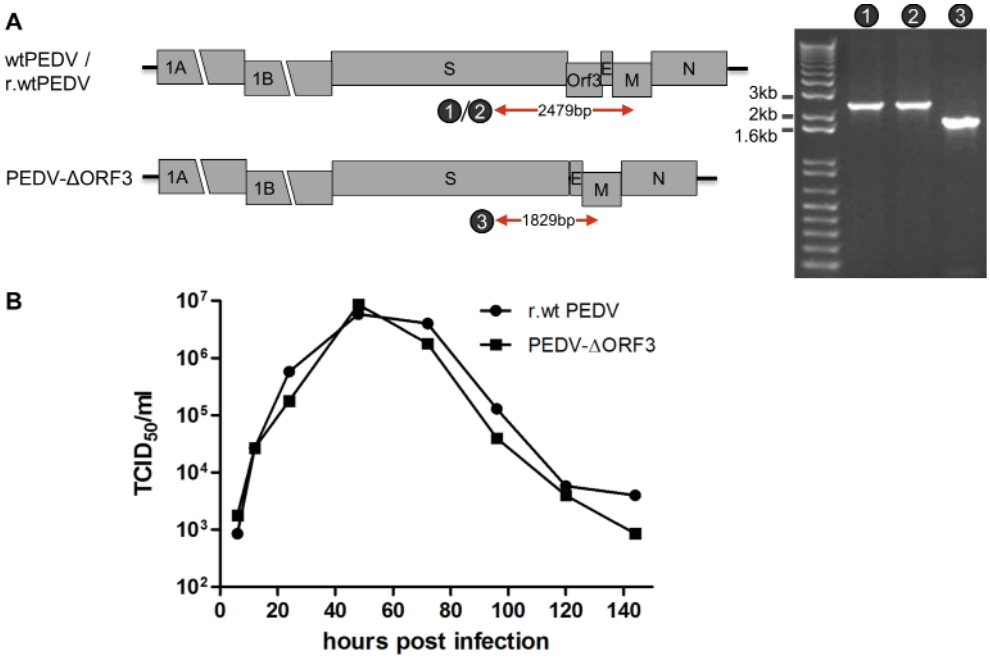

Fig.4 Characterization of a PEDV recombinant virus lacking ORF3. (A) Genetic analysis of PEDV-ΔORF3. RT-PCR was performed covering the S-ORF3-E-M region (primers 4538/4977) using RNA templates isolated from wtPEDV, r-wtPEDV and PEDV-ΔORF3, and analyzed by gel electrophoresis. The expected sizes of the RT-PCR products (numbered 1 to 3) are indicated in the genome maps. For primer sequences, see Table 1. (B) Multi-step growth kinetics of r-wtPEDV and PEDV-ΔORF3. VERO cells were infected with each recombinant PEDV (MOI=0.01), washed after three hours and viral infectivity in the culture media was determined at different times p.i. by a quantal assay on VERO cells from which TCID50 values were calculated.

We studied the luciferase expression by the 2 recombinant viruses carrying a Rluc gene as well as the expression kinetics of one of these viruses, PEDV-Rluc, upon infection of VERO cells at three different MOI's. The result shows (Fig.5B) that luciferase expression levels were linearly related to the MOI during the early phase of infection until 12 hours p.i. whereas at 24 hours p.i. luciferase values converged due to reinfections. Similar kinetics of luciferase expression, but to higher levels, was observed for the PEDV-ΔORF3/Rluc recombinant virus (Fig.5B). Next we studied the GFP expression of the PEDV-ΔORF3/GFP virus upon infection of VERO cells at two MOI's. GFP expression in PEDV-ΔORF3/GFP virus infected cells could be seen starting from 9 hours p.i. and became clearly evident at 12 hours p.i. (Fig.5C). The cell adapted PEDV DR13 p100 strain can propagate in the absence of trypsin in the growth medium but does not form syncytia when trypsin is absent. Yet the clustered appearance of GFP-positive cells suggests that the virus predominantly spreads locally from cell to cell which may correlate with the reported cell surface attachment of progeny viruses released from infected cells in the absence of trypsin (11).

The early detection of the luciferase and GFP reporter proteins during infection can be applied to develop a more rapid PEDV neutralization diagnostic test. The readout of the classical virus neutralization assay with wild-type PEDV is based on the visual inspection of cytopathic effect and can only be done after a multicycle infection which takes at least 2-3 days. Thus, the PEDV-ΔORF3/GFP and PEDV-ΔORF3/RLuc virus were preincubated with dilutions of serum obtained from an experimentally PEDV-infected pig and control serum, and the mixtures were subsequently added to VERO cells and incubated after which the GFP and *Renilla* luciferase expression was recorded at 9 and 6 hours p.i., respectively (Fig.5D). In contrast to the control serum, the PEDV antibody-positive serum was able to neutralize PEDV infection as reflected by the reduction of GFP positive cells and luciferase activity. The results demonstrate that neutralization of the PEDV-ΔORF3/GFP and PEDV-ΔORF3/RLuc virus can already be scored within a single replication cycle, thereby significantly speeding up the assay time. This type of assay is additionally preferred as it avoids the subjectivity that is associated with scoring of cytopathic effects.

Discussion

Here we describe the first reverse genetics system for PEDV. As we illustrate, this system now enables the manipulation of the 3´proximal ~8 kilobases of the PEDV genome including the structural protein genes. Generation of PEDV recombinants was based on the well-known high efficiency of RNA recombination of coronaviruses in combination with host cell tropism switching for selection of the recombinant viruses. Similar recombination systems have been successfully developed for MHV and FIPV coronaviruses by the Masters and Rottier laboratories (12, 13). For a number of coronaviruses genetic engineering of the full length genome has also become accomplished by the development of infectious cDNA clones (14-20). The ability to manipulate the PEDV genome will be extremely valuable to study the molecular and biological features of PEDV infections as well as to develop new tools and strategies for prevention and therapy of this important veterinary pathogen.

Unlike most other coronaviruses, the PEDV genome contains only a single accessory gene, the ORF3 gene, which encodes a multispanning 224-aa long membrane protein. Intriguingly,

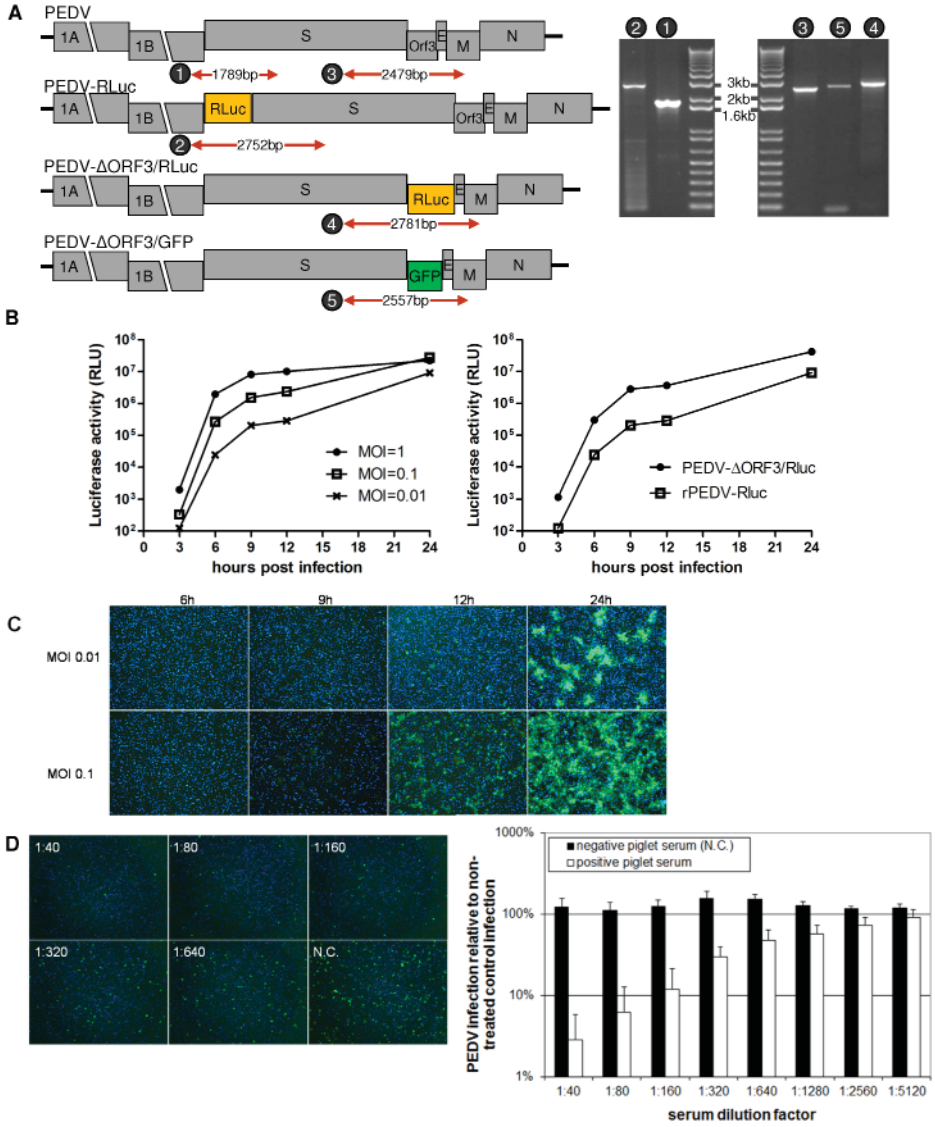

Fig.5 Recombinant PEDVs carrying Renilla luciferase and GFP genes. (A) Genetic analysis of recombinant viruses. RT-PCR was performed covering the 1b-S junction (primers 5109/4535) or the S-M region (primers 4538/4977) using RNA templates isolated from wild-type PEDV, PEDV-Rluc, PEDV-ΔORF3/Rluc or PEDV-ΔORF3/GFP, and analyzed by gel electrophoresis. The expected sizes of the RT-PCR products (numbered 1 to 5) are indicated in the genome maps. For primer sequences, see Table 1. (B) Luciferase expression by the recombinant PEDV-Rluc and PEDV-ΔORF3/Rluc viruses. Left panel: VERO cells were infected with PEDV-Rluc at an MOI of 0.01, 0.1 or 1. Right panel: VERO cells were infected with PEDV-Rluc and PEDV-ΔORF3/Rluc at an MOI of 0.01. Intracellular Renilla luciferase activity (y-axis; Relative Light Units [RLU]) was determined at different times postinfection. (C) GFP expression by the recombinant PEDV-ΔORF3/GFP virus. VERO cells were infected with PEDV-ΔORF3/GFP at an MOI of 0.01 or 0.1 and fluorescence images were taken at different times p.i.. Nuclei of cells were stained with DAPI (blue). (D) A rapid virus neutralization assay based on recombinant PEDVs expressing reporter proteins. PEDV-ΔORF3/Rluc and PEDV-ΔORF3/GFP (8,000 TCID50) were mixed with subsequent dilutions of serum positive for PEDV antibodies and a negative control serum (N.C.) for 30 minutes at room temperature. Mixtures were incubated with VERO cells and Renilla luciferase (left panel) or GFP (right panel) expression was measured at 8 and 9 hours p.i., respectively.

propagation of PEDV isolates in tissue culture cells readily leads to deletions within ORF3 suggesting a dispensable role, at least for the parts deleted from the ORF3 protein, for viral replication *in vitro*. In all these adapted viruses a shorter ORF3 gene product is still translated with a minimal size of 91 amino acids (10). The ORF3 gene of the cell-adapted DR13 vaccine strain (GenBank accession no.: JQ023162.1) employed in our study has a 49 nucleotide deletion compared to that of the parental DR13 virus (GenBank accession no.: JQ023161.1), but still encodes the N-terminal 81 residues long ORF3 protein part including the first transmembrane domain, after which it gets out of frame due to the deletion. The deletion of the entire ORF3 gene from the genome did not have any obvious effect on viral propagation *in vitro*, demonstrating that this ~ 10kD polypeptide does not serve an essential function during replication in culture cells.

The function of the PEDV ORF3 product remains enigmatic. Recently it was shown that the protein exhibits ion channel activity and modulates virus production (5). siRNA knockdown of ORF3 gene in PEDV infected cells reduced the number of particles released from the cells (5). The question remains here why passaging of PEDV in cell culture would lead to the functional loss of a gene beneficial for virus propagation *in vitro*, unless the 91-residue truncated protein still provides that function. Homologues of the ORF3 protein are found in all other alphacoronaviruses. The ORF3 protein of hCoV-NL63 was shown to be N-glycosylated at the amino terminus and incorporated into virions (21). Yet, deletion of the ORF3 gene from the viral genome had little effect on virus replication in cell culture (22). Like for PEDV, loss of ORF3 genes of the alphacoronaviruses TGEV and hCoV-229E (here named ORF4) is associated with unimpaired virus passaging in cell culture (23, 24). Despite a non-essential role in cell culture, the maintenance of the ORF3 gene in alphacoronavirus field isolates strongly points to an important role of the ORF3 protein in natural infection in the animal host. Consistently, the loss of virulence of life-attenuated PEDV vaccine strains has been associated with mutations in the ORF3 gene resulting from cell culture adaptation (10, 25) although a contribution of the numerous additionally acquired mutations in other genes such as the spike gene can obviously not be excluded (26, 27). The specific function of the ORF3 protein (and other viral proteins in the 3′ genome region) in PEDV replication and pathogenesis can now be further investigated using the reverse genetics system.

The introduction of foreign genes at different genomic positions without apparent great fitness loss of the virus *in vitro* (data not shown) once more illustrates the remarkable genome plasticity of the coronavirus genome (28, 29). The insertion of reporter genes like for GFP and luciferase will be very useful for the study of various molecular and virological aspects of PEDV infection. In addition, as we demonstrate here, these reporter properties may also be exploited for applications such as the establishment of convenient virus neutralization assays that provide answers within hours rather than days. Furthermore, genomic insertion of genes encoding foreign antigens using the reverse genetics system opens avenues to the development of PEDV as a vaccine vector for protection against other relevant porcine pathogens in addition to PEDV.

References

1. Song D, Park B. (2012) Porcine epidemic diarrhoea virus: A comprehensive review of molecular epidemiology, diagnosis, and vaccines. Virus Genes . 10.1007/s11262-012-0713-1.
2. Sun RQ, Cai RJ, Chen YQ, Liang PS, Chen DK, et al. (2012) Outbreak of porcine epidemic diarrhea in suckling piglets, china. Emerg Infect Dis 18: 161-163. 10.3201/eid1801.111259; 10.3201/eid1801.111259.
3. Park SJ, Kim HK, Song DS, Moon HJ, Park BK. (2011) Molecular characterization and phylogenetic analysis of porcine epidemic diarrhea virus (PEDV) field isolates in korea. Arch Virol 156: 577-585. 10.1007/s00705-010-0892-9.
4. Tobler K, Ackermann M. (1995) PEDV leader sequence and junction sites. Adv Exp Med Biol 380: 541-542.
5. Wang K, Lu W, Chen J, Xie S, Shi H, et al. (2012) PEDV ORF3 encodes an ion channel protein and regulates virus production. FEBS Lett 586: 384-391. 10.1016/j.febslet.2012.01.005.
6. Li BX, Ge JW, Li YJ. (2007) Porcine aminopeptidase N is a functional receptor for the PEDV coronavirus. Virology 365: 166-172. 10.1016/j.virol.2007.03.031.
7. Hofmann M, Wyler R. (1988) Propagation of the virus of porcine epidemic diarrhea in cell culture. J Clin Microbiol 26: 2235-2239.
8. Shirato K, Matsuyama S, Ujike M, Taguchi F. (2011) Role of proteases in the release of porcine epidemic diarrhea virus from infected cells. J Virol 85: 7872-7880. 10.1128/JVI.00464-11.
9. Kweon CH, Kwon BJ, Lee JG, Kwon GO, Kang YB. (1999) Derivation of attenuated porcine epidemic diarrhea virus (PEDV) as vaccine candidate. Vaccine 17: 2546-2553.
10. Park SJ, Moon HJ, Luo Y, Kim HK, Kim EM, et al. (2008) Cloning and further sequence analysis of the ORF3 gene of wild- and attenuated-type porcine epidemic diarrhea viruses. Virus Genes 36: 95-104. 10.1007/s11262-007-0164-2.
11. Shirato K, Maejima M, Hirai A, Ami Y, Takeyama N, et al. (2010) Enhanced cell fusion activity in porcine epidemic diarrhea virus adapted to suckling mice. Arch Virol 155: 1989-1995. 10.1007/s00705-010-0790-1.
12. Kuo L, Godeke GJ, Raamsman MJ, Masters PS, Rottier PJ. (2000) Retargeting of coronavirus by substitution of the spike glycoprotein ectodomain: Crossing the host cell species barrier. J Virol 74: 1393-1406.
13. Haijema BJ, Volders H, Rottier PJ. (2003) Switching species tropism: An effective way to manipulate the feline coronavirus genome. J Virol 77: 4528-4538.
14. Almazan F, Gonzalez JM, Penzes Z, Izeta A, Calvo E, et al. (2000) Engineering the largest RNA virus genome as an infectious bacterial artificial chromosome. Proc Natl Acad Sci U S A 97: 5516-5521.
15. Casais R, Thiel V, Siddell SG, Cavanagh D, Britton P. (2001) Reverse genetics system for the avian coronavirus infectious bronchitis virus. J Virol 75: 12359-12369. 10.1128/JVI.75.24.12359-12369.2001.
16. Thiel V, Herold J, Schelle B, Siddell SG. (2001) Infectious RNA transcribed in vitro from a cDNA copy of the human coronavirus genome cloned in vaccinia virus. J Gen Virol 82: 1273-1281.
17. Tekes G, Spies D, Bank-Wolf B, Thiel V, Thiel HJ. (2012) A reverse genetics approach to study feline infectious peritonitis. J Virol 86: 6994-6998. 10.1128/JVI.00023-12; 10.1128/JVI.00023-12.
18. Yount B, Curtis KM, Fritz EA, Hensley LE, Jahrling PB, et al. (2003) Reverse genetics with a full-length infectious cDNA of severe acute respiratory syndrome coronavirus. Proc Natl Acad Sci U S A 100: 12995-13000. 10.1073/pnas.1735582100.
19. Yount B, Denison MR, Weiss SR, Baric RS. (2002) Systematic assembly of a full-length infectious cDNA of mouse hepatitis virus strain A59. J Virol 76: 11065-11078.
20. Yount B, Curtis KM, Baric RS. (2000) Strategy for systematic assembly of large RNA and DNA genomes: Transmissible gastroenteritis virus model. J Virol 74: 10600-10611.
21. Muller MA, van der Hoek L, Voss D, Bader O, Lehmann D, et al. (2010) Human coronavirus NL63 open reading frame 3 encodes a virion-incorporated N-glycosylated membrane protein. Virol J 7: 6. 10.1186/1743-422X-7-6.
22. Donaldson EF, Yount B, Sims AC, Burkett S, Pickles RJ, et al. (2008) Systematic assembly of a full-length infectious clone of human coronavirus NL63. J Virol 82: 11948-11957. 10.1128/JVI.01804-08; 10.1128/JVI.01804-08.
23. Dijkman R, Jebbink MF, Wilbrink B, Pyrc K, Zaaijer HL, et al. (2006) Human coronavirus 229E encodes a single ORF4 protein between the spike and the envelope genes. Virol J 3: 106. 10.1186/1743-422X-3-106.
24. Woods RD. (2001) Efficacy of a transmissible gastroenteritis coronavirus with an altered ORF-3 gene. Can J Vet Res 65: 28-32.
25. Song DS, Oh JS, Kang BK, Yang JS, Moon HJ, et al. (2007) Oral efficacy of vero cell attenuated porcine epidemic diarrhea virus DR13 strain. Res Vet Sci 82: 134-140. 10.1016/j.rvsc.2006.03.007.
26. Park SJ, Song DS, Ha GW, Park BK. (2007) Cloning and further sequence analysis of the spike gene of attenuated porcine epidemic diarrhea virus DR13. Virus Genes 35: 55-64. 10.1007/s11262-006-0036-1.
27. Sato T, Takeyama N, Katsumata A, Tuchiya K, Kodama T, et al. (2011) Mutations in the spike gene of porcine epidemic diarrhea virus associated with growth adaptation in vitro and attenuation of virulence in vivo. Virus Genes 43: 72-78. 10.1007/s11262-011-0617-5.
28. de Haan CA, van Genne L, Stoop JN, Volders H, Rottier PJ. (2003) Coronaviruses as vectors: Position dependence of foreign gene expression. J

Virol 77: 11312-11323.

29. de Haan CA, Volders H, Koetzner CA, Masters PS, Rottier PJ. (2002) Coronaviruses maintain viability despite dramatic rearrangements of the strictly conserved genome organization. J Virol 76: 12491-12502.
30. Rottier PJ, Spaan WJ, Horzinek MC, van der Zeijst BA. (1981) Translation of three mouse hepatitis virus strain A59 subgenomic RNAs in xenopus laevis oocytes. J Virol 38: 20-26.
31. Vennema H, Godeke GJ, Rossen JW, Voorhout WF, Horzinek MC, et al. (1996) Nucleocapsid-independent assembly of coronavirus-like particles by co-expression of viral envelope protein genes. EMBO J 15: 2020-2028.
32. Bosch BJ, van der Zee R, de Haan CA, Rottier PJ. (2003) The coronavirus spike protein is a class I virus fusion protein: Structural and functional characterization of the fusion core complex. J Virol 77: 8801-8811.

4

Chapter 5

Proteolytic Activation of the Porcine Epidemic Diarrhea Coronavirus Spike Fusion Protein by Trypsin in Cell Culture

Oliver Wicht[a], Wentao Li[a], Lione Willems[a], Tom J. Meuleman[a], Richard W. Wubbolts[b], Frank J.M. van Kuppeveld[a], Peter J.M. Rottier[a], Berend Jan Bosch[a]

[a]Virology Division, Department of Infectious Diseases and Immunology; [b]Department of Biochemistry and Cell Biology, Faculty of Veterinary Medicine, Utrecht University, Utrecht, The Netherlands

Journal of Virology, *In press*

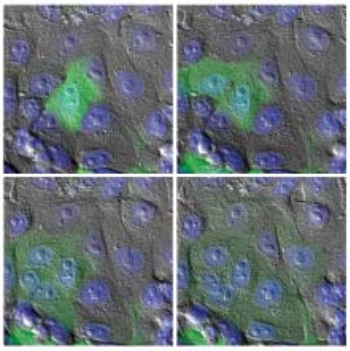

Abstract

Isolation of porcine epidemic diarrhea coronavirus (PEDV) from clinical material in cell culture requires supplementation of trypsin. This may relate to the confinement of PEDV natural infection to the protease-rich small intestine of pigs. Our study focused on the role of protease activity on infection by investigating the spike protein of a PEDV isolate (wtPEDV) using a reverse genetics system based on the trypsin independent cell culture-adapted strain DR13 (caPEDV). We demonstrate that trypsin acts on the wtPEDV spike protein after receptor binding. We mapped the genetic determinant for trypsin dependent cell entry to the N-terminal region of the fusion subunit of this class I fusion protein, revealing a conserved arginine just upstream of the putative fusion peptide as the potential cleavage site. Whereas coronaviruses are typically processed by endogenous proteases of the producer or target cell, PEDV S protein activation strictly required supplementation of a protease, enabling us to study mechanistic details of proteolytic processing.

Introduction

Porcine epidemic diarrhea virus (PEDV) belongs to the genus *Alphacoronavirus* in the family of *Coronaviridae* and is the causative agent of porcine epidemic diarrhea (1). The virus is prevalent in East Asia inflicting severe economic damage due to high mortality rates in young piglets and recently made its first appearance on the North American subcontinent (2-4). PEDV infects the epithelia of the small intestine, an environment rich in proteases, and causes villous atrophy resulting in diarrhea and dehydration. Intriguingly, in vitro propagation of PEDV isolates requires supplementation of trypsin to the cell culture supernatant (5). It has been hypothesized that trypsin mediates activation of virions for membrane fusion by cleaving the Spike (S) glycoprotein (5, 6). Trimeric S proteins decorate the virion envelope and mediate receptor binding and membrane fusion. The S protein has been recognized as a class I fusion protein by its molecular features (7, 8).

Class I fusion proteins are generated in a locked conformation to prevent premature triggering of the fusion mechanism and are subsequently prepared for action by proteolytic processing, a step called priming (reviewed in (9)). This cleavage is separating two functionally distinct protein domains, a soluble head domain responsible for receptor binding and a membrane bound subunit comprising the fusion machinery. A characteristic feature of the cleaved, fusion-ready subunit is an N-terminal fusion peptide. Proteolytic priming can occur in the virus producing cell, in the extracellular environment, or after contact with the target cell membrane. Priming of the PEDV S protein is potentially accomplished by intestinal digestive enzymes.

Some coronaviruses (CoV) such as mouse hepatitis virus (strain A59) and infectious bronchitis virus (IBV) carry S proteins that are cleaved by furin-like proteases in the producer cell at the junction of the receptor binding (S1) and the membrane fusion subunit (S2)(10, 11). However, most CoV like PEDV and severe acute respiratory syndrome coronavirus (SARS-CoV), carry non-cleaved S proteins upon release (12). For an increasing number of coronavirus S proteins an alternative cleavage site within the S2 subunit (S2') has been described that is located upstream of the putative fusion peptide (13-15). Unlike cell culture-adapted PEDV, clinical isolates of PEDV are the only known CoVs for which propagation in cultured cells is dependent on a protease that is not expressed by target cells. The spatiotemporal and mechanistic characteristics of their fusion activation remain unknown.

We focus our investigation on the impact of trypsin on PEDV S protein by using a reverse genetics system based on the cell culture-adapted, trypsin independent PEDV strain DR13 (caPEDV) (16, 17). We substituted the caPEDV S gene (PEDV-Sca) by that of a strictly trypsin dependent PEDV isolate CV777 (PEDVSwt) (18). Indeed, the trypsin dependency of virus propagation was attributed to the S protein. Trypsin was necessary for efficient cell entry and release of PEDV-Swt, whereas it reduced infection of PEDVSca. We demonstrated that trypsin was required for PEDV-Swt entry only after receptor binding. We mapped the genetic determinants for activation of the S protein through trypsin to a site just upstream of the putative fusion peptide by testing various chimeric forms of the S genes and specific point mutations.

Material and Methods

Cells and viruses

Vero-CCL81 cells (ATCC) were maintained in Dulbecco modified Eagle medium (DMEM, Lonza BE12-741F) supplemented with 10% fetal bovine serum (FBS). A Vero-CCL81 derived cell line expressing the MHV receptor - murine carcinoembryonic antigen-related cell adhesion molecule 1a (CCM) - was made by transduction with vesicular stomatitis virus G protein pseudotyped Moloney murine leukemia virus (MLV) using the pQCXIN retroviral vector (Clontech) containing the CCM coding sequence (19). The polyclonal Vero-CCM cell line was selected and maintained with G418 (PAA) and CCM expression was confirmed by immunostaining. To propagate PEDV, cell layers were generally washed twice with phosphate buffered saline (PBS) and maintenance medium was substituted by Eagle's minimum essential medium Alpha Modification (Life Technologies 22571-020) supplemented with 0.3% tryptose phosphate broth (aMEM-TPB, Sigma T9157). The cell culture-adapted PEDV DR13 strain hereafter called caPEDV (gb|JQ023162; isolated from a commercial vaccine of GreenCross, South Korea) and recombinant virus carrying caPEDV S protein including trypsin independent derivatives thereof were propagated and titrated in aMEM-TPB supplemented with 20 mM HEPES in Vero cells (20). PEDV strain CV777 hereafter called wtPEDV (gb|AF353511; kindly provided by Dr. Kristin van Reeth, Gent University) and recombinant virus carrying wtPEDV S protein or derivatives thereof were propagated and titrated in aMEM-TPB supplemented with 20 mM HEPES plus 15 µg/ml trypsin (Sigma T4799) in Vero cells. The S gene of wtPEDV encoded two amino acid deviations from the published CV777 S sequence (G84S and S503L, (7)). For purification of the PEDV-Swt virus particles in the absence of trypsin, Vero cells were inoculated in the presence of trypsin activity reaching a maximum infection rate and the culture supernatant was replenished by aMEM-TPB supplemented with 20 mM HEPES after 4 h. Cells were cultured for 24 h at 37°C and an additional 24 h at 32°C. Virus was harvested by three cycles of freeze-thawing the infected cells and culture supernatant followed by removal of cell debris by centrifugation at 4,000 × *g* for 10 min.

Construction of recombinant viruses

Recombinant PEDV were generated as described by Li et al. (16) except that we used Vero-CCM cells for the recovery of viruses carrying wtPEDV S protein or trypsin dependent derivatives thereof. PEDV-Sca represents the earlier reported PEDV-ΔORF3/GFP (16) that was generated using the transfer vector pPEDV-ΔORF3/GFP. The transfer vectors for novel recombinants were derivatives of pPEDV-ΔORF3/GFP containing a BamHI restriction site between ORF1b and the S gene, as described for prPEDV (16). The chimeric PEDV-S_AB, PEDV-S_Ab, and PEDV-S_aB genes were generated by replacing the PstI X PmlI, PstI X Bsu36I or the Bsu36I X PmlI fragments of the caPEDV S gene by that of wtPEDV sequence. To generate recombinant PEDV with the full length wtPEDV S protein (PEDV-Swt), the entire S gene was replaced by BamHI X PmlI, generating p-PEDV-CV777-ΔORF3/GFP. The FLAG peptide (VQDYKDDDDK) encoding gene fragment was appended to the C-terminal end of the S gene using the PmlI restriction site of p-PEDV-ΔORF3 and p-PEDV-CV777-ΔORF3/GFP resulting in PEDV-Sca_flag and PEDV-Swt_flag, respectively (16). Viral RNA was extracted from virus two to three passages after plaque selection and the genotype confirmed by sequencing.

Infection / virus entry assay

Vero cells were inoculated with caPEDV and wtPEDV (MOI was set to 0.1 in the presence of trypsin) in the presence of 15 µg/ml trypsin or trypsin plus 40 µg/ml soy bean trypsin inhibitor type I (SBTI, Sigma T6522) for 15 h before visualization of the virus infection by immunofluorescence microscopy. For recombinant PEDV containing the GFP reporter gene (MOI was set to 0.1 in the presence of trypsin), inocula contained 15 µg/ml trypsin, 40 µg/ml SBTI or both. After 2 h, inoculum was removed, cell layers were rinsed with PBS, and further incubated with aMEM-TPB supplemented with SBTI. 10-12 h post infection, when GFP signals became apparent, samples were imaged by an EVOS-fl fluorescence microscope (Advanced Microscopy Group) and prepared for flow cytometry analysis. Figures show representative images. The same procedure was used if the inoculum had been pretreated. Prior to infection, trypsin or trypsin plus SBTI were added to the inoculum and incubated for 1 h at 37°C, followed by inoculation of Vero cells for 2 h. The attachment assay was performed (MOI was set to 0.5 in the presence of trypsin before pretreatment) with pretreated or naive virus preparations, while residual trypsin activity was blocked in all cases by an excess of SBTI. Next, the inoculum was allowed to attach to the cells at ~8°C for 1 h before rinsing the cell layer and followed by 2 h inoculation with trypsin or trypsin plus SBTI. Samples were otherwise prepared as in the entry assay.

Flow cytometry

The cell layer was rinsed with PBS and detached with cell culture dissociation solution (Sigma C5914). Cells were resuspended in PBS supplemented with 2% FBS and 0.02% sodium azide, pelleted by centrifugation and fixed in 3.7% formaldehyde in PBS. Subsequently, cells were analyzed for GFP expression using a FACSCalibur flow cytometer (BD Bioscience) recording 20.000 cells. Flowing software 2 (Perttu Terho, Turku Centre for Biotechnology, Finland) was used to analyze the percentage of GFP expressing cells in the live cell gate. The threshold for mock infected cells was set at 0.1% positive cells.

Virus release assay

To assess the release of infectious particles in the absence or presence of trypsin, Vero cells were inoculated with recombinant PEDV at an MOI of 4 for 2 h and further incubated in aMEM-TPB or aMEM-TPB supplemented with 15 µg/ml trypsin. 14-16 h post infection, supernatant was collected, cell debris removed by spinning for 10 min at 10,000 x *g* and pretreated with 15 µg/ml trypsin for 1 h before titration of infectious virus by end point dilution. The trypsin pretreatment was performed to ensure equal trypsin induced reduction of PEDV-Sca infectivity of samples obtained under different conditions. To display the data, ratios of viral titers obtained from supernatants containing trypsin versus lacking trypsin were calculated of paired samples. The p-value was obtained with a paired samples *t*-test between PEDV-Swt and PEDVSca.

The effect of trypsin on the release of viral RNA in the cell culture supernatant was determined by quantitative real-time reverse transcription PCR (qRT-PCR). Vero cells were inoculated with recombinant PEDV at an MOI of 2 for 2 h and further incubated in aMEM-TPB supplemented with 40 µg/ml SBTI or 15 µg/ml trypsin. 16 h post infection RNA was prepared from cell lysates (RNeasy mini kit, Qiagen) and cell culture supernatants (QiaAMP viral RNA mini kit, Qiagen) according to manufacturer's protocols. Reverse transcription and

qRT-PCR were performed using GoTaq 1Step RT-qPCR System (A6020; Promega) with the primer set FW 5'-GAGCACATGTTGTTGGCTCT-3' and RV 5'-GCAACCTTCAGGTCTGACAA-3' on a Light Cycler 480 II (Roche).

PEDV S protein expression vectors

cDNA was recovered from virus preparations and wtPEDV S gene specific PCR products were subcloned into pCAGGS expression vector for transient expression (Swt). To increase cell surface presentation during transient expression, the C-terminus of the S gene was truncated by an equivalent of 20 amino acids which include retrieval signals (21). The point mutation R890G was introduced to the wtPEDV S gene by site directed mutagenesis (Swt_R890G). The entire S protein coding sequence of each construct was confirmed by sequencing.

PEDV S protein mediated cell-cell fusion

Vero cells were transfected with pCAGGS expression plasmids encoding Swt or Swt_R890G using jetPRIME (Polyplus) for 48 h. Alternatively, Vero cells were inoculated with PEDV-Swt for 2 h in the presence of trypsin and cultured from 2 to 20 h in the absence of trypsin. Supplementation of 15 µg/ml trypsin for 1 h resulted in cell-cell fusion which was monitored by immunofluorescence staining against PEDV S protein in the case of overexpression. Cell-cell fusion of cells infected with the GFP-expressing PEDV-Swt was followed by real time confocal fluorescence microscopy using a NIKON A1R microscope with a top climate chamber (Tokai Hit) for live cell imaging at 37°C and 5% CO_2. Image stacks were acquired every 65 s at 40x magnification.

Immunofluorescence microscopy

For immunostaining, the cells were washed twice with PBS and fixed with 3.7% formaldehyde (Merck 1040031000) in PBS, followed by membrane permeabilization with 0.1% Triton-X-100 (Sigma 93426) in PBS for 15 min at room temperature. Cells were blocked by 2% normal goat serum in PBS for 1 h and then incubated with polyclonal rabbit antibody raised against the PEDV (strain D24) S1 ectodomain (amino acids 1-728, anti-PEDV-S1 serum, Davids Biotechnologie GmbH, Germany) or the 3F12 mouse monoclonal antibody detecting PEDV nucleocapsid protein (BioNote, Republic of Korea) for 1 h. After rinsing three times with PBS, staining was completed by goat αrabbit Alexa Fluor®488-conjugated (Life Technologies A11008) or goat αmouse Alexa Fluor®488-conjugated (Life Technologies A11001). For nuclear staining, DAPI (Molecular Probes) was included during blocking. An EVOS-fl fluorescence microscope (Advanced Microscopy Group) was used to visualize staining.

Western blot analysis

Virus containing cell culture supernatants were purified and concentrated (factor 1:400 v/v) by sedimentation of the virus particles through a 20% cushion of sucrose in HCN buffer (50 mM HEPES, 100 mM NaCl, 10 mM $CaCl_2$) at 100,000 x *g* for 1.5 h at 4°C. Virus particles were handled on ice and resuspended in HCN buffer. For trypsin treatment, samples were supplemented with or without 15 µg/ml trypsin before warming to 37°C for 30 min. Samples were chilled and trypsin activity was quenched by the addition of 80 µg/ml SBTI

before determining the titers by end point dilution or denaturing in Laemmli sample buffer at 95°C for 10 min. Samples were subjected to sodium dodecyl sulfatepolyacrylamide gel electrophoresis (SDS-PAGE) in a discontinuous gel with 8% acryl amide in the separating gel. Next, samples were transferred to a polyvinylidene fluoride membrane (BioRad, 1620176) and blocked with bovine serum. PEDV S protein was reacted with mouse monoclonal antiFLAG conjugated to horseradish peroxidase (Sigma, A8592) or anti-PEDV-S1 serum in PBS with 5% FBS and 0.5% Tween20 and the latter subsequently with swine anti-rabbit immunoglobulin G conjugated horseradish peroxidase (Dako, P0217). For detection we used Amersham ECL Western Blotting Analysis System (GE healthcare, RPN2109) with X-Omat LS films (Kodak, Sigma F1149).

Computational analysis

he transmembrane domain of PEDV S protein was predicted by TMHMM 2.0 and the signal peptide by SignalP 4.1. HR1 and HR2 regions are drawn according to Bosch et al. (8). Microscopy images were quantified with ImageJ and GIMP. Amino acid sequence alignment was performed by ClustalW2 using S sequences of PEDV-DR13-par (parental virulent strain DR13, gb|AFE85962.1), Middle East respiratory syndrome coronavirus (MERS-CoV strain HCoV-EMC, gb|AFS88936.1), SARS-CoV strain Tor2, gb|NP_828851.1), IBV (strain Beaudette, gb|NP_040831.1), and murine hepatitis virus (MHV strain A59, gb|NP_045300.1).

Results

In vitro infection with PEDV strains CV777 and caDR13

The requirement for trypsin for the propagation of the PEDV isolate CV777 (wtPEDV) and the cell culture-adapted DR13 strain (caPEDV) was compared. Vero cells were inoculated with either of the two viruses in the absence or presence of trypsin for 15 h. Virus infected cells were visualized by immunofluorescence staining. Numerous multinucleated cells were observed after inoculation with wtPEDV and caPEDV in the presence of trypsin (Figure 1). These syncytial foci, typical for PEDV infection (5), were larger for wtPEDV than for caPEDV. In contrast, when trypsin activity was blocked using soy bean trypsin inhibitor (SBTI), wtPEDV infection was almost absent. caPEDV continued to infect cells, even at a higher rate. Remarkably, no syncytia formation was observed in the absence of trypsin activity.

Recombinant PEDV with different S proteins

Assuming that the addition of trypsin to the inoculum might activate viral S proteins for fusion, we investigated this possible relationship further. We generated recombinant viruses encoding the wtPEDV S gene (PEDV-Swt) or the caPEDV S gene (PEDV-Sca) in an isogenic background, the viruses hence only differing in their S proteins (Figure 2A). In the recombinant viruses the ORF3 was replaced by a GFP gene to enable the detection of infection by fluorescence (16). Recovery and propagation of recombinant PEDVSwt, but not that of PEDVSca, required the presence of active trypsin during inoculation and culturing. We concluded that the contrasting trypsin dependence of wtPEDV and caPEDV was determined by the S protein.

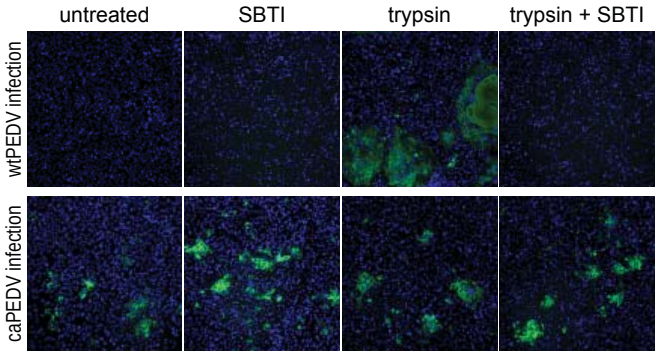

Fig. 1 Infection with the wild-type PEDV isolate, but not with cell culture-adapted PEDV benefits from trypsin activity. Inocula were supplemented with soy bean trypsin inhibitor (SBTI), trypsin, or a combination of both and applied to Vero cells. After 15 h incubation, infected cells were detected by immunofluorescence staining against the nucleocapsid protein (green). Nuclei were stained with DAPI (blue).

Trypsin affects different steps in the viral life cycle

Trypsin might affect virus propagation at different steps in the viral life cycle. First, we focused on virus entry. Vero cells were inoculated in the presence of trypsin for 2 h with PEDVSca or PEDVSwt at an MOI known to infect about 10% of cells. For additional samples, trypsin activity was quenched by addition of SBTI or only SBTI was added. After the virus entry stage, the inoculum was removed and incubation was continued in the presence of SBTI for 9 h to prevent syncytia formation by residual trypsin in the culture supernatant. At 11 h post infection (p.i.), fluorescence microscopy images were acquired. Inoculation with PEDV-Swt and PEDV-Sca in the presence of trypsin yielded ~10% infected cells (Figure 2B). However, in the absence of trypsin activity PEDV-Swt failed to infect Vero cells. SBTI alone had the same effect as when combined with trypsin. In contrast, inoculation with PEDV-Sca was more efficient without trypsin activity. No syncytia were observed with either recombinant virus in the absence of trypsin. Prolonged incubation in the absence of trypsin activity resulted in second round infections by PEDV-Sca but not by PEDV-Swt (data not shown). GFP expressing cells were quantified by flow cytometry to determine the extent of infection. Blocking active trypsin resulted in a > 10-fold reduction of PEDV-Swt infection, where we observed a 3-fold increase of infection for PEDV-Sca (Figure 2C). Thus, PEDV-Swt entry was clearly dependent on active trypsin whereas PEDV-Sca was not.

Besides enhancing its entry, trypsin has been reported to increase the release of PEDV from infected cells (22). We therefore monitored release of PEDVSwt and PEDVSca in the absence or presence of trypsin. Vero cells were inoculated with PEDVSwt and PEDVSca (MOI = 4) and the inoculum was removed after 2 h. Incubation was continued in the absence or presence of trypsin until 14-16 h p.i., after which cell culture supernatants were collected. Trypsin was added to all samples to normalize the trypsin sample conditions before determining viral infectivity in the cell culture supernatant by end-point dilution assay. For both viruses, more infectious virus was detected in the presence than in the absence of trypsin (Figure 2D). However, while for PEDV-Swt this increase was ~500-fold, for PEDV-Sca it was limited to ~15fold. Statistical testing confirmed a significant difference between the increased release of infectious PEDV-Swt over PEDV-Sca from infected cells in the presence of active trypsin. The trypsin-enhanced release of virions in cell culture supernatant was

confirmed by determining the ratio of released viral RNA in the presence compared to absence of trypsin using quantitative real-time reverse transcription PCR (Figure 2E).

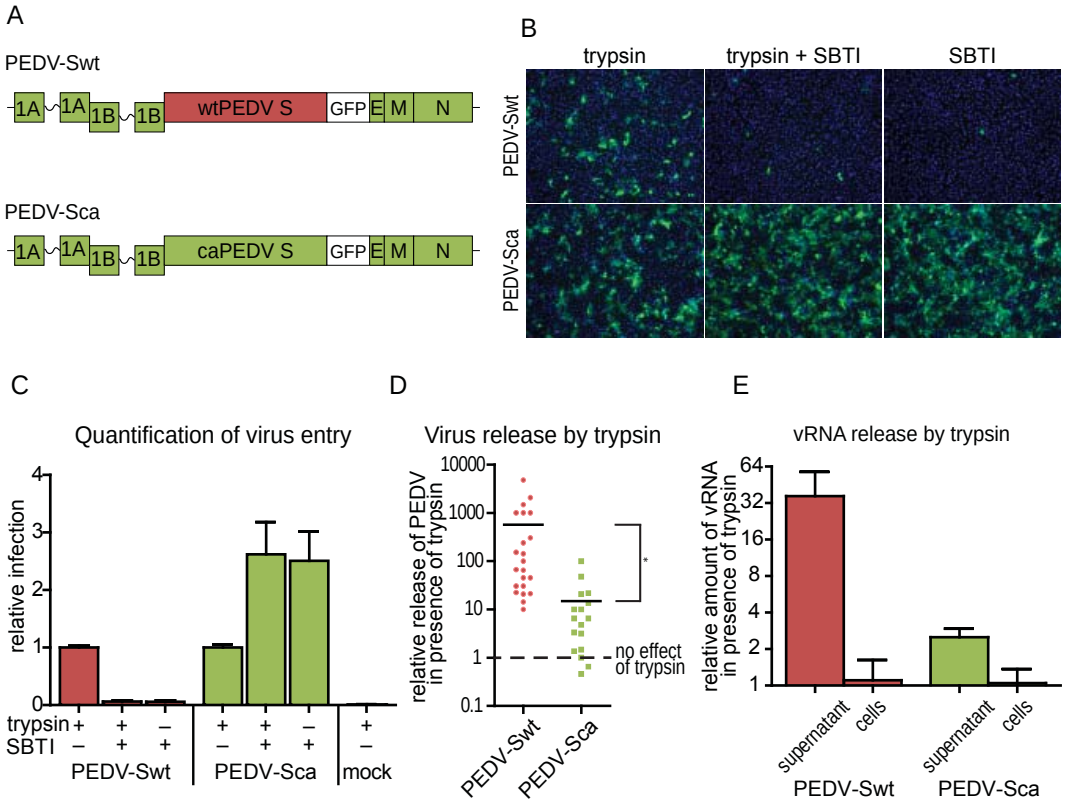

Fig. 2 The S protein determines trypsin dependency of PEDV propagation. (A) Schematic representation of the recombinant PEDV genomes carrying the PEDV-CV777 or the PEDV-caDR13 S gene in the isogenic background of caDR13 (PEDV-Swt and PEDV-Sca, respectively). The ORF3 gene was substituted by a GFP sequence. (B) Vero cells were inoculated in the presence or absence of trypsin or soy bean trypsin inhibitor (SBTI). After 2 h the inoculum was removed and incubation continued in the presence of SBTI to prevent syncytia formation. At 11 h post infection (p.i.), infected cells were examined by GFP expression using fluorescence microscopy (green). Nuclei were stained with DAPI (blue). (C) The percentage of infected cells was determined by quantifying GFP expressing cells using flow cytometry. The averages with standard deviation (s.d.) of 4 experiments are displayed relative to the inoculation in the presence of trypsin. (D) To assess the effect of trypsin on the release of infectious PEDV particles from producer cells, inoculations were performed for 2 h before the medium was refreshed and incubation continued in the absence or presence of trypsin. At 14 to 16 h p.i., supernatants were collected. Trypsin was added to all samples 1 h before infectious virus titers were determined by end point dilution. The ratio of infectivity in samples obtained in presence over absence of trypsin were calculated and displayed (* p-value 0.026 in paired samples t-test). 7 independent experiments with multiple replicates were carried out and each dot represents ratio obtained from one pair of samples. (E) The effect of trypsin on the release of viral RNA (vRNA) from PEDV infected cells was quantified. Vero cells were infected with wtPEDV and caPEDV and cultured from 2 to 16 h p.i. in the presence or absence of trypsin. RNA was subsequently purified from supernatants or cells and vRNA levels were quantified by qRT-PCR. The relative amounts of vRNA of the samples treated with trypsin compared to the samples treated with SBTI are displayed.

Characterization of S protein activation

To facilitate virus entry, trypsin may act on the S protein or the target cells, for example on the virus receptor. In a modified entry assay, either the virus or the target cell monolayer was exposed to trypsin for 60 min prior to inoculation. Trypsin activity was quenched by SBTI before or after pre-incubation or after 2 h of inoculation. Flow cytometry analysis demonstrated that infection by PEDV-Swt was not enhanced by trypsin pretreatment of the inoculum or the cells (Figure 3A), but trypsin was required during inoculation. Similarly, infection with PEDV-Sca did not benefit from trypsin pretreatment of virus or cells. Rather, exposure to active trypsin reduced PEDV-Sca infectivity in the absence of cells and during inoculation, though it did not inactivate the virus entirely.

We performed western blot analysis to study effects of trypsin on the S proteins decorating virus particles. To facilitate monitoring of S proteins, recombinant PEDV-Sca_flag and PEDV-Swt_flag were generated in which the S proteins were Cterminally extended by a FLAGtag. To avoid trypsin exposure during production of PEDV-Swt_flag, we inoculated Vero cells at a high MOI in the presence of trypsin and replaced the cell supernatant by culture medium without trypsin after 4 h. Virus particles were collected from the cell culture supernatants by sedimentation through a 20% sucrose cushion. Purified virus samples were exposed to 15 µg/ml trypsin for 30 min before western blot analysis and infectious titer determination. In the absence of trypsin, full-length PEDV S proteins migrating at ~180 kDa were detected using anti-FLAG antibody or an anti-PEDV-S1 serum (Figure 3B), whereas non-tagged PEDVSca was only detected by anti-S1 serum. Incubation with trypsin cleaved a fraction of PEDVSwt, but essentially all of PEDV-Sca S protein, resulting in two smaller S protein products that migrated at approximately 70 kDa and 50 kDa. The infectivity of PEDV-Swt_flag and PEDV-Sca_flag decreased by 6-fold and >300-fold, respectively. Thus, the extent of trypsin mediated proteolysis of the S proteins correlates with the observed reduction of virus infectivity. While PEDV-Swt_flag was relatively resistant to trypsin, PEDV-Sca_flag was rapidly cleaved.

To further define whether trypsin acts before or after receptor binding we performed a synchronized infection by allowing the viruses to attach to target cells at 8°C in the absence of trypsin. After 60 min, unbound virus was removed and an entry assay was performed. PEDVSwt was able to infect cells exclusively when trypsin activity was present after attachment (Figure 3C, filled bars). Trypsin consistently reduced PEDV-Sca infection whenever present. Nonetheless, we assumed that also PEDV-Sca requires proteolytic activation of its S protein at some stage, but that the beneficial cleavage effect of trypsin might be masked by destructive ones. To probe for a trypsin resistant fraction of PEDV-Sca, virus preparations were pre-treated with trypsin or SBTI for 60 min. Then, trypsin was blocked by an excess of SBTI followed by attachment and subsequent infection as before. In contrast, infection by pre-exposed PEDV-Sca was reduced below the level of infection in the presence of trypsin (Figure 3, compare filled and empty bars) and the remaining infectivity was further decreased by applying trypsin after attachment. The infectivity of pretreated PEDV-Swt was essentially unaffected and required trypsin activity after attachment. Where PEDV-Swt fully depends on trypsin at a post-receptor binding stage, the infectivity of PEDV-Sca is compromised before and after receptor binding.

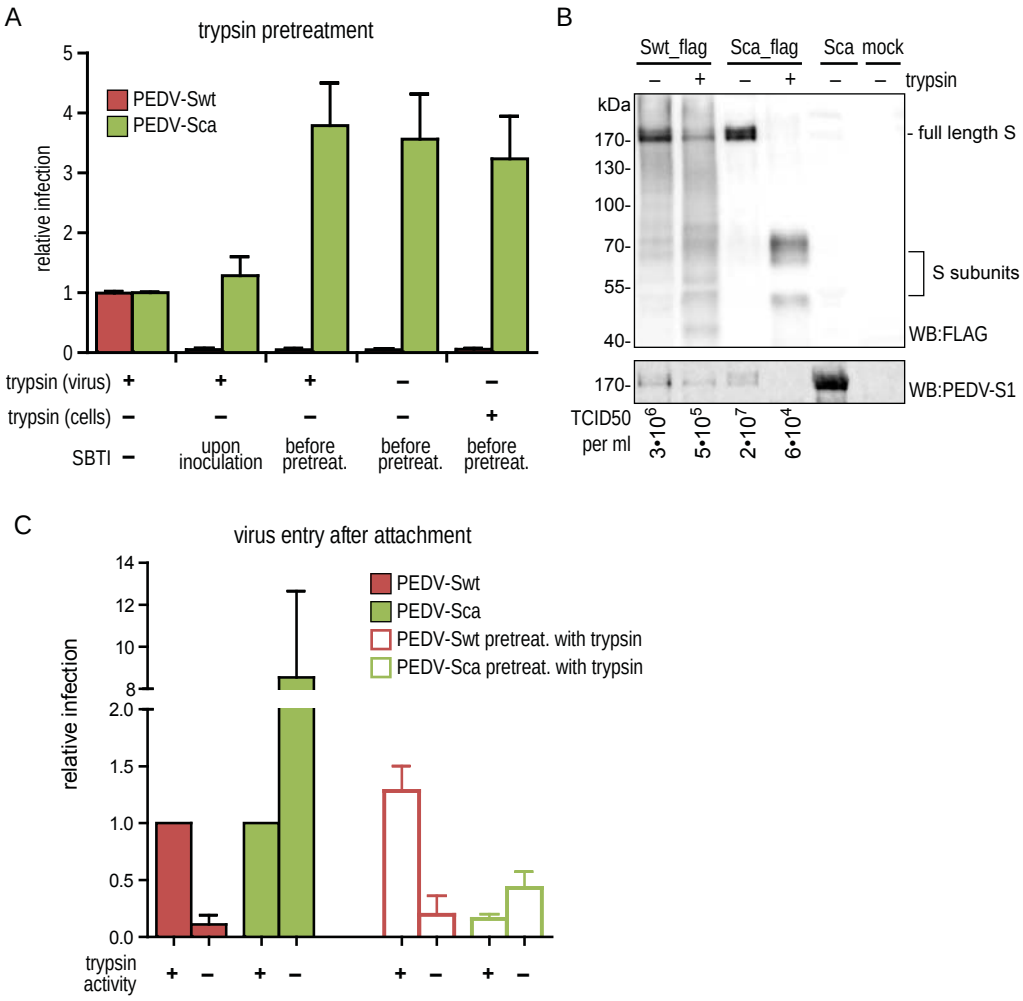

Fig. 3 Characterization of S protein activation. (A) An entry assay was performed as described in Figure 2B. Vero cells were inoculated for 2 h with PEDV Sca or PEDV Swt and infection was quantified by flow cytometry, showing the averages with s.d. of 3 experiments displayed relative to the inoculation in the presence of trypsin. For pretreatment, the inoculum or the target cells were exposed to trypsin for 1 h at 37°C. SBTI was supplemented to quench the trypsin activity at indicated steps. (B) Trypsin treatment of S protein on purified virions. Recombinant viruses carrying a FLAG-tag at the C-terminus of the PEDV-S protein (PEDV-Sca_flag and PEDV-Swt_flag) were produced in the absence of trypsin and purified by pelleting through 20 % sucrose. A similar purification procedure was done with culture medium from PEDV-Sca and mock infected Vero cells (mock). Samples were exposed to 15 µg/ml trypsin or left untreated for 30 min. Infectivity was determined by end point dilution (TCID50/ml) and virus particles were subjected to western blot analysis. Proteins were detected by a mouse monoclonal anti-FLAG antibody conjugated with horse-radish peroxidase or rabbit anti-PEDV-S1 serum. (C) Virus supernatant was pretreated as described above with SBTI (filled bars) or trypsin (open bars). After addition of an excess SBTI, virus was added to cells and attachment was allowed for 1 h at 8°C in the absence of trypsin activity. After binding, an entry assay was performed as described in Figure 2B. Infection was quantified by flow cytometry, showing the averages with s.d. of 4 experiments displayed relative to inoculation in the presence of trypsin without pretreatment.

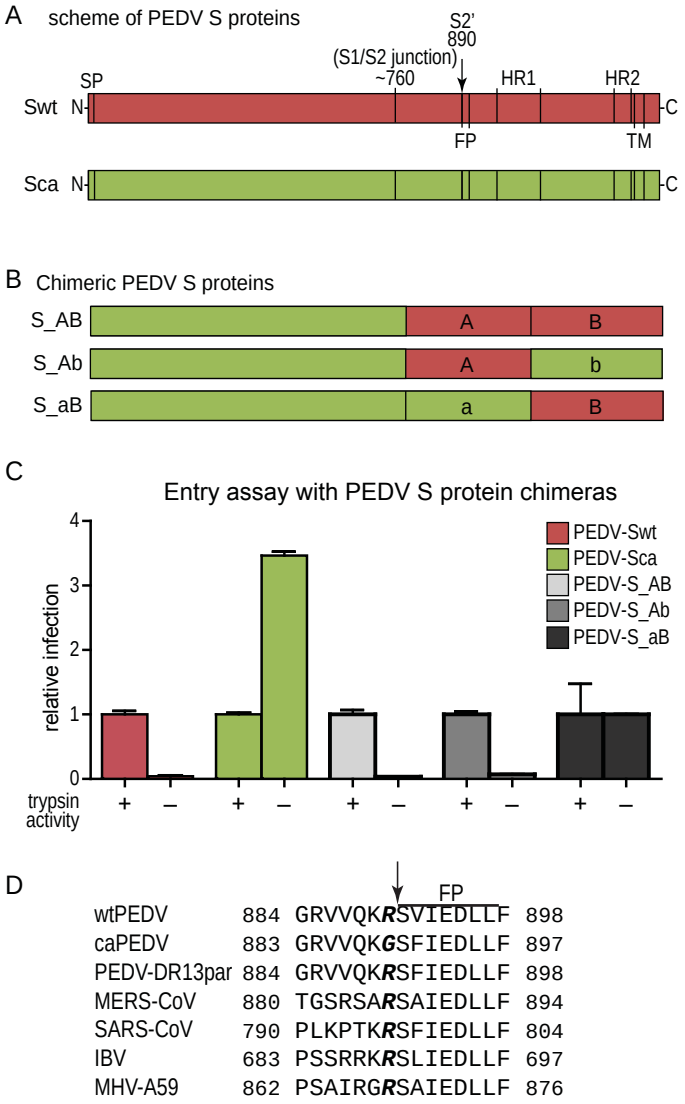

Fig. 4 Mapping the genetic determinant for trypsin enhanced PEDV entry. (A) Putative organization of class I fusion protein features in PEDV S protein. SP = signal peptide, FP = fusion peptide (S891 – V910), HR1 and HR2 = heptad repeat region, TM = transmembrane domain, S1/S2 junction = region of the furin cleavage site in MHV-A59, S2' = location of putative cleavage site within the S2 subunit in SARS-CoV and IBV S protein; drawn to scale. (B) A schematic overview shows the chimeric S proteins of the recombinant PEDV variants. Red and green regions are derived from Swt or Sca protein, respectively. (C) An entry assay was performed as described in Figure 2 to compare the trypsin dependent entry of PEDV variants. (D) The alignment of the amino acid sequence N-terminal of the fusion peptide (FP) depicts a conserved arginine or a glycine substitution (bold italic). Putative S2' cleavage site is indicated with an arrow.

Mapping genetic determinants of trypsin dependent entry

The amino acid sequences of PEDV-Sca and PEDV-Swt differ at 129 amino acid positions. Using a gain of function approach, we aimed to map the genetic determinant for trypsin enhanced entry through substituting fragments of the PEDV-Sca S gene by the corresponding wtPEDV S gene sequences, generating chimeric S proteins. The ultrastructural organization of PEDV S proteins is unknown, but putative functional domains can be identified by theoretical analysis and comparison to other coronaviruses (Figure 4A). We replaced the gene fragment encoding the putative fusion subunit (PEDVS_AB), or its Nterminal part containing the putative S2' cleavage site, fusion peptide, and HR1 domain (PEDVS_Ab), or its Cterminal part containing HR2, the transmembrane domain, and the Cterminus (PEDVS_aB; Figure 4B). Recombinant PEDVS_AB and PEDVS_Ab were recovered in the presence of trypsin, whereas PEDVS_aB could be recovered without trypsin. The chimeric viruses were tested for trypsin dependent entry as described for Figure 2. Clearly, all viruses carrying part A of wtPEDV, as exemplified by PEDVS_AB and PEDVS_Ab, were found to be fully dependent on trypsin for efficient entry, similar to PEDV-Swt (Figure 4C). All other viruses that contain part A of caPEDV such as PEDVS_aB, did not require trypsin for efficient entry. Hence, part A

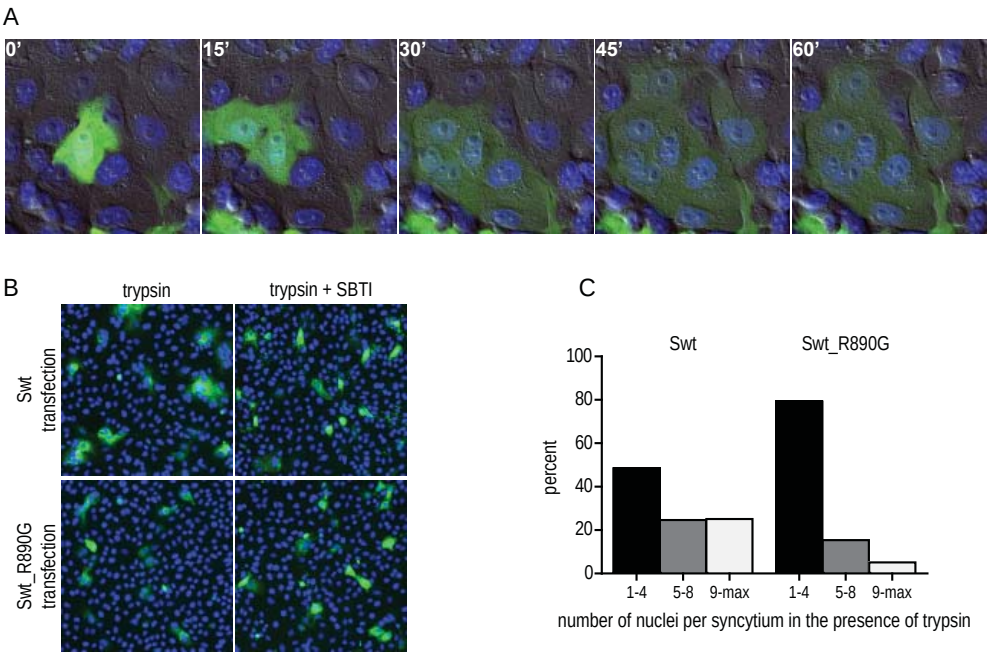

Fig. 5 Substitution of arginine at position 890 results in reduced syncytia formation capacity of transiently expressed S protein. (A) After overnight incubation with PEDV-Swt, infected cells were treated with trypsin for 1 h while live images were obtained. Representative images are shown. (B) Vero cells were transiently transfected with expression plasmids encoding Swt and its point mutant Swt_R890G for 48 h. Cells were treated with trypsin or trypsin plus SBTI for 1 h and subsequently examined by immunostaining against S protein (green). Nuclei were stained with DAPI (blue). Representative images are shown. (C) The numbers of nuclei per focus were quantified and displayed as binned frequency distribution histogram (four independent experiments, Swt n = 390; Swt_R890G n = 330). Syncytia containing 1-4 nuclei were small, 5-8 nuclei were medium and more than 8 were large. The average syncytia size induced by Swt and Swt_R890G significantly differ from each other (p value <0.0001, non-parametric t-test).

contains the determinant for trypsin dependent entry.

To identify the relevant trypsin cleavage site, we compared the amino acid sequences of part A from the PEDV strains CV777, caDR13 and the parental DR13 virus (PEDV-DR13par). We observed 9 amino acid differences including one conspicuous arginine, located at position 890 (R890). The arginine occurred in the S protein of wtPEDV and PEDV-DR13par but was replaced by a glycine in the cell culture-adapted caPEDV (Figure 4D). To investigate the role of R890 in trypsin mediated entry of wtPEDV, attempts were made to generate PEDV-Swt encoding an R890G substitution. Despite multiple efforts this virus could not be recovered by our RNA recombination approach, whereas control recombinations were successful (data not shown). We did not consider introducing the reciprocal G890R substitution in PEDV-Sca, since the resulting recombinant virus would be predicted to remain trypsin independent similar to PEDVS_aB.

Trypsin induced cell-cell fusion mediated by overexpressed S proteins

To otherwise assess the role of R890 in trypsin mediated S protein activation, we made use of a cellcell fusion assay. As indicated in Figure 1, continuous treatment of PEDV infected cells with trypsin results in cell-cell fusion yielding syncytia. Cell-cell fusion was also triggered after overnight infection by addition of trypsin, after which fusion activity continued for more than 1 h (Figure 5A). To test the trypsin-induced cell-cell fusion capacity of the PEDV S proteins, we transiently expressed them in Vero cells for 48 h. Cell-cell fusion by Swt was compared to that of Swt_R890G – containing a point mutation substituting the arginine 890 by a glycine. Trypsin was added for 1 h and syncytium formation examined. Trypsin induced considerable syncytia in Swt expressing cells; in contrast, only small syncytia were induced in the cells expressing Swt_R890G (Figure 5B). Overexpression of Sca results in small-sized syncytia and the Sca mutant bearing the reciprocal G890R mutation did not differ in their ability to induce syncytium formation (data not shown). S proteins were stained by immunofluorescence using anti-PEDV-S1 serum and the sizes of the foci were quantified by counting the number of nuclei (Figure 5C). For Swt about 50% of syncytia were found to be small containing 1 to 4 nuclei, ~25% were medium-sized with 5 to 8 nuclei, and ~25% of syncytia were large, having more than 8 nuclei. In contrast, the Swt_R890G mutant yielded almost 80% of small syncytia, 15% medium and only 5% larger ones. In both cases, incubation with trypsin failed to trigger syncytia formation by all transfected cells. Of note, the number of small syncytia is probably an overestimate because they were not distinguishable from small clusters of PEDV-S positive cells originating from cell division.

Discussion

Proteolytic priming of class I fusion glycoproteins has been reported to occur with different timing and by various host proteases. Human immunodeficiency virus *Env* and HA of highly pathogenic influenza viruses become primed by cellular furin-like proteases in the virus producing cells, hence they are fusionready upon virus release (23, 24). In contrast, the infectivity of viruses carrying uncleaved fusion proteins such as severe acute respiratory syndrome (SARS) coronavirus and low pathogenic influenza viruses rely on host cell proteases like type II transmembrane serine proteases (TTSP) (25), furin-like proteases, or low-pH-dependent, endolysosomal proteases (23, 26-28). Recent progress illustrates

that infection by respiratory syncytial virus, despite its carrying a cleaved F protein, can still be blocked by inhibitors of endosomal proteases as the F protein requires a second cleavage in the target cell (29). PEDV is peculiar because it needs an exogenous protease for propagation in cell culture, thereby providing an excellent model to study proteolytic activation. Our investigation of the spatiotemporal characteristics of trypsin dependent PEDV infection demonstrated that PEDV-Swt undergoes trypsin activation at a post receptor-binding stage. In contrast to influenza virus HA that can be primed at any stage, we suggest that PEDV S protein is protected from premature processing by reduced accessibility of the cleavage site. This mechanism may prevent premature triggering of the fusion machinery in the protease-rich intestine and help to direct the infection to proper target cells. Proteolytic processing after preconditioning has been observed for other CoVs and correlated with conformational changes that expose a cleavage site. A preceding cleavage of SARS-CoV S protein facilitates cleavage at a second site further Cterminal of the first (30). Like PEDV, MHV-2 S protein requires receptor binding before the cleavage occurs that enables the refolding into a post fusion conformation (31). We failed to observe effects of porcine amino peptidase N (pAPN) – the putative receptor for PEDV (32) – because we could not reproduce its receptor function in a variety of assays. Proteolytic processing may constitute a general mechanism to control timing and location of the fusion competence of class I fusion proteins. In fact, the tropism of various enveloped viruses such as low pathogenic influenza virus, SARS-CoV, human coronavirus 229E, infectious bronchitis virus (IBV), and feline infectious peritonitis virus (FIPV), but also of the non-enveloped rotavirus has been correlated with the availability of proteases that mediate fusion activation in the target tissue (28, 33-38).

We used recombinant viruses to attribute specific effects of trypsin to the S protein. For the first time, the function of a strictly trypsin dependent S protein from a PEDV isolate was characterized and compared to the trypsin independent S protein of a cell adapted PEDV variant. A previous study claimed that trypsin exerts its PEDV infection enhancing effect at a post receptor-binding stage (6). However, the PEDV strain used was not trypsin dependent and the impact of trypsin on virus propagation was marginal, jeopardizing the interpretation of the data (6, 39).

In search for the genetic determinant of PEDV cleavage we created viruses with chimeric S proteins by transferring wtPEDV S gene fragments into the trypsin independent caPEDV virus. We mapped the trypsin dependence feature to the Nterminal half of the fusion subunit which includes the putative fusion peptide and HR1 domain (40). A sequence comparison of PEDV S proteins pointed at an arginine (R890) to glycine substitution that has occurred during the serial *in vitro* passaging process, which rendered the original parental PEDVDR13 trypsin independent (41). This arginine was first identified by Whittaker and co-workers in SARS-CoV S protein and sequence alignment by Yamada et al. illustrated the conservation of this arginine in almost all CoV S proteins (14, 30). Recombinant PEDV carrying wild-type S protein encoding the amino acid mutation R890G could not be rescued suggesting that R890 is required for proper functioning of the S protein. Although we were not able to demonstrate trypsin cleavage at R890 biochemically (data not shown), a role of this residue in trypsin-mediated activation of fusion was indicated by the significant reduction in syncytia formation by cells expressing the CV777 S protein encoding the R890G mutation. R890 is located immediately adjacent to the putative fusion peptide and corresponds with the previously described cleavage site within S2 (S2') (40). Consistent with the class I fusion

model, exemplified by influenza virus HA, trypsin cleavage at R890 would enable the bulky receptor binding head domain of the PEDV S protein to move aside, thereby liberating an N-terminal fusion peptide that can then insert into the host cell membrane to initiate membrane fusion (reviewed in (42)).

In contrast to clinical PEDV isolates, entry by cell culture-adapted caPEDV into Vero cells is independent of trypsin. Yet, cell-cell fusion by infected cells still required the addition of trypsin, indicating that proteolysis activates the caDR13 S protein for fusion but does not occur at plasma membrane. Candidate cellular enzymes that could activate the caPEDV S protein in the endolysosomal system are TTSPs and low-pH-activated proteases, by analogy to the SARSCoV, MERS-CoV, human coronavirus 229E, and MHV-2 S proteins (28, 43-46). Moreover, caPEDV infectivity was markedly affected by the action of trypsin, which correlated with a clear proteolysis of S proteins on virions. Trypsin cleavage of virion-bound Sca yielded a dominant 70 kDa-sized S2 fragment with an intact C-terminus (Figure 3B). The size of the product fits with trypsin cleavage in proximity to position G890 (i.e. at R885 or K889) yielding a truncated S2 subunit of approximately 70 kDa (predicted molecular mass of 55 kDa protein and 15 kDa N-glycans). We speculate that alternative trypsin cleavage sites may be more readily accessible in Sca compared to Swt, and hence, prematurely trigger the transition of Sca into a post-fusion form. caPEDV has been used as a live attenuated vaccine and its attenuated phenotype in pigs was suggested to be associated with a deletion in the accessory ORF3 gene product (39, 47, 48). We add that attenuation could also result from reduced viral fitness of the trypsin independent PEDV vaccine strain in the gastric and pancreatic protease-rich environment of the intestine and by reduced syncytia-inflicted damage of the intestinal epithelial layer (41).

It seems counterintuitive that serial passaging of the trypsin dependent PEDV-DR13 parental strain in the presence of trypsin eventually resulted in a cell culture-adapted caPEDV that no longer depended on trypsin for its growth (17). In fact, PEDV strain KPEDV-9 was independently generated by repeated passaging in cell culture and also acquired trypsin independence according to Park et al. (6, 17, 39). Intriguingly, it has been noted that Vero cells inhibit trypsin in cell culture supernatants by secretion of trypsin inhibitory molecules (49). Hence, propagation of the parental PEDV-DR13 in Vero cells may have selected for trypsin independent PEDV mutants.

Comparing virus production in the presence and absence of trypsin we also found that the release of recombinant viruses carrying wtPEDV and caPEDV S proteins from infected cells was increased by trypsin. Release of PEDV-Sca was 15-fold higher in the presence of trypsin, confirming results of Shirato et al. (22). PEDV-Swt was significantly more dependent on trypsin for release than PEDV-Sca, indicating that the S protein is also a determinant for efficient virus release from target cells. Protease activity acts at distinct steps in the viral life cycle of PEDV, although the mechanism of virus retention and the role of proteolysis in virus release are not understood.

Enveloped virus entry is generally directed and controlled by proteolytic processing of the fusion protein, receptor binding and triggering of membrane fusion. Our knowledge about the determinants of PEDV infection is limited and this study aimed at elucidating the requirements for virus entry. Like for other CoVs, we found that activating cleavage of wild-type PEDV S proteins occurs only after receptor binding (50). In vitro, PEDV is unique in its dependence on a protease that is not expressed by the target cell. As for influenza virus,

this trypsin dependence may be an ex vivo requirement. In vivo, the availability of gastric and pancreatic proteases or proteases locally expressed by the intestinal epithelial target cells potentially mediate PEDV virus infection to the intestine (51). TTSPs such as TMPRSS2 are candidate proteases for PEDV activation, since human TMPRSS2 has been shown to activate PEDV S-mediated cell-cell fusion in cell culture (22). It is currently unknown whether PEDV S protein cleavage is a priming event and whether membrane fusion requires yet an additional trigger. So far, trypsin cleavage readily supports the membrane fusion process and can be used as a trigger to investigate virus-cell and cell-cell fusion and to dissect further details of the PEDV fusion machinery. Thus it seems possible that PEDV infection is triggered by proteolysis rather than by alternative environmental cues, thereby abrogating the distinction between priming and triggering events, as was suggested for SARS-CoV (52).

Acknowledgements

We acknowledge Zou Yong for kindly providing Vero cells. This work was supported by E.C. 7th Framework Programme PITN-GA-2009-235649-Virus Entry, NWO MG (40-00506-98-12019). We thank Xander de Haan and Christine Burkard for helpful discussions during the design of this study.

References

1. Pensaert MB, de Bouck P. 1978. A new coronavirus-like particle associated with diarrhea in swine. Archives of virology 58:243-247.
2. AASV. 2013. Porcine Epidemic Diarrhea Information. American Association of Swine Veterinarians
3. Li W, Li H, Liu Y, Pan Y, Deng F, Song Y, Tang X, He Q. 2012. New variants of porcine epidemic diarrhea virus, China, 2011. Emerging infectious diseases 18:1350-1353.
4. Huang YW, Dickerman AW, Pineyro P, Li L, Fang L, Kiehne R, Opriessnig T, Meng XJ. 2013. Origin, evolution, and genotyping of emergent porcine epidemic diarrhea virus strains in the United States. mBio 4.
5. Hofmann M, Wyler R. 1988. Propagation of the virus of porcine epidemic diarrhea in cell culture. Journal of clinical microbiology 26:2235-2239.
6. Park JE, Cruz DJ, Shin HJ. 2011. Receptor-bound porcine epidemic diarrhea virus spike protein cleaved by trypsin induces membrane fusion. Archives of virology 156:1749-1756.
7. Duarte M, Tobler K, Bridgen A, Rasschaert D, Ackermann M, Laude H. 1994. Sequence analysis of the porcine epidemic diarrhea virus genome between the nucleocapsid and spike protein genes reveals a polymorphic ORF. Virology 198:466-476.
8. Bosch BJ, van der Zee R, de Haan CA, Rottier PJ. 2003. The coronavirus spike protein is a class I virus fusion protein: structural and functional characterization of the fusion core complex. Journal of virology 77:8801-8811.
9. White JM, Delos SE, Brecher M, Schornberg K. 2008. Structures and mechanisms of viral membrane fusion proteins: multiple variations on a common theme. Critical reviews in biochemistry and molecular biology 43:189-219.
10. Frana MF, Behnke JN, Sturman LS, Holmes KV. 1985. Proteolytic cleavage of the E2 glycoprotein of murine coronavirus: host-dependent differences in proteolytic cleavage and cell fusion. Journal of virology 56:912-920.
11. Cavanagh D. 1983. Coronavirus IBV: structural characterization of the spike protein. The Journal of general virology 64 (Pt 12):2577-2583.
12. Xiao X, Chakraborti S, Dimitrov AS, Gramatikoff K, Dimitrov DS. 2003. The SARS-CoV S glycoprotein: expression and functional characterization. Biochemical and biophysical research communications 312:1159-1164.
13. Watanabe R, Matsuyama S, Shirato K, Maejima M, Fukushi S, Morikawa S, Taguchi F. 2008. Entry from the cell surface of severe acute respiratory syndrome coronavirus with cleaved S protein as revealed by pseudotype virus bearing cleaved S protein. Journal of virology 82:11985-11991.
14. Yamada Y, Liu DX. 2009. Proteolytic activation of the spike protein at a novel RRRR/S motif is implicated in furin-dependent entry, syncytium formation, and infectivity of coronavirus infectious bronchitis virus in cultured cells. Journal of virology 83:8744-8758.
15. Matsuyama S, Taguchi F. 2002. Receptor-induced conformational changes of murine coronavirus spike protein. Journal of virology 76:11819-11826.
16. Li C, Li Z, Zou Y, Wicht O, van Kuppeveld FJ, Rottier PJ, Bosch BJ. 2013. Manipulation of the porcine epidemic diarrhea virus genome using targeted

RNA recombination. PloS one 8:e69997.

17. Song DS, Yang JS, Oh JS, Han JH, Park BK. 2003. Differentiation of a Vero cell adapted porcine epidemic diarrhea virus from Korean field strains by restriction fragment length polymorphism analysis of ORF 3. Vaccine 21:1833-1842.
18. Egberink HF, Ederveen J, Callebaut P, Horzinek MC. 1988. Characterization of the structural proteins of porcine epizootic diarrhea virus, strain CV777. American journal of veterinary research 49:1320-1324.
19. Rossen JW, Bekker CP, Strous GJ, Horzinek MC, Dveksler GS, Holmes KV, Rottier PJ. 1996. A murine and a porcine coronavirus are released from opposite surfaces of the same epithelial cells. Virology 224:345-351.
20. Park SJ, Moon HJ, Yang JS, Lee CS, Song DS, Kang BK, Park BK. 2007. Sequence analysis of the partial spike glycoprotein gene of porcine epidemic diarrhea viruses isolated in Korea. Virus genes 35:321-332.
21. Shirato K, Maejima M, Matsuyama S, Ujike M, Miyazaki A, Takeyama N, Ikeda H, Taguchi F. 2011. Mutation in the cytoplasmic retrieval signal of porcine epidemic diarrhea virus spike (S) protein is responsible for enhanced fusion activity. Virus research 161:188-193.
22. Shirato K, Matsuyama S, Ujike M, Taguchi F. 2011. Role of proteases in the release of porcine epidemic diarrhea virus from infected cells. Journal of virology 85:7872-7880.
23. Kido H, Okumura Y, Takahashi E, Pan HY, Wang S, Chida J, Le TQ, Yano M. 2008. Host envelope glycoprotein processing proteases are indispensable for entry into human cells by seasonal and highly pathogenic avian influenza viruses. Journal of molecular and genetic medicine : an international journal of biomedical research 3:167-175.
24. Kantanen ML, Leinikki P, Kuismanen E. 1995. Endoproteolytic cleavage of HIV-1 gp160 envelope precursor occurs after exit from the trans-Golgi network (TGN). Archives of virology 140:1441-1449.
25. Bugge TH, Antalis TM, Wu Q. 2009. Type II transmembrane serine proteases. The Journal of biological chemistry 284:23177-23181.
26. Bottcher E, Matrosovich T, Beyerle M, Klenk HD, Garten W, Matrosovich M. 2006. Proteolytic activation of influenza viruses by serine proteases TMPRSS2 and HAT from human airway epithelium. Journal of virology 80:9896-9898.
27. Simmons G, Gosalia DN, Rennekamp AJ, Reeves JD, Diamond SL, Bates P. 2005. Inhibitors of cathepsin L prevent severe acute respiratory syndrome coronavirus entry. Proceedings of the National Academy of Sciences of the United States of America 102:11876-11881.
28. Matsuyama S, Nagata N, Shirato K, Kawase M, Takeda M, Taguchi F. 2010. Efficient activation of the severe acute respiratory syndrome coronavirus spike protein by the transmembrane protease TMPRSS2. Journal of virology 84:12658-12664.
29. Krzyzaniak MA, Zumstein MT, Gerez JA, Picotti P, Helenius A. 2013. Host cell entry of respiratory syncytial virus involves macropinocytosis followed by proteolytic activation of the F protein. PLoS pathogens 9:e1003309.
30. Belouzard S, Chu VC, Whittaker GR. 2009. Activation of the SARS coronavirus spike protein via sequential proteolytic cleavage at two distinct sites. Proceedings of the National Academy of Sciences of the United States of America 106:5871-5876.
31. Matsuyama S, Taguchi F. 2009. Two-step conformational changes in a coronavirus envelope glycoprotein mediated by receptor binding and proteolysis. Journal of virology 83:11133-11141.
32. Li BX, Ge JW, Li YJ. 2007. Porcine aminopeptidase N is a functional receptor for the PEDV coronavirus. Virology 365:166-172.
33. Bertram S, Dijkman R, Habjan M, Heurich A, Gierer S, Glowacka I, Welsch K, Winkler M, Schneider H, Hofmann-Winkler H, Thiel V, Pohlmann S. 2013. TMPRSS2 activates the human coronavirus 229E for cathepsin-independent host cell entry and is expressed in viral target cells in the respiratory epithelium. Journal of virology 87:6150-6160.
34. Bertram S, Heurich A, Lavender H, Gierer S, Danisch S, Perin P, Lucas JM, Nelson PS, Pohlmann S, Soilleux EJ. 2012. Influenza and SARS-coronavirus activating proteases TMPRSS2 and HAT are expressed at multiple sites in human respiratory and gastrointestinal tracts. PloS one 7:e35876.
35. Licitra BN, Millet JK, Regan AD, Hamilton BS, Rinaldi VD, Duhamel GE, Whittaker GR. 2013. Mutation in spike protein cleavage site and pathogenesis of feline coronavirus. Emerging infectious diseases 19:1066-1073.
36. Kido H, Okumura Y, Takahashi E, Pan HY, Wang S, Yao D, Yao M, Chida J, Yano M. 2012. Role of host cellular proteases in the pathogenesis of influenza and influenza-induced multiple organ failure. Biochimica et biophysica acta 1824:186-194.
37. Tay FP, Huang M, Wang L, Yamada Y, Liu DX. 2012. Characterization of cellular furin content as a potential factor determining the susceptibility of cultured human and animal cells to coronavirus infectious bronchitis virus infection. Virology 433:421-430.
38. Baker M, Prasad BV. 2010. Rotavirus cell entry. Current topics in microbiology and immunology 343:121-148.
39. Kweon CH, Kwon BJ, Lee JG, Kwon GO, Kang YB. 1999. Derivation of attenuated porcine epidemic diarrhea virus (PEDV) as vaccine candidate. Vaccine 17:2546-2553.
40. Madu IG, Roth SL, Belouzard S, Whittaker GR. 2009. Characterization of a highly conserved domain within the severe acute respiratory syndrome coronavirus spike protein S2 domain with characteristics of a viral fusion peptide. Journal of virology 83:7411-7421.
41. Park SJ, Song DS, Ha GW, Park BK. 2007. Cloning and further sequence analysis of the spike gene of attenuated porcine epidemic diarrhea virus DR13. Virus genes 35:55-64.
42. Harrison SC. 2008. Viral membrane fusion. Nature

structural & molecular biology 15:690-698.

43. Qiu Z, Hingley ST, Simmons G, Yu C, Das Sarma J, Bates P, Weiss SR. 2006. Endosomal proteolysis by cathepsins is necessary for murine coronavirus mouse hepatitis virus type 2 spike-mediated entry. Journal of virology 80:5768-5776.
44. Huang IC, Bosch BJ, Li F, Li W, Lee KH, Ghiran S, Vasilieva N, Dermody TS, Harrison SC, Dormitzer PR, Farzan M, Rottier PJ, Choe H. 2006. SARS coronavirus, but not human coronavirus NL63, utilizes cathepsin L to infect ACE2-expressing cells. The Journal of biological chemistry 281:3198-3203.
45. Kawase M, Shirato K, Matsuyama S, Taguchi F. 2009. Protease-mediated entry via the endosome of human coronavirus 229E. Journal of virology 83:712-721.
46. Gierer S, Bertram S, Kaup F, Wrensch F, Heurich A, Kramer-Kuhl A, Welsch K, Winkler M, Meyer B, Drosten C, Dittmer U, von Hahn T, Simmons G, Hofmann H, Pohlmann S. 2013. The spike protein of the emerging betacoronavirus EMC uses a novel coronavirus receptor for entry, can be activated by TMPRSS2, and is targeted by neutralizing antibodies. Journal of virology 87:5502-5511.
47. Sato T, Takeyama N, Katsumata A, Tuchiya K, Kodama T, Kusanagi K. 2011. Mutations in the spike gene of porcine epidemic diarrhea virus associated with growth adaptation in vitro and attenuation of virulence in vivo. Virus genes 43:72-78.
48. Park SJ, Moon HJ, Luo Y, Kim HK, Kim EM, Yang JS, Song DS, Kang BK, Lee CS, Park BK. 2008. Cloning and further sequence analysis of the ORF3 gene of wild- and attenuated-type porcine epidemic diarrhea viruses. Virus genes 36:95-104.
49. Kaverin NV, Webster RG. 1995. Impairment of multicycle influenza virus growth in Vero (WHO) cells by loss of trypsin activity. Journal of virology 69:2700-2703.
50. Belouzard S, Millet JK, Licitra BN, Whittaker GR. 2012. Mechanisms of coronavirus cell entry mediated by the viral spike protein. Viruses 4:1011-1033.
51. Zamolodchikova TS. 2012. Serine proteases of small intestine mucosa--localization, functional properties, and physiological role. Biochemistry. Biokhimiia 77:820-829.
52. Simmons G, Zmora P, Gierer S, Heurich A, Pohlmann S. 2013. Proteolytic activation of the SARS-coronavirus spike protein: Cutting enzymes at the cutting edge of antiviral research. Antiviral research 100:605-614

Summarizing Discussion

Viruses must gain access to cells for replication. Enveloped viruses use fusion glycoproteins to merge their envelope with a host cell membrane. Structural and biochemical studies elucidated how fusion proteins function, but many questions remain. Generally, the fusion event is controlled at multiple checkpoints that have to be passed by the fusion protein: i) receptor binding, ii) acquisition of fusion-competence by priming, and iii) triggering of membrane fusion (Chapter 1 Figure 2). However, considerable differences concerning the nature and sequential order of these checkpoints exist between virus families.

The present PhD project focused on priming and triggering of the coronavirus spike (S) fusion proteins. No detailed structural information of any coronavirus S protein has been reported that would elucidate the conformational stages that lead to fusion. Nevertheless, proteolytic processing of coronavirus S proteins evidently plays a pivotal role in controlling of its fusion function. S proteins can be cleaved at two distinct sites: the S1/S2 junction and the S2' site. I will discuss molecular details and consequences of S protein cleavage at both sites. To that end, coronavirus S proteins are compared to the general model of class I fusion proteins discussing particularities and parallels. The availability of appropriate proteases and corresponding cleavage sites also appears to influence the tropism of coronaviruses. I will also elaborate on proteases as potential targets for antiviral intervention strategies. Besides proteolytic processing of the S proteins, I will evaluate the role of membrane-anchored peptidases as receptors for coronaviruses. Finally, a future perspective of the coronavirus entry research will be discussed.

The role of cleavage of spike proteins at the S1/S2 junction in cell-cell fusion

Proteolytic priming of the viral fusion machinery was initially recognized as an essential activation step for the virus entry of enveloped influenza virus. Since then proteolytic cleavage of viral fusion proteins has been observed in many virus families. Moreover, nonenveloped viruses such as reoviruses also require proteolysis of viral components to acquire the ability to enter a cell (1).

Consistently, some coronavirus S proteins undergo cleavage by furin-like proprotein convertases in the trans-Golgi network. The basic furin recognition motif is located at the S1/S2 junction (Table 1). Initially, this site was thought to correspond to that of other class I fusion proteins like influenza virus hemagglutinin (Chapter 1 Figure 2), and to be available in all coronavirus S proteins. Since then it appeared that not all coronavirus S proteins are cleaved. Furin cleavage at the S1/S2 junction is even dispensable for virus infectivity (reviewed in (2)). Unlike in other class I fusion proteins, the fusion peptide is located in some distance from novel N-terminus of the S2 subunit (Chapter 1, Figure 3).

One way to characterize fusion events is by studying the cell-cell fusion capacity of coronavirus infected cells or of cells expressing S proteins. The capability to form syncytia was found to be enhanced by the addition of exogenous proteases to cells infected by coronaviruses (3). This initial discovery suggested that coronavirus fusion proteins generally require proteolytic priming.

Cleavage at the S1/S2 junction by endogenous proteases like furin can stimulate efficient cell-cell fusion (4, 5). Hence, it was believed that cleavage at the S1/S2 junction is sufficient for priming of coronavirus S proteins. Further support for this hypothesis came from studies of MHV S proteins with distinct configurations of the S1/S2 cleavage site. The probability of

cleavage at the S1/S2 junction showed a positive correlation with cell-cell fusion activity. MHV-2 and MHV/BHK (a derivative of MHV-A59) S proteins lack a functional furin cleavage site R-X-(R/K)-R (R = arginine, K = lysine, X = any aa) at the S1/S2 junction and infected cells display none or limited cell-cell fusion activity (6, 7). MHV2f and MHV-A59 S proteins contain minimal furin cleavage sites at the S1/S2 junction and infection results in syncytia formation under physiological conditions (8). MHV-JHM S protein contains two overlapping furin cleavage sites for optimal chance of cleavage (9). All S proteins on MHV-JHM virions are cleaved by furin and cell-cell fusion is more efficient than for other MHV strains, and can actually occur independent of the receptor (10, 11).

Although cell-cell fusion assays are convenient and certainly informative, the results appeared to be inconsistent with those of virus-cell fusion. This led to misinterpretations of the proteolytic requirements for coronavirus fusion. Plasma membrane fusion occurs under particular conditions like neutral pH, at large membrane surfaces, involving potentially large numbers of participating fusion proteins, and with a distinct composition of lipids and receptor molecules. Diverging characteristics of cell-cell fusion and virus-cell fusion have been reported multiple times (4, 12-14). These findings put the relevance of cell-cell fusion assays for studying virus-cell fusion into question. Moreover, syncytia formation may be a mere artifact of cell culture-based propagation of coronaviruses and thus, provide limited insight into the virus-cell fusion process (15). More research is required to understand the particular conditions under which cell-cell fusion can occur. It is currently unclear how cell-cell fusion observed in vitro corresponds to the in vivo situation.

Cleavage of spike proteins at the S1/S2 junction may enhance the fusion capability

Furin cleavage of S proteins at the S1/S2 junction has been reported to be dispensable for coronavirus entry using different approaches. In the presence of furin inhibitors or by disruption of the furin cleavage site using mutagenesis, virus entry was not affected (4, 16, 17). Even the substitution of all basic amino acids at the furin cleavage site of the spike protein did not abolish MHV-A59 infection (Chapter 2). Nevertheless, some coronaviruses maintain a furin cleavage site and carry furin-cleaved S proteins on the surface of released virions (Table 2). The purpose of cleavage at the S1/S2 junction may be to augment the membrane fusion capability. This is already indicated by the increased cell-cell fusion activity of viruses with a FCS at the S1/S2 junction. Independent of cell-cell fusion, it was also found to enhance virus entry of particular coronaviruses. For cell culture-adapted infectious bronchitis virus (IBV) strain Beaudette (18), a FCS at the S1/S2 junction of the S protein was found dispensable but increased IBV entry (5). Also the proteolytic activation of the SARS-CoV S protein is more efficient after a preceding cleavage at the S1/S2 junction, although S proteins is not naturally cleaved by furin in this case (19). In our study, most MHV-A59 S proteins that were part of fusion virions, were cleaved downstream of the S1/S2 junction (Chapter 2). By analogy to IBV and SARS-CoV, MHV S proteins that are cleaved at the S1/S2 junction may become more efficiently processed at a sequential cleavage site during entry.

The studies prove that disconnecting the covalent linkage between the S1 and S2 subunits by furin can enhance the membrane fusion capacity of coronavirions. In agreement with the model of influenza virus hemagglutinin, we believe that proteolytic cleavage at the S1/S2 junction allows the bulky receptor binding unit to be displaced, relieving steric restrictions on the fusion subunit (1, 20). More importantly, sequestered cleavage sites in the coronavirus S

protein may become accessible to proteases after cleavage at the S1/S2 junction. This would then improve the chance of sequential cleavage and stimulate fusion activity. The molecular and structural details thereof remain to be elucidated in future studies.

Detrimental effects of cleavage at the S1/S2 junction

If cleavage at the S1/S2 junction enhances S protein activity, why do most coronavirus S proteins lack a genuine furin cleavage site and carry uncleaved S proteins? In my opinion, a covalent link between the S1 and S2 subunits could be crucial to preserve the receptor binding function of the S protein. The subunits of influenza virus hemagglutinin and Ebola virus glycoprotein remain covalently attached by disulfide bonds (Chapter 1 Figure 3). In contrast, the subunits of human immunodeficiency virus Env and coronavirus S proteins are associated by noncovalent interactions (21). The coronavirus S1 subunit has been found to dissociate upon incubation at pH 8 (22, 23) and by >1 M urea (unpublished observation in our laboratory). Hence, the coronavirus subunits could be separated in the extracellular phase of the viral life cycle, resulting in an irreversible loss of receptor binding capability. A delay of coronavirus S protein cleavage ensures that the S1 receptor binding domain remains in place until the virions reach the host cells. Indeed, pretreatment of cell culture-adapted PEDV-DR13 S proteins with trypsin resulted in reduction of infectivity, reduced binding to the host cells, and cleavage of the S protein (Chapter 5). The wild-type PEDV S proteins resisted cleavage by trypsin and infectivity was not affected. Likewise, cell entry of pseudotyped particles carrying SARS-CoV S proteins was disrupted if they were exposed to trypsin prior to attachment. Cleavage occurred at the S1/S2 junction (13). We sought to address the effects of cleavage experimentally by creating an MHV-A59 S protein that would always become cleaved by furin. Therefore, the furin cleavage site at the S1/S2 junction was optimized by mutagenesis. We tried to generate this recombinant MHVA59, but could not recover the virus carrying only cleaved S proteins (unpublished observation in our laboratory). Furthermore, the cleaved S proteins could not be incorporated into retrovirus-like particles (Chapter 3). Future studies may investigate the role of covalent linkage in maintaining the receptor binding capacity. With more structural information on the S proteins at hand, it might be possible to engineer disulfide bonds between the S1 and S2 domain in combination with an optimized cleavage site. This S protein might maintain receptor binding without inhibiting the fusion capabilities.

After cleavage, the fusion-ready and metastable coronavirus S protein might also become more labile and may more easily transit into the irreversible post-fusion conformation. To approach this issue, we determined the specific infectivity of the earlier mentioned MHV/BHK, MHV-A59, and MHV-JHM; i.e., their average infectivity per particle. The specific infectivity of MHV/BHK and MHV-A59 was approximately 100fold higher than that of MHV-JHM, the latter carrying cleaved S proteins (data kindly provided by Christine Burkard). This demonstrates that viruses with readily cleaved S proteins are be less infectious. We interpret this as a result of premature activation of the fusion protein. This view is supported by the receptor-independent cell-cell fusion capacity of MHV-JHM as mentioned earlier. A fusion trigger checkpoint could prevent premature structural rearrangements of a labile fusion protein. Until today no genuine trigger of coronavirus fusion has been identified as I will discuss later. Instead, the proteolytic priming of S protein is delayed, which might help to preserve the fusion capacity until the appropriate host cell is encountered.

Coronavirus fusion proteins are activated by cleavage at the S2' cleavage site

Initial research was unable to define a precise role for cleavage at the S1/S2 junction of coronavirus S proteins. In the last 5 years refined experiments and the intensive study of the SARS-CoV S protein provided more insight. Cleavage at the S1/S2 junction was reported to be dispensable for virus-cell fusion as shown by mutagenesis of the cleavage site (13, 19). Eventually, a crucial arginine was identified as the more important S2' cleavage site (19) (Table 1). By using amino acid sequence comparison and mutagenesis of the S protein, the S2' site was found to be located C-terminal of the S1/S2 junction and just upstream of the fusion peptide (24). High sequence conservation of the fusion peptide and the adjacent arginine are illustrated by a comprehensive amino acid sequence alignment of coronavirus S proteins (5).

In our opinion, the S2' site is the common cleavage site for coronavirus S protein activation. Its position upstream of the conserved fusion peptide (25) corresponds to the typical cleavage site described in the model of class I fusion proteins(20). In this thesis, we demonstrated MHV-A59 S protein cleavage at sequential cleavage sites during infection. In chapter 2, we provide evidence that cleavage downstream of the S1/S2 junction yields the fusion-ready S protein subunit (S2*), which corresponds to the primed, pre-fusion metastable intermediate conformation of class I fusion proteins. Whether this cleavage site in MHV-A59 S proteins corresponds exactly to the S2' cleavage site in SARS-CoV S proteins will be discussed towards the end of the present discussion. In contrast to influenza virus hemagglutinin, human immunodeficiency virus Env, and paramyxovirus F protein, none of the studied wild-type coronavirus S proteins were found to be cleaved at the S2' site after release of the virions, i.e. are not fusion-ready (21). However, the current model of class I fusion proteins would dictate that uncleaved precursor S proteins must be proteolytically activated at or in the target cell.

A number of coronavirus S proteins have been studied in detail. They seem to require a distinctive set of stimuli and proteases for the activation of the fusion capability. I will depict examples of the preconditions that must be fulfilled to facilitate S2' cleavage. For MHV2, receptor interaction enables cleavage at S2' equivalent position, yielding the protease K resistant post-fusion conformation of the S protein (26). We suggest that S2' cleavage of MHV-A59 S protein also requires inoculation of cells (Chapter 2). Thus, receptor interaction is probably required for MHVA59 S protein activation.

The S protein of SARS-CoV is also activated by cleavage at or in the host cell. The S1/S2 junction (R667) can be cleaved by trypsin, which promotes fusion events at the cell surface (12). Although trypsin is not present at the natural site of SARS-CoV infection, it demonstrates that the fusion process can be independent of low pH. Alternatively, low-pH dependent protease cathepsin L can activate SARS-CoV S proteins in the endosome (27). Compounds that prevent endolysosomal acidification (lysosomotropic agents) and specific cathepsin L inhibitors block entry of SARS-CoV (28). However, the above mentioned proteases may not be of pivotal importance for SARS-CoV infections, as S proteins are rather activated by cleavage at the downstream S2' site. The cleavage at the S1/S2 junction augments the sequential cleavage at the S2' site (19, 29). In natural infections, type II transmembrane serine proteases (TTSP) present on the host cells can facilitate infection by cleavage at the S2' site (30).

Table 1. Putative cleavage sites in coronavirus S proteins

Coronavirus	abbreviation	strain	host	Protein receptor	S1/S2 junction	S2' site prediction	adjacent fusion peptide
Genus Alphacoronavirus							
Canine coronavirus	CCoV		canine	APN	YTNARTR	SHNSKRKY**R**	SAIEDLLFDKVVTSGLGT
Feline coronavirus	FECV	79-1683	feline	APN	YTNERTR	SHNSKRKY**R**	SAIEDLLFDKAVTSGLGT
	FIPV	79-1146			YTSERTR	SHNSKRKY**G**	SAIEDLLFDKVVTSGLGT
Transmissible gastroenteritis virus	TGEV		porcine	APN	YTNDRTR	SHNSKRKY**R**	SAIEDLLFDKVVTSGLGT
human coronavirus 229E	HCoV 229E		human	APN	AVQPR	TSGSRVAG**R**	SAIEDILFSKLVTSGLGT
human coronavirus NL63	HCoV NL63		human	ACE2	PVRPR	IRSSRIAG**R**	SALEDLLFSKVVTSGLGT
Porcine epidemic diarrhea virus	PEDV	caDR13	porcine	APN	GYVPLQ	ASGRVVQKG	SFIEDLLFNKVVTNGLGT
		CV777			GYVPSQ	ASGRVVQK**R**	SVIEDLLFNKVVTNGLGT
Genus Betacoronavirus							
Human coronavirus	HCoV OC43	ATCC	human	Sugars	RRSRG	----KASS**R**	SAIEDLLFDKVKLSDVGF
Bovine coronavirus	BCoV	Mebus	bovine	Sugars	RRSRR	----KVSS**R**	SAIEDLLFSKVKLSDVGF
Human coronavirus	HKU1		human		RRKRR	-PHCGSSS**R**	SFFEDLLFDKVKLSDVGF
Murine coronavirus	MHV	A59	murine	CCM	RRAHR	NGPSAIRG**R**	SAIEDLLFDKVKLSDVGF
		JHM			RRARR	NGPSAIRG**R**	SAIEDLLFDKVKLSDVGF
		2			HRARS	VTMAAQTG**R**	SAIEDVLFDKVKLSDVGF
		DIVM			HRARR	GTMAAQG-**R**	STVEDLLFDKVKLSDVGF
Middle East respiratory syndrome coronavirus	MERS-CoV		human	DPP4	PRSVR	ISTGSRSA**R**	SAIEDLLFDKVTIADPGY
Severe acute respiratory syndrome coronavirus	SARS-CoV	Tor2	human	ACE2	VSLLR	PDPLKPTK**R**	SFIEDLLFNKVTLADAGF
Genus Gammacoronavirus							
Infectious bronchitis virus	IBV	Beaudette	avian		RRFRR	TNPSSRRK**R**	SLIEDLLFTSVESVGLPT
		M41			RRFRR	TTPSSPRR**R**	SFIEDLLFTSVESVGLPT
Genus Deltacoronavirus							
bulbul coronavirus	HKU11		avian		KFTRTIA	IITSKSGG**R**	SAIEDLLFNKVVTNGLGT
munia coronavirus	HKU13		avian		FQRVIPT	ILSNKIGEK	SVIEDLLFNKVVTNGLGT
thrush coronavirus	HKU12		avian		FKSRIAT	ILPNKQGG**R**	SAIEDLLFDKVVTNGLGT

Putative cleavage sites in coronavirus S proteins
S1/S2 junction: putative border between the S1 and S2 subunit as predicted by the location of the furin cleavage site in some beta- and gamma-coronaviruses. The conserved arginine marking the S2' cleavage site (bold) is typically directly adjacent to the highly conserved fusion peptide.

Proteolytic priming of coronavirus S protein can be controlled by receptor binding, low pH, as well as the access to and function of appropriate proteases. New studies will probably identify alternative cues. Novel cofactors for virus entry, like the discovery of Niemann Pick C1 protein for Ebola virus, may be found (31). Another possible stimulus may be the distinct ion concentrations in the lumen of the endosomal vesicles (reviewed in (32)). The ionic composition changes considerably as endosomes mature and can affect virus entry. For example, influenza virus infection is dependent on the flux of ions across the viral envelope in the endosome (reviewed in (33)).

In chapter 5, we studied the conditions for the proteolytic activation of PEDV entry. PEDV infection in cell culture is peculiar for coronaviruses in that it requires the supplementation with exogenous trypsin (34). We believe that receptor-bound PEDV S protein can be activated by trypsin cleavage at the S2' site (Chapter 5). Therefore, PEDV S proteins may be a reductionistic tool to accurately study stimulation, mechanism, and consequences of S protein mediated fusion. Intriguingly, cell culture-adapted PEDV strains propagate independent of trypsin (35) indicating that serial passaging can alter virus fusion requirements. Trypsin-independent PEDV may still require cleavage of the S protein by cellular proteases, as no cell-cell fusion was observed in the absence of trypsin in the cell culture supernatant. However, trypsin independence does not provide PEDV infection an advantage in vivo, because all PEDV field strains isolated so far appear trypsin dependent. It remains to be investigated whether PEDV fusion requires additional stimuli as co-factors like the endosomal milieu.

Priming and triggering of coronavirus fusion proteins

Influenza virus hemagglutinin, dengue virus E protein, and VSV G protein are prototypic examples of class I, II, and III fusion proteins, respectively. They adopt their metastable intermediate conformation either after proteolytic processing in the producer cells or do not require cleavage for it (20). Their virions carry fusion-ready fusion proteins. Subsequently, the spatiotemporal characteristics of membrane fusion are regulated by the fusion trigger that typically comes in the form of receptor binding or low pH (21). The trigger lowers the energy barrier that prevents the structural rearrangements leading to the post-fusion conformation (Chapter 1 Figure 2). This classical distinction between priming, i.e. conversion into the metastable conformation, and fusion activation by a trigger may not apply to coronavirus S proteins. I will discuss how particular coronaviruses control the membrane fusion capabilities of their S proteins.

There is no clear evidence for a pH-induced fusion process of coronavirus S proteins. Main argument is that syncytia formation by cells infected with different coronavirus species occurs at physiological pH. Initially, it was found that SARS-CoV, MHV-JHM and MHV-2 infection is blocked by lysosomotropic agents. However, the block of infection can be bypassed by the treatment of cell-bound virions with pH-independent proteases (36-39). Furthermore, coronavirus infectivity is not compromised by low-pH incubation (22). This indicates that acidic pH cannot trigger the S protein to adopt its post-fusion conformation.

Yet, MHV-A59 and also infectious bronchitis virus infection were independently found to rely on acidic pH (40, 41). Membrane fusion by MHV-A59 fusion-ready S2* subunits was not observed when acidification of the endolysosomal compartment was prevented (Chapter 2 and 3). However, pH-perturbing agents have several secondary effects and can disturb endosome maturation and ion concentrations, for example. Pitfalls in studying endocytosis of virions are extensively reviewed by Mercer et al. (42).

If independent of low pH, the coronavirus S protein fusion activity must be initiated at the susceptible cells by other means. In my opinion, control over the fusion proteins is at least partially applied by crucial timing of the proteolytic processing of coronavirus S proteins. Until their arrival at a susceptible cell, S proteins maintain a precursor conformation. Only then, proteolytic cleavage releases the S proteins into a metastable, fusion-ready, pre-fusion conformation which readily progresses into a post-fusion conformation, possibly without

subsequent trigger (43). We could observe cell-cell fusion by PEDV S proteins within minutes after addition of trypsin by live cell microscopy (Chapter 5). Precise timing of fusion protein activation could also be essential to prevent premature transitions into an irreversible post-fusion conformation as discussed earlier.

The main checkpoint which controls coronavirus S protein fusion activity seems to be proteolytic priming and not triggering. Proteolysis may substitute for the low pH trigger for some coronaviruses and combine priming and triggering. Besides, additional co-factors like auxiliary receptors, low pH, ion gradients, or membrane composition may fine-tune the fusion process of particular coronaviruses.

For example, the redox potential at the fusion site can be of importance, because disulfide bonds play an important role in structuring fusion proteins (reviewed in (44)). Membrane fusion by the HIV Env protein can be blocked by inhibitors of the protein disulfide isomerase (45). Generally, little is known about the impact of the redox potential on virus entry.

Fusion protein cleavage can determine tropism and pathogenicity of coronavirus infections

I discussed above the stimuli and molecular consequences of cleavage of coronavirus S proteins with a focus on the membrane fusion mechanics, and I will continue to debate the role of cleavage for virus tropism, and how alterations of the proteolytic event can change virus entry.

Viruses carrying uncleaved class I fusion proteins may only infect cells that provide particular proteases for activation. Consequently, differences in cleavage can determine pathology and tropism of infection as illustrated by influenza viruses (46, 47). Highly pathogenic avian influenza virus hemagglutinin typically contains a multiple basic cleavage site, which is cleaved by ubiquitously expressed furin-like proteases in the producer cells. Virus progeny is fusion-ready when released and can cause systemic infections. Viruses carrying primed fusion proteins cannot use cleavage as a checkpoint to regulate tropism. In contrast, low pathogenic influenza virus hemagglutinin has a mono basic cleavage site. Virions carry uncleaved, inactive fusion protein and rely on trypsin-like proteases secreted or expressed by gastrointestinal and respiratory cells for activation. Thus, infection is restricted to the gut and airways. This illustrates how fine-tuning of the cleavage site properties might be a strategy of viruses that require proteolytic activation to adjust to specific proteases. Dependence on a specific protease may restrain the virus infection to tissues providing optimal growth conditions and high chances for transmission such as the airways or the gut.

In the last 5 years, the tropism and pathogenesis of coronaviruses was demonstrated to correlate with proteolytic activation of the S fusion proteins. In particular type II transmembrane serine proteases (TTSP) like TMPRSS2 received much attention, because they process the S proteins of many human pathogenic coronaviruses including Middle East respiratory syndrome CoV (48), SARS-CoV (49), human CoV-229E (50), and also enhance influenza virus (51) and metapneumovirus (52) entry. TTSP are endogenously expressed by epithelial cells of the aerodigestive tract (reviewed in (53)) and cellular expression correlates with susceptibility to virus infections (30). However, not all coronavirus S proteins can be activated by TMPRSS2. Virus entry of protease dependent PEDV, for instance, was not enabled by TMPRSS2 overexpression (unpublished observation).

The pathogenesis of the two biotypes of feline coronavirus might be modulated by proteolytic activation. The nonpathogenic feline enteric coronavirus (FECV) is dependent on

cathepsin L and B, while the highly pathogenic feline infectious peritonitis virus (FIPV) was only dependent on cathepsin L in vitro (54). Divergent from the example of high and low pathogenic avian influenza virus, a recent study suggests that FIPV, which causes systemic infections, differs from FECV, which is restricted to the gut, by losing the S1/S2 furin cleavage site (55).

Apparently, the contribution of distinct proteases or protease classes to natural virus infections needs further investigation, for example by using knockout animal models. A recent study showed that influenza virus infection is limited in TMPRSS2 knockout mice (56). This is the first clear evidence for the role of TMPRSS2 in natural infections. Moreover, specific protease inhibitors like Camostat can also be used to assess the relevance of proteases for infection and tropism in vivo.

Proteases as entry effectors and pharmacologic targets

If coronaviruses engage specific proteases for proteolytic activation of the fusion proteins, they can chose between various cellular proteases. About 1000 known and putative protease genes constituting five principle classes of proteases are known in humans, whereof some 500 proteases may be expressed by individual cells (overview in table 2) (57, 58). Secretory organs such as pancreas, kidney and salivary glands secrete substantial amounts of proteases. They establish a characteristic milieu of proteases and potentially enhance the susceptibility of adjacent tissues to virus infections. About half of the proteases expressed by a cell are predicted to cleave extracellular targets. Those could potentially affect virus entry.

Inhibition of virus entry by blocking of proteases that activate the fusion protein is considered an alternative option for antiviral drug therapy (60-62). Proof of principle studies showed effectiveness of such inhibitors in vivo, but none are currently used in the clinics. For example, the broad spectrum inhibition of serine proteases reduced the pathogenicity of influenza virus infection in mice (63) and humans (reviewed in (64). Cathepsin cysteine proteases are an example of proteases that can activate fusion proteins of different viruses. Specific inhibitors of cathepsin proteases are investigated as antiviral drugs (reviewed in (65)). In combination with serine protease inhibitors the more natural infection of a human bronchial epithelial cell model by SARS-CoV can be blocked (66).

Of concern, inhibitors of cellular proteases have a considerable potential to cause side effects. Proteases have essential functions in cell metabolism and catabolism, as proprotein

Table 2. Protease classes of mammalian cells (59)

Catalytic type	# Known proteases	Examples	Typical inhibitors
Aspartate	21	pepsin, cathepsin E	pepstatin A
Cysteine	148	papain, cathepsin K	E64, N-ethylmaleimide, leupeptin
Metallo	194	thermolysin, vertebrate collagenase, carboxypeptidase A	1,10-phenanthroline*, phosphoramidon
Serine	175	trypsin, lysosomal Pro-Xaa carboxypeptidase, prolyl oligopeptidase	Diisopropyl fluorophosphates*, leupeptin, AEBSF, aprotinin
Threonine	28	proteasome	lactacystin for some

*Toxic to cells

convertases, and digestive enzymes. Catalytically active proteases are usually generated from zymogens. Their activity is fine-tuned by the level of expression, the presence of protease inhibitors, cofactors, and subcellular localization. Dysregulation of protease function has been implicated in many diseases including cancer (67), haemophilia A (68), and Alzheimer disease (69). To reduce harmful side effects, one would typically design highly specific therapeutic compounds. However, protease inhibitors with a narrow specificity can be inefficient due to redundant proteolytic activity or flexible cleavage sites as discussed below.

Another approach to prevent S protein activation on coronavirions could be to limit the chance of exposure to the priming protease. Enveloped viruses typically fuse after endocytosis (42). The endolysosomal compartment provides protease activity to degrade extracellular material, but can also activates viral fusion proteins. Blocking the endocytic route or specific endosomal proteases may inhibit virus entry. However, Ebola virus and influenza viruses can use alternative endocytic routes for productive infection (70, 71). Since the contribution of individual entry routes to natural virus infection remains elusive, it is challenging to design a specific intervention strategy.

An alternative source of fusion-protein activating proteases are the proteases of commensal or pathogenic microbes in the gut and upper air ways. Microbial proteases often have distinct catalytic centers compared to host proteases or are members of a different class of proteases (72). Hence, specific inhibitors might be easier to select. Treatment might result in fewer side effects. Unclear is, whether microbial proteases can enhance virus entry by activating the viral fusion proteins. For example, influenza virus hemagglutinin can be cleaved by bacterial proteases (73). The pathogenicity of influenza infections in waterfowl (74) and swine (75) has been implicated to be affected by bacterial colonization. However, microbes modulate the immune response against virus infection, which obscures effects of protease inhibition (76). This makes the impact of microbial proteases on virus infection difficult to study.

In addition to virus entry, virus replication can also require proteases. Especially the processing of viral polyproteins typically requires specific proteases that can be a pharmacological target. Along these lines, inhibitors of hepatitis virus C protease NS3/4A and human immunodeficiency virus-1 protease are used in the clinics (reviewed in (77) and (78), respectively).

Proteolytic activation of PEDV in the gut

PEDV causes substantial economic losses in East Asia and is spreading in North America since 2013. Current vaccination strategies are ineffective. PEDV propagation in vitro is unique among coronaviruses in its requirement for the supplementation with exogenous proteases. The protease that enables PEDV infection in vivo could be a novel target for antiviral therapy.

In vivo, gastric and pancreatic proteases probably assist PEDV infection in the small intestine analogous to trypsin in cell culture. It would be interesting to explore the feeding of trypsin inhibitors to infected animals as a potential treatment for PEDV infections.

Intriguingly, the typical pig diet provides natural protease inhibitors, but it has not been studied whether they modulate virus infections. Soybean meals contribute up to 68% of protein meals in animal farming worldwide (79). Soy beans contain large amounts of the Bowman-Birk inhibitor and the Kunitz inhibitor, both blocking trypsin (latter one is used in

Chapter 5). Conspicuously, severe PED is predominantly observed in suckling piglets. Older pigs, perhaps due to their more inhibitor-rich diet, display considerably milder symptoms.

In fact, it has been demonstrated that ingested trypsin inhibitors reach the small intestine, where they can cause pancreatic growth in rats (reviewed in (80)). There are indications that protease inhibitors contained in the diet can inhibit the infection by rotavirus, a nonenveloped, trypsin-dependent DNA virus infecting the gastrointestinal tract. Soybean meals fed to mice and breastfeeding of human neonates are believed to protect from rotavirus infection (81, 82). However, we cannot exclude that alternative endoproteases, locally expressed by the gut epithelium could also enable PEDV infection (83).

Specificity of the proteolytic priming

Success of protease inhibitor therapies largely relies on the identification of a protease that is crucial for virus entry. An appropriate protease specific inhibitor may not necessarily abolish virus infection, yet it may reduce viremia and allow the immune system to control the infection. As mentioned before, TMPRSS2 activates a variety of viral fusion proteins. This stimulated the development of highly specific inhibitors of TMPRSS2 (84, 85). Other protease inhibitors developed for treatment of diseases related to protease-malfunctions are already clinically approved and may be tested for off-label use against virus infections (reviewed in (86)). Intensive research continues to seek out the most important proteases and design inhibitors.

The fusion-ready subunits of prototype class I fusion proteins appear to be cleaved at a distinct amino acid position. The model implies that cleavage occurs just upstream of the fusion peptide. Thereby, the fusion peptide is positioned at the novel N-terminus of the fusogenic subunit. Intriguingly, SARS-CoV S protein activation seems to occur at different positions (reviewed in (2)). The SARS-CoV S protein has been found to be cleaved at positions T795 or R797 by mutagenesis of the respective amino acids ((19) and (29), respectively). Additionally, proteolytic processing at a minimal furin cleavage site 758-RNTR-761 and at T678 by cathepsin L facilitates membrane fusion ((13) and (27)).

In my opinion, diverse or redundant proteases can activate MHV and SARS-CoV S proteins by cleavage at different positions rather than relying on one precise cleavage site. Our investigations indicated that the fusion-ready S2* subunit of MHV-A59 is not cleaved at a distinct position either (Chapter 2). Instead, we observed heterogeneous product after virus-cell fusion. Furthermore, we could block neither S protein processing nor MHV infection by broad spectrum protease inhibitors. The cleavage position will affect the relative location of the fusion peptide within the fusion-ready subunit. It will be interesting to compare the function of an N-terminal fusion peptide – by analogy to influenza virus – with the function of an internal fusion peptide, as found in Ebola virus (87).

Diversity in the cleavage reaction must be considered when designing antiviral intervention strategies. Inhibition of a specific protease may not abolish activation of coronavirus S proteins. The fusion proteins could be activated by an alternative protease that may cleave at the same or a nearby position.

Not relying on a single critical cleavage position may also explain why many coronaviruses S proteins are found to be activated by the cathepsin L. A large variety of diverse peptides can be cleaved by cathepsin L as shown by peptide library screening (88). It may activate the S proteins of different coronaviruses and cleave individual S proteins multiple times.

Cathepsin L is expressed ubiquitously. If it activates viral fusion proteins in vivo, the presence of the receptor would be the main determinant of tropism left.

No clear role for multiple cleavages has been established, yet. As previously discussed, initial cleavage events may facilitate subsequent cleavage at a crucial position. For other fusion proteins, successive cleavage seems to gradually increase the fusion capability. Ebola virus GP and respiratory syncytial virus F are cleaved multiple times at the N-terminus while they move along the endosomal pathway towards the lysosomes. This successively shortens the fusion proteins and gradually increases the fusion capability (89-91).

To study the precise requirements for coronavirus fusion protein activation in the future, one might employ viruses that were found to depend on individual proteases like PEDV. In addition, applying our conditional biotinylation assay to other coronaviruses might allow us to further characterize the proteolytic processing in combination with protease inhibitors.

Receptor interaction

Besides the important role of proteases for coronavirus entry, the expression of a receptor largely determines whether a cell is susceptible. According to the Fields Virology textbook, the receptor is a catalyst that lowers the energy barrier required to initiate the irreversible structural reorganization of the fusion protein into the post-fusion conformation (1). However, receptor interaction by many coronavirus S proteins is apparently necessary for S protein activation by cleavage. As described above, receptor interactions may ensure colocalization of S proteins with appropriate proteases, uptake into a particular endocytic compartment where proteolysis can occur, or result in structural rearrangements that expose the S2' cleavage site. Additional studies may elucidate if receptor interaction functions beyond the support of activating cleavage, for example by triggering of the fusion process.

Three membrane-anchored peptidases are described as receptors for different coronaviruses: ACE2, aminopeptidase N, a receptor for various alpha coronaviruses, and the recently identified dipeptidyl peptidase 4 as receptor for MERS-CoV. Is there a common denominator, which makes peptidases effective coronavirus receptors? Peptidases typically process zymogens into their active form, but their catalytic activity is not critical for their function as coronavirus receptor (92-94). Instead, peptidases could serve as a scaffold for interaction of viral structural proteins with the peptidase substrates. Recruiting substrate molecules may provide cofactors such as coreceptors for entry. Alternatively, peptidases could be internalized with distinct kinetics or via particular internalization pathways, for example the recycling endosome (42). Distinct uptake routes may be beneficial for coronavirus entry.

Recent investigations demonstrated that the SARS-CoV receptor angiotensin-converting enzyme 2 (ACE2) can become cleaved by TTSPs, resulting in an increased SARS-CoV infection (95, 96). Cleaved ACE2 receptors were suggested to be internalized more efficiently, resulting in enhanced uptake of SARS-CoV. However, coronaviruses may have evolved to use peptidases as receptors simply for their abundance and accessibility on epithelial and endothelial tissues (94).

Studying virus fusion

Studying virus entry has been hampered by technical obstacles and principle limitations arising from the nature of the process. In particular, the rapid sequence of events after attachment of a virion remains largely elusive. Endocytosis, hemi-fusion, and pore formation by vesicular stomatitis virus can occur within a few minutes (97). Notable progress has been made studying the spatiotemporal characteristics of virus entry by employing optical techniques. Single influenza virions and individual human immunodeficiency virus particles could be tracked by microscopy and different entry stages were distinguished (98, 99).

Most studies on virus entry rely on viral replication to amplify viral or reporter genes for convenient readout. To measure virus entry directly and differentiate virion attachment, internalization, and fusion, our lab developed a novel assay (Christine Burkard, manuscript submitted). It enables quantitative measurements, supports high-throughput approaches, and can detect small numbers of virions at any stage of the entry process.

Low amounts of viral antigen involved in the fusion process and the high abundance of nonfunctional virus particles impose a challenge in unraveling further details at molecular level. Structural information contributed to the model of prototype fusion proteins, yet, no coronavirus S protein structure has been determined. Information about the function of coronavirus fusion proteins was mostly deduced from data generated by genetic modifications of the virus, pharmacologic treatment during infection and in vitro systems that mimic natural virus infections.

We combined these classical experiments with a novel conditional biotinylation assay for direct biochemical analysis (Chapter 2). The assay allowed us to characterize particular fusion glycoproteins from virions that had accomplished membrane fusion. Thus, fused S proteins are intracellularly labeled with biotin. We focused on priming and triggering of the coronavirus S proteins.

Using the conditional biotinylation assay, we could identify a novel proteolytically processed subunit of MHV-A59 S proteins, which displayed post-fusion characteristics. To my knowledge, we were the first to isolate viral fusion proteins directly after virus entry via a genuine infection route. A major difficulty was the detection of the S proteins. Since not all virions appeared to undergo fusion, infection only yielded a fraction of biotin-labeled S proteins. Our method required many virions to fuse and subsequent purification of the involved fusion proteins. With the goal of identifying possible cleavage sites in the S protein, additional large scale experiments may generate enough post-fusion S protein for an in-depth biochemical analysis like N-terminal sequencing or mass spectrometry.

We managed to refine our understanding of the function of S proteins during coronavirus entry, but many unanswered questions remain that are of genuine scientific interest to other viruses as well. One of the most intriguing questions is how many fusion proteins actively participate in an individual virus fusion event. The biotinylation assay will not be able to provide an answer, since all BAP-tagged proteins of a fusing virion will be labeled. Nevertheless, we have noticed equal processing of almost all biotinylated fusion proteins, arguing for a fusion-ready status of most S proteins at the time of fusion. By manipulating the number of fusion proteins that are incorporated into a virus envelope, one might be able to approximate the number of fusion proteins required for entry.

Also unknown is, from what precursor S protein the fusion-ready subunits are generated. In the case of MHV-A59, S2* subunits were found to be derived from S2 subunits by

subsequent cleavage. However, additional intermediate cleavage products may exist and be functional, because a knockout of all arginines at the S1/S2 junction of MHV-A59 S protein did not affect virus fusion. A hint may come from further studies of the Middle East respiratory syndrome human coronavirus. The S proteins are cleaved during biogenesis at the S1/S2 junction. Since a furin cleavage site is absent in the S protein, alternative cellular proteases may be identified that can cleave S proteins (48).

The biotinylation assay may be further used to track the fate of fusion proteins for an extended period time. One could monitor the location and kinetics of a potential degradation processes in the endosomal compartment. For coronaviruses, this may help to characterize the window of opportunity for membrane fusion between proteolytic activation of the fusion machinery during endocytosis and degradation in the lysosomes.

The trigger for fusion is another determinant of coronavirus entry that needs further characterization. At this moment it remains obscure whether coronaviruses require fusion triggers and if so, of what nature. Coronavirus entry seems to be a rather slow process (Chapter 2 and unpublished observation in our lab) that cannot be readily triggered by any of the known stimuli. Besides relying on the function of low-pH-activated proteases, some coronaviruses seem to require acidification of the endosomal compartment for entry as discussed earlier.

Virus entry will be different for individual coronavirus species. Nevertheless, underlying common mechanisms may exist. Specific questions could be answered best by choosing a virus with simple and well-known fusion characteristics. For example, to confirm our hypothesis of the coronavirus S2' cleavage site, it would be advantageous to adopt the conditional biotinylation assay to a virus with a single protease requirement like PEDV. Those can be blocked by specific inhibitors and may allow a precise analysis of the cleavage site.

Concluding Remarks

Virus entry requires dedicated protein functions that enable viruses to cross the host cell membrane. Intensive studies of prototype viruses helped to generate models for the virus-cell fusion process and to understand the mechanics of this process. The classification of coronavirus fusion proteins as class I fusion proteins was based on structural features. However, similarities are mainly of structural nature, as I reviewed in the introduction. In contrast, control over the fusion competence, priming, and triggering of coronavirus S proteins has proven to be distinct.

Determining the pre- or post-fusion structure of a coronavirus S protein would allow scientists to deduce the impact of environmental stimuli and protease cleavage on fusion. One could design new experiments on knowledge-based hypotheses and understand how CoV S proteins differ from well-known class I fusion proteins.

Especially the zoonotic potential of coronaviruses and the unforeseeable consequences of such an occurrence impose a threat to public health. The ability of coronaviruses to cross the species barrier also depends on the spike fusion protein. Knowledge concerning the structure and function of these peculiar fusion proteins is essential to deal with coronavirus infections in humans and animals. S proteins mediate host cell entry, the first step in the viral life cycle. Hence, they are a prime target for treatment and prevention strategies.

References

1. Fields BN, Knipe DM, Howley PM. 2013. Fields virology, Sixth edition ed. Wolters Kluwer/ Lippincott Williams & Wilkins Health, Philadelphia.
2. Belouzard S, Millet JK, Licitra BN, Whittaker GR. 2012. Mechanisms of coronavirus cell entry mediated by the viral spike protein. Viruses 4:1011-1033.
3. Otsuki K, Tsubokura M. 1981. Plaque formation by avian infectious bronchitis virus in primary chick embryo fibroblast cells in the presence of trypsin. Archives of virology 70:315-320.
4. de Haan CA, Stadler K, Godeke GJ, Bosch BJ, Rottier PJ. 2004. Cleavage inhibition of the murine coronavirus spike protein by a furin-like enzyme affects cell-cell but not virus-cell fusion. Journal of virology 78:6048-6054.
5. Yamada Y, Liu DX. 2009. Proteolytic activation of the spike protein at a novel RRRR/S motif is implicated in furin-dependent entry, syncytium formation, and infectivity of coronavirus infectious bronchitis virus in cultured cells. Journal of virology 83:8744-8758.
6. Yamada YK, Takimoto K, Yabe M, Taguchi F. 1997. Acquired fusion activity of a murine coronavirus MHV-2 variant with mutations in the proteolytic cleavage site and the signal sequence of the S protein. Virology 227:215-219.
7. Schickli JH, Zelus BD, Wentworth DE, Sawicki SG, Holmes KV. 1997. The murine coronavirus mouse hepatitis virus strain A59 from persistently infected murine cells exhibits an extended host range. Journal of virology 71:9499-9507.
8. Sturman LS, Ricard CS, Holmes KV. 1985. Proteolytic cleavage of the E2 glycoprotein of murine coronavirus: activation of cell-fusing activity of virions by trypsin and separation of two different 90K cleavage fragments. Journal of virology 56:904-911.
9. Taguchi F. 1993. Fusion formation by the uncleaved spike protein of murine coronavirus JHMV variant cl-2. Journal of virology 67:1195-1202.
10. Krueger DK, Kelly SM, Lewicki DN, Ruffolo R, Gallagher TM. 2001. Variations in disparate regions of the murine coronavirus spike protein impact the initiation of membrane fusion. Journal of virology 75:2792-2802.
11. Talbot PJ, Buchmeier MJ. 1985. Antigenic variation among murine coronaviruses: evidence for polymorphism on the peplomer glycoprotein, E2. Virus research 2:317-328.
12. Follis KE, York J, Nunberg JH. 2006. Furin cleavage of the SARS coronavirus spike glycoprotein enhances cell-cell fusion but does not affect virion entry. Virology 350:358-369.
13. Simmons G, Bertram S, Glowacka I, Steffen I, Chaipan C, Agudelo J, Lu K, Rennekamp AJ, Hofmann H, Bates P, Pohlmann S. 2011. Different host cell proteases activate the SARS-coronavirus spike-protein for cell-cell and virus-cell fusion. Virology 413:265-274.
14. Kim SH, Xiao S, Shive H, Collins PL, Samal SK. 2013. Mutations in the fusion protein cleavage site of avian paramyxovirus serotype 4 confer increased replication and syncytium formation in vitro but not increased replication and pathogenicity in chickens and ducks. PloS one 8:e50598.
15. Yamada Y, Liu XB, Fang SG, Tay FP, Liu DX. 2009. Acquisition of cell-cell fusion activity by amino acid substitutions in spike protein determines the infectivity of a coronavirus in cultured cells. PloS one 4:e6130.
16. Bos EC, Luytjes W, Spaan WJ. 1997. The function of the spike protein of mouse hepatitis virus strain A59 can be studied on virus-like particles: cleavage is not required for infectivity. Journal of virology 71:9427-9433.
17. Gombold JL, Hingley ST, Weiss SR. 1993. Fusion-defective mutants of mouse hepatitis virus A59 contain a mutation in the spike protein cleavage signal. Journal of virology 67:4504-4512.
18. Otsuki K, Noro K, Yamamoto H, Tsubokura M. 1979. Studies on avian infectious bronchitis virus (IBV). II. Propagation of IBV in several cultured cells. Archives of virology 60:115-122.
19. Belouzard S, Chu VC, Whittaker GR. 2009. Activation of the SARS coronavirus spike protein via sequential proteolytic cleavage at two distinct sites. Proceedings of the National Academy of Sciences of the United States of America 106:5871-5876.
20. Harrison SC. 2008. Viral membrane fusion. Nature structural & molecular biology 15:690-698.
21. White JM, Delos SE, Brecher M, Schornberg K. 2008. Structures and mechanisms of viral membrane fusion proteins: multiple variations on a common theme. Critical reviews in biochemistry and molecular biology 43:189-219.
22. Sturman LS, Ricard CS, Holmes KV. 1990. Conformational change of the coronavirus peplomer glycoprotein at pH 8.0 and 37 degrees C correlates with virus aggregation and virus-induced cell fusion. Journal of virology 64:3042-3050.
23. Zelus BD, Schickli JH, Blau DM, Weiss SR, Holmes KV. 2003. Conformational changes in the spike glycoprotein of murine coronavirus are induced at 37 degrees C either by soluble murine CEACAM1 receptors or by pH 8. Journal of virology 77:830-840.
24. Madu IG, Roth SL, Belouzard S, Whittaker GR. 2009. Characterization of a highly conserved domain within the severe acute respiratory syndrome coronavirus spike protein S2 domain with characteristics of a viral fusion peptide. Journal of virology 83:7411-7421.
25. Epand RM. 2003. Fusion peptides and the mechanism of viral fusion. Biochimica et biophysica acta 1614:116-121.
26. Matsuyama S, Taguchi F. 2009. Two-step conformational changes in a coronavirus envelope glycoprotein mediated by receptor binding and proteolysis. Journal of virology 83:11133-11141.

27. Bosch BJ, Bartelink W, Rottier PJ. 2008. Cathepsin L functionally cleaves the severe acute respiratory syndrome coronavirus class I fusion protein upstream of rather than adjacent to the fusion peptide. Journal of virology 82:8887-8890.

28. Simmons G, Gosalia DN, Rennekamp AJ, Reeves JD, Diamond SL, Bates P. 2005. Inhibitors of cathepsin L prevent severe acute respiratory syndrome coronavirus entry. Proceedings of the National Academy of Sciences of the United States of America 102:11876-11881.

29. Belouzard S, Madu I, Whittaker GR. 2010. Elastase-mediated activation of the severe acute respiratory syndrome coronavirus spike protein at discrete sites within the S2 domain. The Journal of biological chemistry 285:22758-22763.

30. Bertram S, Heurich A, Lavender H, Gierer S, Danisch S, Perin P, Lucas JM, Nelson PS, Pohlmann S, Soilleux EJ. 2012. Influenza and SARS-coronavirus activating proteases TMPRSS2 and HAT are expressed at multiple sites in human respiratory and gastrointestinal tracts. PloS one 7:e35876.

31. Cote M, Misasi J, Ren T, Bruchez A, Lee K, Filone CM, Hensley L, Li Q, Ory D, Chandran K, Cunningham J. 2011. Small molecule inhibitors reveal Niemann-Pick C1 is essential for Ebola virus infection. Nature 477:344-348.

32. Scott CC, Gruenberg J. 2011. Ion flux and the function of endosomes and lysosomes: pH is just the start: the flux of ions across endosomal membranes influences endosome function not only through regulation of the luminal pH. BioEssays : news and reviews in molecular, cellular and developmental biology 33:103-110.

33. Schnell JR, Chou JJ. 2008. Structure and mechanism of the M2 proton channel of influenza A virus. Nature 451:591-595.

34. Hofmann M, Wyler R. 1988. Propagation of the virus of porcine epidemic diarrhea in cell culture. Journal of clinical microbiology 26:2235-2239.

35. Song DS, Yang JS, Oh JS, Han JH, Park BK. 2003. Differentiation of a Vero cell adapted porcine epidemic diarrhea virus from Korean field strains by restriction fragment length polymorphism analysis of ORF 3. Vaccine 21:1833-1842.

36. Qiu Z, Hingley ST, Simmons G, Yu C, Das Sarma J, Bates P, Weiss SR. 2006. Endosomal proteolysis by cathepsins is necessary for murine coronavirus mouse hepatitis virus type 2 spike-mediated entry. Journal of virology 80:5768-5776.

37. Matsuyama S, Ujike M, Morikawa S, Tashiro M, Taguchi F. 2005. Protease-mediated enhancement of severe acute respiratory syndrome coronavirus infection. Proceedings of the National Academy of Sciences of the United States of America 102:12543-12547.

38. Simmons G, Reeves JD, Rennekamp AJ, Amberg SM, Piefer AJ, Bates P. 2004. Characterization of severe acute respiratory syndrome-associated coronavirus (SARS-CoV) spike glycoprotein-mediated viral entry. Proceedings of the National Academy of Sciences of the United States of America 101:4240-4245.

39. Nash TC, Buchmeier MJ. 1997. Entry of mouse hepatitis virus into cells by endosomal and nonendosomal pathways. Virology 233:1-8.

40. Eifart P, Ludwig K, Bottcher C, de Haan CA, Rottier PJ, Korte T, Herrmann A. 2007. Role of endocytosis and low pH in murine hepatitis virus strain A59 cell entry. Journal of virology 81:10758-10768.

41. Chu VC, McElroy LJ, Chu V, Bauman BE, Whittaker GR. 2006. The avian coronavirus infectious bronchitis virus undergoes direct low-pH-dependent fusion activation during entry into host cells. Journal of virology 80:3180-3188.

42. Mercer J, Schelhaas M, Helenius A. 2010. Virus entry by endocytosis. Annual review of biochemistry 79:803-833.

43. Simmons G, Zmora P, Gierer S, Heurich A, Pohlmann S. 2013. Proteolytic activation of the SARS-coronavirus spike protein: cutting enzymes at the cutting edge of antiviral research. Antiviral research 100:605-614.

44. Fenouillet E, Barbouche R, Jones IM. 2007. Cell entry by enveloped viruses: redox considerations for HIV and SARS-coronavirus. Antioxidants & redox signaling 9:1009-1034.

45. Ryser HJ, Levy EM, Mandel R, DiSciullo GJ. 1994. Inhibition of human immunodeficiency virus infection by agents that interfere with thiol-disulfide interchange upon virus-receptor interaction. Proceedings of the National Academy of Sciences of the United States of America 91:4559-4563.

46. Rott R, Klenk HD, Nagai Y, Tashiro M. 1995. Influenza viruses, cell enzymes, and pathogenicity. American journal of respiratory and critical care medicine 152:S16-19.

47. Steinhauer DA. 1999. Role of hemagglutinin cleavage for the pathogenicity of influenza virus. Virology 258:1-20.

48. Gierer S, Bertram S, Kaup F, Wrensch F, Heurich A, Kramer-Kuhl A, Welsch K, Winkler M, Meyer B, Drosten C, Dittmer U, von Hahn T, Simmons G, Hofmann H, Pohlmann S. 2013. The spike protein of the emerging betacoronavirus EMC uses a novel coronavirus receptor for entry, can be activated by TMPRSS2, and is targeted by neutralizing antibodies. Journal of virology 87:5502-5511.

49. Matsuyama S, Nagata N, Shirato K, Kawase M, Takeda M, Taguchi F. 2010. Efficient activation of the severe acute respiratory syndrome coronavirus spike protein by the transmembrane protease TMPRSS2. Journal of virology 84:12658-12664.

50. Bertram S, Dijkman R, Habjan M, Heurich A, Gierer S, Glowacka I, Welsch K, Winkler M, Schneider H, Hofmann-Winkler H, Thiel V, Pohlmann S. 2013. TMPRSS2 activates the human coronavirus 229E for cathepsin-independent host cell entry and is expressed in viral target cells in the respiratory epithelium. Journal of virology 87:6150-6160.

51. Bottcher E, Matrosovich T, Beyerle M, Klenk HD, Garten W, Matrosovich M. 2006. Proteolytic activation of influenza viruses by serine proteases TMPRSS2 and HAT from human airway epithelium. Journal of virology 80:9896-9898.

52. Shirogane Y, Takeda M, Iwasaki M, Ishiguro N, Takeuchi H, Nakatsu Y, Tahara M, Kikuta H,

Yanagi Y. 2008. Efficient multiplication of human metapneumovirus in Vero cells expressing the transmembrane serine protease TMPRSS2. Journal of virology 82:8942-8946.

53. Bugge TH, Antalis TM, Wu Q. 2009. Type II transmembrane serine proteases. The Journal of biological chemistry 284:23177-23181.
54. Regan AD, Shraybman R, Cohen RD, Whittaker GR. 2008. Differential role for low pH and cathepsin-mediated cleavage of the viral spike protein during entry of serotype II feline coronaviruses. Veterinary microbiology 132:235-248.
55. Licitra BN, Millet JK, Regan AD, Hamilton BS, Rinaldi VD, Duhamel GE, Whittaker GR. 2013. Mutation in spike protein cleavage site and pathogenesis of feline coronavirus. Emerging infectious diseases 19:1066-1073.
56. Hatesuer B, Bertram S, Mehnert N, Bahgat MM, Nelson PS, Pohlman S, Schughart K. 2013. Tmprss2 Is Essential for Influenza H1N1 Virus Pathogenesis in Mice. PLoS pathogens 9:e1003774.
57. Overall CM, Blobel CP. 2007. In search of partners: linking extracellular proteases to substrates. Nature reviews. Molecular cell biology 8:245-257.
58. Rawlings ND, Barrett AJ, Bateman A. 2012. MEROPS: the database of proteolytic enzymes, their substrates and inhibitors. Nucleic acids research 40:D343-350.
59. Barrett AJ. 2001. Proteases. Current protocols in protein science / editorial board, John E. Coligan ... [et al.] Chapter 21:Unit 21 21.
60. Zhirnov OP, Ovcharenko AV, Bukrinskaya AG. 1984. Suppression of influenza virus replication in infected mice by protease inhibitors. The Journal of general virology 65 (Pt 1):191-196.
61. Watanabe M, Hirano A, Stenglein S, Nelson J, Thomas G, Wong TC. 1995. Engineered serine protease inhibitor prevents furin-catalyzed activation of the fusion glycoprotein and production of infectious measles virus. Journal of virology 69:3206-3210.
62. Shen X, Zhang X, Liu S. 2013. Novel hemagglutinin-based influenza virus inhibitors. Journal of thoracic disease 5:S149-159.
63. Bahgat MM, Blazejewska P, Schughart K. 2011. Inhibition of lung serine proteases in mice: a potentially new approach to control influenza infection. Virology journal 8:27.
64. Zhirnov OP, Klenk HD, Wright PF. 2011. Aprotinin and similar protease inhibitors as drugs against influenza. Antiviral research 92:27-36.
65. Zhou Y, Simmons G. 2012. Development of novel entry inhibitors targeting emerging viruses. Expert review of anti-infective therapy 10:1129-1138.
66. Kawase M, Shirato K, van der Hoek L, Taguchi F, Matsuyama S. 2012. Simultaneous treatment of human bronchial epithelial cells with serine and cysteine protease inhibitors prevents severe acute respiratory syndrome coronavirus entry. Journal of virology 86:6537-6545.
67. Saini N, Mahindra A. 2013. Therapeutic strategies for the treatment of multiple myeloma. Discovery medicine 15:251-258.
68. Eckhardt CL, van der Bom JG, van der Naald M, Peters M, Kamphuisen PW, Fijnvandraat K. 2011. Surgery and inhibitor development in hemophilia A: a systematic review. Journal of thrombosis and haemostasis : JTH 9:1948-1958.
69. Crump CJ, Johnson DS, Li YM. 2013. Development and mechanism of gamma-secretase modulators for Alzheimer's disease. Biochemistry 52:3197-3216.
70. de Vries E, Tscherne DM, Wienholts MJ, Cobos-Jimenez V, Scholte F, Garcia-Sastre A, Rottier PJ, de Haan CA. 2011. Dissection of the influenza A virus endocytic routes reveals macropinocytosis as an alternative entry pathway. PLoS pathogens 7:e1001329.
71. Bhattacharyya S, Mulherkar N, Chandran K. 2012. Endocytic pathways involved in filovirus entry: advances, implications and future directions. Viruses 4:3647-3664.
72. Travis J, Potempa J. 2000. Bacterial proteinases as targets for the development of second-generation antibiotics. Biochimica et biophysica acta 1477:35-50.
73. Bottcher-Friebertshauser E, Klenk HD, Garten W. 2013. Activation of influenza viruses by proteases from host cells and bacteria in the human airway epithelium. Pathogens and disease 69:87-100.
74. King MD, Guentzel MN, Arulanandam BP, Bodour AA, Brahmakshatriya V, Lupiani B, Chambers JP. 2011. Effects of bacterial microflora of the lower digestive tract of free-range waterfowl on influenza virus activation. Applied and environmental microbiology 77:4119-4125.
75. Callan RJ, Hartmann FA, West SE, Hinshaw VS. 1997. Cleavage of influenza A virus H1 hemagglutinin by swine respiratory bacterial proteases. Journal of virology 71:7579-7585.
76. Chertow DS, Memoli MJ. 2013. Bacterial coinfection in influenza: a grand rounds review. JAMA : the journal of the American Medical Association 309:275-282.
77. Scheel TK, Rice CM. 2013. Understanding the hepatitis C virus life cycle paves the way for highly effective therapies. Nature medicine 19:837-849.
78. Hill A. 2013. Optimizing HIV treatment. Current opinion in HIV and AIDS 8:34-40.
79. American-Soybean-Association. 2013. A Reference Guide to Important Soybean Facts & Figures.
80. Watanapa P, Williamson RC. 1993. Experimental pancreatic hyperplasia and neoplasia: effects of dietary and surgical manipulation. British journal of cancer 67:877-884.
81. Haffejee IE. 1991. Neonatal rotavirus infections. Reviews of infectious diseases 13:957-962.
82. Katyal R, Rana S, Vaiphei K, Ojha S, Singh K, Singh V. 2000. Influence of soybean trypsin inhibitor on small bowel enzyme activities during rotavirus infection in malnourished infant mice. Annals of nutrition & metabolism 44:198-206.
83. Zamolodchikova TS. 2012. Serine proteases of small intestine mucosa--localization, functional properties, and physiological role. Biochemistry. Biokhimiia 77:820-829.
84. Meyer D, Sielaff F, Hammami M, Bottcher-

Friebertshauser E, Garten W, Steinmetzer T. 2013. Identification of the first synthetic inhibitors of the type II transmembrane serine protease TMPRSS2 suitable for inhibition of influenza virus activation. The Biochemical journal 452:331-343.

85. Bottcher-Friebertshauser E, Lu Y, Meyer D, Sielaff F, Steinmetzer T, Klenk HD, Garten W. 2012. Hemagglutinin activating host cell proteases provide promising drug targets for the treatment of influenza A and B virus infections. Vaccine 30:7374-7380.
86. Turk B. 2006. Targeting proteases: successes, failures and future prospects. Nature reviews. Drug discovery 5:785-799.
87. Ruiz-Arguello MB, Goni FM, Pereira FB, Nieva JL. 1998. Phosphatidylinositol-dependent membrane fusion induced by a putative fusogenic sequence of Ebola virus. Journal of virology 72:1775-1781.
88. Biniossek ML, Nagler DK, Becker-Pauly C, Schilling O. 2011. Proteomic identification of protease cleavage sites characterizes prime and non-prime specificity of cysteine cathepsins B, L, and S. Journal of proteome research 10:5363-5373.
89. Brecher M, Schornberg KL, Delos SE, Fusco ML, Saphire EO, White JM. 2012. Cathepsin cleavage potentiates the Ebola virus glycoprotein to undergo a subsequent fusion-relevant conformational change. Journal of virology 86:364-372.
90. Krzyzaniak MA, Zumstein MT, Gerez JA, Picotti P, Helenius A. 2013. Host cell entry of respiratory syncytial virus involves macropinocytosis followed by proteolytic activation of the F protein. PLoS pathogens 9:e1003309.
91. Hunt CL, Lennemann NJ, Maury W. 2012. Filovirus entry: a novelty in the viral fusion world. Viruses 4:258-275.
92. Li W, Moore MJ, Vasilieva N, Sui J, Wong SK, Berne MA, Somasundaran M, Sullivan JL, Luzuriaga K, Greenough TC, Choe H, Farzan M. 2003. Angiotensin-converting enzyme 2 is a functional receptor for the SARS coronavirus. Nature 426:450-454.
93. Delmas B, Gelfi J, L'Haridon R, Vogel LK, Sjostrom H, Noren O, Laude H. 1992. Aminopeptidase N is a major receptor for the entero-pathogenic coronavirus TGEV. Nature 357:417-420.
94. Raj VS, Mou H, Smits SL, Dekkers DH, Muller MA, Dijkman R, Muth D, Demmers JA, Zaki A, Fouchier RA, Thiel V, Drosten C, Rottier PJ, Osterhaus AD, Bosch BJ, Haagmans BL. 2013. Dipeptidyl peptidase 4 is a functional receptor for the emerging human coronavirus-EMC. Nature 495:251-254.
95. Heurich A, Hofmann-Winkler H, Gierer S, Liepold T, Jahn O, Pohlmann S. 2014. TMPRSS2 and ADAM17 Cleave ACE2 Differentially and Only Proteolysis by TMPRSS2 Augments Entry Driven by the Severe Acute Respiratory Syndrome Coronavirus Spike Protein. Journal of virology 88:1293-1307.
96. Shulla A, Heald-Sargent T, Subramanya G, Zhao J, Perlman S, Gallagher T. 2011. A transmembrane serine protease is linked to the severe acute respiratory syndrome coronavirus receptor and activates virus entry. Journal of virology 85:873-882.
97. Johannsdottir HK, Mancini R, Kartenbeck J, Amato L, Helenius A. 2009. Host cell factors and functions involved in vesicular stomatitis virus entry. Journal of virology 83:440-453.
98. Floyd DL, Ragains JR, Skehel JJ, Harrison SC, van Oijen AM. 2008. Single-particle kinetics of influenza virus membrane fusion. Proceedings of the National Academy of Sciences of the United States of America 105:15382-15387.
99. Koch P, Lampe M, Godinez WJ, Muller B, Rohr K, Krausslich HG, Lehmann MJ. 2009. Visualizing fusion of pseudotyped HIV-1 particles in real time by live cell microscopy. Retrovirology 6:84.

Summaries

Nederlandse Samenvatting

Virussen zijn kleine deeltjes die genetische informatie (het genoom) bevatten. Virussen zijn zelf geen levende organismen en zijn derhalve voor hun vermenigvuldiging volledig afhankelijk van de machinerie van gastheercellen. Co-evolutie tussen gastheercellen en virussen vindt plaats sinds het begin van het cellulaire leven. Vrijwel alle bekende organismen kunnen geïnfecteerd worden door virussen. Sommige virale infecties veroorzaken ziekten. Bekende voorbeelden van veel voorkomende virale ziekten zijn griep, AIDS, mazelen en koortslip.

De familie van coronavirussen bevat belangrijke ziekteverwekkers van mensen en dieren. De aandacht voor coronavirussen is sterk toegenomen sinds de opkomst van het severe acute respiratory syndrome coronavirus (SARS-CoV) in 2003 en het Middle East respiratory syndrome coronavirus (MERS-CoV) in 2012. Beide virussen infecteren de luchtwegen van de mens, vaak met dodelijke afloop. De overdracht van deze coronavirussen van dier naar mens toont het potentiële gevaar van coronavirussen voor de volksgezondheid aan. Coronavirussen veroorzaken ook ernstige ziekten onder vee en gezelschapsdieren. Het porcine epidemic diarrhea virus (PEDV) bijvoorbeeld is een belangrijk pathogeen voor varkens en repliceert in de darmen. PEDV-epidemieën komen regelmatig voor in Oost-Azië, en veroorzaken ernstige economische schade als gevolg van een hoge sterfte onder met name jonge biggen. PEDV verscheen en verspreidde zich op het Noord-Amerikaanse subcontinent voor het eerst in 2013, en sindsdien blijft het aantal nieuwe infecties oplopen. De beschikbare, commerciële PEDV vaccins bieden niet afdoende bescherming in varkens. Meer kennis over de moleculaire mechanismen van PEDV-infectie en -replicatie zijn belangrijk om nieuwe, meer effectieve vaccins te ontwikkelen. Naast PEDV werd in dit proefschrift het muizen hepatitis virus (MHV) onderzocht. De MHV-stam A59 is een prototype coronavirus en diende in dit onderzoek als een modelvirus om de details van coronavirus infecties verder uit te zoeken.

Verspreiding van virussen tussen cellen en individuele organismen vereist de overdracht van virale genetische informatie. Hiertoe wordt het virale genoom door een beschermende mantel van eiwitten verpakt en in de omgeving vrijgelaten. Coronavirussen zijn membraan omhulde virussen en zijn extra omsloten door een lipide-membraan met daarin virale eiwitten (de envelop). Om in een nieuwe gastheer cel terecht te komen, moeten de virusdeeltjes door het cellulaire membraan heen dat de cel omhult en een barrière vormt. Dit binnentreden in de cel wordt beschouwd als de eerste, cruciale stap in de vermeerderingscyclus van virussen. Onder de juiste omstandigheden en door specifieke stimuli, kan de virale membraan-envelop versmelten met het cellulaire membraan. Bij die versmelting (fusie) met de cel brengt het virus zijn genoom in de gastheercel.

Om toegang te krijgen tot de gastheercellen brengen coronavirussen gespecialiseerde “fusiemachines” mee: de zogenaamde ‘Spike’ eiwitten welke in het virale membraan zijn verankerd. Deze eiwitten kunnen met de elektronenmicroscoop worden waargenomen als uitsteeksels van het virus wat een karakteristieke kroonachtige verschijning geeft (de corona). Spike-eiwitten hebben meerdere functies, zoals binding aan receptor-moleculen van de cel en het mogelijk maken van membraanfusie. De acties van de spike-eiwitten worden strak gereguleerd om het irreversibele membraanfusie proces op de juiste plaats en tijd te laten gebeuren. De membraanfusie-actieve toestand wordt bereikt door het in tweeën knippen van het spike-eiwit middels cellulaire enzymen. Belangrijke kenmerken van

coronavirus membraanfusie zijn weliswaar bekend, maar de noodzakelijke biochemische en moleculaire processen en de volgorde van de gebeurtenissen die tot de fusie leiden zijn nog onduidelijk.

In de dit proefschrift bestudeerden we de details van MHV-membraanfusie. Onze focus was gericht op de activering van het spike-eiwit door proteolytische klieving. Op basis van onze resultaten, beschrijven we een meer geavanceerd model van de door het MHV spike-eiwit gemedieerde fusie met de gastheercel. Verder onderzochten we de basis-mechanismen van PEDV-infectie met behulp van recombinante virussen. Het fusie-mechanisme werd vergeleken met het bestaande model voor virus-fusie. Samen bieden deze bevindingen nieuw inzicht in hoe coronavirussen in de cellen terecht komen, de essentiële eerste stap van een infectie. Deze kennis kan het ontwerp van nieuwe interventiestrategieën ter voorkoming van het binnendringen van virus in gastheercellen ondersteunen.

Inhoud van dit proefschrift

In hoofdstuk 2 onderzochten we de activering van MHV spike-eiwit door proteolytische klieving. Hiervoor ontwikkelden we een methode zonder bias om de klievingstatus van MHV spike-eiwitten direct na membraanfusie te bepalen. Dit maakte het mogelijk virale spike-eiwitten te identificeren en biochemisch te analyseren specifiek van gefuseerde virussen. Daarmee konden we de geknipte MHV spike-eiwitten bestuderen, die voor de membraanfusie met de gastheercel verantwoordelijk zijn.

De studie in hoofdstuk 3 is ontworpen om de proteolytische enzymen (proteasen) te bestuderen die de MHV spike-eiwitten klieven. We gebruikten RNA-interferentie technologie en pseudogetypeerde virus-achtige deeltjes. Blijkbaar is de activatie van MHV spike-eiwitten niet afhankelijk van een specifiek protease omdat de activatie van spike-eiwit niet door enkele remmers van dergelijke enzymen geblokkeerd worden. De plaatsen van klieving en/of de proteases zijn kennelijk variabel. Deze bevinding verklaart waarom MHV infectie ongevoelig is voor specifieke remmers.

In hoofdstuk 4 leggen we de grondslag voor ons onderzoek naar PEDV. Om het virale genoom te kunnen modificeren, hebben we een reverse-genetics systeem ontwikkeld op basis van de trypsine-onafhankelijke en celkweek-geadapteerde PEDV-stam DR13. Hiermee hebben we onder andere mutanten van PEDV met reporter-genen kunnen maken.

We onderzochten de bijzondere vereisten voor de verspreiding van PEDV in celkweek in hoofdstuk 5. Infectie van cellen door natuurlijke PEDV-stammen is strikt afhankelijk van toevoeging van actieve trypsine. We vergeleken de spike-eiwitten van de natuurlijke stam CV777 en de trypsine-onafhankelijke, celkweek-geadapteerde PEDV-stam DR13. Genetische manipulatie van het spike gen maakte het mogelijk details van membraanfusie van PEDV te bepalen. We vonden de genetische determinanten in het spike gen verantwoordelijk voor trypsine-afhankelijke virus vermeerdering.

In het laatste hoofdstuk worden de huidige inzichten in de verschillende stappen die tot membraan fusie van coronavirussen leiden besproken en vergeleken met die van andere virale fusie eiwitten. Gebaseerd op de samengevatte resultaten van onze MHV- en PEDV-studies, bespreken we het onderliggende mechanisme en de vermeende biologische rol van klieving van spike-eiwitten in de vermeerderingscyclus van coronavirussen.

English Summary

Viruses are small biological particles containing selfish genetic information. They are no living organisms themselves; instead viruses hijack the host cells machinery for their multiplication. Viruses coevolved with their hosts since the beginning of cellular life. Virtually all life forms on earth can be infected by viruses. Evidently, some viral infections can cause sickness. The general public is aware of common viral diseases such as flu, AIDS, measles, and cold sore.

The family of coronaviruses studied in the present dissertation comprises many pathogenic viruses of concern to man. Coronaviruses have received attention because of infections with the severe acute respiratory syndrome coronavirus (SARS-CoV) in 2003 and the Middle East respiratory syndrome coronavirus (MERS-CoV) in 2012, both infecting the airways of humans. Their emergence demonstrates the potential of animal viruses to infect humans and the consequential threat to human health. Coronaviruses can also cause severe diseases among farm and companion animals. Porcine epidemic diarrhea virus (PEDV) infects the intestines of pigs. Epidemics frequently recur in East-Asia causing severe economic damage due to high mortality rates amongst piglets. PEDV has emerged on the North American subcontinent in 2013 and since then, the number of reported cases continues to rise. The current vaccines do not provide effective protection to the pigs, and greater knowledge about the molecular mechanisms of PEDV infection and replication are required to devise effective vaccines. Besides PEDV, the mouse hepatitis virus (MHV), a virus that infects mice, was investigated. This prototype coronavirus served as a model to investigate coronavirus infection.

Transmission of viruses between cells and individual organisms requires the transfer of viral genetic information. Therefore, the viral genome is packaged into a protective shell and released into the environment. Enveloped virus particles, like coronaviruses, are additionally enclosed by a lipid membrane. To enter a new host cells, virus particles must overcome the cellular membrane barrier. Virus entry is the initial step of the next infection. Under particular conditions and by certain stimuli, the virus can fuse its envelope with a cellular membrane and thereby release the genetic information into the cell.

To gain access to the host cell, coronaviruses carry specialized fusion machines: Spike proteins that are anchored in the viral membrane envelope. These proteins can be observed as protrusions in electron microscopy images resulting in the characteristic crown-like appearance (the corona). Spike proteins have multiple functions including binding to host cell receptor molecules and facilitating membrane fusion. The actions of the spike protein are tightly controlled to regulate the timing and place of fusion. Proteolytic cleavage of the spike protein is required to render them fusion-ready. The characteristics of membrane fusion by coronaviruses have been studied extensively, however biochemical and molecular requirements and sequence of events of the viral entry into the host cell are elusive.

In the present dissertation, we probed the details of MHV entry. Our focus was set on the activation of the virus-cell fusion process. Based on our results, we describe a more advanced model of MHV spike protein-mediated fusion. Furthermore, we elucidated the basic mechanism of PEDV entry using recombinant viruses. The fusion mechanism was compared with the existing virus fusion model. Together, this provides novel insight into virus entry, the essential first step of an infection. This will help to understand how viruses

are transferred between hosts and it will aid the design of novel intervention strategies based on the inhibition of virus entry.

Outline of this thesis

In the second chapter, we investigated the activation of MHV spike protein by proteolytic cleavage. We developed an unbiased assay to determine the cleavage status of MHV spike proteins directly after membrane fusion has occurred. Our entry assay enables the identification and biochemical characterization of viral spike proteins of fusing virions, specifically. Thereby, we could study the MHV spike protein cleavage product that actually mediates membrane fusion with the host cell.

The study in chapter 3 was designed to identify the proteases, which cleave the MHV spike protein by RNA interference technology and by using pseudotyped virus-like particles. We found that MHV spike proteins are not dependent on a specific protease. The cleavage site and/or the proteases are rather promiscuous and thereby enable MHV to infect a variety of different cell types. This finding explains why MHV infection is insensitive to specific protease inhibitors.

In chapter 4, we set the stage for the investigation of PEDV. To modify the viral genome, we established a reverse genetic system based on the trypsin-independent cell culture-adapted PEDV strain DR13. Using this system, we generated PEDV derivatives containing reporter genes.

We investigated the particular requirements for propagation of PEDV in cell culture in chapter 5. Infection of cells by PEDV field isolates is strictly dependent on the supplementation of active trypsin to cell culture medium. Genetic manipulation of the spike gene enabled us to study details of PEDV entry. We compared the S proteins of the trypsin-dependent field isolate CV777 and the trypsin-independent cell culture-adapted PEDV DR13 and were able to map the genetic determinants within the spike gene responsible for trypsin-dependent entry.

In the final chapter, the current understanding of the various steps leading to coronavirus membrane fusion is discussed and compared to other class I viral fusion proteins. Reviewing our results from the MHV and PEDV studies, we discuss the underlying mechanism and the putative biological role of spike protein proteolysis in the coronavirus life cycle.

Deutsche Zusammenfassung

Viren sind kleine Partikel, die genetische Erbinformationen (das Genom) enthalten. Viren sind keine lebenden Organismen, weil ihre Vermehrung vollständig von Wirtszellen abhängig ist. Dazu übernimmt das Virus die Wirtszelle und nutzt deren Funktionen. Seit Beginn des zellulären Lebens findet somit eine ständige Anpassung (Koevolution) zwischen Viren und ihren Wirtszellen statt. Es wird davon ausgegangen, dass alle Organismen von Viren infiziert werden können. Einige virale Infektionen verursachen Krankheiten. Bekannte Beispiele von Viruserkrankungen des Menschen sind die Grippe, AIDS, Masern und Lippenherpes.

Zur Familie der Coronaviren gehören für Mensch und Tier gefährliche Krankheitserreger. Coronaviren machten Schlagzeilen durch das Auftreten des severe acute respiratory syndrome coronavirus (SARS-CoV) im Jahr 2003 und des Middle East respiratory syndrome coronavirus (MERS-CoV) 2012. Beide Viren führen zu Atemwegserkrankungen beim Menschen und enden oft tödlich. Die Übertragung dieser Coronaviren vom Tier auf den Menschen verdeutlichte die Gefahr von bisher unbekannten viralen Erkrankungen für die öffentliche Gesundheit. Coronaviren verursachen auch schwere Krankheiten in Nutz- und Haustieren. Das porcine epidemic diarrhea virus (PEDV) befällt Schweine in Mastbetrieben und führt zu hohen Sterblichkeitsraten insbesondere bei Ferkeln. Vor allem in Ost-Asien entsteht großer ökonomischer Schaden. Im Jahr 2013 wurde das Virus zum ersten Mal auf dem Nordamerikanischen Subkontinent nachgewiesen und verursacht seitdem eine ansteigende Zahl von Infektionen. Die kommerziell erhältlichen Impfstoffe gegen PEDV verleihen keinen hinreichenden Schutz. Unser Wissen über die molekularen Mechanismen der PEDV-Infektion und Vermehrung ist begrenzt. Diese Dissertation legt Grundlagen zur Erforschung von PEDV-Infektionen und kann somit zur Entwicklung von neuen, effektiveren PEDV-Impfstoffen beitragen. Neben PEDV wurde das Maus Hepatitis Virus (MHV) weiter erforscht. Der MHV Stamm A59 stellt ein typisches Coronavirus dar und diente als Modelvirus für die Untersuchung weiterer Details von Coronavirusinfektionen.

Die Verbreitung von Viren zwischen Zellen und individuellen Organismen erfordert die Übertragung der viralen Erbinformationen. Das Genom wird dazu in eine Schutzhülle aus Eiweißmolekülen verpackt und in die Umgebung ausgeschieden. Coronaviren sind behüllte Viren. Die Viruspartikel zeichnen sich durch eine zusätzliche Ummantelung mit einer Lipidmembran aus, die wiederum virale Eiweiße mit verschiedenen Funktionen enthält. Der Eintritt in die Wirtszelle wird als erster und notwendiger Schritt des viralen Vermehrungszyklus angesehen. Um Zugang zu einer neuen Wirtszelle zu erlangen, müssen Viruspartikel die zelluläre Membran überwinden, welche alle Zellen umgibt und sie gegen die Außenwelt abschirmt. Dazu verschmilzt unter günstigen Umständen und durch spezifische Auslöser die virale Membranhülle mit der Zellmembran. Durch die Fusion mit der Zellmembran wird das virale Genom eingeschleust.

Um Zugang zur Wirtszelle zu erzwingen, enthalten Coronaviruspartikel eine hoch spezialisierte Fusionsmachinerie: die sogenannten ‚Spike'-Eiweiße, die in der Membranhülle verankert sind. Spike-Eiweiße sind im Elektronenmikroskop als Kranz um das Viruspartikel sichtbar (lat. corona: Kranz, Krone). Sie haben mehrere Aufgaben, unter anderem das Binden an Rezeptormoleküle der Zelle und Durchführen der Membranfusion. Die Funktionen der Spike-Eiweiße werden genau gesteuert, damit der unumkehrbare Fusionsprozess am richtigen Ort und zum richtigen Zeitpunkt stattfindet. Zelluläre Verdauungsenzyme können das Spike-Eiweiß entzwei schneiden. Dadurch wird die Fähigkeit zur Membranfusion

aktiviert. Grundlegende Merkmale der Coronavirus-Membranfusion sind bekannt, aber die notwendigen biochemischen und molekularen Prozesse sowie die Abfolge der einzelnen Ereignisse, die zur Fusion führen, sind unzureichend erforscht.

In dieser Dissertation beschreibe ich unsere Detailstudien der MHV-Membranfusion. Dabei konzentrierten wir uns auf die Aktivierung des Spike-Eiweißes durch die oben erwähnte enzymatische Spaltung. Auf der Basis unserer Ergebnisse haben wir ein detaillierteres Model der durch das MHV Spike-Eiweiß ausgelösten Membranfusion entworfen. Außerdem haben wir die Grundlagen von PEDV-Infektionen unter Zuhilfenahme von Virusmutanten studiert. Den Fusionsmechanismus von PEDV haben wir mit dem bestehenden Model der Virusfusion verglichen. Zusammengefasst liefern unsere Studien neue Erkenntnisse über das Eintreten von Coronaviren in die Wirtszellen. Mit Hilfe dieses Wissens können neue antivirale Therapiemöglichkeiten entwickelt werden, die auf dem Blockieren der Virusfusion basieren.

Gliederung der Dissertation

Im zweiten Kapitel beschreiben wir unsere Untersuchungen zur Aktivierung der MHV Spike-Eiweiße durch die enzymatische Spaltung von Verdauungsenzymen. Wir entwickelten eine neue, objektive Methode, um den Zustand der MHV Spike-Eiweiße direkt nach der Membranfusion zu isolieren. Dadurch waren wir erstmals in der Lage, die viralen Spike-Eiweiße von fusionierten Viren zu identifizieren und biochemisch zu analysieren. Wir konnten einen definierten Abschnitt im Spike-Eiweiß nachweisen, in dem eine Spaltung stattfinden muss, um das Spike-Eiweiß zu aktivieren.

Die in Kapitel drei vorgestellte Studie wurde entworfen, um die Verdauungsenzyme (Proteasen) der Zelle zu erforschen, die die MHV Spike-Eiweiße schneiden. Dazu machten wir von der RNA-Interferenz-Technologie und pseudotypisierten virusähnlichen Partikeln Gebrauch. Die Aktivierung von MHV Spike-Eiweißen war unabhängig von speziellen Proteasen. Wir untersuchten den Effekt von verschiedenen Protease hemmenden Agenzien, konnten jedoch keine Auswirkungen erkennen. Die Schnittstelle im Spike-Eiweiß und die Spaltungsenzyme waren offensichtlich variabel. Dies erklärt auch, warum MHV-Infektionen nicht durch spezifische Proteasehemmer gestoppt werden können.

Im vierten Kapitel werden die Grundlagen für unsere Untersuchungen an PEDV dargestellt. Um das virale Erbgut zu modifizieren, entwickelten wir ein reverses Genetiksystem. Es basiert auf dem Trypsin (Verdauungsenzym) unabhängigen, auf Zellkultur angepassten PEDV Stamm DR13. Unter anderem konnten wir somit PEDV-Virusmutanten herstellen, die zusätzliche Reportergene enthalten.

Die Untersuchungen der besonderen Eigenschaften der Vermehrung von PEDV in Zellkultur wurden in Kapitel fünf beschrieben. Infektion von Zellen mit einem in der Natur vorkommenden PEDV-Stamm ist abhängig von der Zugabe des Verdauungsenzyms Trypsin. Wir haben die Spike-Eiweiße eines Wildstamms mit dem Trypsin-unabhängigen, Zellkultur angepassten PEDV-Stamm DR13 verglichen. Manipulation des viralen Erbgutes ermöglichte die detaillierte Studie der Membranfusion von PEDV. Wir konnten die Teile des PEDV Spike-Eiweißes identifizieren, welche für die zur Infektion benötigte Aktivierung durch Trypsin verantwortlich sind.

Im letzten Kapitel werden aktuelle Erkenntnisse über die verschiedenen Schritte, die zur Membranfusion von Coronaviren führen, besprochen und mit anderen viralen

Fusionseiweißen verglichen. Auf Grundlage der zusammengefassten Resultate unserer Studien an MHV und PEDV, diskutieren wir den zugrundeliegenden Mechanismus und die mutmaßliche Rolle der Spaltung von Spike-Eiweißen im Vermehrungszyklus von Coronaviren.

Acknowledgements

I want to express my sincere gratitude to the people who paved my way to a successful doctoral degree. Respect and honors to my promoter Peter Rottier and co-promoter Berend Jan Bosch, who made this achievement possible. Their warm, cheerful personality and dedication to science created an inspiring and fruitful environment. I was granted the independence to develop and follow my own theories. Implementation and execution of my ideas was made possible by the endless and unconditional support I received from my colleagues. Most of you have moved on; new colleagues joined. I am grateful for all lessons taught on experimental, scientific, and personal level. All of you have made an impact and I remember the individual characters with joy. I wish you a long, pleasant, and prosperous future. A special shout out to Christine Burkard and Nancy Schuurman, whose efforts continue by being my paranimfen during the defense. I am also grateful for my previous mentors Volker Lohmann and Marco Binder at University of Heidelberg. I am optimistic that I could pass on some of the spirit and knowledge you taught me by being a good tutor to my students Eelke Béguin, Lione Willems, and Tom Meuleman. I enjoyed working with you so much.

Some of my colleagues became friends. Christine, we always managed to create a comfortable and fun atmosphere to enjoy the good things in life. I want to thank Qiushi Wang and Marne Hagemeijer for their honest opinions and support. Arno de Vliet, Nancy Schuurman, Alan Rigter, Hélène Verheije, and Inge Marie Stub, you made my arrival in the Netherlands pleasant, invited me to the Dutch culture, and offered so much help. Thank you. I was glad when Lucian Albulescu, Cristina Dorobantu, Qian Feng, and Rachel Ulferts joined the lab and spiced up my life. Thank you for all your enthusiasm and frankness. Special thanks to Huihui Mou, Wentao Li, Julio Padilla, and Kazuya Shirato for introducing and sharing their news and views.

It took some time until I completely arrived in Utrecht. By now, I call it my second home, packed with good friends. First of all, Petra Vrancken and Marjolein Hooykaas - sharing a passion for table top gaming and chocorozijnen, spiced with philosophical discussions. Regards go out to Mette Roesgaard and Markus Sobora, first neighbors, then friends. Also many thanks to Raimond Heukers, Willem Bartelink, and Roxana Dragusel for their positive nature and enthusiasm – keep that excitement about the future. I want to thank the excellent dancers from Danscentrum Cornelissen for all the enjoyable evenings and interactive Dutch lessons.

Der Umzug nach Holland, erneut über 600 Kilometer entfernt vom letzten Standort, hat viele gute Freunde, aber nicht Freundschaften zurückgelassen. Ich habe mich riesig über jeden Besucher gefreut. Ich bedanke mich bei denjenigen, die den Kontakt und die Freundschaft halten. Lucie Behnke, Verena Heise, Familie Klein, Miriam Meyer, Simon Murmann, Paul Paepke, Robert Rauchut, Friederike Schlumm, Broder Schmidt, Toni Woelk, und Alexander Wolff. Ihr habt mein Leben bereichert und mich geerdet. Auch wenn wir uns selten sehen; ihr sollt wissen, dass es immer eine Freude ist, euch zu sehen und euren Geschichten zu lauschen.

Mein Leben wäre leer, öde und weniger ambitioniert ohne meine Familie. Ich danke meinen Eltern und meinem Bruder, die mir mit ihrer Unterstützung, ihrem Antrieb und ihrer Liebe dieses Doktorat ermöglicht haben. Ich danke auch meinen Großeltern, die durch Pakete und Nachrichten oft einen Teil Heimat nach Utrecht geschickt haben. Viele glückliche Momente habe ich mit allen anderen Familienmitgliedern erlebt und immer ein wohliges Gefühl davongetragen. Ich bin glücklich ein Teil dieser bunten Sippe zu sein. Ich bin in besonderem Maße der Familie Gram dankbar, deren Kreis ich mittlerweile auch als Heimat empfinde.

Ein Teil meines Lebens ist auch ein Teil aller drei Heimaten Berlin-Basel-Utrecht. Liebe Anna, du hast mich verzaubert und dieser Zauber hält an. Magisch hast du immer Recht, auch wenn ich‘s nicht hören will. Wie durch Zufall, ergänzen wir uns jeden Tag. Aber ich weiß, dass alles ein lang ausgeheckter Plan von dir ist. Wir sind ein fantastisches Team, deine Voraussicht und meine innere Ruhe sind unsere Geheimwaffe, die uns durch Tiefs führte und Hochs genießen lässt. Ich werde immer für dich da sein und will gemeinsam mit dir und an dir weiter wachsen.

Curriculum vitae

Postdoctoral Scientist	2013 - today	Scientist at National Institute for Public Health and the Environment, Bilthoven, The Netherlands
Doctorate	2009 - 2013	Molecular Virology, University of Utrecht, The Netherlands
Master of Science	2007 - 2009	Molecular Biosciences, University of Heidelberg, Germany
Bachelor of Science	2004 - 2007	Molecular Cell Biology, University of Heidelberg, Germany

Scientific output & publications

Bachelor Thesis	Functional analysis of chimeric RNA polymerases from two hepatitis C virus strains. Supervised by Volker Lohmann, Molecular Virology, University of Heidelberg, 2007
Master Thesis	Screening for novel kinases in RIG-I mediated IRF3 signaling. Supervised by Ralf Bartenschlager, Molecular Virology, University of Heidelberg, 2009
Poster presentation	Coronavirus cell entry: kinetics and cleavage of its fusion protein. International conference Eurovirology, Como, Italy, 2010
Presentation	Coronavirus cell entry: Visualization and characterization of viral fusion protein after fusion with the target cell. International conference GfV in Essen, Germany, 2012
Poster presentation	Coronavirus cell entry: Visualization and characterization of viral fusion protein after fusion with the target cell. Virus Assembly Meeting, Menorca, 2012
Invited presentation	Identification and characterization of Coronavirus spike proteins after fusion with the target cell. German Primate Center, Göttingen, Germany, 2012
Presentation	Genetic determinants for trypsin-dependent propagation of porcine epidemic diarrhea virus. American Society of Virology Meeting, Penn State University, USA, 2013
Presentation	Identification and characterization of coronavirus spike proteins after fusion with the target cell. American Society of Virology Meeting, Penn State University, USA, 2013

Wicht O, Li W, Willems L, Meuleman TJ, Wubbolts RW, van Kuppeveld FJ, Rottier PJ, Bosch BJ. 2014. Proteolytic Activation of the Porcine Epidemic Diarrhea Coronavirus Spike Fusion Protein by Trypsin in Cell Culture. Journal of virology 88, in press.

Wicht O, Burkard C, de Haan CA, van Kuppeveld FJ, Rottier PJ, Bosch BJ. 2014. Identification and characterization of a proteolytically primed form of the murine coronavirus spike proteins after fusion with the target cell. Journal of virology 88:4943-4952.

Li C, Li Z, Zou Y, Wicht O, van Kuppeveld FJ, Rottier PJ, Bosch BJ. 2013. Manipulation of the porcine epidemic diarrhea virus genome using targeted RNA recombination. PloS one 8:e69997

Schmitt M, Scrima N, Radujkovic D, Caillet-Saguy C, Simister PC, Friebe P, Wicht O, Klein R, Bartenschlager R, Lohmann V, Bressanelli S. 2011. A comprehensive structure-function comparison of hepatitis C virus strain JFH1 and J6 polymerases reveals a key residue stimulating replication in cell culture across genotypes. Journal of virology 85:2565-2581.

Simister P, Schmitt M, Geitmann M, Wicht O, Danielson UH, Klein R, Bressanelli S, Lohmann V. 2009. Structural and functional analysis of hepatitis C virus strain JFH1 polymerase. Journal of virology 83:11926-11939.